Field Theoretical Description of Exchange Terms and Pairing Correlations in Nuclear Systems

Dissertation
von
Milena Serra

Institut für Theoretische Physik T30
Physik–Department
Technische Universität München

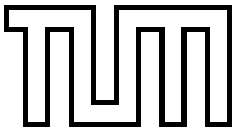

Juli 2001

Physik–Department der Technischen Universität München
Theoretische Physik T30

Field Theoretical Description of Exchange Terms and Pairing Correlations in Nuclear Systems

Milena Serra

Vollständiger Abdruck der von der Fakultät für Physik der Technischen Universität München zur Erlarung des akademischen Grades eines

Doktors der Naturwissenschaften (Dr. rer. nat.)

genehmigten Dissertation.

Vorsitzender:		Univ.–Prof. Dr. H.-J. Körner
Prüfer der Dissertation:	1.	Univ.–Prof. Dr. P. Ring
	2.	Univ.–Prof. Dr. Dr. h. c. K. Dietrich

.

Die Dissertation wurde am 03.07.2001 bei der Technischen Universität München eingereicht und durch die Fakultät für Physik am 16.07.2001 angenommen.

An dieser Stelle gilt mein besonderer Dank Herrn Prof. Dr. Peter Ring für die Themenstellung dieser Arbeit. Damit hat er mir eine einmalige Gelegenheit geboten, viel Neues zu lernen. Er hat diese Arbeit die ganzen Jahre über mit großen Engagement betreut und hat immer bedingungslos zu mir gehalten.

Sehr danke ich auch den Herren Prof. Dr. Dario Vretenar und Prof. Dr. George Lalazissis dafür, daß sie mir mit vielen Ratschlägen geholfen haben, diese Arbeit zu verbessern. Ein herzlicher Dank gilt Dario: ohne ihn wäre ich nicht bei T30 gelandet.

Des weiteren bedanke ich mich bei allen Institutsmitgleidern für die nette Aufnahme und das freundschaftliche Arbeitsklima.

Contents

Introduction

The study of nuclear many-body systems plays an outstanding role in the development of many-body theories [RS80]. One of the most active areas of research since the beginning of last century, nuclear physics has always demanded for a strong link between experiments and theories of atomic nuclei. Early experimental techniques allowed only the study of nuclei on or close to the β-stability line, and, in addition, they were limited to energy scales considerably smaller than the nucleon mass $M \approx 939.0$ MeV/c^2. Thus, the nucleus has traditionally and successfully been described as a collection of non-relativistic nucleons interacting through an instantaneous two-body potential, with the dynamics given by the Schrödinger equation.

For the last two decades, the new generation of accelerators has been providing an always larger amount of valuable informations for a better understanding of the nuclear force. Although intimately related, three main areas of investigation of the strong interaction may be distinguished: heavy ion collisions at relativistic energies, as for example at LHC and at RHIC, probe the nature of quark-gluon confinement and the assumptions of the underlying QCD. Electron and muon scattering experiments probe the quark-gluon structure of hadrons and of nuclei, and, finally, experiments at lower energies with beams of stable and unstable nuclei, performed with Radioactive Nuclear Beams (RNB) facilities in Europe, Japan, and in the USA, probe the structure and the dynamics of nuclei on and far from the stability line [RIA00, NuP00]. In particular, the study of exotic nuclei with RNB techniques encompasses new aspects of nucleonic matter: limits of nuclear existence, extended distributions of neutron matter, nuclei with large N to Z ratio, pairing correlations in both $T = 1$ and $T = 0$ channels are some of the most interesting issues that RNB techniques may address.

From the theoretical point of view, it is well established that quantum chromodynamics (QCD) is the fundamental theory of strong interactions. However, due to the mathematical problems raised by the non-perturbative character of QCD in the low energy regime, a quantitative understanding of the structure and interactions of nucleons in terms of QCD, and therefore of nuclei as bound systems of nucleons, remains an essential long-term goal of nuclear theory.

Since the early days of nuclear physics diverse quantitative theoretical approaches have been developed in order to describe and predict nuclear structure properties. One of the most fundamental challenges of the nuclear many-body theory is to derive the bulk properties of nuclei from a bare nucleon-nucleon (NN) interaction, viewed as residual interaction of the underlaying quark-gluon dynamics of QCD. Here, the term bare refers to nuclear potentials which reproduce NN scattering data. Representative examples are the Bonn [Ma89], Paris [LLR80], Argonne [WSA84], and Nijmegen [MRS89] potentials. Typically, these forces contain a very repulsive core which accounts for NN correlations at short

internucleonic distances, an intermediate attraction and as long range part a one-pion exchange potential. For very light nuclei, using a bare interaction plus a phenomenological three-body potential as only inputs, Quantum Monte Carlo methods provide an exact solution for the few-body problem and allow to calculate various properties of nuclear bound, and low energy continuum states. At present, this is possible only up to $A = 10$ [WPC00]. For the description of heavier nuclei, bare NN interactions may be used for example in the framework of the Brueckner-Hartree-Fock (BHF) approximation. In this approach, starting from an appropriate model wave function of the system under investigation, the Bethe-Goldstone equation determines an effective interaction, the so-called G-matrix, which takes into account the effects of NN correlations as, for example, the Pauli principle and dispersion effects. For many years, non-relativistic BHF calculations have been performed with only limited success. Well known is the so-called phenomenon of the Coester band, which stands for the fact that many-body calculations based on various realistic models of the NN interaction lead to predictions for the saturation point of nuclear matter that either fail to yield enough binding energy or predict a saturation density larger than the empirical value [CCD70]. Such a Coester band can also be observed in non-relativistic studies of finite nuclei: in this case BHF calculations yield either correct binding energies but too small radii, or correct radii but too small binding energies [SMM91]. Through the years it has turned out that relativistic effects cannot be neglected, and Dirac-Brueckner-Hartree-Fock (DBHF) calculations have given results for the saturation point of nuclear matter in quite a good agreement with the empirical saturation point [BM90]. So far no self-consistent solutions of the DBHF equations for finite nuclei have been established.

In parallel, since Brueckner calculations suggested a density dependence of the effective interaction, phenomenological approaches based on energy functionals have been developed and successfully applied to the nuclear many-body problem. In full analogy with the Kohn-Sham approach [KS65] to the density functional theory [DG90], the minimization of the energy functional determines the exact ground state energy and density of a given system. In particular, these approaches are mainly used in the mean field approximation in which atomic nuclei are described as systems of A nucleons moving independently in an average field produced by other nucleons. With this assumption hamiltonian and density reduce to single-particle operators. Then, the variational principle determines the equilibrium density of the ground state which provides the Hartree-Fock equations and defines at the same time the average field in the system. Therefore, in this sense, a mean field description contains already exchange and short-range correlation effects, and in the relativistic case in particular also contribution from the vacuum. However, in nuclear physics such a density functional theory does not allow *ab initio* calculations because it gives no practical guide for the construction of the effective energy functional, and therefore, several phenomenological parametrizations have been adopted (well known non-relativistic examples are the Skyrme interactions [Sk59] and Gogny forces [DG80]): they contain a certain number of fit parameters which are adjusted to reproduce experimental data. Successful in many applications, with only a few fixed parameters, they can explain many experimental data encompassing nuclei over a large range of the periodic table.

Over the past decades, the phenomenological models have been fined tuned primarily to reproduce the properties of nuclei close to the valley of stability. For this reason, they

may not always be appropriate for use in the calculations of nuclei far from this valley. In this contest, it is expected that the spectroscopy of exotic nuclei by means of RNB techniques will test the existing forces in the exotic region of the periodic table and will lead to a better determination of the effective nuclear forces and their isospin dependence.

In recent years, since the work of Walecka and collaborators [SW86], who re-introduced an idea proposed already in the Fifties by Schiff [Sc51] and Teller [JT55, DT56], relativistic approaches to nuclear physics have been studied and applied to problems of scattering, nuclear matter at zero and finite temperature, and nuclear structure. Starting from a relativistic Lagrangian density containing mesonic and nucleonic degrees of freedom, a relativistic theory of the nuclear many-body problem is formulated on the basis of the three following assumptions: first, it is fully Lorentz invariant; second, it obeys strictly causality; and third, the nucleons are treated as point-like particles. Therefore, from its definition, it is a relativistic quantum field theory. However, it cannot be treated in perturbation theory because of the strong coupling constants. The lowest order of the full quantum field theory is the mean field approximation.

Relativistic Mean Field (RMF) models form a phenomenological effective theory for the relevant degrees of freedom of QCD at very low energy. The relativistic Lagrangian, whose parameters are fitted to nuclear data, is an effective functional of the density and, therefore, describes the nuclear many-body system exactly. In this approach independent nucleons are treated as Dirac spinors and they interact only by the exchange of virtual mesons characterized by their masses, coupling constants, and by the quantum numbers spin, parity, and isospin. Although from scattering experiments at intermediates energies it is well known that many mesons play a role in a quantitative description of the bare NN interaction, in the RMF theory, being a phenomenological approach, one tries to include as few mesons as possible, classified by their quantum numbers, in order to reproduce the experimental data with a minimal number of fit parameters. In particular one is tempted to incorporate those mesons which are experimentally known to exist in free space and to use their properties as far as possible.

Most of the applications of the RMF theory to the study of nuclear systems have been performed at the Hartree level. In this approach the nucleons and the virtual mesons σ, ω, and ρ are the only degrees of freedom of the theory: σ is an isoscalar scalar meson which mediates the attractive intermediate-range of the nuclear interaction, ω is an isoscalar vector meson that is responsible for the short-range repulsion of the nuclear force, and, finally, ρ provides the isospin dependence of the nuclear force. Furthermore, it was recognized very early that relativistic models based only on one-meson exchange could not reproduce quantitatively essential nuclear properties such as the incompressibility or surface properties, as for example nuclear deformations [PRB87]. Therefore, Boguta and Bodmer [BB77] extended the model by including a non-linear self-coupling amongst the σ-meson of the form of a cubic and quartic potentials. The parameters of the non-linear terms are adjusted to the surface properties of finite nuclei, and since the σ field is strongly dependent on the nuclear density, non-linearities in the potential corresponds in some sense to a density dependence of the σ mass. Finally, at this level the pion, responsible of the tensor term of the nuclear force, is not included because its corresponding mean field has a negative parity, while in real nuclei the mean field is parity conserving to a very high degree of accuracy.

Starting from the corresponding local Lagrangian density, the variational principle

determines the equations of motions of the fields which are then solved self-consistently. In particular, the nucleons obey the Dirac equation and the mesons Klein Gordon equations. In the relativistic Hartree (RH) approximation the meson fields are replaced by their expectation values, i.e. they are considered as classical fields. Furthermore, the no-sea approximation is used in almost all the applications of the RMF theory. This means that one neglects the negative energy solutions of the Dirac equation which should be taken into account for a fully relativistic description of the system. It has been argued that effects of vacuum polarization are taken into account in the fit of the parameters.

A large number of calculations of ground state properties of nuclei in many regions of the periodic table have argued that the RMF theory is at least as successful as non-relativistic mean field theories based on density-dependent forces as the Skyrme or Gogny interactions [VB72, DG80]. Amongst the successes: ground state properties (such as nuclear radii, isotopes shifts, and magnetic moments) of closed shell spherical nuclei and nuclei with deformations are successfully predicted by the RMF theory. As well, nuclei far from the line of β-stability and collective vibrations of small amplitudes and giant resonances in time-dependent problems are well described. A review of the RMF theory is given in Ref. [Ri96].

As the RMF theory is a completely phenomenological approach, in spirit very similar to the non-relativistic DDHF models of Skyrme and Gogny, the question arises whether it is really necessary to choose a relativistic description of the nuclear many-body system. Although on the phenomenological level non-relativistic approaches may explain all data maybe at the cost of a larger number of parameters, a relativistic, even phenomenological, description of the nuclear many-body problem goes beyond these "classical" theories. In particular, because the kinetic energy of the system turns out to be small in comparison to the rest mass, it has to be stressed that the consequences of relativity are dynamical and not kinematic.

Several are the motivations which may lead to prefer a relativistic theory for the description of nuclear systems. First of all, it starts on a more fundamental level, treating mesonic degrees of freedom explicitly and it includes the spin properties in a natural way. Another essential point is the classification of different physical quantities by their behavior under Lorentz transformation, for example the distinction between scalar and vector densities (ρ_s and ρ_v), and between the Lorentz scalar field S and the Lorentz vector field $V^\mu = (V, \mathbf{V})$. In particular, it has been shown that the difference between ρ_s and ρ_v, a purely relativistic effect, introduces a new mechanism of saturation. It seems that also in non-relativistic DDHF calculations this effect is considered in a phenomenological way and it is hidden amongst other many-body effects in the strongly repulsive density dependent terms which produce saturation. Concerning the scalar field S and the time-like component of the vector field V, their absolute sizes are large and cannot be neglected in comparison to the rest mass, and from Lorentz invariance it follows that S is attractive and V is repulsive. They are particularly important as they characterize the essential properties of the nuclear systems: in fact, their difference determines the weak mean field in which nucleons move and their sum the strong spin-orbit term. Thus one derives the existence of the traditional nuclear shell model and the validity of its assumptions. Another important point in favor of a relativistic description of the nuclear many-body system is the fact that $|S| \approx |V|$ leads to the pseudo-spin symmetry in nuclear spectra, a symmetry which has been known for thirty years in nuclear physics but which could be understood

only recently as a consequence of the relativistic content of nuclear structure [Gi97]. A further example that shows the advantage of being relativistic is the nuclear magnetism phenomenon. In systems, where the time-reversal symmetry is broken, such as in those with an odd number of particles or in the rotating ones, one has to consider currents. In a relativistic system they induce potentials connected with the spatial components of the vector field $\mathbf{V}$. Thus they lead to time-reversal breaking mean fields and to polarization currents playing an important role in a quantitative understanding of nuclear magnetic moments of odd-mass nuclei and of moments of inertia in rotating nuclei. Finally, from the mathematical and numerical point of view, the relativistic models considered at the Hartree level are in many respects easier to handle than non-relativistic DDHF calculations. In fact, in the former case only local terms enter into the RH equations, which may be solved rather easily by using several techniques, for example by expansion in an oscillator basis [GRT90] or in coordinate space.

Although a RH approach provides a successful nuclear phenomenology, the variational principle and the classical treatment of the meson fields do not allow a satisfactory description of pairing correlations in the *pp*-channel, neither do they take into account explicitly the Fock term of one-meson exchange potentials in the *ph*-channel.

Starting from a quantized version of the theory and using Green's functions techniques relativistic Hartree-Fock-Bogoliubov (RHFB) equations can be derived as shown by Kucharek and Ring in Ref. [KR91]. The explicit energy dependence of the relativistic nuclear wave function, the non-localities introduced by the Fock terms in the *ph*-channel, and the presence of pairing correlations in the *pp*-channel make these equations much more complicated than the non-relativistic HFB and the RH equations. So far, in the relativistic framework the problems of exchange terms and pairing correlations have been considered separately.

Of course, in going from a RH to a relativistic Hartree-Fock (RHF) approximation of the nuclear many-body problem the parameters of the effective Lagrangian must be readjusted. Up to now the RHF equations have been solved for infinite nuclear matter [BMM85, GRW89] and for spherical nuclei [BMG87, HS83, BI87], but due to the involved numerics no satisfactory parameters sets have been determined, and RHF results do not reproduce experimental data as well as calculations performed with the most recent parameters sets of RH models. As previously alluded, the latters already contain the exchange effects. In fact, although relativistic forces have finite ranges, the heavy mass of the mesons σ, ω, and ρ, and the local character of their corresponding interaction, allow one to consider these fields in the limit of infinite mass, i.e. as zero-range forces. Analogously to the non-relativistic case [VB72], it can be shown that the exchange terms of zero-range relativistic forces have the same form of the direct terms, but different coefficients. Therefore, adjusting the parameters of these mesons in the RH calculations to the experimental data takes already into account in a phenomenological way a large part of the Fock terms contribution. This approximation does not apply to the case of the pion: in fact it is a light particle and the corresponding interaction has a non-local character.

Concerning the treatment of pairing correlations, at the Hartree level they are usually taken into account in the constant gap approximation, a variational procedure first introduced for density dependent Skyrme forces [Va73]. In the BCS scheme, using the experimental value of the gap parameters taken from the odd-even mass formula, one

calculates the occupation probabilities, which are then used in the calculation of the physical observables. Although for nuclei close to the β-stability line, the RMF calculations performed within this scheme are in good agreement with experimental data and non-relativistic HFB calculations, this method is not satisfactory when applied to very exotic nuclei. In the first instance no data are available, and, in addition, it has been proved that the BCS approximation is not the proper way to treat pairing correlations as it does not provide a correct description of the scattering of nucleonic pairs from bound states to the positive energy continuum [DNW96], leading to unbound systems. Therefore, for a proper description of pairing correlations relativistic Hartree-Bogoliubov (RHB) equations, as those derived in Ref. [KR91], have to be used. In the same work the authors have shown that the one-boson exchange interaction used in for the description of the nuclear mean field leads to unrealistic pairing correlations. On the other hand, the effective force in the pairing channel should be the K-matrix [La59, Mi68], which is the sum over all the particle-particle irreducible diagrams and it has probably very little to do with the Brueckner's G-matrix which enters in the ph-channel. However, very little is known about this matrix in the relativistic framework and up to now only phenomenological forces have been used to describe pairing correlations in finite nuclei. On one side, since it is supposed that relativistic effects do not play a role in the pp-channel, a RHB model with a non-relativistic finite-range pairing interaction has been successfully applied in the study of several isotope chains of spherical nuclei [GLE96], and exotic systems: for example it has been used for the investigation of the halo phenomenon in light nuclei [MR96, PVL97], properties of light nuclei near the neutron drip line [LVP98a], reduction of the spin-orbit potential in nuclei with extreme isospin values [LVP98b], ground state properties of Ni and Sn isotopes [LVR98], properties of proton rich nuclei [VLR98, LVR01]. Although extremely successful, pairing correlations are not treated in a fully self-consistent relativistic way. On the other side a RHB model with a phenomenological relativistic delta interaction has been developed in Ref. [CH00] and applied to several isotopic chains of even-even spherical and deformed nuclei.

The present status of the RMF theories of the nuclear many-body problem may be summarized as follows:

- Although very successful, RH approximations presents two main shortcomings: first, it does not allow a satisfactory description of pairing in nuclei and second it does not allow to take into account tensor terms of the nuclear force, introduced by the pion exchange potential.

- RHF theories exist, but no satisfactory parameters sets have been determined yet. This is due to the fact that the numerical methods used for the iterations of the RHF equations are too slow to fit accurately the parameters sets of the new effective force.

- A fully relativistic theory of pairing is still an open question.

In this thesis a new RHF and a fully relativistic HB approaches are developed. Applications in infinite nuclear matter and spherical finite nuclei are presented.

With respect to the RHF approximation, our principal goal is to study the effect of the tensor term of the nuclear force on the ground state properties of finite nuclei. Our starting point is then an effective relativistic Lagrangian density containing nucleons and

the mesons σ, ω, ρ, and π, and the the non-linear self-interactions of σ as degrees of freedom. By using the experimental values for the pion mass and coupling constant, the parameters which have to be fitted to experimental data are the same as those of standard RH approximations. Due to the complexity of the RHF equations, in order to determine the parameters set of the model in the most effective way, we have developed a new numerical techniques which allows a fast iteration of the RHF equations. The fit of the parameters of the new force is now in progress. As test for our numerics we have used our method for solving the RHF equations in the case of RHF models already existing. Calculations of ground state properties of finite spherical nuclei carried out with our expansion method are in excellent agreement with the results obtained solving the RHF in coordinate space (see for example Ref. [BMG87]) and the calculation time is much shorter, once that the matrix elements have been calculated. Furthermore, we have investigated the contribution of the contribution of the Fock term to several nuclear properties, as for example binding energy, rms radii and energy splittings of spin-orbit partners. In the latter case, we have found that the inclusion of the π-meson produces a large effect in comparison with RH calculations.

With respect to the relativistic theory of pairing, we aim to solve the RHB equations for finite nuclei fully relativistically, i.e. by using a relativistic interaction also in the *pp*-channel. We start with an investigation of pairing correlations in infinite nuclear matter: we solve the relativistic BCS equations for the pairing gap using the relativistic bare potential adjusted by the Bonn group [Ma89], which corresponds to the first order of the K-matrix, the interaction which should be used in the *pp*-channel. The results for the $^1S_0$ pairing gap are in good agreement with non-relativistic calculations based on realistic forces fitted to reproduce pairing properties of finite nuclei. This is a first hint that a relativistic field theoretical description of nuclear many-body problem is able to reproduce pairing properties of finite systems.

Moving to finite nuclei, we propose a fully relativistic HB model which uses the standard relativistic force NL3 in the *ph*-channel and which treats fully relativistically also the *pp*-channel. Although the most ambitious goal would be to use a realistic pairing interaction, as in the case of the relativistic Hartree-Fock model, it is considerably more difficult to solve the RHB equations than the RH + BCS equations, and in particular a fully relativistic treatment of the *pp*-channel with realistic OBE interactions requires a big numerical effort. Therefore we have constructed a phenomenological pairing interaction based on the exchange of the σ- and ω-meson and, in first approximation, we have considered a limit of infinite mass. In this way, the interaction reduces to a zero-range force for which it is easier to solve the RHB equations. With this model we have calculated ground state properties of isotopic chain of Sn nuclei and we have compared the results with existing RHB calculations which use a non-relativistic approximation for the *pp*-channel. In particular we have investigate whether relativity plays a role also in the *pp*-channel which has always be considered as non-relativistic.

The work in organized as follows: in Chapter 1 the Lagrangian density of the RMF theory is presented, the corresponding equations of motions are derived, and the approximations of the theory are discussed. Here RMF is treated as a classical field theory; in Chapter 2, through a quantization of the theory, the relativistic HFB equations are derived. They allow a self-consistent treatment of pairing correlations and of the effects of the Fock terms in the description of nuclear systems; in Chapter 3 the relativistic

Hartree-Bogoliubov equations derived in Chapter 2 are applied for an investigation of the ${}^0S_1$ pairing in infinite nuclear matter. In particular, a BCS approximation is used for the study of the pairing gap at the Fermi surface produced by a realistic pairing potential; in Chapter 4 relativistic Hartree-Bogoliubov equations for finite nuclei are given explicitly and a fully relativistic solution for a isotopic chain of Sn nuclei is presented. Ground state properties are discussed and in particular the effects of relativity in the pairing channel are investigated; in Chapter 5 a relativistic Hartree-Fock model is introduced and applications to nuclear matter and finite nuclei are presented. In particular, the strength of the Fock term is compared with the direct term of the total OBE interaction and of the single one-meson exchange potential, and the effect of the spin-isospin and of the tensor term introduced by the exchange of the pion on the spin-orbit partners is investigated. Isotopes of Ca and Sn nuclei are considered; in the Conclusion we summarize our work and we give some hints for possible investigations and extensions which could be done in the future.

Chapter 1

Relativistic Mean Field Theory

The Relativistic Mean Field (RMF) theory, based on a local, Lorentz-invariant Lagrangian density, is an effective theory of the nuclear many-body problem [SW86]. It describes nuclear systems in terms of hadronic degrees of freedom, i.e.

- nucleons, treated as point-like particles, obey the Dirac equation;
- effective, point-like mesons mediate the interaction between the nucleons.

Mesons are characterized by their quantum numbers as spin J, parity P, isospin T, by their masses m_m and coupling constants g_m. Because the theory is phenomenological, these parameters are fitted to reproduce bulk nuclear properties and therefore they are different from the values in free space.

From nucleon-nucleon (NN) scattering data (see for example Ref. [Ma89]), it is known that for the description of the nuclear force in the low energy domain the following mesons are necessary:

- The isovector pseudo-scalar $\pi-$meson $(0^-, 1)$. It mediates the long-range (essentially tensor) attraction between nucleons. Although in nuclear physics it is one of the most important meson, closely connected to the chiral properties of QCD, its corresponding parity breaking mean field gives no contribution if the nuclear many-problem is treated at the Hartree level. However, in the case of the Hartree-Fock theory or in an investigation of pairing in nuclear systems, the role of the π-meson must be included explicitly.
- The isoscalar scalar $\sigma-$meson $(0^+, 0)$. It is a phenomenological meson which parametrizes the scalar part of the nuclear force. Namely, it is well known that the exchange of two or an even number of pions contribute to positive parity scalar fields and, although it is possible to form mean fields out of meson pairs, one prefers to introduce the phenomenological σ-meson, which is thus understood as an approximation of a two-pion exchange and other diagrams of higher order. It mediates the intermediate-range attraction;
- The isoscalar vector $\omega-$meson $(1^-, 0)$. It mediates the short-range repulsion;
- The isovector vector $\rho-$meson $(1^-, 1)$. It provides an isospin dependence of the nuclear force.

1.1 Relativistic Lagrangian Density

The starting point of a relativistic field theory of the nuclear many-body problem is the following classical Lagrangian density [Ri96]

$$\mathcal{L} = \mathcal{L}_N + \mathcal{L}_M + \mathcal{L}_{int}, \tag{1.1}$$

where $\mathcal{L}_N$, $\mathcal{L}_M$ and $\mathcal{L}_{int}$ describe free nucleons, free mesons and nucleon-meson interactions respectively. Explicitly

- $\mathcal{L}_N$ reads

$$\mathcal{L}_N = \bar{\psi}(i\gamma^\mu\partial_\mu - M)\psi \tag{1.2}$$

  where M is the bare nucleon mass and ψ is a Dirac spinor.

- Considering only the mesons previously mentioned, $\mathcal{L}_M$ contains

$$\begin{aligned}
\mathcal{L}_\sigma &= \frac{1}{2}(\partial_\mu\sigma\partial^\mu\sigma - m_\sigma^2\sigma^2), && (1.3)\\
\mathcal{L}_\pi &= \frac{1}{2}(\partial_\mu\vec{\pi}\partial^\mu\vec{\pi} - m_\pi^2)\vec{\pi}^2, && (1.4)\\
\mathcal{L}_\omega &= -\frac{1}{2}(\Omega_{\mu\nu}\Omega^{\mu\nu} - m_\omega^2\omega^\mu\omega_\mu), && (1.5)\\
\mathcal{L}_\rho &= -\frac{1}{2}(\vec{R}_{\mu\nu}\vec{R}^{\mu\nu} - m_\rho^2\vec{\rho}^\mu\vec{\rho}_\mu), && (1.6)\\
\mathcal{L}_A &= -\frac{1}{2}F_{\mu\nu}F^{\mu\nu} && (1.7)
\end{aligned}$$

  where m_σ, m_π, m_ω and m_ρ are the rest masses of the mesons, and

$$\begin{aligned}
\Omega^{\mu\nu} &= \partial^\mu\omega^\nu - \partial^\nu\omega^\mu, && (1.8)\\
\vec{R}^{\mu\nu} &= \partial^\mu\vec{\rho}^\nu - \partial^\nu\vec{\rho}^\mu, && (1.9)\\
F^{\mu\nu} &= \partial^\mu A^\nu - \partial^\nu A^\mu, && (1.10)\\
& && (1.11)
\end{aligned}$$

  are the field tensors of the $\omega-$ and the $\rho-$ mesons and of the photon. The arrows indicate vectors in isospin space.

- $\mathcal{L}_{int}$ reads

$$\begin{aligned}
\mathcal{L}_{int} = &- g_\sigma\bar{\psi}\sigma\psi - U(\sigma) - ig_\pi\bar{\psi}\gamma_5\vec{\tau}\vec{\pi}\psi\\
&- g_\omega\bar{\psi}\gamma_\mu\omega^\mu\psi - g_\rho\bar{\psi}\gamma_\mu\vec{\tau}\vec{\rho}^\mu\psi - e\bar{\psi}\gamma_\mu A^\mu\psi
\end{aligned} \tag{1.12}$$

  where $U(\sigma)$ is the non-linear self-coupling term amongst the $\sigma-$mesons and represents a sort of density dependence of the σ-mass. It was recognized that the original linear (σ,ω)-model of Walecka [Wa74] with linear parameter sets is not able to reproduce essential nuclear properties as incompressibility, surface properties and deformations. Therefore, Boguta and Bodmer [BB77] extended the model including

a non-linear self-coupling amongst the $\sigma-$mesons. They added to the mass term $\frac{1}{2}m_\sigma^2\sigma^2$ a quartic σ- potential of the form

$$U(\sigma) = \frac{1}{3}g_2\sigma^3 + \frac{1}{4}g_3\sigma^4 \tag{1.13}$$

where the parameters g_2 and g_3 are adjusted to the surface properties of nuclei. In principle, such a density dependence of the effective parameters is expected also from more fundamental arguments. For example, starting from the bare NN interaction Brockmann and Toki [BT92] have carried out relativistic Brueckner-Hartree-Fock calculations to determine the properties of nuclear matter at various densities. For each value of ρ they found density dependent coupling constants g_σ and g_ω.

In principle, the Lagrangian (1.1) defines a fully fledged relativistic field theory [IZ80] and, therefore, it should be quantized and treated by methods of quantum field theory. In this way one encounters the usual problems of divergent terms in many orders of perturbation theory. Although it may be shown that this theory is renormalizable, in practice the Lagrangian (1.1) is treated in mean field approximation, i.e. on the classical level and its parameters are adjusted by comparing the results with experimental data. In a way the situation is similar to non-relativistic density-dependent Hartree-Fock theory with a phenomenological ansatz for the energy functional [Va73] and to the Kohn-Sham theory in condensed matter physics [DG90, JG89].

In $\mathcal{L}_{int}$, instead of the pseudo-scalar coupling of the pion the pseudo-vector coupling is often used

$$\mathcal{L}_{pv} = -\frac{f_\pi}{m_\pi}\bar{\psi}\gamma_5\gamma_\mu\partial^\mu\vec{\pi}\vec{\tau}\psi \tag{1.14}$$

because it provides a better description of πN scattering data.

The dynamics of the system is determined by the variational principle

$$\delta S = 0, \qquad S = \int d^4x\mathcal{L}(x) \tag{1.15}$$

through the Euler-Lagrange equations

$$\partial_\mu\left(\frac{\partial\mathcal{L}}{\partial(\partial_\mu q_i)}\right) - \frac{\partial\mathcal{L}}{\partial q_i} = 0, \tag{1.16}$$

where the generalized coordinates q_i are the nucleon field ψ, and the meson fields $\sigma, \omega_\mu, \vec{\rho}_\mu$ and A_μ. Explicitly

- nucleons obey the Dirac equation

$$[\gamma^\mu(\partial_\mu - g_\omega\omega_\mu - g_\rho\vec{\rho}_\mu\vec{\tau} - e\frac{1-\tau_3}{2}A_\mu) - (M + g_\sigma\sigma) + ig_\pi\gamma_5\vec{\tau}\vec{\pi}]\psi = 0 \tag{1.17}$$

and the baryon current $\mathcal{B}^\mu = \bar{\psi}\gamma^\mu\psi$ is conserved, i.e.

$$\partial_\mu\mathcal{B}^\mu = 0. \tag{1.18}$$

- the mesons σ and π obey Klein-Gordon equations

$$(\partial_\mu \partial^\mu + m_\sigma^2)\sigma = -g_\sigma \bar{\psi}\psi - g_2\sigma^2 - g_3\sigma^3, \tag{1.19}$$
$$(\partial_\mu \partial^\mu + m_\pi^2)\vec{\pi} = -g_\pi \bar{\psi}\gamma_5 \vec{\tau}\psi. \tag{1.20}$$

- the mesons ω and ρ obey the Proca equations

$$\partial_\nu \Omega^{\nu\mu} + m_\omega^2 \omega^\mu = g_\omega \bar{\psi}\gamma^\mu \psi, \tag{1.21}$$
$$\partial_\nu \vec{R}^{\nu\mu} + m_\rho^2 \vec{\rho}^\mu = g_\rho \bar{\psi}\gamma^\mu \vec{\tau}\psi, \tag{1.22}$$

  which, using the conservation of the baryon current (1.18), can be rewritten as Klein-Gordon equations

$$(\partial_\mu \partial^\mu + m_\omega^2)\omega^\mu = g_\omega \bar{\psi}\gamma^\mu \psi, \tag{1.23}$$
$$(\partial_\mu \partial^\mu + m_\rho^2)\vec{\rho}^\mu = g_\rho \bar{\psi}\gamma^\mu \vec{\tau}\psi, \tag{1.24}$$

- the electromagnetic field obeys the Maxwell equations

$$\partial_\nu F^{\nu\mu} = e\bar{\psi}\gamma^\mu \frac{1-\tau_3}{2}\psi \tag{1.25}$$

  which in the Lorentz-gauge are reduced to

$$\partial_\nu \partial^\nu A^\mu = e\bar{\psi}\gamma^\mu \frac{1-\tau_3}{2}\psi \tag{1.26}$$

The energy-momentum tensor of the system is calculated as usually from $\mathcal{L}$ and it is given by

$$T^{\mu\nu} = -g^{\mu\nu}\mathcal{L} + \frac{\partial q_i}{\partial x_\nu}\frac{\mathcal{L}}{\partial(\partial q_i/\partial x^\nu)}. \tag{1.27}$$

It obeys the continuity equation

$$\partial_\mu T^{\mu\nu} = 0, \tag{1.28}$$

and therefore the four-momentum

$$P^\mu = \int d^3x\, T^{0\mu}, \tag{1.29}$$

is conserved. The energy is defined as the integral over the Hamiltonian density

$$P^0 = E = \int d^3r\ \mathcal{H} \tag{1.30}$$

with

$$\mathcal{H} = T^{00} = \frac{\partial \mathcal{L}}{\partial \dot{q}_j}\dot{q}_j - \mathcal{L}. \tag{1.31}$$

The transition from a classical field theory to a quantum field theory [IZ80] is achieved

by introducing the anti-commutator relations for fermions at equal-time points

$$\{\psi_\alpha(\boldsymbol{x},t),\psi^\dagger_\beta(\boldsymbol{y},t)\} = \delta_{\alpha\beta}\delta(\boldsymbol{x}-\boldsymbol{y}) \tag{1.32}$$

$$\{\psi_\alpha(\boldsymbol{x},t),\psi_\beta(\boldsymbol{y},t)\} = \{\psi^\dagger_\alpha(\boldsymbol{x},t),\psi^\dagger_\beta(\boldsymbol{y},t)\} = 0, \tag{1.33}$$

where α and β are Dirac indices and the commutator relations for mesons

$$[\phi_\mu(\boldsymbol{x},t),\Pi^\dagger_\nu(\boldsymbol{y},t)] = i\delta_{\mu\nu}\delta(\boldsymbol{x}-\boldsymbol{y}) \tag{1.34}$$

$$[\phi_\mu(\boldsymbol{x},t),\phi_\nu(\boldsymbol{y},t)] = [\Pi^\dagger_\mu(\boldsymbol{x},t),\Pi^\dagger_\nu(\boldsymbol{y},t)] = 0. \tag{1.35}$$

Here $\phi_\mu(x)$ are the meson fields and $\Pi_\mu(x)$ the conjugate momenta

$$\Pi_\mu = \frac{\partial\mathcal{L}}{\partial(\partial_0 q_\mu)}. \tag{1.36}$$

In the case of the vector mesons the Greek indices are Lorentz indices and the Kronecker symbol $\delta_{\mu\nu}$ has to be replaced by the metric tensor $-g_{\mu\nu}$.

1.2 Approximations and Equations of Motion of the RMF Theory

The RMF theory is formulated on the basis of two approximations of the effective Lagrangian density $\mathcal{L}$ given by Eq.s (1.2)-(1.7): The Mean Field and the No-Sea approximations.

- The Mean Field approximation corresponds to a classical treatment of the field theory defined by $\mathcal{L}$. It removes all quantum fluctuations of the meson fields using their expectation values

  $$\sigma,\vec{\pi},\omega^\mu,\vec{\rho}^\mu \longrightarrow <\sigma>,<\vec{\pi}>,<\omega^\mu>,<\vec{\rho}^\mu>$$

  In this way the handling of the nucleons is simplified: in fact they interact only via the mean field moving as independent particles in the meson fields. Derived from a classical variational principle, the RMF equations of motion are a relativistic Hartree approximation. Exchange corrections can be taken into account starting from the quantized version of the theory and using Greens function techniques [KR91]. Solving the relativistic Hartree-Fock equations for nuclear matter [BMM85, GRW89] and finite spherical nuclei [HS83, BMG87] it turns out that the effects due to the exchange terms are not negligible and consequently the parameters of the Lagrangian have to be readjusted. On the other side this could mean that fitting the parameters of the Lagrangian in the relativistic Hartree approximation to the experimental data takes already into account the effects of exchange terms in a phenomenological way. This is easy to understand for non-relativistic Hartree-Fock calculations with zero-range: in fact, in this case, apart from a different factor, the exchange term has essentially the same form as the direct term, and, as a consequence in this case, the only difference between the Hartree and the hartree-Fock approximation consists in different values of the parameters which are adjusted

anyway. However, since in a relativistic framework the forces do not have zero-range, the exchange terms are much more complicated. On the other side, in the case of the mesons with large mass, as σ, ω, and ρ the range of these forces is very small and therefore it may be argued that there is not a big difference between the relativistic Hartree and the relativistic Hartree-Fock approximation. This argument does not apply to the case of the π-meson because of its light mass and its tensor nature.

- The spectrum of the Dirac equation (1.17) for the nucleons consists of the negative energy continuum, a large number of negative energy bound states, positive energy bound states, which correspond to the usual nuclear shell model states, and the positive energy continuum. In principle, all the solutions should be taken into account for a fully relativistic description: In other words, one should allow for a polarization of the vacuum. This leads to divergent terms, which have to be removed by a proper renormalization. Analytically this has been done only for infinite nuclear matter, see for example Ref.s [CW74, Ch77]. Due to the fact that only numerical solutions can be obtained, in the case of finite nuclei an exact renormalization is not possible. To avoid this problem a local density approximation has been proposed by Horowitz and Serot in Ref. [HS84], and semi-classical extensions of this method have been used by Wasson in Ref. [Wa88] and Zhu et al. in Ref. [ZMR91] to study the influence of the vacuum polarization in spherical and deformed nuclei respectively. It has turned out that the renormalization effects are of the order of 20-30%. Therefore, if one takes into account vacuum polarization, the parameter set of the Lagrangian has to be readjusted, and with new force one finds approximately the same results as in the case of neglecting vacuum polarization. This means that by fitting the parameters of the Lagrangian in the no-sea approximation a large part of the effect of the vacuum polarization is already taken into account. Most of the application of the relativistic mean field theory to finite nuclei are done in the no-sea approximation.

Consistently with the Mean Field approximation, to each nucleon corresponds a spinor ψ_i, $i = 1, \ldots A$ satisfying the Dirac equation

$$\{\gamma_\mu(i\partial^\mu + V^\mu) + M + S + i\gamma_5 P\}\psi_i = 0 \tag{1.37}$$

where the relativistic fields read

$$\begin{aligned} S(x) &= g_\sigma \sigma(x), & (1.38)\\ P(x) &= g_\pi \vec{\tau}\vec{\pi}(x), & (1.39)\\ V^\mu(x) &= g_\omega \omega^\mu(x) + g_\rho \vec{\tau}\vec{\rho}^\mu(x) + eA^\mu(x). & (1.40) \end{aligned}$$

The mesons fields obey the Klein-Gordon equations

$$\begin{aligned} (\Box + m_\sigma)\sigma &= -g_\sigma \rho_s - g_2\sigma^2 - g_3\sigma^3, & (1.41)\\ (\Box + m_\pi)\vec{\pi} &= -g_\pi \vec{\rho}_{ps}, & (1.42)\\ (\Box + m_\omega)\omega^\mu &= g_\omega j^\mu, & (1.43)\\ (\Box + m_\rho)\vec{\rho}^\mu &= g_\rho \vec{j}^\mu, & (1.44)\\ \Box A^\mu &= e j_c^\mu, & (1.45) \end{aligned}$$

with the scalar density defined as

$$\rho_s(x) = \sum_i^A \bar{\psi}_i(x)\psi_i(x) \tag{1.46}$$

the pseudo-scalar density

$$\vec{\rho}_{ps}(x) = \sum_i^A \bar{\psi}_i(x)\gamma_5\vec{\tau}\psi_i(x), \tag{1.47}$$

the baryon current

$$j^\mu(x) = \sum_i^A \bar{\psi}_i(x)\gamma^\mu\psi_i(x), \tag{1.48}$$

the isocurrent

$$\vec{j}^\mu(x) = \sum_i^A \bar{\psi}_i(x)\gamma^\mu\vec{\tau}\psi_i(x), \tag{1.49}$$

and the electromagnetic current

$$j_c^\mu(x) = \sum_i^A \bar{\psi}_i(x)\frac{1}{2}(1+\tau_3)\gamma^\mu\psi_i(x). \tag{1.50}$$

For the description of even-even nuclei only stationary states with good parity of the Dirac equation (1.37) are concerned. In the static approximation it is assumed that the nucleon wave functions oscillate with the single-particle energies ε_i and that the meson fields are time-independent functions. Moreover, as the nuclear ground state of even-even nuclei is even under time-reversal and has a good parity, the space-like components of all currents $\boldsymbol{j}$, $\vec{\boldsymbol{j}}$, and $\boldsymbol{j}_c$, of the vector fields $\boldsymbol{\omega}$, $\vec{\boldsymbol{\rho}}$ and $\mathbf{A}$, and the pion field vanish. Finally, as the nucleon single-particle states do not mix isospin, only the third component of the isospin vector is needed. With these further simplifications, the equations of motion of the system read

$$\begin{aligned}
\{-i\boldsymbol{\alpha}\nabla + \beta(M+S) + V\}\psi_i &= \varepsilon_i\psi_i, && (1.51)\\
\{-\Delta + m_\sigma\}\sigma &= -g_\sigma\rho_s - g_2\sigma^2 - g_3\sigma^3, && (1.52)\\
\{-\Delta + m_\omega\}\omega^0 &= g_\omega\rho_v, && (1.53)\\
\{-\Delta + m_\rho\}\rho_3^0 &= g_\rho\rho_3, && (1.54)\\
-\Delta\rho_c^0 &= e\rho_c, && (1.55)
\end{aligned}$$

where now the scalar density ρ_s reads

$$\rho_s(x) = \sum_i^A \bar{\psi}_i\psi_i, \tag{1.56}$$

the baryon density ρ_v

$$\rho_v(x) = \sum_i^A \psi_i^\dagger\psi_i, \tag{1.57}$$

the isovector density ρ_3

$$\rho_v(x) = \sum_i^A \psi_i^\dagger \tau_3 \psi_i, \tag{1.58}$$

and the charge density ρ_c

$$\rho_c(x) = \sum_i^A \psi_i^\dagger \frac{1}{2}(1+\tau_3)\psi_i, \tag{1.59}$$

In the Dirac equation (1.51) V is the vector potential and reads

$$V(\mathbf{r}) = g_\omega \omega^0(\mathbf{r}) + g_\rho \tau_3 \rho_3^0(\mathbf{r}) + eA^0(\mathbf{r}), \tag{1.60}$$

and S the scalar potential

$$S(\mathbf{r}) = g_\sigma \sigma(\mathbf{r}) \tag{1.61}$$

which contributes to the effective Dirac mass

$$M^* = M + S(\mathbf{r}). \tag{1.62}$$

Using Eq.(1.30) and the Klein-Gordon equations given by (1.52)-(1.55), the total energy of the system can be written as

$$E = \sum_{i=1}^A \varepsilon_i - \frac{1}{2}\int d^3r \, (g_\sigma \rho_s \sigma + \frac{1}{3} g_2 \sigma^3 + \frac{1}{2} g_3 \sigma^4 + g_\omega \rho_v \omega^0 + g_\rho \rho_3 \rho_3^0 + e\rho_c A^0). \tag{1.63}$$

1.3 Parameters of the RMF Theory

The parameters of the model are

- the meson masses m_σ, m_ω, and m_ρ
- the coupling constants g_σ, g_2, g_3, g_ω and g_ρ.

In Mean Field approximation there is no mass-renormalization for the nucleon, which is then fixed to an average of the experimental values of the neutron and proton masses

$$M = 938.0 \text{ MeV} \qquad \text{or} \qquad M = 939.0 \text{ MeV}.$$

The mass of the ρ-meson is fixed to the empirical value

$$m_\rho = 763.0 \text{ MeV},$$

and the photon coupling e^2 to the known value

$$\frac{e^2}{4\pi} = \frac{1}{137.03602}$$

requiring that the Coulomb field of the nucleus has the right asymptotic behavior. The seven free parameters are usually obtained by a least-squared fit to bulk properties of nuclear matter and spherical nuclei. The fitting procedure is done in such a way to

Parameter	NL1	NL-SH	NL3
M [MeV]	938.0	939.0	939.0
m_σ [MeV]	492.25	526.059	508.194
m_ω [MeV]	795.359	783.0	782.501
g_σ	10.138	10.444	10.217
g_ω	13.285	12.945	12.868
g_ρ	4.976	4.383	4.474
g_2 [fm^{-1}]	-12.172	-6.9099	-10.431
g_3	-36.265	-15.8337	-28.885

Table 1.1: Parameters of the effective interactions NL1, NL-SH and NL3 in the RMF theory.

minimize the sum of the squared deviations from the data whose selection is restricted to some observables, that is to quantities which can be measured and computed reliably by the model.

Several parametrizations of the RMF theory exist, and amongst them NL1 [RRM86], NL-SH [SNR93], and NL3 [LKR97] are particularly used in nuclear structure calculations. In these parametrizations the main fitted properties are the charge radii, the binding energies and the available neutron radii of spherical nuclei. In NL-SH six nuclei (^{16}O, ^{40}Ca, ^{90}Zr, ^{116}Sn, ^{124}Sn and ^{208}Pb) are used, while for NL1 also ^{48}Ca and ^{58}Ni are considered. The experimental informations used in this last case are the total binding energy, the diffraction radii and the surface thickness. For NL3, in order to take into account a larger variation in isospin, also the nuclei ^{132}Sn and ^{214}Pb are included in the fit and for open shell nuclei pairing was considered using the BCS formalism (see Chapter 2).

Chapter 2

Relativistic Theory of Pairing

Pairing plays an essential role in the understanding of nuclei with open shells. Therefore, a relativistic theory of the nuclear many-body problem without pairing as presented in the previous Chapter, can only be applied to a few doubly magic nuclei as ^{16}O, ^{40}Ca, ^{48}Ca, ^{208}Pb. Early extensions of the RMF theory to open shell nuclei [GRT90] could only achieve a satisfactory agreement with the experimental data treating pairing with the constant gap approximation, a procedure first introduced in Ref. [Va73] for non-relativistic density-dependent Hartree-Fock calculations. It corresponds to the variation of an energy functional containing a pairing energy of the form

$$E_{pair} = -G \sum_{k>0} (v_k u_k)^2 \tag{2.1}$$

where the constant G is fixed and is connected to the pairing gap by the self-consistency condition

$$\Delta = G \sum_{k>0} u_k v_k. \tag{2.2}$$

At each step of the iterative solution one uses the single-particle energies of the Hartree-Fock potential and the experimental gap Δ_n and Δ_p to calculate the BCS-occupation probabilities. The experimental value of the gap parameter is taken from the odd-even mass difference

$$\Delta = \frac{1}{2}[E(N+2) - E(N+1) - (E(N+1) - E(N))], \tag{2.3}$$

and the occupation probabilities v_k^2 are calculated according to the BCS formula (see for example Ref. [RS80])

$$v_k^2 = \frac{1}{2}[1 - \frac{\varepsilon_k - \lambda}{\sqrt{(\varepsilon_k - \lambda)^2 + \Delta^2}}] \tag{2.4}$$

where λ is the chemical potential. All the sums over the occupied orbitals are replaced by a sum over all orbitals multiplied with the corresponding occupation probabilities:

$$\sum_{i=1}^{A} \cdots \Longrightarrow \sum_{k} v_k^2 \cdots \tag{2.5}$$

For fixed values of the gap parameters for neutrons and protons the self-consistent solution is obtained by iteration.

Unfortunately, this method has a major problem: if the sum over k is not restricted, the sums in Eq.s (2.1) and (2.2) diverge. Therefore, in these sums one has to introduce a cut-off energy which cannot be taken from experiments and it defines the so-called pairing window. For fixed values of the gap parameter Δ this problem occurs only in the evaluation of E_{pair} given in Eq. (2.1), which is usually very small as compared to the total energy and can often be neglected. The importance of pairing is largest in the occupation numbers for the evaluation of the densities, and these quantities are completely determined by the value of the gap.

From assumption (2.3) it follows that the predictive power of this method is limited to the ground state of the nuclei for which experimental values of the gap parameters are available. Moreover, apart from the dependence on a cutoff which cannot be controlled by experimental data, this approximation cannot be applied in the study of rotating nuclei and of those close to the driplines. In fact, in the first case time-reversal is broken and the corresponding alignment effect lead to a large off-diagonal contributions of Δ, while in the second case it leads to unbound states, because one populates states in the continuum.

Finally, it can be summarized that, although being successful, the constant gap approximation is a recipe and therefore a better understanding and a self-consistent treatment of pairing in a relativistic field theory of the nuclear many-body systems is needed. In the next section a derivation of the relativistic Hartree-Fock-Bogoliubov theory [KR91] is presented: in particular it is shown that from the microscopical point of view, pairing correlations may originate from relativistic OBE interactions.

2.1 Relativistic Hartree-Fock-Bogoliubov Theory

As seen in Section (1.2), RMF theory treats mesons as classical fields. As a consequence, the relativistic Hamiltonian which describes the nuclear system, is a single-particle operator and contains only terms of the structure $\psi^\dagger\psi$. Therefore, in this classical framework, it is impossible to describe a superfluid behavior of the nuclear many-body system for which a two-body interaction of the form $\psi^\dagger\psi^\dagger\psi\psi$ or a generalized single-particle potential of the form $\psi^\dagger\psi^\dagger + \psi\psi$ are needed. In order to derive these terms the meson fields have to be quantized too (see Eq.s (1.34)-(1.35)). In the following considerations we neglect in a first step the non-linear coupling of the σ-field.

For the nuclear system defined by $\mathcal{L}$ in Eq.s (1.2)-(1.7) with $U(\sigma) = 0$, the Hamiltonian H consists of three parts

$$H = H_N + H_M + H_{int}$$

which read explicitly:

- for nucleons

$$H_N = \int d^3x\, \psi^\dagger(\boldsymbol{\alpha}\mathbf{p} + \beta M)\psi, \tag{2.6}$$

- for free mesons

$$H_M = H_\sigma + H_\pi + H_\omega + H_\rho$$

with the σ-term is given by

$$H_\sigma = \frac{1}{2}\int d^3x\,(\Pi_\sigma^2 + [\nabla\sigma]^2 + m_\sigma^2\sigma^2), \tag{2.7}$$

the π-term

$$H_\pi = \frac{1}{2}\int d^3x\,([\vec{\Pi}]_\pi^2 + [\nabla\vec{\pi}]^2 + m_\pi^2\vec{\pi}^2), \tag{2.8}$$

the ω-term

$$H_\omega = -\frac{1}{2}\int d^3x\,(\Pi_\omega^\mu\Pi_{\omega\mu} + \nabla\omega^\mu\nabla\omega_\mu + m_\omega^2\omega^\mu\omega_\mu), \tag{2.9}$$

and the ρ-term

$$H_\rho = -\frac{1}{2}\int d^3x\,(\vec{\Pi}_\rho^\mu\vec{\Pi}_{\rho\,\mu} + \nabla\vec{\rho}^\mu\nabla\vec{\rho}_\mu + m_\rho^2\vec{\rho}^\mu\vec{\rho}_\mu); \tag{2.10}$$

- for the nucleon-meson interaction

$$H_{int} = \int d^3x\,\bar{\psi}_\alpha(x)\Gamma^\mu_{\alpha\beta}\psi_\beta(x)\phi_\mu(x), \tag{2.11}$$

which contains the nucleon-nucleon-meson vertices $\Gamma^\mu_{\alpha\beta}$

$$\Gamma_{\alpha\beta} = g_\sigma\delta_{\alpha\beta} \qquad \sigma \tag{2.12}$$

$$\Gamma^\mu_{\alpha\beta} = g_\omega\gamma^\mu_{\alpha\beta} \qquad \omega \tag{2.13}$$

$$\vec{\Gamma}_{\alpha\beta} = g_\pi\gamma^5_{\alpha\beta}\vec{\tau} \qquad \pi\ (\mathrm{p}s) \tag{2.14}$$

$$\vec{\Gamma}^{pv}_{\alpha\beta} = \frac{f_\pi}{m_\pi}(\gamma^5\not{\partial}\,)_{\alpha\beta}\,\vec{\tau} \qquad \pi\ (\mathrm{p}v) \tag{2.15}$$

$$\vec{\Gamma}^\mu_{\alpha\beta} = g_\rho\gamma^\mu_{\alpha\beta}\vec{\tau} \qquad \rho \tag{2.16}$$

To simplify the notation of the equations which will follow, in analogy to Ref. [BW63], a Latin index combining the Dirac- or meson-indices and the space-time coordinates

$$a = (\alpha, \boldsymbol{x}, t) \qquad\qquad m = (\mu, \boldsymbol{x}, t), \tag{2.17}$$

is introduced, and the convention to sum or integrate over the indices occurring twice in a formula is used. The interaction (2.11) is then written as

$$H_{int} = \bar{\psi}_a\Gamma^m_{ab}\psi_b\phi_m, \tag{2.18}$$

where the local vertices now read

$$\Gamma^m_{ab} = \Gamma^\mu_{\alpha\beta}(x_a, x_b, x_m) = \Gamma^\mu_{\alpha\beta}\delta(x_a - x_b)\delta(x_a - x_m). \tag{2.19}$$

In this notation the Green's functions are defined by

$$G_{ab} = -i\langle A|T\psi_a\bar{\psi}_b|A\rangle, \tag{2.20}$$

where $|A\rangle$ is the exact ground state of a $A-$nucleon system, ψ the time-dependent field operator in the Heisenberg representation

$$\psi_a(\boldsymbol{x}, t) = \mathrm{e}^{iHt}\psi_a(\boldsymbol{x}, 0)\mathrm{e}^{-iHt}, \tag{2.21}$$

and T is the time-ordering operator. The equations of motion of the field operators

$$\partial_t \psi(x) = i[H, \psi(x)] \tag{2.22}$$

lead to the following equation of motion for the two-point Green's function G_{ab}

$$(\not{p} - M)_{ac} G_{cb} = \delta_{ab} - i\Gamma^m_{ac} \langle A|T\psi_c \phi_m \bar{\psi}_b|A\rangle, \tag{2.23}$$

where

$$\not{p} = \gamma_0(i\partial_t - \boldsymbol{\alpha}\mathbf{p}). \tag{2.24}$$

Eq. (2.23) is exact, but not closed. As the goal is to describe pairing correlations in nuclei, relativistic anomalous Green's functions F_{ab} and $\tilde{F}_{ab}$ can be introduced:

$$F_{ab} = -i\langle A+2|T\,\bar{\psi}_a \bar{\psi}_b|A\rangle \qquad \text{and} \tag{2.25}$$

$$\tilde{F}_{ab} = -i\langle A|T\,\psi_a \psi_b|A+2\rangle \tag{2.26}$$

and their equation of motion can be obtained by using Eq. (2.22). For F_{ab} it reads

$$(\not{\bar{p}} - M)_{ca} F_{cb} = -i\,\Gamma^m_{ca} \langle A+2|T\,\bar{\psi}_c \phi_m \bar{\psi}_b|A\rangle, \tag{2.27}$$

in which $\not{\bar{p}}$ is defined as

$$\not{\bar{p}} = \gamma_0(-i\partial_t - \boldsymbol{\alpha}\mathbf{p}). \tag{2.28}$$

In Eq.s (2.25)-(2.27) $|A+2\rangle$ is the exact ground state of a $(A+2)$-nucleon system. In order to eliminate the meson field operators ϕ_m from Eq.s (2.23) and (2.27), the following procedure, valid for an arbitrary vertex function, can be applied. First, the equation of motion of ϕ_m (in this case they are Klein-Gordon equations) are derived, and they read

$$(\partial^\nu \partial_\nu + m^2_\mu)\phi^m = \mp \bar{\psi}_a \Gamma^m_{ab} \psi_b. \tag{2.29}$$

in which the $\pm$ signs hold for scalar and vector meson fields respectively. Then, the equations of motion are solved for the meson field operator by inversion. This gives

$$\phi_m = \mp D_{mm'}\, \bar{\psi}_a \Gamma^{m'}_{ab} \psi_b, \tag{2.30}$$

where $D_{mm'}$ represents the meson-propagator [IZ80]:

$$D_{mm'} = -\int \frac{d^4}{(2\pi)^4} \frac{\mathrm{e}^{-ik(x-x')}}{k^2 - m^2_m + i\epsilon} \delta_{\mu\mu'}. \tag{2.31}$$

For vector mesons the Kronecker symbol $\delta_{\mu\mu'}$ has to be replaced by the metric tensor $g_{\mu\mu'} - \frac{k_\mu k_{\mu'}}{m}$.

Substituting Eq. (2.30), the meson field operators may be eliminated and Eq.s (2.23) and (2.27) become

$$(\not{p} - M)_{ac} G_{cb} = \delta_{ab} \mp i\Gamma^m_{ac} D_{mm'} \Gamma^{m'}_{de} \langle A|T\,\psi_e \bar{\psi}_d \psi_c \bar{\psi}_b|A\rangle, \tag{2.32}$$

$$(\not{\bar{p}} - M)_{ac} F_{cb} = \mp i\Gamma^m_{ca} D_{mm'} \Gamma^{m'}_{de} \langle A+2|T\,\psi_e \bar{\psi}_d \bar{\psi}_c \bar{\psi}_b|A\rangle. \tag{2.33}$$

The rh.s. of these equations, which, as before, are still exact but not closed, depends on the four-point Green's functions. The Gorkov factorization [Go58], which approximates the four-point by products of two-point Green's functions

$$\langle A|T\,\psi_e\bar{\psi}_d\psi_c\bar{\psi}_b|A\rangle \approx -G_{ed}G_{cb} + G_{cd}G_{eb} + \tilde{F}_{ec}F_{db}, \tag{2.34}$$

$$\langle A+2|T\,\psi_e\bar{\psi}_d\bar{\psi}_c\bar{\psi}_b|A\rangle \approx -G_{ed}F_{cb} + G_{ec}F_{db} - G_{eb}F_{dc}. \tag{2.35}$$

allows one to close the system of Eq.s (2.32)-(2.33). In the second equation G_{ab} is actually the normal Green's functions of the $A+2$ system. Neglecting this difference in particle number and replacing it by the normal Green's functions of the $A-$particle system leads to the well known violation of particle number symmetry in BCS-theory.
The first and the second terms of rhs of Eq.s (2.34)- (2.35) are the well known Hartree-term and the Fock-term. In addition the third term, commonly called Gorkov-term, describes correlations between particles. Neglecting the last two terms in Eq.s (2.34)-(2.35), the classical mean field theory, i.e. the relativistic Hartree approximation is recovered. Together with the second term, this theory represents the relativistic Hartree-Fock theory [Br78, BMG87]. Taking into account all three terms leads to the following system of equations:

$$\begin{aligned}(\not{p} - M)_{ac}G_{cb} = \delta_{ab} &\pm i\Gamma^m_{ac}D_{mm'}\Gamma^{m'}_{de}G_{ed}G_{cb} \\ &\mp i\Gamma^m_{ae}D_{mm'}\Gamma^{m'}_{dc}G_{ed}G_{cb} \\ &\mp i\Gamma^m_{ad}D_{mm'}\Gamma^{m'}_{ce}\tilde{F}_{ed}F_{cb}\end{aligned} \tag{2.36}$$

and

$$\begin{aligned}(\not{\hat{p}} - M)_{ca}F_{cb} = &\pm i\Gamma^m_{ca}D_{mm'}\Gamma^{m'}_{de}G_{ed}F_{cb} \\ &\mp i\Gamma^m_{da}D_{mm'}\Gamma^{m'}_{ce}G_{ed}F_{cb} \\ &\pm i\Gamma^m_{ea}D_{mm'}\Gamma^{m'}_{dc}F_{de}G_{cb}.\end{aligned} \tag{2.37}$$

This system of equations is obviously not closed yet, because it still contains the unknown function $\tilde{F}_{ab}$.

Because of the invariance of the Lagrangian under translation in time and the time-dependence of the normal and anomalous Green's functions, one can show that

- G_{ab} depends only on the difference in time $t_a - t_b$

$$\begin{aligned}\hat{G}_{ab}(t_a - t_b) &\equiv \hat{G}_{\alpha\beta}(\boldsymbol{x}_a, \boldsymbol{x}_b; t_a - t_b) \\ &= G_{\alpha\beta'}(\boldsymbol{x}_a, t_a, \boldsymbol{x}_b, t_b)\gamma^0_{\beta'\beta};\end{aligned} \tag{2.38}$$

- the other two functions F_{ab} and $\tilde{F}_{ab}$ can be decomposed in functions $\hat{F}_{ab}$ and $\hat{\tilde{F}}_{ab}$, depending only on this difference and an exponential part, depending on t_a,

$$\begin{aligned}\hat{F}_{ab}(t_a - t_b) &\equiv \hat{F}_{\alpha\beta}(\boldsymbol{x}_a, \boldsymbol{x}_b; t_a - t_b) \\ &= \mathrm{e}^{-i2\lambda t_a}F_{\alpha'\beta'}(\boldsymbol{x}_a, t_a, \boldsymbol{x}_b, t_b)\gamma^0_{\alpha'\alpha}\gamma^0_{\beta'\beta}, \\ \hat{\tilde{F}}_{ab}(t_a - t_b) &\equiv \hat{\tilde{F}}_{\alpha\beta} \\ &= \mathrm{e}^{+i2\lambda t_a}\tilde{F}_{\alpha\beta}(\boldsymbol{x}_a, t_a, \boldsymbol{x}_b, t_b)\end{aligned} \tag{2.39}$$

where $2\lambda = E_{A+2} - E_A$ is the difference of the ground state energy of the $A+2$ and the A particle system and therefore twice the chemical potential ($\lambda = \frac{\partial E}{\partial N}$).

In Eq.s (2.38), (2.39), the time dependence is treated explicitly, and the Latin indices now contain, apart from the Dirac indices α, only the spatial coordinates $\boldsymbol{x}_a$.

Using the instantaneous approximation, i.e. neglecting the retardation effects in the interactions which determine the mass operator Σ and the pairing potential Δ, these quantities become time-independent, and a time-independent two-body potential can be defined as follows

$$\begin{aligned} V_{abcd} = & \mp \delta(\boldsymbol{x}_a - \boldsymbol{x}_c)\delta(\boldsymbol{x}_b - \boldsymbol{x}_d) \\ & \times \sum_\mu (\gamma^0\Gamma^\mu)_{\alpha\gamma}(\gamma^0\Gamma_\mu)_{\beta\delta} \int \frac{d^3k}{(2\pi)^3} \frac{\mathrm{e}^{i\boldsymbol{k}(\boldsymbol{x}_a - \boldsymbol{x}_b)}}{\boldsymbol{x}^2 + m_\mu^2}, \end{aligned} \tag{2.40}$$

with the usual convention for the signs.
Introducing the normal density matrix

$$\rho_{ab} \equiv \rho_{\alpha\beta}(\boldsymbol{x}_a, \boldsymbol{x}_b) = \langle A|\psi^\dagger_\beta(\boldsymbol{x}_b)\psi_\alpha(\boldsymbol{x}_a)|A\rangle \tag{2.41}$$

and the anomalous density matrix (pairing tensor)

$$\kappa_{ab} \equiv \kappa_{\alpha\beta}(\boldsymbol{x}_a, \boldsymbol{x}_b) = \langle A|\psi_\beta(\boldsymbol{x}_b)\psi_\alpha(\boldsymbol{x}_a)|A\rangle, \tag{2.42}$$

respectively, hermitian and skew symmetric tensors

$$\rho^\dagger = \rho, \qquad\qquad \kappa^T = -\kappa \tag{2.43}$$

the mass operator in Hartree-Fock approximation and the pairing field read explicitly

$$\begin{aligned} \Sigma_{ac} &= \delta_{ac}M + \Gamma_{ac} \\ \Gamma_{ac} &= V_{adce}\rho_{ed} - V_{adec}\rho_{ed} && (2.44) \\ \Delta_{ac} &= V_{acde}\kappa_{de}. && (2.45) \end{aligned}$$

Eq.s (2.36) and (2.37) can thus be written in the following form:

$$\begin{pmatrix} (i\partial_t - \boldsymbol{\alpha}\mathbf{p} - \beta\Sigma)_{ac} & -\Delta_{ac} \\ \Delta^*_{ca} & (-i\partial_t + 2\lambda - \boldsymbol{\alpha}\mathbf{p} - \beta\Sigma)_{ca} \end{pmatrix} \begin{pmatrix} \hat{G}_{cb}(t) \\ \hat{F}_{cb} \end{pmatrix} = \begin{pmatrix} \delta_{ab} \\ 0 \end{pmatrix}. \tag{2.46}$$

The time-dependence is taken into account explicitly by a Fourier transformation:

$$\begin{aligned} G_{ab}(\omega) &\equiv G_{\alpha\beta}(\boldsymbol{x}_a, \boldsymbol{x}_b; \omega) = \int \hat{G}_{\alpha\beta}(\boldsymbol{x}_a, \boldsymbol{x}_b; t)\mathrm{e}^{i(\omega+\lambda)t}dt, \\ F_{ab}(\omega) &\equiv F_{\alpha\beta}(\boldsymbol{x}_a, \boldsymbol{x}_b; \omega) = \int \hat{F}_{\alpha\beta}(\boldsymbol{x}_a, \boldsymbol{x}_b; t)\mathrm{e}^{i(\omega+\lambda)t}dt. \end{aligned} \tag{2.47}$$

this transforms Eq. (2.46) into the following matrix-equation

$$(\omega - \mathcal{H}) \begin{pmatrix} G(\omega) \\ F(\omega) \end{pmatrix} = \begin{pmatrix} 1 \\ 0 \end{pmatrix}, \tag{2.48}$$

where the matrix $\mathcal{H}$

$$\mathcal{H} = \begin{pmatrix} h-\lambda & \Delta \\ -\Delta^* & -h^*+\lambda \end{pmatrix} \tag{2.49}$$

is the relativistic form of the Hartree-Fock-Bogoliubov-Matrix. We call it Hartree-Fock-Bogoliubov Matrix because the Hamiltonian h is the Dirac Hamiltonian h

$$h = \boldsymbol{\alpha}\mathbf{p} + \beta\Sigma. \tag{2.50}$$

The indices of this matrix are combinations of Dirac index and coordinates. In particular matrix multiplication means then a summation over the Dirac index and an integration over the coordinates.
Like in nonrelativistic physics we obtain the eigenfunction by a spectral decomposition

$$G_{ab}(\omega) = \sum_\nu \frac{U_{a\nu}U^*_{b\nu}}{\omega-\varepsilon_\nu+i\eta} + \frac{V_{a\nu}V^*_{b\nu}}{\omega-\varepsilon_\nu-i\eta} \tag{2.51}$$

$$F_{ab}(\omega) = \sum_\nu \frac{V_{a\nu}U^*_{b\nu}}{\omega-\varepsilon_\nu-i\eta} + \frac{U_{a\nu}V^*_{b\nu}}{\omega-\varepsilon_\nu-i\eta} \tag{2.52}$$

where the poles of these functions are the quasi particle energies ε_ν, and the residues are given by the amplitudes

$$U_{\nu a} = \langle A|\psi_a|A+1,\nu\rangle \qquad \text{and} \qquad V_{\nu a} = \langle A|\psi^\dagger_a|A-1,\nu\rangle, \tag{2.53}$$

containing the wave functions plus BCS-occupation numbers. Finally we obtain the relativistic form of the Hartree-Fock-Bogoliubov -Equations, which we have called the Dirac-Hartree-Fock-Bogoliubov equations:

$$\begin{pmatrix} h-\lambda & \Delta \\ -\Delta^* & -h^*+\lambda \end{pmatrix} \begin{pmatrix} U_\nu \\ V_\nu \end{pmatrix} = E_\nu \begin{pmatrix} U_\nu \\ V_\nu \end{pmatrix} \tag{2.54}$$

where E_ν are the quasi-particle energies. These equations can be applied for a fully self-consistent description of open-shell nuclei, where the possibly deformed mean fields and the pairing field are determined simultaneously.

Let us consider the pairing field Δ. Its components (see Eq.(2.45) are given by the product of the two-body matrix elements of the interaction V_{adce} and the pairing density κ. One of the biggest open question is which interaction has to be used in the *pp*-channel.

Following the Fermi's Liquid theory proposed first by Landau in Ref. [La59] and then by Migdal in Ref.s [Mi67, Mi68] the effective force in the pairing channel should be the particle-particle $K-$matrix, which is the sum over all particle-particle irreducible diagrams.

In this theory the pairing field Δ is defined as the sum of all diagrams converting a particle into a hole and a correlated pair (or two particles into a correlated pair), which cannot be divided into parts connected by one line of any direction. These graphs have the following structure. (see the Figures in the next page). First, there is an interaction (since Δ does not include free states by definition). This is followed by the complete set of graphs modifying the direction of the particles, which represent the anomalous Green's functions F. Since, by definition, F includes the ends, all the interaction diagrams that

may be split into parts connected by two lines of any direction enter in the equation for F. It follows that only the graphs which do not contain parts connected by two lines of any direction enter in the gap equation, i.e.

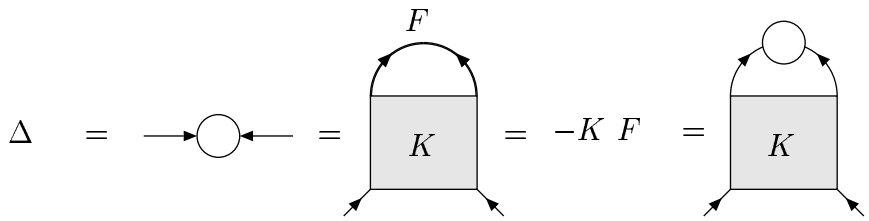

The block K does not contain parts connected by two vertical lines of any direction as such graphs are contained in F and for this reason K is represented in form of a narrow rectangle. The first terms in perturbation series for K are

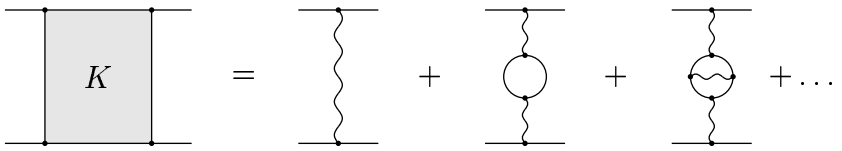

Chapter 3

Relativistic Theory of Pairing for Infinite Nuclear Matter

As first application of the relativistic Hartree-Fock-Bogoliubov (HFB) theory presented in Chapter 2, we calculate the pairing gap ${}^1S_0$ at zero temperature in infinite nuclear matter. Since pairing correlations are concentrated mostly at the Fermi surface, we have performed the calculation of the gap and other pairing properties by using a relativistic BCS approximation to the fully relativistic HFB equations given in Eq. (2.54). A similar investigation was already performed by Kuchareck and Ring in Ref. [KR91] and by using the relativistic BCS approximation with the same force in the *ph*- and in the *pp*-channel, they found a pairing gap of a factor three too large with respect to standard calculations in infinite nuclear matter, see for example Ref.s [KRS89a, BCL90, CCD93]. That result has been justified by the fact that although from the microscopical point of view pairing correlations may originate from relativistic OBE interactions, the force in these two channels is not the same: in particular, the effective force in the *ph*-channel has large contributions in the region of high momenta, i.e. it does not contain a cutoff. Therefore, in our investigation, we have used a relativistic bare potential adjusted by the Bonn group [Ma89] which is adjusted to scattering data and has an appropriate cutoff. Therefore it corresponds to the first diagram of the K-matrix, i.e. the interaction which should be used in the *pp*-channel.

We are particularly interested in the study of the pairing gap in symmetric nuclear matter for the link that may be established with pairing in finite nuclei through a local-density approximation [KRS89b]. In particular, from experimental evidences it is well known that in the latter case the largest contribution to pairing comes from the ${}^1S_0$ channel. For example, scattering data show that this is the most attractive channel of the NN interaction, and therefore it should favorite the formation of a nucleonic pair. In addition, nuclei with even N and even Z are more stable than others. Pairs of neutrons and also pairs of protons couple to total spin 0, with a little extra binding. That feature, which accounts for the fact that all known even-even nuclei have ground state angular momentum of 0, motivates the study of the pairing gap ${}^1S_0$ in nuclear matter.

We have compared our results for the pairing properties of nuclear matter obtained with the bare relativistic Bonn potential with non-relativistic calculations based on the Gogny force [DG80], a very successful phenomenological effective interaction whose parameters have been determined by fitting properties of finite nuclei obtained with HFB

calculations to the experimental data. Since it is supposed to describe pairing properties of finite nuclei properly, with the help of the local-density approximation one can pass to infinite nuclear matter and this interaction with the aim to set a benchmark against which pairing properties of other forces could be compared.

In the following Sections we introduce the Dirac-Hartree-Bogoliubov equations for infinite nuclear matter and we solve the gap equation by using the bare Bonn potential as pairing interaction. Further pairing properties as for example pairing densities in momentum and in coordinate space, and coherence length are studied. The results are always compared with non-relativistic calculations based on the Gogny force, parameter set D1 [DG80]. Finally, phenomenological relativistic interactions in the pairing channel are discussed in order to extend the relativistic theory of pairing to finite nuclei.

3.1 Relativistic BCS Equations for Nuclear Matter

To derive the BCS equations in infinite nuclear matter we neglect for simplicity the Fock term and the vacuum polarization as it is usually done in RMF theory. Because of the translational invariance of the system, the mass operator Σ in Eq. (2.44) has the simple form

$$\Sigma = S + \beta V, \tag{3.1}$$

with the fields

$$S = -\frac{g_\sigma^2}{m_\sigma^2}\rho_s, \tag{3.2}$$

$$V = \frac{g_\omega^2}{m_\omega^2}\rho_v \tag{3.3}$$

determined by the scalar density

$$\rho_s = \langle A|\bar{\psi}\psi|A\rangle \tag{3.4}$$

and by the vector density

$$\rho_v = \langle A|\psi^\dagger\psi|A\rangle. \tag{3.5}$$

The RHBF equations (2.54) become

$$\begin{pmatrix} \boldsymbol{\alpha}\mathbf{p} + \Sigma - M - \lambda & \Delta \\ -\Delta^* & -\boldsymbol{\alpha}\mathbf{p} - \Sigma + M + \lambda \end{pmatrix} \begin{pmatrix} U_\nu \\ V_\nu \end{pmatrix} = E_\nu \begin{pmatrix} U_\nu \\ V_\nu \end{pmatrix} \tag{3.6}$$

and they should be solved self-consistently. In analogy with h, the relativistic pairing field Δ, whose components are given in Eq. (2.45), is a 2×2-matrix. Δ contains the same terms of the relativistic OBE interaction V_{abcd}. For example, in the simple case of an interaction based only on the exchange of the two mesons σ and ω, Δ contains a scalar term, and a vector term with time-like and space-like components, i.e.

$$\Delta^{\sigma,\omega} = \begin{pmatrix} \Delta^s_{++} + \Delta^0_{++} + \boldsymbol{\Delta}_{++} & \Delta^s_{+-} + \Delta^0_{+-} + \boldsymbol{\Delta}_{+-} \\ \Delta^s_{-+} + \Delta^0_{-+} + \boldsymbol{\Delta}_{-+} & \Delta^s_{--} + \Delta^0_{--} + \boldsymbol{\Delta}_{--} \end{pmatrix} \tag{3.7}$$

where the signs + and − refer to the large and small components of the U_k and V_k. Although for a fully RHB calculation (see also Guimãeres et al. in Ref. [GCF96]), all the components of Δ should be taken into account, since in infinite nuclear matter pairing correlations play only a minor role in the neighborhood of the Fermi surface, a BCS approximation, in which pairing is considered only on top of a simple Hartree solution, is still a good framework for this calculation. Consistently with this scheme we first diagonalize the hamiltonian h, i.e. we solve the usual Dirac equation for infinite nuclear matter. Writing the RHB equations given in (3.6) in this basis the h part is diagonal, and the pairing field Δ is transformed into another field $\tilde{\Delta}$ which is not diagonal. Up to now the equations are still equivalent to the full HFB equations. Neglecting the off-diagonal elements of the new matrix $\tilde{\Delta}$, the problem decomposes in a large number of small 2×2 matrices where h and Δ are both diagonal. The diagonalization of these new matrices leads to the BCS solution on top of Hartree. It must be remarked that in this approximation only the effects of the off-diagonal matrix elements of Δ are neglected. Fully relativistic HB calculations in finite nuclei (see Chapter 4) will show that they are negligible. No antiparticle solutions are considered in the calculations.

We start from the eigenvalues and eigenfunctions of the Dirac equation of a nucleon propagating in a uniform nuclear medium

$$(\boldsymbol{\gamma} \cdot \mathbf{p} + M^*)u(\mathbf{p}, s) = \gamma_0 E^* u(\mathbf{p}, s). \tag{3.8}$$

They are characterized by the momentum $\boldsymbol{k}$ and the spin index s, the eigenvalues are

$$\epsilon(k) = V \pm E^*(k), \tag{3.9}$$

with $E^*(k) = \sqrt{k^2 + M^{*2}}$, where $M^* = M + S$ is the effective mass, and the eigenfunctions are the well known Dirac spinors for positive and negative energies [see Appendix B]. Moreover, as usual in RMF, the densities ρ in Eq. (2.41) and κ in eq. (2.42) are calculated in the no-sea approximation and, as usually done in BCS, time reversed orbits with the quantum numbers $(\boldsymbol{k}, s)$ and $(-\boldsymbol{k}, -s)$ are assumed to be pairwise occupied with occupation amplitudes $v(k)$ $(u^2 + v^2 = 1)$. Then, in the basis characterized by the quantum numbers $(\boldsymbol{k}, s)$ the matrices for scalar and vector densities are diagonal

$$\rho_s(\boldsymbol{k}s, \boldsymbol{k}'s') = \delta(\boldsymbol{k} - \boldsymbol{k}')\delta_{ss'}v^2(k)\frac{M^*}{E^*(k)}, \tag{3.10}$$

$$\rho_v(\boldsymbol{k}s, \boldsymbol{k}'s') = \delta(\boldsymbol{k} - \boldsymbol{k}')\delta_{ss'}v^2(k), \tag{3.11}$$

and the pairing tensor skew diagonal

$$\kappa(\boldsymbol{k}s, \boldsymbol{k}'s') = (-)^{1/2-s}\delta(\boldsymbol{k} + \boldsymbol{k}')\delta_{s-s'}u(k)v(k). \tag{3.12}$$

The density matrices allow the calculation of the densities

$$\rho_s = \frac{4}{2\pi^2}\int_0^\infty \frac{M^*}{E^*(k)}v^2(k)k^2dk, \tag{3.13}$$

$$\rho_v = \frac{4}{2\pi^2}\int_0^\infty v^2(k)k^2dk, \tag{3.14}$$

and consequently of the potentials V and S given in Eq.s (3.2) and (3.3). The factor 4 originates from the spin-isospin degeneracy.

Analogously, the pairing tensor κ leads to the skew diagonal pairing field

$$\Delta(\boldsymbol{k}s, \boldsymbol{k}'s') = (-)^{1/2-s}\delta(\boldsymbol{k}+\boldsymbol{k}')\delta_{s-s'}\Delta(k), \tag{3.15}$$

where the gap parameter $\Delta(k)$ obeys the gap equation

$$\Delta(k) = -\int_0^\infty \frac{d^3p}{(2\pi)^3} v_{pp}(\boldsymbol{k},\boldsymbol{p})u(p)v(p), \tag{3.16}$$

where $v_{pp}(\boldsymbol{k},\boldsymbol{p})$ is the interaction in the $pp-$channel. In the following we will use the relativistic bare Bonn potential.

Substituting these expressions into the DHFB equations (2.54), one notices that it decomposes into $(2\times 2)-$matrices of BCS-type as in the case of non-relativistic HFB equations in infinite nuclear matter

$$\begin{pmatrix} \epsilon(k)-\lambda & \Delta(k) \\ \Delta(k) & -\epsilon(k)+\lambda \end{pmatrix} \begin{pmatrix} u(k) \\ v(k) \end{pmatrix} = E(k) \begin{pmatrix} u(k) \\ v(k) \end{pmatrix}. \tag{3.17}$$

This yields the well known occupation numbers

$$v^2(k) = \frac{1}{2}\left(1 - \frac{\epsilon(k)-\lambda}{\sqrt{(\epsilon(k)-\lambda)^2+\Delta^2(k)}}\right) \tag{3.18}$$

with the eigenvalues

$$\epsilon(k) = V + E^*(k), \tag{3.19}$$

and

$$E(k) = \sqrt{(V+\sqrt{k^2+M^{*2}}-\lambda)^2+\Delta^2(k)}. \tag{3.20}$$

The effective mass is obtained from the solution of the implicit equation

$$M^* = M - \frac{g_\sigma^2}{m_\sigma^2}\frac{4}{2\pi^2}\int_0^\infty \frac{M^*}{E^*(k)} v^2(k)k^2dk. \tag{3.21}$$

The gap parameter is determined by the non-linear gap equation given in Eq. (3.16)

$$\Delta(k) = -\frac{1}{4\pi^2}\int_0^\infty v_{pp}(k,p)\frac{\Delta(p)}{\sqrt{(\epsilon(p)-\lambda)^2+\Delta^2(p)}}p^2dp, \tag{3.22}$$

where $v_{pp}(k,p)$ is the average over the angle of the amplitude $v_{pp}(\mathbf{k},\mathbf{p})$

$$v_{pp}(k,p) = \int d\cos\theta v_{pp}(\boldsymbol{k},\boldsymbol{p}), \tag{3.23}$$

with θ angle between the vectors $\boldsymbol{k}$ and $\boldsymbol{p}$. In appendix B the amplitudes $v_{pp}(\mathbf{k},\mathbf{p})$ are given for a arbitrary nucleon-meson vertex and the resulting integral (3.23) for the Bonn potential and two phenomenological relativistic pairing interactions discussed at the end of this chapter. The equations (3.21) and (3.22) are solved iteratively.

3.2 Pairing with Bonn Potential

In this Section we present a BCS solution of the gap equation (3.22) obtained by using a relativistic version of the Bonn potential (for more details see Appendix B and Ref. [Ma89]) as $v_{pp}(k,p)$, which corresponds to the first diagram of the $K-$matrix. In the $ph-$channel we use the RMF Lagrangian density, and, as we are dealing with infinite nuclear matter, the $\sigma-$ and $\omega-$meson only are considered. The eigenvalues of the Dirac equation are given in Eq. (3.19) where the effective mass M^* and the vector field V are given by

$$M^* = M + g_\sigma \sigma \tag{3.24}$$
$$V = g_\omega \omega \tag{3.25}$$

and the fields σ and ω are determined by the meson equations of the non-linear Walecka model [Ri96]

$$\sigma = -\frac{4g_\sigma}{m_\sigma^2}\int \frac{d^3k}{(2\pi)^3}\frac{M^*}{\sqrt{k^2+M^{*2}}}v^2(k) + g_2\sigma^2 + g_3\sigma^3 \tag{3.26}$$
$$\omega = +\frac{4g_\omega}{m_\omega^2}\frac{d^3k}{(2\pi)^3}v^2(k). \tag{3.27}$$

In Eq.s (3.26)-(3.27) the BCS occupation numbers $v^2(k)$, the Fermi energy λ which is related to the Fermi momentum k_F by the relation

$$\lambda = V + \sqrt{k_F^2 + M^{*2}}. \tag{3.28}$$

are thus determined by the density of the system $\rho = m_\omega^2\omega/g_\omega$. The coupling constants g_σ, g_ω, g_2 and g_3, and the meson masses m_σ, m_ω are taken from the parameter set NL1 of the non-linear Walecka model [GRT90, RRM86]. We have also performed the calculations with the parameters sets NL2 and NL3 and we have found no differences in the results for the pairing gap at the Fermi surface. The numerical technique used for the solution of Eq.s (3.21)-(3.22) is described in detail in Ref.s [BCL90, Ru94, EEH96] and references therein.

3.2.1 Gap Parameter at the Fermi Surface

In Fig. 3.1 we show the resulting gap parameter at the Fermi surface k_F $\Delta_F = \Delta(k = k_F)$ as a function of the density represented by the Fermi momentum k_F for the relativistic Bonn-B potential Δ_F^B (solid line) and compare it with the same quantity obtained in a non-relativistic calculation [KRS89a] based on the Gogny force D1 [DG80] Δ_F^G (dashed line). Apart from the difference at larger densities, the solutions are in excellent agreement. In both cases we find maximal pairing correlations of roughly 2.8 MeV at the Fermi momentum $k_F \approx 0.8$ fm^{-1}, i.e. at roughly one fifth of nuclear matter density. In particular, for the Bonn B potential we have

$$\Delta_F^{B_B} \approx 2.84 \text{ MeV} \qquad \text{at} \qquad k_F \approx 0.76 \text{ fm}^{-1} \tag{3.29}$$

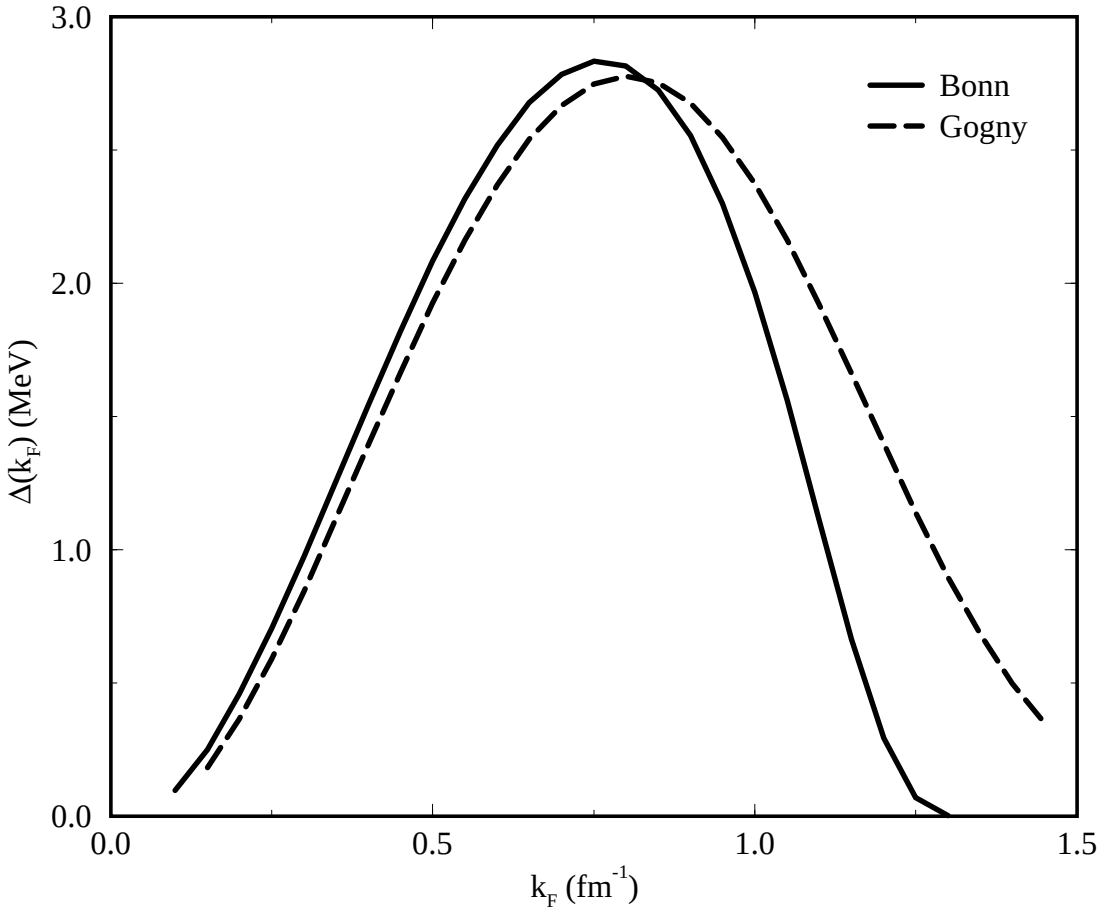

Figure 3.1: The gap parameter at the Fermi surface Δ_F as a function of the density represented by the Fermi momentum k_F for the relativistic Bonn potential (version B) and for the Gogny force D1.

and for the Gogny force

$$\Delta_F^G \approx 2.78 \text{ MeV} \qquad \text{at} \qquad k_F \approx 0.8 \text{ fm}^{-1} \tag{3.30}$$

Since pairing correlations are largest for small densities, i.e. in the surface of the nucleus, this result agrees with the usual observation that pairing in nuclei is a surface phenomenon. Moreover, the agreement between Δ_F^B and Δ_F^G is a particularly interesting result as in the latter case it has been shown [KRS89a] that using this density dependence of the gap parameter in a semiclassical calculations the average pairing properties of finite nuclei can be reproduced rather well. Therefore we hope that this remains true also for the Bonn potential. At the saturation density ($k_F^S = 1.35$ fm^{-1}), it is rather difficult to decide whether nuclear matter is superfluid. In any case it seems to depend crucially on the interaction. For Gogny forces a small pairing gap of roughly 0.5 MeV is left at saturation,

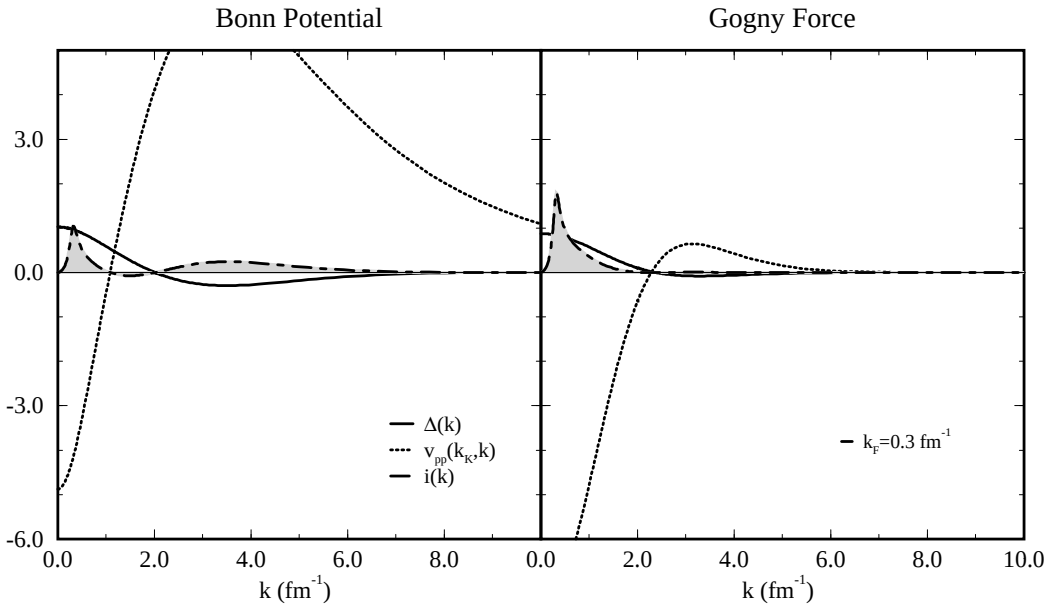

Figure 3.2: Various contributions to the integral in the gap equation (3.16) for the density corresponding to the Fermi momentum $k_F = 0.3$ fm^{-1}. Comparison of the relativistic Bonn-B potential and the Gogny force. The details are discussed in the text.

whereas for the Bonn-B potential there seems to be no pairing. In the next paragraph we will explain the origin of this discrepancy.

Till now we have presented relativistic calculations based on the version B of the Bonn potential [MHE87]. The version A and C of the potential produce nearly identical pairing; in particular at $k_F = 0.76$ fm^{-1} for the maximum of the gap parameter we find

$$\Delta_F^{B_A} \approx 2.80 \text{ MeV}, \qquad \Delta_F^{B_C} \approx 2.83 \text{ MeV}. \tag{3.31}$$

In Ref.s [BCL90, CCD93, EEH96] non-relativistic calculations of the pairing gap $^1S_0$ based on the bare Paris potential [LLR80], a non-relativistic version Bonn potential, and on the CBF method respectively leads to a very similar result for Δ_F.

To understand the difference between Δ_F^B and Δ_F^G at higher densities, we analyze the behavior of $\Delta(k)$ and $v_{pp}(k_F, k)$ for different values of k_F in both cases. We choose $k_F = 0.3,\ 0.8$ fm^{-1} for which the agreement between the relativistic and the non-relativistic solutions is good and $k_F = 1.2$ fm^{-1} for which Δ_F^B drops more rapidly than Δ_F^G. From Eq. (3.22) we see that the gap parameter at the Fermi surface is given by the integral of

$$i(k) = -\frac{k^2}{4\pi^2} v_{pp}(k_F, k) \frac{\Delta(k)}{\sqrt{(\epsilon(k) - \lambda)^2 + \Delta^2(k)}}. \tag{3.32}$$

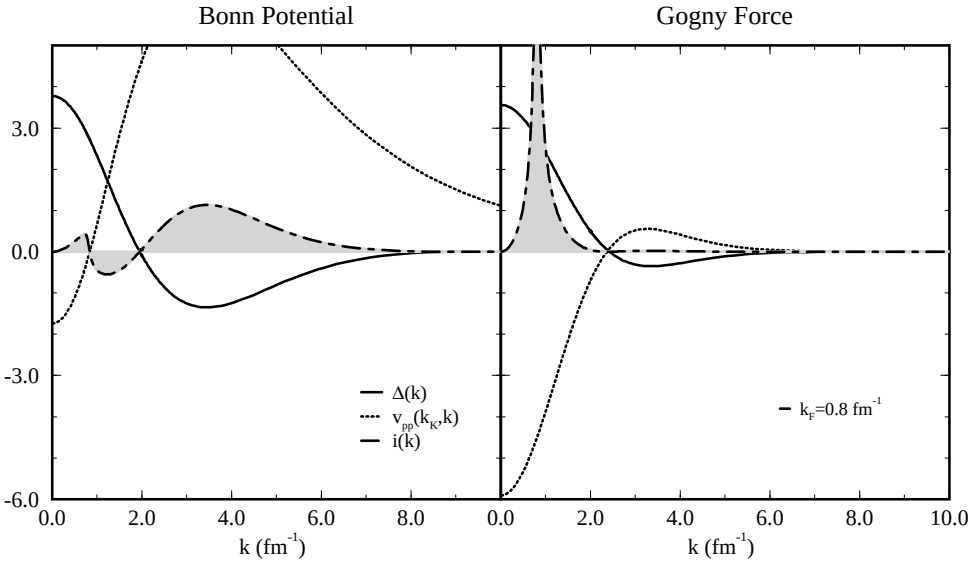

Figure 3.3: Various contributions to the integral in the gap equation (3.16) for the density corresponding to the Fermi momentum $k_F = 0.8$ fm^{-1}. Comparison of the relativistic Bonn-B potential and the Gogny force. The details are discussed in the text.

In the following considerations we focus our attention on $v_{pp}(k_F, k)$ and on $\Delta(k)$. In Fig. 3.2, 3.3 and 3.4 we show $v_{pp}(k_F, k)$, $\Delta(k)$ and $i(k)$ for the three previously mentioned values of k_F. On the left side the graphs refer to the Bonn potential and on the right side to the Gogny force. First of all, we consider the interactions which are plotted with dotted lines: we observe that the behavior of the Bonn potential differs considerably from the behavior of the Gogny force. In the first two cases, Fig. 3.2 and Fig. 3.3, the relativistic force consists of two parts: one negative at small momenta and one positive at larger momenta, its zeros k_0 are located at around 1.0 fm^{-1}. Moreover, going up to higher Fermi momenta, we notice that the strength of the negative part decreases, and for $k_F = 1.2$ fm^{-1} (see Fig. 3.4), it has disappeared. On the contrary, the non-relativistic force consists of a negative part at small momenta and a positive one at large momenta for each value of the Fermi momentum. Its zeros k_0 are located at around $2.0 - 3.0$ fm^{-1} independently of k_F and the strength of the positive part is always negligible. Next, we consider the pairing fields $\Delta(k)$, plotted with solid lines. For both the interactions and for each k_F, they show a maximum at $k = 0$, decrease with a zero at $k \approx 2.0$ fm^{-1}, reach a minimum at $k \approx 3.0$ fm^{-1}, and, finally, go to zero at large momenta. For $k_F = 0.3$ and 0.8 fm^{-1} the maxima and the minima of $\Delta^B(k)$ and $\Delta^G(k)$ have comparable magnitudes, while for $k_F = 1.2$ fm^{-1} $\Delta^G(k)$ is far greater than $\Delta(k)^B$. This last observation agrees also with the fact that Δ_F^B goes to zero faster than Δ_F^G. Finally, in the figures we show the integrand $i(k)$ given in Eq.(3.32), plotted with dot-dashed lines and whose shaded areas represent

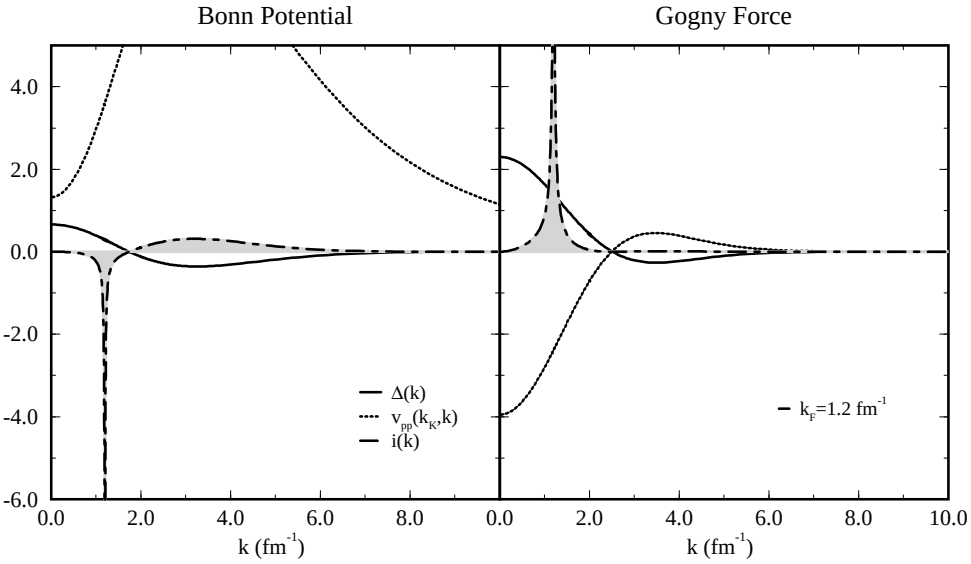

Figure 3.4: Various contributions to the integral in the gap equation (3.16) for the density corresponding to the Fermi momentum $k_F = 1.2$ fm^{-1}. Comparison of the relativistic Bonn-B potential and the Gogny force. The details are discussed in the text.

Δ_F, and we examine how $v_{pp}(k_F, k)$ and $\Delta(k)$ contribute to it. As before we observe differences in the quantities calculated with the Bonn potential and with the Gogny force. In the latter case, for each value of k_F and for momenta smaller than k_0, $\Delta(k)$ is positive, while $v_{pp}(k_F, k)$ is negative. Together with the minus sign in $i(k)$ in Eq. (3.32), this gives a positive contribution to the gap parameter at the Fermi surface, as we may from the shaded area. In the interval $k > k_0$, $\Delta(k)$ is negative and v_{pp} is positive, but because they have rather small strengths the total contribution to Δ_F^G of this interval is negligible. Thus we may conclude that for the non-relativistic interaction Δ_F originates mainly from the interval of small momenta only.

For the Bonn potential, the way $\Delta(k)$ and $v_{pp}(k_F, k)$ contribute to Δ_F^B depends on k_F. For $k_F = 0.3$ and 0.8 fm^{-1}, as we may see Fig. 3.2 and Fig. 3.3, we distinguish three intervals: for $k < 1.0$ fm^{-1} $\Delta(k)$ is positive and $v_{pp}(k_F, k)$ negative, then, because of the minus sign in $i(k)$, the contribution of this interval to Δ_F is positive (positive area). For $1.0 \leq k$ fm^{-1} ≤ 2.0 $\Delta(k)$ and $v_{pp}(k_F, k)$ are both positive and consequently the contribution to Δ_F is negative (negative area). Finally, due to the fact that $\Delta(k)$ is negative and v_{pp} positive, the contribution to Δ_F of the interval $k > 2.0$ (fm)$^{-1}$ is again positive. Therefore, as it can also be seen from the shaded areas in the figures, $\Delta_F(k_F = 0.3$ fm$^{-1})$ and $\Delta_F(k_F = 0.8$ fm$^{-1})$ are given by the sum of two positive and one negative contributions. For $k_F = 1.2$ fm^{-1} v_{pp} is positive for $k > 0$. At small momenta $\Delta(k)$ is also positive, then the contribution of the interval for which $k < 2.0$ fm^{-1} is

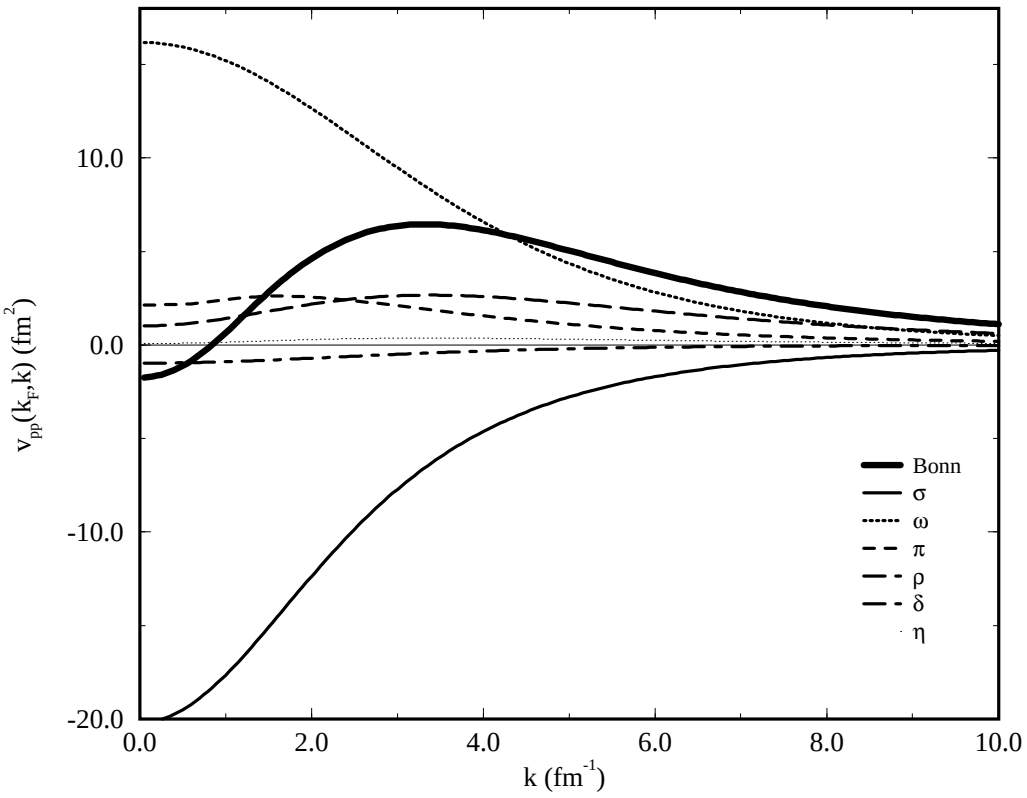

Figure 3.5: Matrix elements of the relativistic Bonn-B potential in momentum space $v_{pp}(k_F, k)$ at the Fermi momentum of maximal pairing correlations $k_F = 0.8$ fm^{-1}. The thick solid line corresponds to the full potential, the thin lines to the various one-meson exchanges.

negative. In the interval $k > 2.0$ fm^{-1} $\Delta(k)$ is negative so that the contribution to Δ_F is positive. Therefore, in this last case, we observe that Δ_F is given by the algebraic sum of two areas only: one positive and one negative, and since they are of comparable size they cancel each other. In conclusion, the fact that Δ_F^B drops to zero faster Δ_F^G is due to the strong dependence of the Bonn potential on the Fermi momentum.

From Fig.s 3.2, 3.3, and 3.4 we notice that for both the interactions and for each Fermi momentum, the integrand $i(k)$ presents a peak at $k \approx k_F$. This is simply due to the fact that for this value of the momentum the denominator in Eq. (3.32) is minimum. In the relativistic case, we observe the presence of a second peak that is a maximum for each k_F. It corresponds to the maximum of the positive part of v_{pp}.
The fact that also the large momentum part of the bare interaction contributes sensitively to the gap parameter was already pointed out in Ref. [BCL90].

In order to understand the discrepancy between the relativistic and the non-relativistic calculations, one should also mentioned that it could be due to the effects of the polarization. In fact, while the Gogny force is an effective force, i.e. it adjusted to the data and

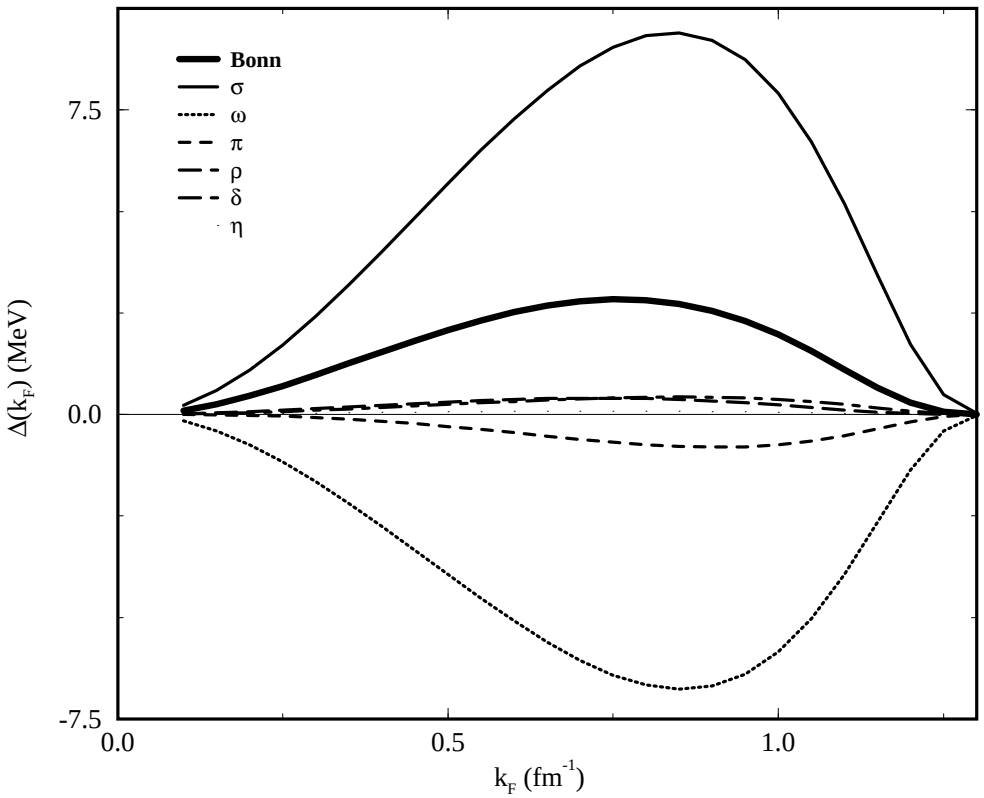

Figure 3.6: Contributions of the different one-meson exchange potentials to the gap parameter at the Fermi surface as a function of the density represented by the Fermi momentum k_F. The thick solid line corresponds to the full gap, the thin lines to the various mesons gaps.

all the effects are already taken into account, the Bonn potential is a bare interaction, and therefore one has to say that the full pairing force contains an additional part that it is induced by the presence of the background medium and as a consequence the effect of the polarization diagram in the K-matrix should be investigated.

We now concentrate on the relativistic $pp-$interaction. The Bonn potential is defined as the sum of OBE contributions of six mesons, namely σ, ω, π, ρ, δ, and η (see Appendix B). In Fig. 3.5 we show the different meson contributions and the resulting Bonn potential at the Fermi momentum $k_F = 0.8$ fm^{-1}. We observe that the full interaction results from the cancellation of two main terms: the negative and the positive contributions of σ and ω respectively. The other mesons play only a minor role, for example, at $k \approx 0$ the size of the π and ρ potential is only 10% of the size of the $\sigma - \omega$ exchanges. Anyway, their contribution cannot be neglected because of the large cancellation between σ and ω. The influence of δ and η is even smaller, and although they are considered in the calculations, we neglect them in the following discussion. Since we are working in momentum space

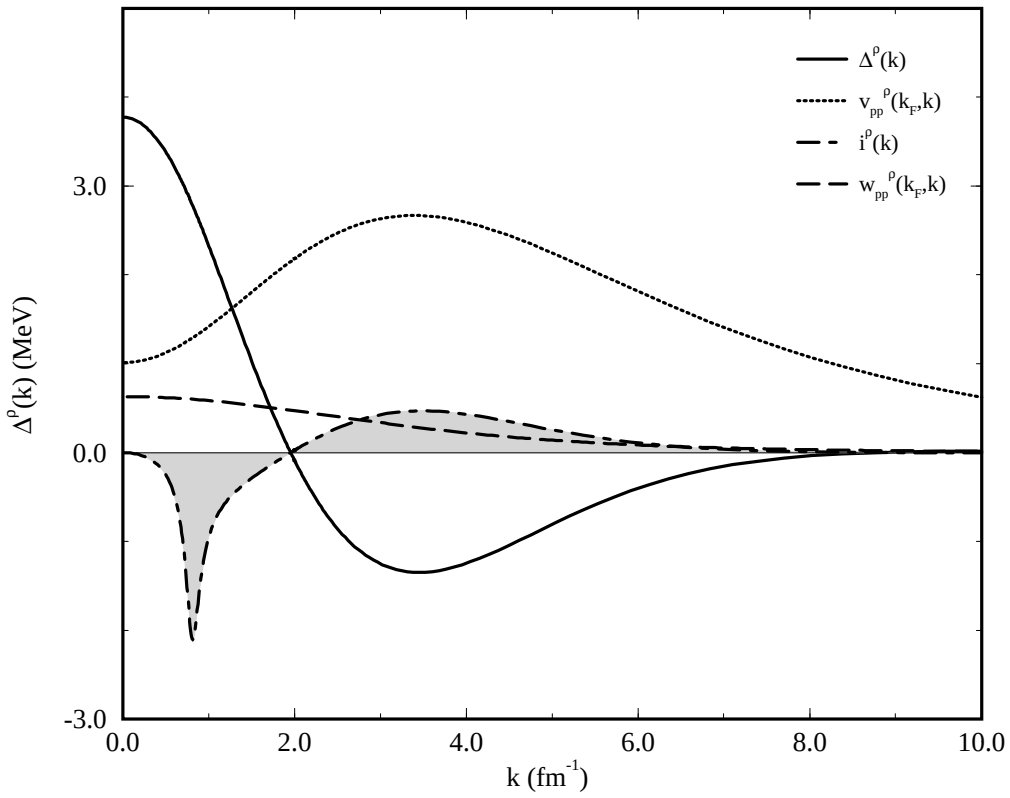

Figure 3.7: $\rho-$meson contributions to the integral in the gap equation (3.16) for the density corresponding to the Fermi momentum $k_F = 0.8$ fm^{-1}. Comparison of one-ρ exchange potential matrix elements: the dotted line corresponds to the full potential, i.e. vector+tensor+tensor-vector terms; the long-dashed line to the vector term only.

for a fixed value of the Fermi momentum, we cannot infer any further properties of the $pp-$interaction. In Fig. 3.6 we study how the exchange of the different mesons contributes to Δ_F. As we have just seen for the potential, the pairing gap at the Fermi surface mainly results from the the exchange of σ and ω whose corresponding pairing gaps at the Fermi surface $\Delta_F^{\sigma,\omega}$ are of the order of $+9.5$ MeV and -6.8 MeV for maximal pairing correlations respectively, and, as before, the other mesons play a minor role. Among them $\Delta_F^{\pi} \approx -0.85$ MeV and $\Delta_F^{\rho} \approx +0.42$ MeV for the same k_F. Quite surprising is the case of the $\rho-$meson whose contribution to the total gap at the Fermi surface Δ_F^{ρ} has the same sign of the interaction, while for every other meson we observe an inversion of the signs of v_{pp} and Δ_F^m. This behavior is due to the tensor V_T and vector-tensor V_{VT} terms in the one-rho exchange potential. To understand this property, in Fig. 3.7 we show $\Delta^{\rho}(k)$, $v_{pp}^{\rho}(k_F,k)$, $w_{pp}^{\rho}(k_F,k)$, and $i^{\rho}(k)$, where $v_{pp}^{\rho}(k_F,k)$, plotted with a dotted line, is the one-rho exchange potential with V_T and V_{VT} calculated at $k_F = 0.8$ fm^{-1} and $w_{pp}^{\rho}(k_F,k)$, plotted with a long-dashed line, contains the vector term only. Comparing v_{pp}^{ρ} and w_{pp}^{ρ} we observe that the presence of V_T and V_{VT} modifies the potential: it is no longer a monotonic

decreasing function of k as w^{ρ}_{pp}, but it has now a maximum at $k \approx 3.5$ fm^{-1} and then goes to zero. In addition, the strength of v^{ρ}_{pp} is considerably greater than the strength of w^{ρ}_{pp}. Proceeding as in the previous considerations for the full potential in the figures 3.2, 3.3, and 3.4, we notice that Δ^{ρ}_{F} is given by the sum of a negative contribution in the interval $0 < k$ (fm^{-1}) < 2.0 and a positive contribution for $k > 2.0$ fm^{-1}, the interval where the effects of V_T and V_{VT} on v^{ρ}_{pp} are stronger. As Δ^{ρ}_{F} is positive, we may therefore deduce that the effect of the tensor and vector-tensor terms in one-ρ meson exchange cannot be neglected.

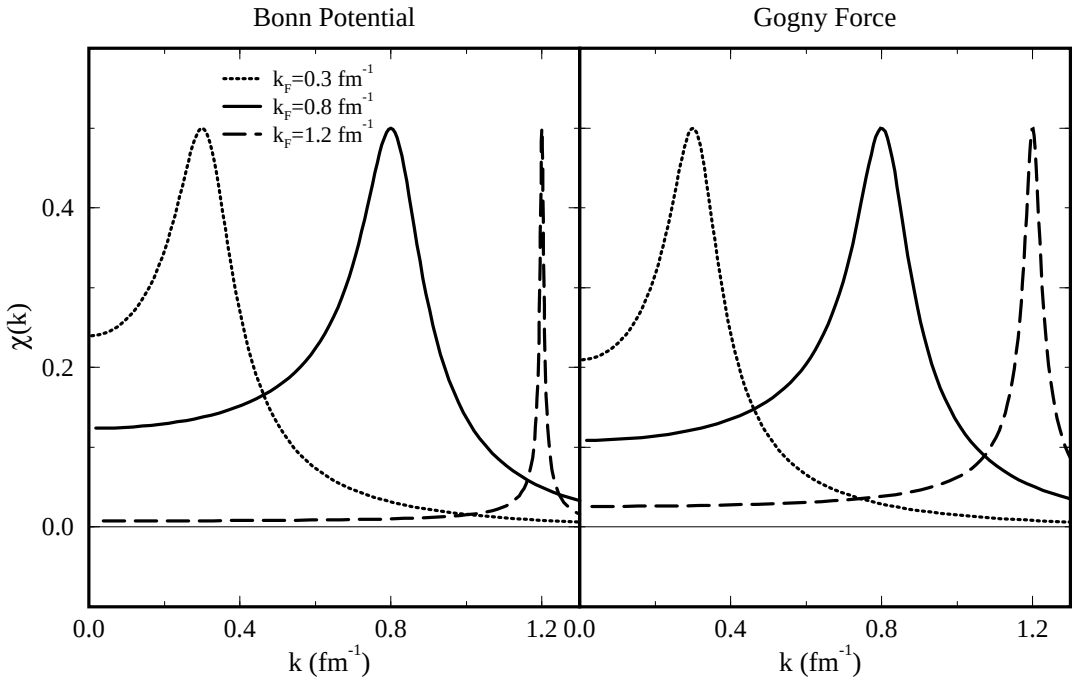

Figure 3.8: Cooper pair wave functions in momentum space $\chi(k)$ calculated at different values of the Fermi momentum k_F as functions of the momentum k for the relativistic Bonn-B potential and for the Gogny force.

3.2.2 Cooper Pair Wave Function and Coherence Length

For a better understanding of the pairing properties we study the Cooper Pair wave function. In momentum space it is defined by

$$\chi(k) = \frac{\Delta(k)}{2\sqrt{(\epsilon(k) - \lambda)^2 + \Delta^2(k)}}. \tag{3.33}$$

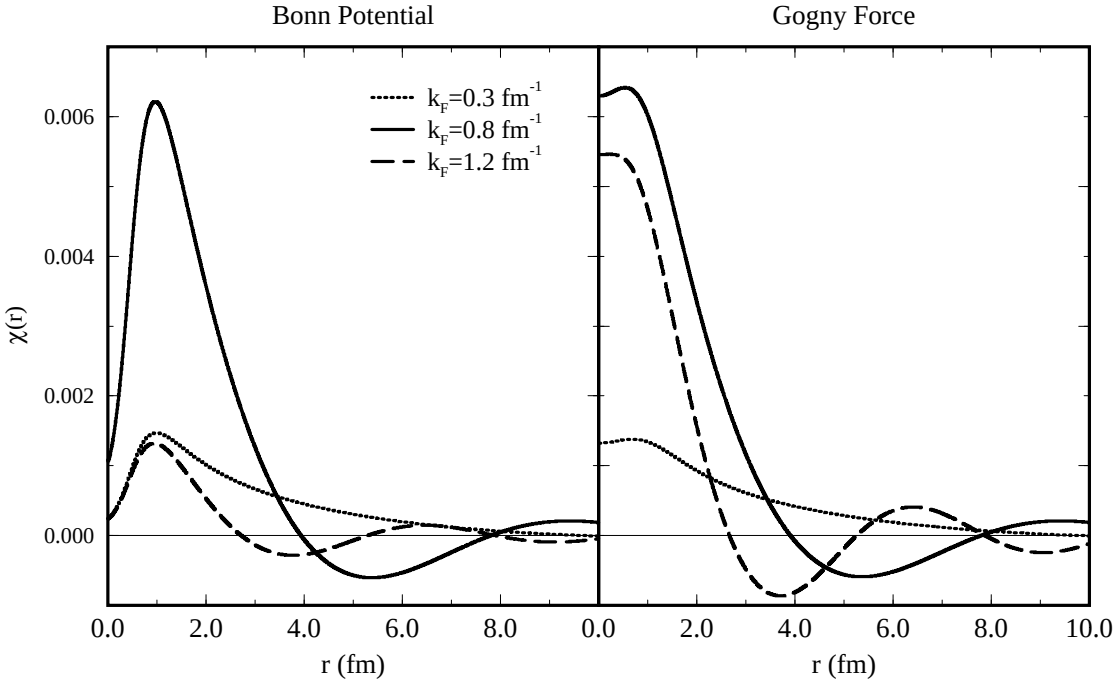

Figure 3.9: Cooper pair wave functions in coordinate space $\chi(r)$ calculated at different values of the Fermi momentum k_F as functions of the coordinate r for the relativistic Bonn-B potential and for the Gogny force.

By comparing the equations (3.16) and (3.22), it is immediately clear that the function $\chi(k)$ just defined in Eq. (3.33) is simply proportional to the product $u(k)v(k)$ that is the pairing tensor. In the formalism of the second quantization it is given by

$$\kappa_{ab} = \kappa_{\alpha\beta}(\mathbf{x}_a\mathbf{x}_b) = \langle A|\psi_\beta(\mathbf{x}_b)\psi_\alpha(\mathbf{x}_a)|A\rangle$$

and from this it follows that χ is the wave function which describes a pair of nucleons. In Fig. 3.8 on the left we show $\chi(k)$ obtained with the Bonn potential and with the Gogny force on the right at the three values of the Fermi momentum previously considered, i.e. $k_F = 0.3,\ 0.8$ and 1.2 fm^{-1}. First of all, we observe that every wave function is peaked at $k = k_F$. As already said before, this is due to the fact that the denominator in Eq.(3.33) at $k = k_F$ is minimum: in fact it reduces to $\Delta(k_F)$. Moreover, the pair wave functions asymmetry in the momenta intervals $k < k_F$ and $k > k_F$ may be explained as a consequence of the variation of the gap function $\Delta(k)$ with k. For both the interactions, the widths of the peaks, which represent the inverse of the coherence length, have the same size for $k_F = 0.3,$ and 0.8 fm^{-1}, while they are smaller for $k_F = 1.2$ fm^{-1}. In addition, the fact that for $k_F = 1.2$ fm^{-1} the width of the peak is narrower for the Bonn

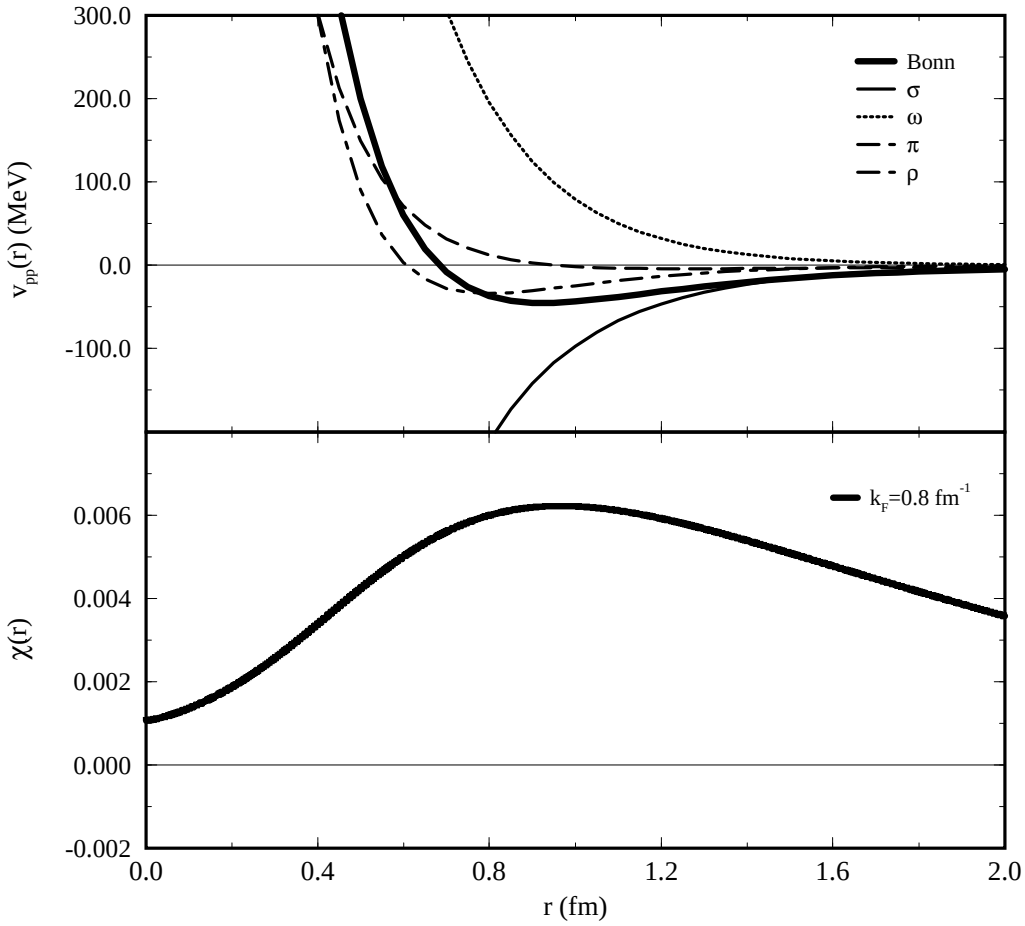

Figure 3.10: Upper part: even-singlet central part of the Bonn potential in coordinate space and its one-meson exchange contributions. The former is plotted with a thick solid line and the latters with thinner lines. Lower part: Cooper pair wave function at $k_F = 0.8$ (fm^{-1}). It is peaked where the interaction is mostly attractive. $\chi(r)$ is given in fm^{-3}.

potential than for the Gogny force is consistent with the observation that in the former case the gap parameter at the Fermi surface Δ_F drops faster than in the latter. Apart from this, in momentum space there are no big differences between the wave functions $\chi(k)$ calculated with the relativistic and non-relativistic forces. A similar behavior of $\chi(k)$ has been found also in Ref. [EH98].

In order to look further into the physical content, we now turn to the dependence on r, that represents the distance between the two nucleons forming a Cooper pair. In Fig. 3.9 we plot the pair wave functions in coordinate space of the Bonn potential and of the Gogny force $\chi(r)$, with

$$\chi(r) = \int \frac{d^3k}{(2\pi)^3} \mathrm{e}^{-i\mathbf{k}\cdot\mathbf{r}} \chi(k) \tag{3.34}$$

at the three values of k_F used before. Here r is the interparticle distance. For both the interactions they are oscillating functions of r, and the oscillation rate increases with the

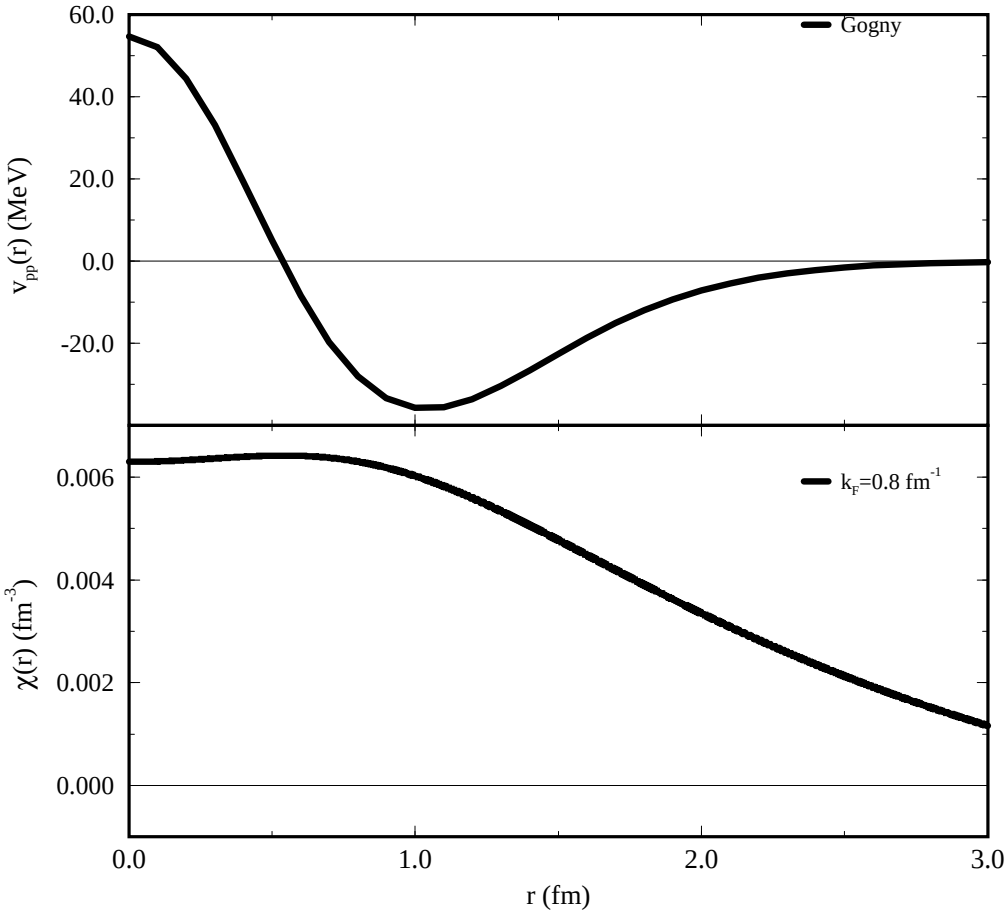

Figure 3.11: Upper part: channel $^1S_0$ for the Gogny force in coordinate space. Lower part: Cooper pair wave function at $k_F = 0.8$ (fm^{-1}). It is maximal where the interaction is mostly repulsive.

density represented by k_F. However, we also observe important differences between the relativistic and the non-relativistic calculations. In the former case, for each k_F, $\chi(r = 0)$ is close to zero, then increases till a maximum at $r_{max} \approx 1.0$ fm and thereafter it starts to oscillate at different rates for each k_F. We observe that the highest maximum of the pair wave functions $\chi(r_{max}) \approx 0.0062$ fm^{-3} corresponds to the Fermi momentum for which pairing correlations are maximal, i.e. $k_F = 0.8$ fm^{-1}. For $k_F = 0.3$ and 1.2 fm^{-1}, we have $\chi(r_{max}) \approx 0.0015$ fm^{-3}. In principle there is no reason why the height of the $\chi(r)$s corresponding to these two k_F is the same. However, from Fig. 3.1, we observe that the magnitude of the pairing gap at the Fermi surface is roughly 0.9 MeV for both these two values of k_F, and this could explain why we obtain the same height in the two Cooper pair wave functions. In the case of the Gogny force, the situation is quite different. First of all, the pair wave functions $\chi(r)$ do not present any pronounced peak at small distances. In particular they are almost constant in the interval $k < 1.0$ fm^{-1} for each k_F, then decrease and oscillate with an oscillation rate increasing with k_F as we have noticed for the relativistic interaction. Comparing the strength of $\chi^B(r)$ and $\chi^G(r)$ at the different densities, we observe that they are of the same order for $k_F = 0.3$ and 0.8 fm^{-1}, for which,

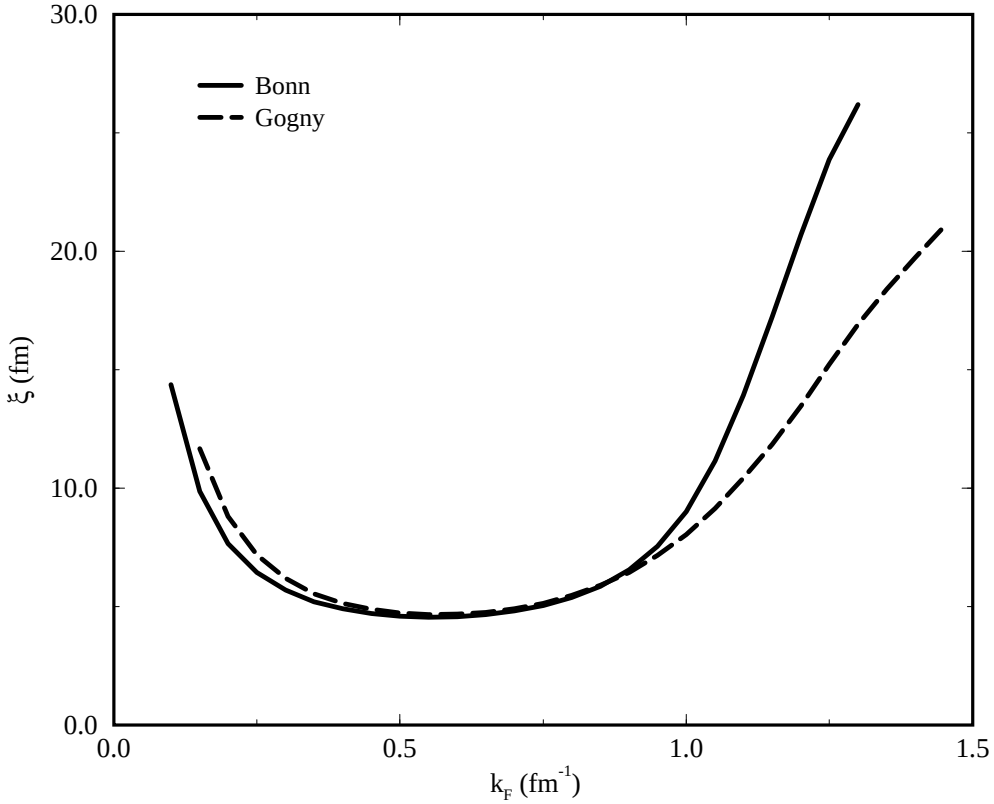

Figure 3.12: Coherence length as function of the Fermi momentum k_F for the relativistic Bonn-B potential and for the Gogny force.

as it can be noticed from Fig. 3.1, also the agreement between the corresponding pairing gap at the Fermi surface is very good, namely $\Delta_F^B(k_F = 0.3\,\mathrm{fm}^{-1}) \approx \Delta_F^G(k_F = 0.3\,\mathrm{fm}^{-1}) \approx 0.9$ MeV and $\Delta_F^B(k_F = 0.8\,\mathrm{fm}^{-1}) \approx \Delta_F^G(k_F = 0.8\,\mathrm{fm}^{-1}) \approx 2.8$ MeV. On the contrary, for $k_F = 1.2\,\mathrm{fm}^{-1}$ the strength of $\chi^G(r)$ is far greater than the strength of $\chi^B(r)$. This agrees with the observation that at this Fermi momentum the pairing gap obtained with the Gogny force is much greater than the pairing gap obtained with the Bonn potential, namely we find $\Delta_F^G(k_F = 1.2\,\mathrm{fm}^{-1}) \approx 1.9$ MeV and $\Delta_F^B(k_F 1.2\,\mathrm{fm}^{-1}) \approx 0.9$ respectively. In both cases the interparticle distance for which the Cooper pair wave function is maximal is ≈ 1.0 fm.

Starting from the fact that the Bonn potential is a rather complicated function of r, the Cooper pair wave functions in coordinate space allow us to find an answer to the following question: which part of the interaction is responsible for pairing correlations? Let us consider the Bonn potential. In the upper part of Fig. 3.10, we show the even-singlet ($^1S_0$) central part of the bare interaction in coordinate space. We have to remark that we have used here a non-relativistic reduction of the potential in coordinate space, which is however a good approximation of the relativistic one at small distances, since the

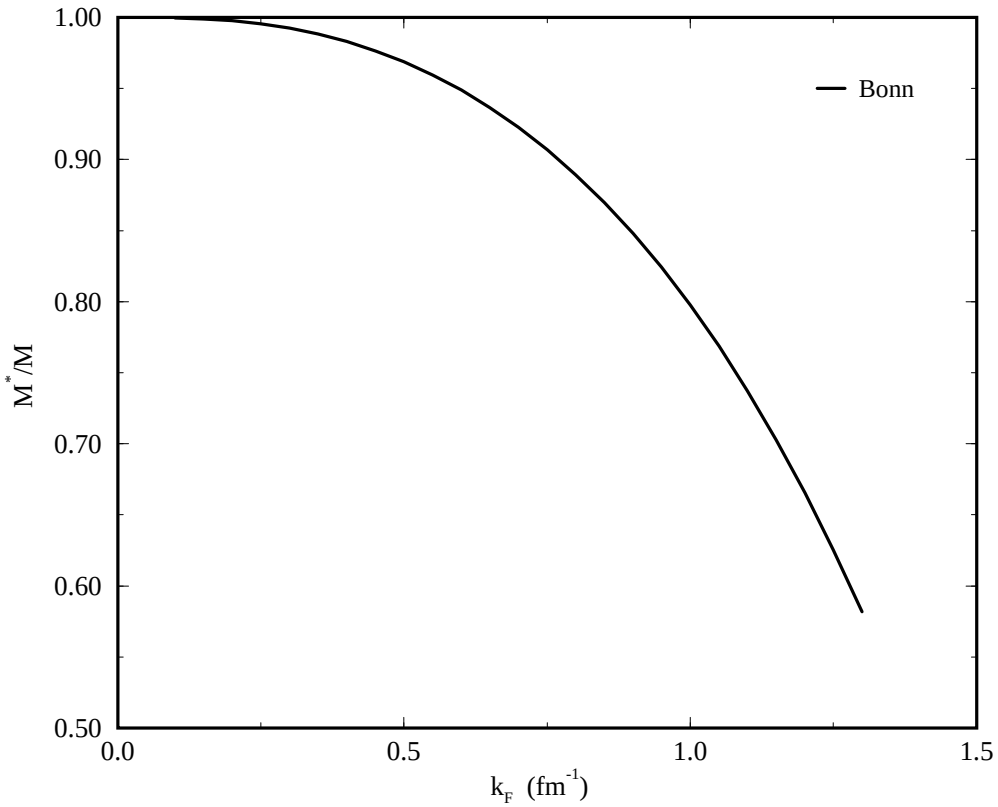

Figure 3.13: Ratio M^*/M as function of the Fermi momentum k_F for the relativistic Bonn-B potential.

Fourier transformation of the latter from momentum to coordinate space cannot be carried out analytically because of the presence of non-local terms [Ma89]. We observe that the full potential, represented in the figure by a thick solid line, is repulsive at short distances, has a zero at $r \approx 0.7$ fm and then a minimum of the order of -50 MeV at $r_{mim} \approx 0.9$ fm and, finally, goes to zero for larger distances. The thinner lines represent the single meson contributions. In particular we notice the monotonic increasing and decreasing potentials corresponding to the attractive $\sigma-$ and to the repulsive $\omega-$mesons, the contribution of the one-pion exchange that in this channel of the $pp-$interaction is strongly repulsive for $r \leq 1.0$ fm and weakly attractive for $r \geq 1.0$ fm, the one-rho exchange potential which is also strongly repulsive at small distances, has a zero at $r \sim 0.6$ fm and gives an attractive contribution of the order of -40 MeV at 0.8 fm much stronger than the contribution of π. This is probably due not only to fact that ρ is heavier than π but also to the presence of the tensor and vector-tensor in the potential. Moreover, we also remark that the $\delta-$functions in the spin-spin (central) force of the one-pion and of the one-rho exchanges are removed by the form factors applied to the nucleon-meson-nucleon vertices of the potential. In the picture we have omitted the contributions of the $\delta-$ and $\eta-$meson as they are negligible. In the lower part of Fig. 3.10 we show the Cooper pair

wave function in coordinate space for $k_F = 0.8$ fm^{-1} and we observe a correspondence between the potential and the $\chi(r)$ behaviors: at small distances, where the interaction is strongly repulsive, the size of $\chi(r)$ is small, in particular for interparticle distances less than 0.1 fm it seems very unlikely that two nucleons condensate into a Cooper pair. At larger distances the strength of $\chi(r)$ clearly increases together with the decreasing in the strength of the potential, in particular $\chi(r)$ has a maximum of 0.006 at $r_{min} \approx 0.8$ fm at which the interaction is mostly attractive. The same observations can be repeated also for the other values of the Fermi momentum, as we have seen that every Cooper pair wave function in coordinate space shows a peak at the same $r = r_{mim}$ independently k_F. From these considerations, we may conclude that pairing correlations in nuclei are mainly due to the attractive part of the interaction and that the effect of the repulsive part is to shift the peak of the Cooper pair wave function outwards.

The relativistic Bonn potential gives a good quantitative description of pairing correlations, which result in a extra-binding energy of the system, in infinite nuclear matter and we have just seen that in the interval where it is repulsive, it is unlikely to find two nucleons bounded into a Cooper pair. On the other side, from Fig. 3.10 and Fig. 3.6 we may see that to a potential repulsive along the whole $r-$axis (for example ω) corresponds a finite gap. Therefore, we could deduce that the exchange of mesons producing a repulsive potential generates a finite energy which would loose the system.

As we have done for the relativistic interaction, in Fig. 3.11 we show the Gogny force in coordinate space in the upper part of the figure and the Cooper pair wave function in coordinate space for $k_F = 0.8$ fm^{-1} in the lower part. In this case the situation does not seem to be realistic, since $\chi(r)$ is not suppressed by the repulsive part of the force, indeed its strength is maximal in the corresponding interval. In comparison with the Bonn potential, the Gogny force is far less repulsive at small distance and less attractive at intermediate distances.

Another important quantity that we investigate for a better understanding of the pairing properties in nuclear systems is the coherence length ξ that, from a microscopic point of view, represents the squared mean distance of two paired particles on top of the Fermi surface. In terms of the Cooper pair wave functions it is defined as

$$\xi^2 = \frac{\int d^3r |\chi(\mathbf{r})|^2 r^2}{\int d^3r |\chi(\mathbf{r})|^2} = \frac{\int_0^\infty dk k^2 |\partial\chi(k)/\partial k|^2}{\int_0^\infty dk k^2 |\chi(k)|^2} \tag{3.35}$$

and for our calculation we have chosen the coordinate space representation since it is more convenient on the numerical point of view. In Fig. 3.12 we show the resulting ξ as a function of the Fermi momentum k_F for the Bonn potential, plotted with a solid line, and for the Gogny force, plotted with a dashed line. In both cases, we observe that in the interval $0.4 \leq k_F(\text{fm}^{-1}) \leq 0.9$, ξ has a minimum of the order of $5.0 - 6.0$ MeV and it is an almost constant function of the Fermi momentum. This is in agreement with the fact that in this interval pairing correlations are maximal, namely we find $\Delta_F \geq 1.5$ MeV as it may be seen from Fig. 3.1. For low densities ($k_F \leq 0.25$ fm^{-1}) and high densities ($k_F \geq 1.0$ fm^{-1}) the strength of the coherence length increases rapidly, meaning that the two nucleons becomes more and more separated, i.e. do not form a Cooper pair. The difference of the coherence length obtained with the Bonn potential and the coherence length calculated with the Gogny force at larger densities agrees with the observation that

the pairing gap drops faster for the relativistic interaction than for the non-relativistic force. Furthermore our calculations are in good agreement with the results given in Ref. [EH98].

Finally, since, as we have mentioned at the beginning of the section, the pairing gap at the Fermi surface k_F Δ_F is given by the solution of the system of non-linear differential equations for the pairing field $\Delta(k)$ and for the effective mass M^* given in Eq.s (3.22)-(3.21), we show the ratio M^*/M in Fig. 3.13. As expected, it is a decreasing function of the Fermi momentum and for maximal pairing at $k_F = 0.8$ fm^{-1} correlations its value is 0.88.

3.3 Pairing with Relativistic Phenomenological Interactions

As the relativistic bare Bonn potential reproduces fairly well the pairing gap at the Fermi surface and other pairing properties obtained with non-relativistic calculations [KRS89a] based on phenomenological interactions [DG80] adjusted to finite nuclei experimental data, our next goal is to investigate pairing properties in finite nuclei in a fully relativistic Hartree-Bogoliubov approach. Unfortunately, as we solve the RHB equations by expanding the wave functions and nuclear densities in terms of harmonic oscillator wave functions, the relativistic Bonn potential cannot be used as interaction in the *pp*-channel. In fact, by using this expansion method the energy associated to a nuclear shell with principal number N is

$$E_N = N\hbar\omega_0 \tag{3.36}$$

where $\omega_0 = 41/A^{1/3}$, and for finite nuclei that $\hbar\omega_0$ is approximately 10 MeV. As 16-20 shells are needed for the convergence of the RHB equations, the maximal energy in the spectrum is around 200 MeV. On the other side, the cutoff masses Λ_m associated to the nucleon-meson vertex functions Λ_m are of the order of $1500 - 2000$ MeV. This means that the effect of the Bonn potential cutoffs cannot be totally included in the calculations performed by using such an expansion method. In [TM99] a relativistic phenomenological particle-particle channel interaction is presented. It is based on the exchange of a σ- and a ω-meson and suits the gap equation for nuclear matter. This is done by introducing a density independent momentum cutoff parameter Λ to the relativistic mean field model so as to reproduce the pairing properties obtained by the Bonn-B potential and not to change the saturation property. Nevertheless, as the cutoff mass Λ is fixed to the value of ≈ 700 MeV, which, as for the Bonn potential, is too high to be used in the framework of an expansion method. Therefore, we have constructed a relativistic phenomenological particle-particle channel interaction, also based on the exchange of a σ and a ω-meson, but for the form factor $F(\mathbf{q}^2)$ we we have chosen a gaussian function in order to assure the convergence of the RHB equations solved by the HOWF expansion method. Starting from the parameters set NL2 and keeping constant the meson masses, we have fixed the cutoff mass μ and changed the coupling constants in order to reproduce the pairing gap at the Fermi surface obtained by using the relativistic Bonn potential. In Fig. 3.14 we display the gap parameter at the Fermi surface Δ_F as a function of the Fermi momentum k_F for the different pairing interactions. On the left side we show the calculations obtained by

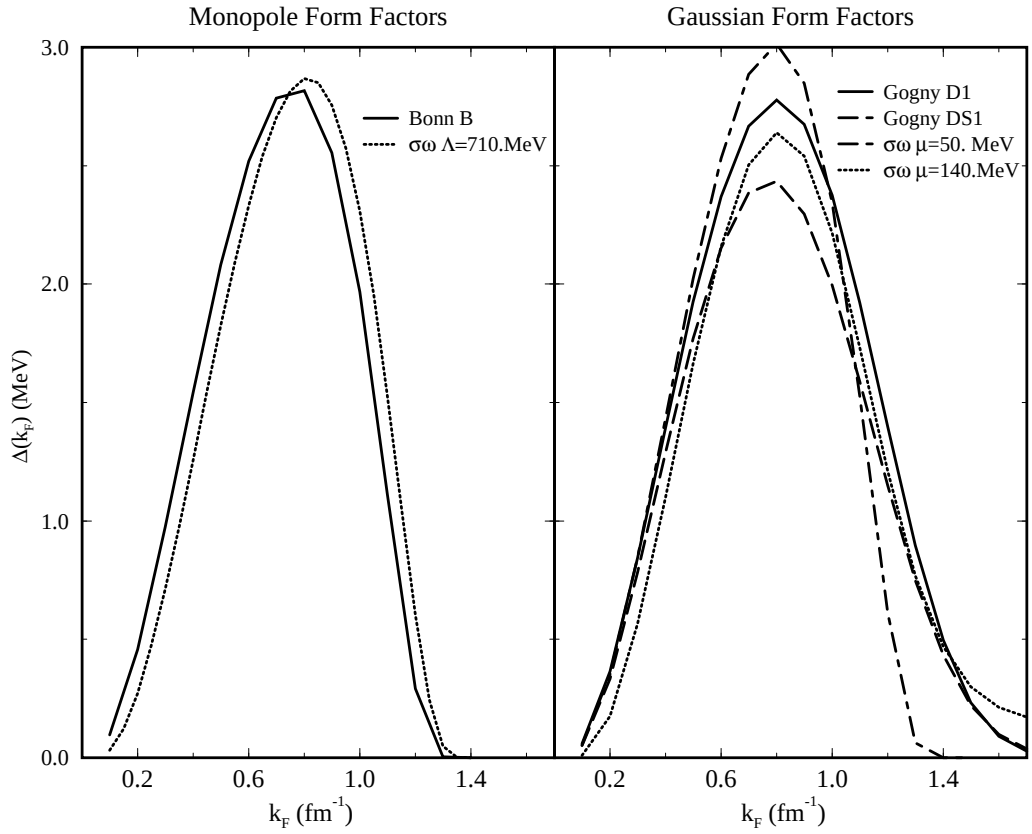

Figure 3.14: The gap parameter at the Fermi surface Δ_F as a function of the density represented by the Fermi momentum k_F for the different pairing interactions. On the left side form factors of monopole type are used, while on the right side form factors of gaussian type are used.

using the relativistic Bonn B potential (solid line), and the phenomenological interaction introduced in [MT99], based on the exchange of a σ- and a ω-meson and whose form factor $F_m(\mathbf{q}^2)$ given in Eq.(B.25) is of monopole type (dotted line). The relativistic phenomenological interaction produces a pairing gap which is in excellent agreement with Δ_F^B for all the values of the densities k_F. On the right hand side of the figure we plot the same quantity obtained by using non-relativistic Gogny forces, parameters sets D1 [DG80] and D1S [BGG84], and by using our new phenomenological relativistic interactions based on the exchange of a σ- and a ω-meson and with the form factor $F_m(\mathbf{q}^2)$ given in (B.27) of gaussian type. First, we notice that the two Gogny forces D1 and D1S plotted with a solid and long-dashed line respectively, show the same functional dependence on k_F although there is a difference of 0.3 MeV in the strength of the maximal pairing correlations at $k_F = 0.8$ fm^{-1}. The other two curves dot-dashed and the dotted lines display $\Delta_F(k_F)$ that we obtain by using the new phenomenological relativistic interaction. The dot-dashed line is obtained with a cutoff mass μ of 50. MeV for which g_σ and g_ω have been reduced of the 15% of the original NL2 parameters set. The dotted line is obtained with a cutoff mass μ of 140. MeV for which g_σ and g_ω have been reduced of the 40% of the original NL2 parameters. We are in particular interested in the gap parameter produce by the new force with the cutoff of 140. MeV as it corresponds to the same cutoff value of the

non-relativistic Gogny force D1. From the figure, we may see that in these two cases the agreement of Δ_F in the strength of the pairing for each value of the density is excellent. Finally, from the comparison of the results for Δ_{k_F} displayed in this figure, we may say that at large densities the pairing gap is very sensitive to the interaction.

Chapter 4

Relativistic HB Theory for Finite Nuclei

In the previous Chapters it has been explained that a relativistic theory with classical meson fields does not allow the description of superfluid nuclei, because it contains only terms $\psi^\dagger\psi$ and not Cooper pairs $\psi^\dagger\psi^\dagger$ or $\psi\psi$. A reformulation of the theory in terms of an energy functional (in analogy to what was done in Skyrme models) allows one to take into account monopole pairing within the BCS approximation. However, although successful for the nuclei close to stability, it has been shown in Ref.s [DNW96, DFT84] that the BCS scheme cannot be applied to the study of very neutron rich nuclei close to the dripline, where pairing is embedded in the continuum. In this case a HFB theory has to be used. As discussed in Chapter 2, relativistic HFB (RHFB) equations have been derived by Kucharek and Ring in Ref. [KR91], where it was shown that, microscopically, pairing correlations originate from a one-meson exchange interaction. However, a fully relativistic solution of the RHFB equations with meson exchange forces for finite nuclei has not been carried out yet. All the investigations of superfluid nuclei which have been done so far neglect the Fock term in the *ph*-channel, and most of them use non-relativistic forces with finite or zero range in the *pp*-channel. For recent reviews see Ref.s [LVR99, Me98] and the references therein. In this Chapter we present a fully relativistic Hartree-Bogoliubov (RHB) approximation for finite nuclei and we study in detail the relativistic effects in pairing correlations in finite nuclei.

In Section 4.1 we give the general expressions of the RHB equations for finite nuclei. In Section 4.2 we discuss our phenomenological relativistic potential in the pairing channel, and in Section 4.3 we show the results for an isotopic chain of Sn nuclei.

4.1 Relativistic Hartree-Bogoliubov Equations

The fully relativistic HFB equations have been already introduced in Chapter 2. Starting from the usual relativistic Lagrangian density of the RMF theory, the quantization of the meson fields together with Green's functions techniques allows the derivation of the relativistic HFB equations:

$$\begin{pmatrix} h-\lambda & \Delta \\ \Delta^\dagger & -h^*+\lambda \end{pmatrix} \begin{pmatrix} U_k \\ V_k \end{pmatrix} = E_k \begin{pmatrix} U_k \\ V_k \end{pmatrix} \tag{4.1}$$

where h and Δ are the single-nucleon Dirac Hamiltonian and the relativistic pairing field respectively, λ is the chemical potential, E_k are the quasi-particle energies and the eigenvector $(U_k,\, V_k)$ is defined by

$$\begin{pmatrix} U_k \\ V_k \end{pmatrix} = \begin{pmatrix} f_{U_k} \\ ig_{U_k} \\ f_{V_k} \\ -ig_{V_k} \end{pmatrix} \tag{4.2}$$

(For details on the HFB theory see Ref. [RS80]). In Eq. (4.2) f and g are the large and the small components of the Dirac spinor given in Eq. (D.2). The phases in Eq. (4.2) have been chosen in such a way that we finally obtain real RHB equations. We write the pairing field Δ in analogy to the Dirac Hamiltonian as

$$\Delta = \begin{pmatrix} \Delta_{++} & i\Delta_{+-} \\ i\Delta_{-+} & -\Delta_{--} \end{pmatrix} \tag{4.3}$$

with real matrices Δ_{++}, Δ_{+-}, Δ_{-+} and Δ_{--}. The $+$ and $-$ denote the relativistic indices p_i, which refer to the large or small component of a Dirac spinor. They are defined in Eq. (D.7). A generic matrix element of the relativistic pairing field reads

$$\Delta_{a_1p_1a_2p_2} = \frac{1}{2} \sum_{a_3p_3a_4p_4} \langle a_1p_1a_2p_2|V^{pp}|a_3p_3a_4p_4\rangle_a \;\kappa_{a_3p_3a_4p_4} \tag{4.4}$$

where $\langle V^{pp}\rangle_a$ is the relativistic antisymmetrized two-body matrix element (see Eq.s (D.1) and (D.7) for notations and definitions) and the total pairing energy E_{pair} is given by

$$E_{pair} = \frac{1}{4} \sum_{a_1p_1a_2p_2a_3p_3a_4p_4} \kappa_{a_2p_2a_1p_1} \langle a_1p_1a_2p_2|V^{pp}|a_3p_3a_4p_4\rangle_a \kappa_{a_3p_3a_4p_4}. \tag{4.5}$$

In the relativistic case one has to sum also over the relativistic index p_i, and for a fully relativistic self-consistent solution of the Eq.s (4.1), all the four matrices in Eq. (4.3) have to be considered. Since we solve the RHB equations by expanding nuclear wave functions and densities in terms of a finite basis of the Harmonic Oscillator (see Ref.s [GRT90, GR93]), the two-body matrix elements of the pairing interaction V^{pp} which appear in Eq.s (4.4)-(4.5) are calculated in terms of the Harmonic Oscillator wave functions. The expressions of these matrix elements are given explicitly in Appendices D, E, and F. The choice of the phase given in Eq. (4.2) allows one to write the DHFB Eq.s (4.1) as a real eigenvalue problem. Explicitly, considering only the scalar and vector mesons with time-reversal symmetry in the Dirac Hamiltonian, and neglecting the Fock term in the ph-channel, the relativistic Hartree-Bogoliubov (RHB) equations read

$$\begin{pmatrix} M^*+V-\lambda & \boldsymbol{\sigma}\cdot\boldsymbol{\nabla} & \Delta_{++} & \Delta_{+-} \\ (\boldsymbol{\sigma}\cdot\boldsymbol{\nabla})^\dagger & -M^*+V-\lambda & \Delta_{-+} & \Delta_{--} \\ \Delta^T_{++} & \Delta^T_{-+} & M^*+V+\lambda & \boldsymbol{\sigma}\cdot\boldsymbol{\nabla} \\ \Delta^T_{+-} & \Delta^T_{--} & (\boldsymbol{\sigma}\cdot\boldsymbol{\nabla})^\dagger & -M^*+V+\lambda \end{pmatrix} \begin{pmatrix} f_{U_k} \\ g_{U_k} \\ f_{V_k} \\ g_{V_k} \end{pmatrix} = E_k \begin{pmatrix} f_{U_k} \\ g_{U_k} \\ f_{V_k} \\ g_{V_k} \end{pmatrix}. \tag{4.6}$$

This equation has solutions for the quasi-particle creation operators $\alpha^\dagger$ (U, V) and solutions for the quasi-particle annihilation operators α (U^*, V^*). In addition, there are particle solutions (f, g) and antiparticle solutions $(\tilde{f}, \tilde{g})$.

The relativistic coefficients U_k and V_k of the Bogoliubov transformation, can be combined to the unitary matrix $\mathcal{W}$

$$\mathcal{W} = \begin{pmatrix} U & V^* \\ V & U^* \end{pmatrix} = \begin{pmatrix} f_U & \tilde{f}_U & f_V^* & \tilde{f}_V^* \\ ig_U & i\tilde{g}_U & ig_V^* & i\tilde{g}_V^* \\ f_V & \tilde{f}_V & f_U^* & \tilde{f}_U^* \\ -ig_V & -i\tilde{g}_V & -ig_U^* & -i\tilde{g}_U^* \end{pmatrix} \tag{4.7}$$

from which, as in the non-relativistic case (see for example Ref. [RS80]), the relativistic generalized density matrix $\mathcal{R}$ is obtained as

$$\begin{aligned} \mathcal{R} &= \mathcal{W} \begin{pmatrix} 0 & \\ & 1 \end{pmatrix} \mathcal{W}^\dagger \\ &= \begin{pmatrix} V^*V^T & V^*U^T \\ U^*V^T & U^*U^T \end{pmatrix} = \begin{pmatrix} \rho & \kappa \\ -\kappa^* & 1-\rho^* \end{pmatrix}. \end{aligned} \tag{4.8}$$

In Eq.s (4.7) $\tilde{f}$ and $\tilde{g}$ are the large and small components of the antiparticle solutions of the Dirac equation. The relativistic density matrix ρ is given by

$$\begin{aligned} \rho &= V^*V^T \\ &= \begin{pmatrix} f_V f_V^T + \tilde{f}_V \tilde{f}_V^T & -i(f_V g_V^T + \tilde{f}_V \tilde{g}_V^T) \\ i(g_V f_V^T + \tilde{g}_V \tilde{f}_V^T) & g_V g_V^T + \tilde{g}_V \tilde{g}_V^T \end{pmatrix} = \begin{pmatrix} \rho_{++} & -i\rho_{+-} \\ i\rho_{-+} & \rho_{--} \end{pmatrix} \end{aligned} \tag{4.9}$$

and the relativistic pairing tensor κ by

$$\begin{aligned} \kappa &= V^*U^T \\ &= \begin{pmatrix} f_V f_U^T + \tilde{f}_V \tilde{f}_U^T & i(f_V g_U^T + \tilde{f}_V \tilde{g}_U^T) \\ i(g_V f_U^T + \tilde{g}_V \tilde{f}_U^T) & -(g_V g_U^T + \tilde{g}_V \tilde{g}_U^T) \end{pmatrix} = \begin{pmatrix} \kappa_{++} & i\kappa_{+-} \\ i\kappa_{-+} & -\kappa_{--} \end{pmatrix}. \end{aligned} \tag{4.10}$$

As before, in Eq.s (4.9) and (4.10) the indices + and − refer to the large and small component of the Dirac spinor, and, as given in Eq.s (4.9) and (4.10), the relativistic ρ and κ contain also the contributions of the antiparticles. Similarly to the non-relativistic case, the density matrix is a symmetric tensor, while the pairing tensor is skew symmetric Since as we work in the no-sea approximation in the *ph*-channel, the antiparticles are not included in the expression for ρ given in Eq. (4.9), i.e. we neglect the terms $\tilde{f}_V \tilde{f}_V^T$, $\tilde{f}_V \tilde{g}_V^T$, $\tilde{g}_V \tilde{f}_V^T$, and $\tilde{g}_V \tilde{g}_V^T$ in ρ. The effect of the antiparticles on the pairing tensor is still a complete open question. It is argued that as pairing correlations are concentrated on the Fermi surface and that at the same time the antiparticles have an energy of about -1200 MeV, they should not contribute to κ, but this should be clarified. We will address the problem later on. In any case κ is antisymmetric only with respect to the complete basis, i.e. only if the antiparticle solutions $(\tilde{f}, \tilde{g})$ are taken into account in its calculation.

4.2 A Relativistic Pairing Interaction for Finite Nuclei

In Chapter 3 it has been shown that the relativistic Bonn potential gives a fairly good description of pairing correlations in infinite nuclear matter. Being a bare interaction, it corresponds to the first diagram of the K-matrix, i.e. the interaction that should be used in the *pp*-channel. Therefore, it seems reasonable to describe ground state properties of finite nuclei by solving the RHB Eq.s (4.6) using the Bonn potential as interaction in the relativistic pairing field given in Eq. (4.3). However, the mathematical properties of the potential make the numerical solution of the RHB equations quite a difficult task: due to its high cutoff no convergence is achieved in a reasonable oscillator space and therefore they should be solved in coordinate space. Although it would be preferable to have a relativistic pairing force with a finite range with a cutoff fixed by reproducing the pairing properties of nuclear matter, for this study we have constructed a relativistic pairing interaction with zero-range. Starting from the fact that on the microscopic point of view, pairing correlations originate from a one-meson exchange interaction, our phenomenological relativistic pairing potential consists of the exchange of the two mesons σ and ω, and the zero-range approximation of the force simply means to work in the limit $m_\sigma, m_\omega \to \infty$. In other words, we have considered a point-coupling model (see Appendix A) based on two isoscalar relativistic fields: a Lorentz scalar s and a Lorentz vector field $v^\mu = (v^0, \mathbf{v}$. As coupling constants we have used the parameters of NL3. In addition, because in this approximation it is a δ-force which enters into the RHB equations, we needed to introduce a cutoff which assures the convergence of Eq.s (4.6). This has been done by multiplying the s- and v-field couplings for a constant parameter c_0, fixed to reproduce the pairing energy of a given nucleus to the value obtained with other HFB calculations. Explicitly, the pairing interaction reads

$$V_\delta^{pp}(\mathbf{r}_1, \mathbf{r}_2) \;=\; c_0 \left\{ -C_s^2 \; \gamma_{13}^0 \gamma_{24}^0 + C_v^2 \; \mathbf{I}_{13} \mathbf{I}_{24} - C_v^2 \; \boldsymbol{\alpha}_{13} \cdot \boldsymbol{\alpha}_{24} \right\} \delta(\mathbf{r}_1 - \mathbf{r}_2) \qquad (4.11)$$

where the coupling constants are defined by

$$C_s = \frac{g_\sigma}{m_\sigma} \qquad\qquad C_v = \frac{g_\omega}{m_\omega} \qquad (4.12)$$

(see also Appendix A). Then, V_δ^{pp} results from three terms: the two attractive terms of s and of the spacelike component of the v-field $\mathbf{v}$, and the repulsive term of the timelike component of the v-field v^0. Since it will be shown that a fully relativistic treatment of the *pp*-channel induces a new production mechanism of pairing correlations in finite nuclei, we write explicitly the expression Δ_{++}, Δ_{+-}, Δ_{-+}, and Δ_{--} given in Eq. (4.3) for the pairing force given in Eq. (4.11). Writing

$$\Delta_{a_1 p_1 a_2 p_2}(\mathbf{r}_1, \mathbf{r}_2) \;=\; \delta(\mathbf{r}_1 - \mathbf{r}_2) \Delta_{a_1 p_1 a_2 p_2}(\mathbf{r}_1) \qquad (4.13)$$

$$\kappa_{a_1 p_1 a_2 p_2}(\mathbf{r}_1, \mathbf{r}_2) \;=\; \kappa_{a_1 p_1 a_2 p_2}(\mathbf{r}_1) \qquad (4.14)$$

the components of the relativistic pairing field read

$$\Delta_{a_1 + a_2 +}(\mathbf{r}_1) \;=\; \frac{1}{2} c_0 \sum_{a_3 a_4} \left[-C_s^2 + C_v^2 \right] \kappa_{a_3 + a_4 +}(\mathbf{r}_1) - 3 C_v^2 \kappa_{a_3 - a_4 -}(\mathbf{r}_1), \qquad (4.15)$$

$$\Delta_{a_1+a_2-}(\mathbf{r}_1) = \frac{1}{2}c_0 \sum_{a_3 a_4} \left[C_s^2 + C_v^2\right] \kappa_{a_3+a_4-}(\mathbf{r}_1) - C_v^2 \kappa_{a_3-a_4+}(\mathbf{r}_1), \tag{4.16}$$

$$\Delta_{a_1-a_2-}(\mathbf{r}_1) = \frac{1}{2}c_0 \sum_{a_3 a_4} \left[-C_s^2 + C_v^2\right] \kappa_{a_3-a_4-}(\mathbf{r}_1) - 3C_v^2 \kappa_{a_3+a_4+}(\mathbf{r}_1). \tag{4.17}$$

We have omitted the component $\Delta_{a_1-a_2+}$ since it has similar expression of $\Delta_{a_1+a_2-}$. From Eq.s (4.15)-(4.17) an interesting characteristic of the relativistic structure appears: the matrix elements of the relativistic pairing field result from a combination of two components of the relativistic pairing tensor given in Eq. (4.10): namely, to a given $\Delta_{p_1 p_2}$ (here the indices a_1 and a_2 have been omitted for simplicity), both $\kappa_{p_1 p_2}$ and $\kappa_{\bar{p}_1 \bar{p}_2}$ contribute: in particular, the fields s and v^0, which constitute the central part of the interaction (4.11), are connected to the term $\kappa_{p_1 p_2}$, while the field $\mathbf{v}$, which is the spin dependent part of the interaction, is connected to $\kappa_{\bar{p}_1 \bar{p}_2}$. This is a relativistic effect and originates from the structure of the Dirac matrices in the nucleon-meson vertices of the interaction (4.11). Finally, due to the simple structure of the δ force, the pairing field and tensor are diagonal in $\mathbf{r}$, i.e. $\mathbf{r}_1 = \mathbf{r}_2$.

Also the total pairing energy results from a combination of different terms:

$$\begin{aligned}
E_{pair} &= \frac{1}{4}c_0 \sum_{a_1 a_2 a_3 a_4} \int d\mathbf{r} \left\{ \left[-C_s^2 + C_v^2\right] \kappa_{a_2+a_1+}(\mathbf{r}) \kappa_{a_3+a_4+}(\mathbf{r}) \right. && (4.18)\\
&+ \left[-C_s^2 + C_v^2\right] \kappa_{a_2-a_1-}(\mathbf{r}) \kappa_{a_3-a_4-}(\mathbf{r}) && (4.19)\\
&- 2C_v^2 \kappa_{a_2+a_1+}(\mathbf{r}) \kappa_{a_3-a_4-}(\mathbf{r}) && (4.20)\\
&+ \left. 2\left(\left[C_s^2 + C_v^2\right] \kappa_{a_2+a_1-}(\mathbf{r}) \kappa_{a_3-a_4+}(\mathbf{r}) - C_v^2 \kappa_{a_2+a_1-}(\mathbf{r}) \kappa_{a_3+a_4-}(\mathbf{r})\right)\right\}. && (4.21)
\end{aligned}$$

In order to see the differences induced by a fully relativistic treatment of the pairing channel, we compare these expressions with those used in the RHB model NL3+Gogny (for a recent review see Ref. [LVR99]). The Gogny force was used for the first RHB calculations for finite nuclei by Gonzales-Llarena et al. in Ref. [GLE96] where it was argued that since the matrix elements of a two-body force in the *pp*-channel are of a few MeV only, a non-relativistic force could be used also in the solution of the RHB equations. Comparisons of binding energies and pairing energies showed a good agreement between the calculations carried out by the RHB model NL3+Gogny and non-relativistic HFB model based on the Gogny force. However, since this interaction is non-relativistic in the calculations of the two-body matrix elements given in Eq. (4.4) the relativistic index p_i remains arbitrary and it has to be decided in which part of the relativistic pairing field the Gogny force acts. On the basis of the previous considerations, the Gogny force is used only with κ_{++}. The pairing field and energy reduce then

$$\Delta_{a_1+a_2+}(\mathbf{r}_1, \mathbf{r}_2) = \frac{1}{2} \sum_{a_3 a_4} V^{pp}_{Gogny}(\mathbf{r}_1, \mathbf{r}_2) \kappa_{a_3+a_4+}(\mathbf{r}_1, \mathbf{r}_2) \tag{4.22}$$

$$E_{pair} = \frac{1}{4} \sum_{a_1 a_2 a_3 a_4} V^{pp}_{Gogny}(\mathbf{r}_1, \mathbf{r}_2) \kappa_{a_2+a_1+}(\mathbf{r}_1, \mathbf{r}_2) \kappa_{a_3+a_4+}(\mathbf{r}_1, \mathbf{r}_2). \tag{4.23}$$

Therefore by comparing the equations for the pairing field (4.15)-(4.17) and (4.22) and the pairing energy (4.18)-(4.21) and (4.23), the situation with a fully relativistic interaction

is more complicated. In particular, relativity leads to the fact that in the pp-channel, the spin dependent part of the interaction mixes large and small components of the pairing density κ.

4.2.1 Applications to Sn Isotopes

We present here an investigation of the ground state properties of an even isotopic chain of Sn. Particular attention is focused on the relativistic structure of the pairing tensor κ and of the pairing field Δ and the energy E_{pair}. We have solved the RHB equations given in Eq. (4.6) using as pairing interaction the relativistic point-coupling potential introduced in the last Section and taking into account the contribution of the antiparticles in the calculation of the pairing tensor in order to have an antisymmetric κ (see Eq. (4.10)).

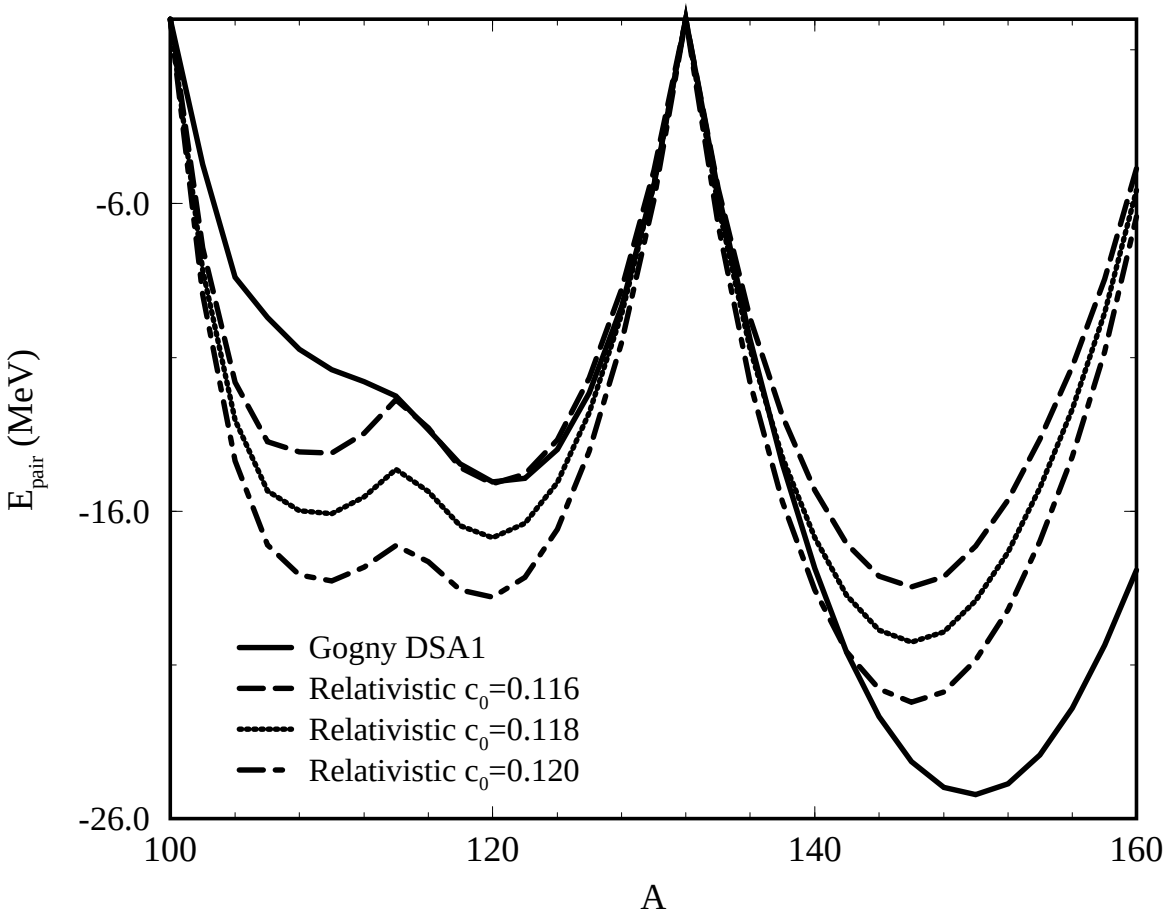

Figure 4.1: Neutron pairing energy of the even isotopes of Sn, as a function of the mass number A, calculated with the relativistic pairing interaction given in Eq. (4.11) for three values of the parameter c_0, and with non-relativistic Gogny force DSA1.

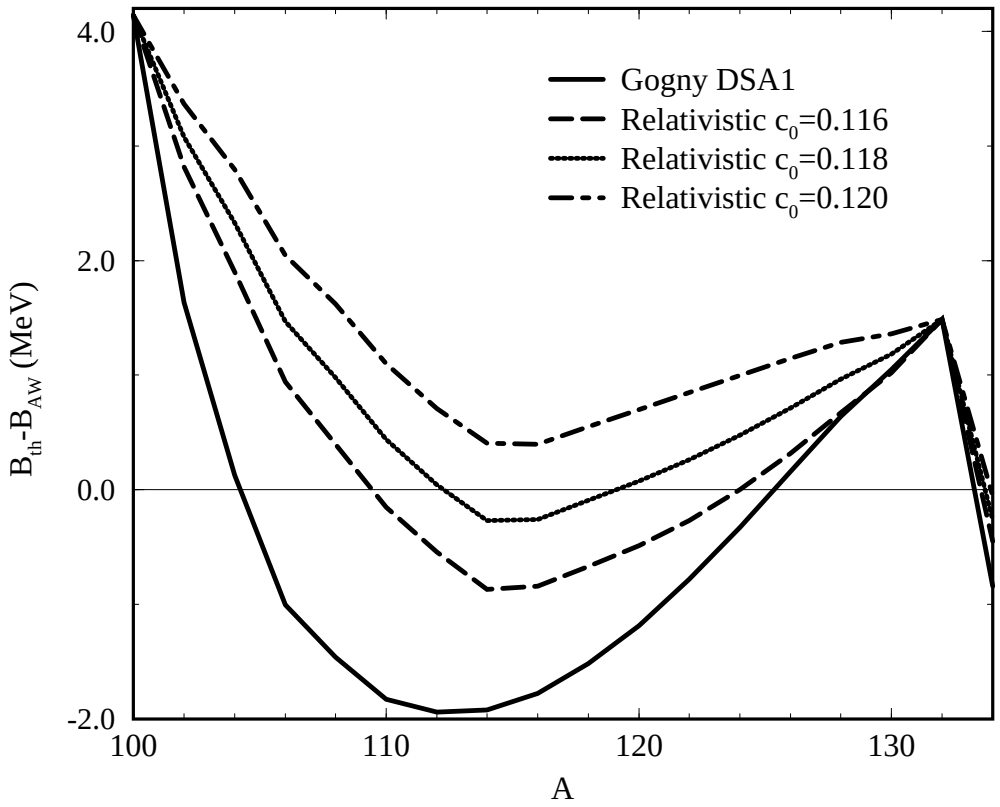

Figure 4.2: Difference between the calculated binding energy and the Audi-Wapstra experimental energy [AW93], for the even isotopes of Sn, as a function of the mass number A. The RHB calculations are performed by using the relativistic pairing interaction given in Eq. (4.11) for three values of the parameter c_0, and with non-relativistic Gogny force DSA1.

Comparisons have been made with RHB calculations based on NL3 and on the Gogny force with the parameter set DSA1 [BGG84]. The parameter c_0 has been fixed in such a way to reproduce the pairing energy of the nucleus ^{120}Sn obtained with the RHB model NL3+Gogny. In principle, the choice of the nucleus used to fix c_0 is completely arbitrary, but we have chosen the isotope $A = 120$ because it is stable and the NL3+Gogny model gives reasonable results as compared to the experiments.

In Fig. 4.1 we display the neutron pairing energies E_{pair} given in Eq.s (4.18)-(4.21) for different values of c_0 as a function of the mass number. The solid line corresponds to the Gogny force calculations, whereas the long-dashed, the dotted and the dot-dashed lines refer to the relativistic pairing interaction. Three different values for the strength parameter c_0, namely 0.116, 0.118, and 0.120, have been used. First of all, we observe that very small variations of the value of c_0 change E_{pair} quite considerably. This is due to the high non-linearity of the RHB equations. The value of c_0 which reproduces the pairing energy of ^{120}Sn obtained with the Gogny force E^G_{pair} is 0.116. With this value for c_0 the

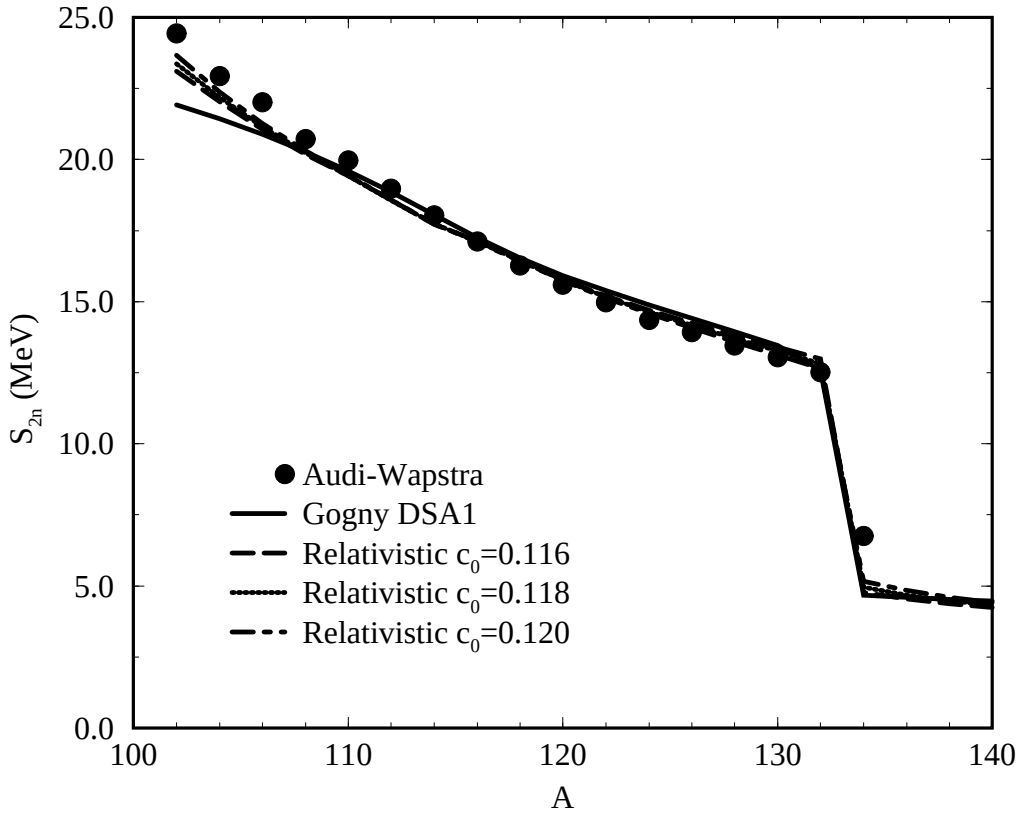

Figure 4.3: Two-neutron separation energy of the even isotopes of Sn, as a function of the mass number A. The filled dots are the values obtained from the experimental masses of Ref. [AW93]. The lines show RHB calculations performed by using the relativistic pairing interaction given in Eq. (4.11) for three values of the parameter c_0, and with non-relativistic Gogny force DSA1.

agreement between the two RHB models is excellent in the mass region $114 \leq A \leq 132$. For $100 \leq A \leq 114$ the behavior of E^{δ}_{pair} differs considerably from the behavior of E^{G}_{pair}. In particular, E^{G}_{pair} decreases almost monotonically with the mass number till $A = 120$, while E^{δ}_{pair} shows two minima one at $A = 110$ and one at $A = 120$ and it is roughly symmetric with respect to $A = 114$. This effect is particularly interesting as it seems to be due to the fully relativistic structure of the pairing interaction. For $134 \leq A \leq 160$ E^{δ}_{pair} is smaller than E^{G}_{pair}, but it shows a similar behavior, i.e. it decreases till a minimum at about $A = 146$ and then it increases again.

In Fig. 4.2 we plot the difference between the binding energies calculated with the theoretical models and the experimental values of Audi-Wapstra given in Ref. [AW93] as a function of the mass number A. As before, the solid line corresponds to the RHB model NL3+Gogny and the dashed lines refer to the fully relativistic RHB calculations performed with the same three values of c_0. We observe that $B_{th} - B_{AW}$ depends quite sensitively on the choice of the interaction in the *pp*-channel. In the region $N \approx Z$, the calculations give

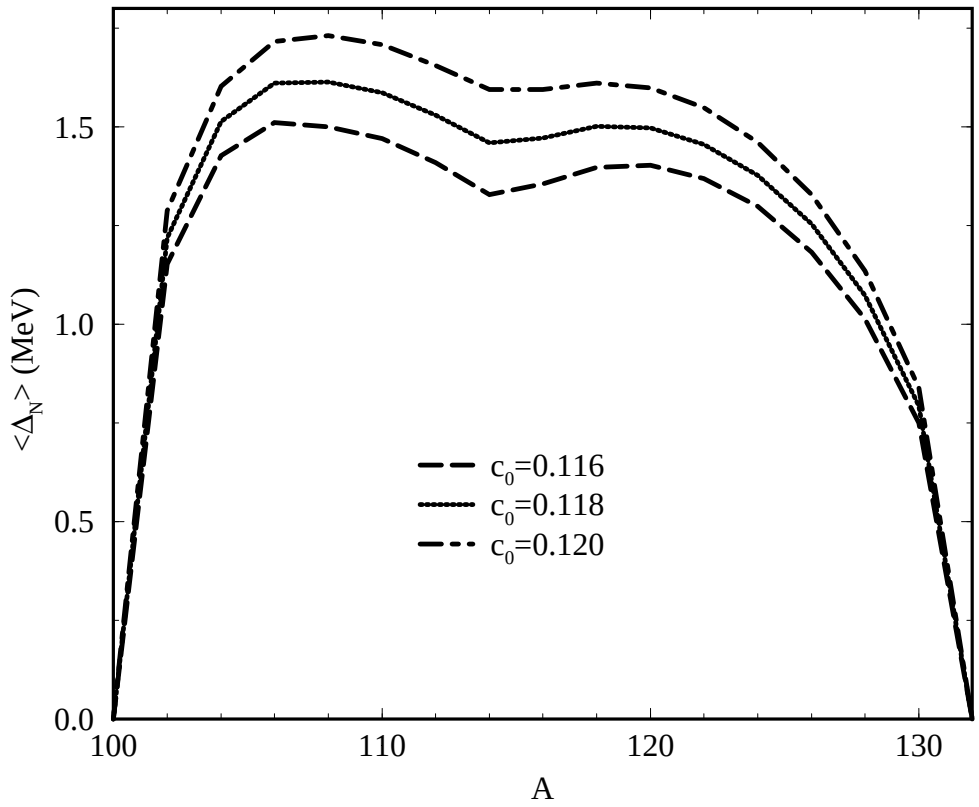

Figure 4.4: Average neutron pairing gaps $\langle \Delta_N \rangle$ for the even Sn isotopes, as a function of the mass number A. RHB calculations performed with the relativistic pairing potential given in Eq. (4.11) are shown for the three values of c_0.

an overbinding with the respect to the experimental value. This discrepancy is largest at $A = 100$ with a value of about 4 MeV. Since ^{100}Sn is a double magic nucleus, this result does not depend on pairing and it can be attributed to some deficiencies in the isospin dependence of the NL3 parameter set. The best average agreement seems to be yielded by the fully relativistic RHB calculations for the strength parameter values $c_0 = 0.116$ and 0.118. In particular, it is interesting to remark that although E^G_{pair} and $E^\delta_{pair}(c_0 = 0.116)$ agree extremely well in the range $114 \leq A \leq 132$, the relativistic RHB calculations give a total binding energy closer to the experimental value for the lighter isotopes. At the shell closure $A = 132$ the discrepancy of about 2 MeV between theoretical and experimental values depends once more on some deficiency of NL3 in the *ph*-channel.

In Fig. 4.3 we show the two-neutron separation energy S_{2n}

$$S_{2n} = B(Z, N) - B(Z, N-2) \tag{4.24}$$

for the even Sn isotopes as a function of A. In the mass region $102 \leq A \leq 108$ the NL3+Gogny model underestimates the two-neutron separation energies of about $2.5 - 1.5$

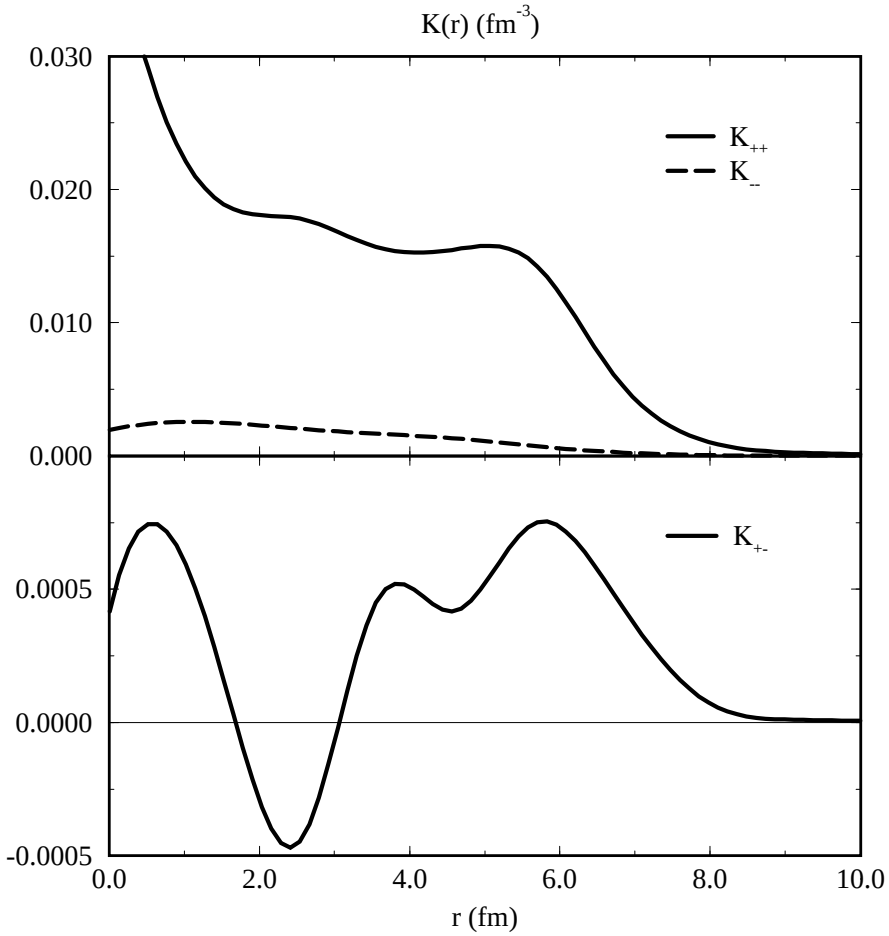

Figure 4.5: The components κ_{++},κ_{+-},and κ_{--} of the pairing tensor given in Eq. (4.10) for the nucleus ^{120}Sn, as a function of the radial coordinate. The calculations are performed by using the relativistic pairing potential given in Eq. (4.11) for $c_0 = 0.116$.

MeV, while a relativistic description of the *pp*-channel yields a better agreement between the theoretical calculations and the experimental values. Up to the shell closure at $A = 132$ both models agree fairly well with the experimental data, although it seems that the Gogny force gives a two-neutron separation energy slightly larger that the pairing potential. All the calculations reproduce the two-neutron separation energy at $A = 134$ and for $A \geq 136$. The agreement between the results obtained with non-relativistic and relativistic pairing interactions is excellent, but the fully RHB calculations give a slightly larger two-neutron separation energy. Finally, we compare only the RHB calculations performed with the relativistic pairing interaction. Although the two-neutron separation energies almost coincide, the calculation with $c_0 = 0.120$ is closer to the S_{2n} calculated from the experimental data. From Fig. 4.1, we observe that for this value of c_0, E^{δ}_{pair} differs mostly from E^{G}_{pair}. In the same figure it is also shown that for the nuclei from $100 < A < 108$ E^{δ}_{pair} decreases faster than E^{G}_{pair}, and this is responsible for the larger S_{2n} obtained with the relativistic pairing interaction. However, it cannot be concluded that a better result for S_{2n} comes only from the pairing energies.

In Fig. 4.4 we plot the average of the neutron pairing gaps $\langle \Delta_N \rangle$ in the mass region

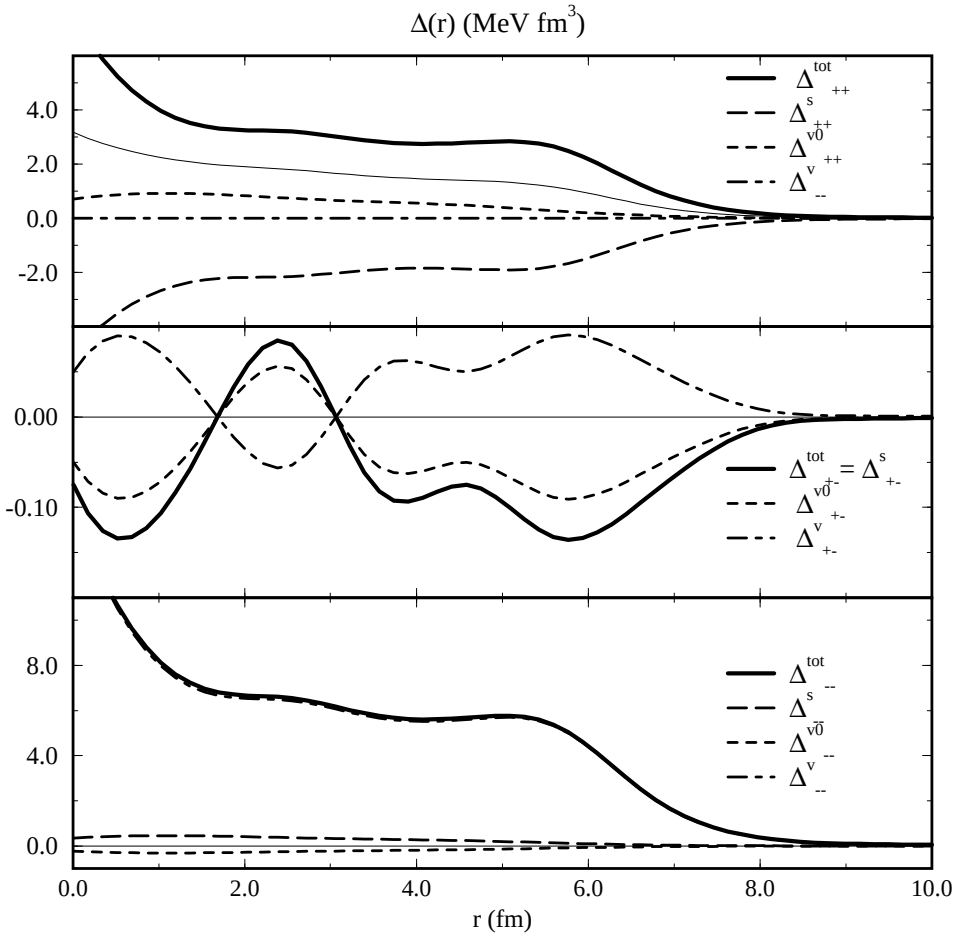

Figure 4.6: Neutron pairing field components Δ_{++},Δ_{+-},and Δ_{--} given in Eq.s (4.15)-(4.17) for the nucleus ^{120}Sn as a function of the radial coordinate. The calculations are performed by using the relativistic pairing potential given in Eq. (4.11) for $c_0 = 0.116$.

$100 \leq A \leq 132$. It is defined by

$$\langle \Delta_N \rangle = \frac{\sum_{nlj} \Delta_{nlj} v^2_{nlj}}{\sum_{nlj} v^2_{nlj}} \tag{4.25}$$

where v^2_{nlj} are the occupation probabilities, and it provides a quantitative measure of pairing correlations. Calculations are shown for the relativistic pairing potential for the three values of c_0. $\langle \Delta_N \rangle$ reflects the behavior of the pairing energies shown in Fig. 4.1. Two maxima appear at $A = 106$ and at $A = 120$ and they correspond to the two minima observed in E^{δ}_{pair}. For $100 \leq A \leq 114$ the values of $\langle \Delta_N \rangle$ are larger than those in the mass region $114 \leq A \leq 132$. This result agrees with the observation that the decrease of E^{δ}_{pair} is faster in the first interval than in the second one. The values of $\langle \Delta_N \rangle$ are between 1.3 and 1.5 MeV for $c_0 = 0.116$ and slightly larger for the other values of c_0. In Fig. 12 of Ref. [LVR98] $\langle \Delta_N \rangle$ obtained with the Gogny force is a quasiparabolic function, almost constant in the central interval. This comparison reflects also the difference between the non-relativistic and the relativistic interactions already pointed out through the discrepancy in the neutron pairing energies. Moreover, the values of $\langle \Delta_N \rangle$ obtained with the Gogny force are about 2 MeV, therefore 0.5 MeV larger than the ones resulting from the relativistic pairing potential.

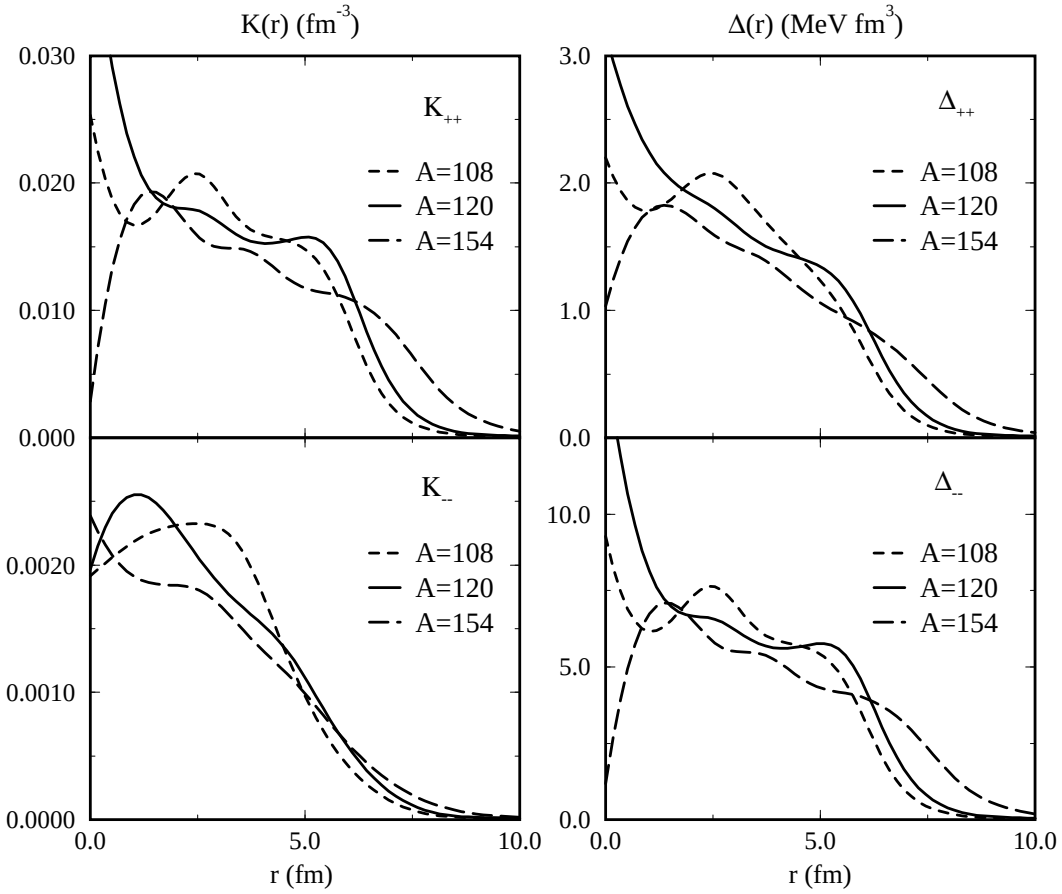

Figure 4.7: Neutron pairing tensor components κ_{++},κ_{+-},and κ_{--} given in Eq. (4.10), and neutron pairing field components Δ_{++},Δ_{+-},and Δ_{--} given in Eq.s (4.15)-(4.17) as a function of the radial coordinate for ^{108}Sn, ^{114}Sn, and ^{120}Sn. The calculations are performed by using the relativistic pairing potential given in Eq. (4.11) for $c_0 = 0.116$.

In the following we concentrate on the relativistic structure of the pairing tensor κ given in Eq. (4.10) and of the pairing field Δ given in Eq.s (4.15)-(4.17). In particular, we investigate the contributions to these quantities coming from the large and small components of the Dirac spinors and the effects of the antiparticles.

In Fig. 4.5 we display the three components of the relativistic pairing tensor given in Eq. (4.10) for ^{120}Sn, namely κ_{++}, κ_{--}, and κ_{+-}, as a function of the radial coordinate $r = |\mathbf{r}|$. In the upper part of the figure, the solid line shows κ_{++}, given by the product of the large components f_V and f_U of the Dirac spinors, and the dashed line shows κ_{--}, given by the product of the small components g_V and g_U of the Dirac spinors, i.e.

$$\kappa_{++}(r,r) = \sum f_V(r) f_U(r) \tag{4.26}$$

$$\kappa_{--}(r,r) = \sum g_V(r) g_U(r) \tag{4.27}$$

Both the functions are largest at the origin and decrease towards the surface. This behavior has already been observed in non-relativistic HFB calculations with the interaction SkP$^\delta$ (see Ref. [DNW96]). κ_{++} is a factor 10 larger than κ_{--}, and both are always positive. In the lower part, we show κ_{+-}, given by the product of large and small components

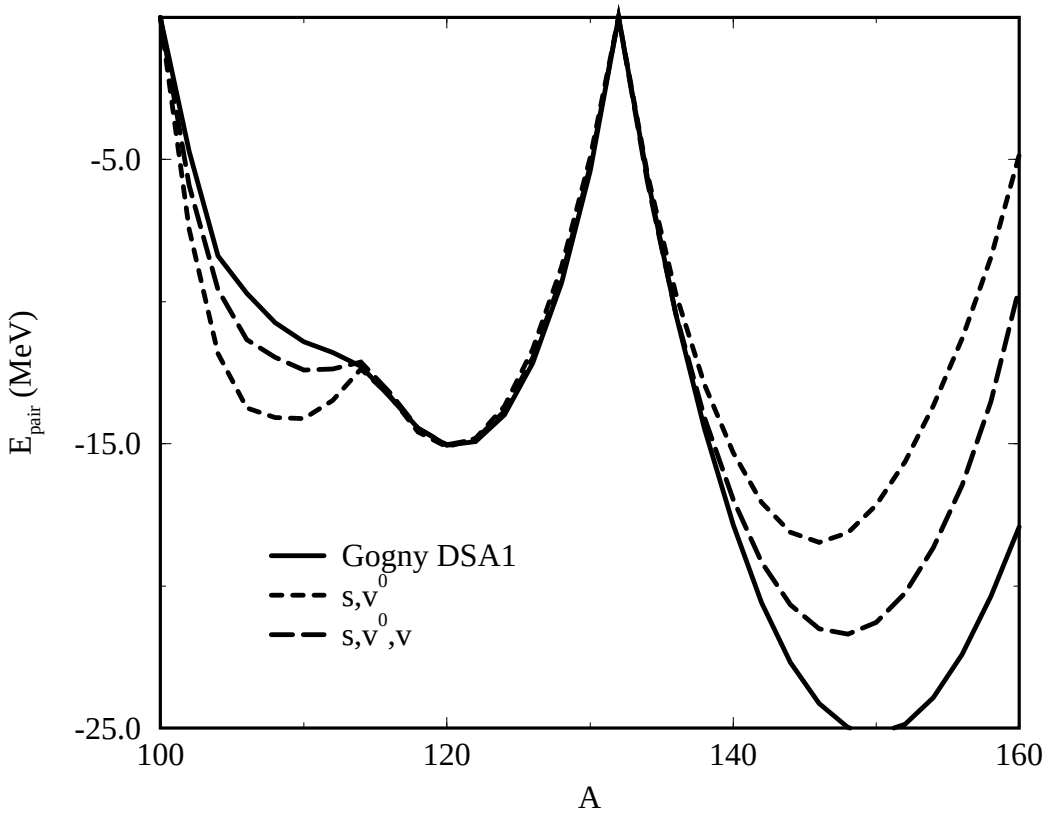

Figure 4.8: Neutron pairing energy of the even isotopes of Sn, as a function of the mass number A, calculated with the relativistic pairing interaction given in Eq. (4.11) for $c_0 = 0.116$, with the relativistic (s, v^0) pairing interaction for $c_0 = 0.207$ and with non-relativistic Gogny force DSA1.

f_V and g_U of the Dirac spinor, as a function of the coordinate,

$$\kappa_{+-}(r, r) = \sum f_V(r) g_U(r) \tag{4.28}$$

In this case the pairing tensor has an oscillating structure and it is of the same magnitude of κ_{--}. Later on, the study of the pairing field and energy will show that the contribution of κ_{+-} is almost negligible, whereas it is crucial to consider κ_{--} in the solution of the RHB equations. This is due to the the vector part of the relativistic pairing interaction.

In Fig. 4.6 we show the three components of the relativistic pairing field, namely Δ_{++}, Δ_{--}, and Δ_{+-}, given in Eq.s (4.15)-(4.17) for ^{120}Sn, as a function of the coordinate. The thick solid line displays the total pairing field, and the thin lines show the contributions of the different parts of the relativistic pairing interaction: the long dashed line is the contribution of s, the dotted line gives the contribution of v^0, and the dot-dashed line the contribution of the $\mathbf{v}$. Δ_{++}, Δ_{--}, and Δ_{+-} behave similarly to κ_{++}, κ_{--}, and κ_{+-}, i.e. they are largest at small r and then decrease to zero in the first two cases,

and they oscillate in the third case. From the upper and the lower parts of the figure it follows that the relativistic interaction produces Δ_{++} and Δ_{--} through completely different mechanisms. Δ_{++} is given by the cancellation of the large positive s term, the large negative v^0 term, and the smaller but not negligible $\mathbf{v}$ term. The first two terms are proportional to κ_{++}, while the last one to κ_{--}. On the contrary, Δ_{--} originates mostly from the large positive contribution of $\mathbf{v}$, which enters into the expression (4.17) with the large κ_{++}. s and v^0, being proportional to κ_{--} are, in this case, almost negligible. Finally, it is interesting to observe that Δ_{--} is of a factor 2 larger than Δ_{++}. This is due to the fact that the large matrix elements of the spin dependent part of V_{pp} are even amplified with the multiplication by κ_{++}. In the middle part of the figure the mixed component of the pairing field Δ_{+-} is plotted. It is an oscillating function of the coordinate, negative at $r = 0$ and it originates from the s-field only, as the contributions of v^0 and $\mathbf{v}$ cancel exactly. This is true only in the case of a δ interaction. The size of this component of the pairing field is negligible with respect of the other two components. This means that nearly no mixing of the large and small components of the Dirac spinors originates from pairing and therefore the operator $\boldsymbol{\sigma} \cdot \boldsymbol{\nabla}$ of the Dirac Hamiltonian which describes the ph-channel remains the only responsible for it.

In Fig. 4.7 we plot κ_{--}, Δ_{--}, and κ_{++}, Δ_{++} as functions of the radial coordinate for the three even Sn isotopes $A = 108$, 120, and 154. We have not shown κ_{+-} and Δ_{+-} because their contributions are negligible. By adding more neutrons, the essential features of the pairing tensor and field do not vary in a sensitive way; i.e. they are largest at small r, and then they decrease to zero. However, we observe that at small r, κ and Δ are larger for the lighter isotopes, and that they decrease to zero more slowly for the heavier nucleus. This is due to the fact that in the case of the ligther isotopes the s level gives the largest contribution, while in the case of the heavier nuclei the largest contribution comes from higher levels because changes in the shell structure.

We now go back to Fig. 4.1, and we concentrate on the discrepancy between E^{δ}_{pair} and E^{G}_{pair} in the mass regions $100 \leq A \leq 114$ and $A \geq 136$. In order to understand the origin of this difference, we first compare the expressions of the pairing field and energy for the pairing potential given in Eq.s (4.15)-(4.17) and (4.18)-(4.21), and for the Gogny force given in Eq.s (4.22) and (4.23). It has already been remarked that the Gogny force is used only with the elements of the pairing tensor given by the product of two large components of the Dirac spinor, while the relativistic pairing interaction uses all the components of κ. In particular we have seen that the spin dependent part of the relativistic model, i.e. $\mathbf{v}$, enters into the expression of Δ always with matrix elements of κ which are different from those connected to the spin independent term. Therefore, one may ask whether it is the spin dependent part of the interaction which is responsible for the discrepancies in the pairing energies. In order to answer this question, we have constructed a relativistic pairing interaction based only on the Lorentz scalar field s and on the timelike component of the Lorentz vector v-field, v^0, i.e. V_{pp}^{s,v^0} reduces only to the first line of Eq. (4.11). In this way the expressions of the pairing field given by Eq.s (4.15)-(4.17) and energy given by Eq.s (4.18)-(4.21), become very similar to the correspondent expressions used with the Gogny force given in Eq.s (4.22) and (4.23) respectively.

In Fig. 4.8 we display the pairing energies obtained by RHB calculations with different pairing interactions. The solid line shows the results obtained with the Gogny force, the long dashed line those obtained by using all the components of the relativistic interaction

with the cutoff $c_0 = 0.116$, and the dashed line refers to the calculations performed with the new relativistic s, v^0 interaction. We find that by switching off $\mathbf{v}$, the strength parameter c_0 has to be readjusted in order to reproduce $E_{pair}(A = 120)$. We observe that without $\mathbf{v}$, the discrepancy between E^{s,v^0}_{pair} and E^{G}_{pair} is reduced in particular in the mass region $100 \leq A \leq 114$. Although the effect of the $\mathbf{v}$ seems to be stronger in this mass range, also in the region $134 \leq A \leq 160$ the difference between E^{s,v^0}_{pair} and E^{G}_{pair} is also reduced. However, from this investigation we may only conclude that in particular for the lighter Sn isotopes the effect of $\mathbf{v}$ is very strong and changes the non-relativistic description of the pairing properties in finite nuclei. Unfortunately, it is not possible to make any statement about the realistic case. It can also be noticed that the use of the Gogny force in the pairing channel of the RHB equations does not take properly into account the spin degree of freedom.

Next, we consider the expression of the pairing energy given in Eq.s (4.18)-(4.21) for the (σ, ω) pairing potential of Eq. (4.11). As already discussed for the relativistic pairing field components, the Dirac matrices in the nucleon-meson vertices of the interaction (4.11) introduce some selection rules for the expression of the total pairing energy. In particular, the central spin independent part of Eq. (4.11) enters into E^{δ}_{pair} with terms proportional to $\kappa_{++}\kappa_{++}$ $\kappa_{--}\kappa_{--}$ $\kappa_{+-}\kappa_{+-}$, while the spin dependent part of the interaction shows terms proportional to $\kappa_{++}\kappa_{--}$ and $\kappa_{+-}\kappa_{-+}$. In the following we denote the terms $\kappa_{++}\kappa_{++}$ with E^{++++}, $\kappa_{--}\kappa_{--}$ with E^{----}, and so on. In Table 4.1 we show the the total neutron pairing energy for the three isotopes ^{108}Sn, ^{114}Sn, and ^{120}Sn, and the different contribution originating from the terms just discussed. We notice that the main contributions to E_{pair} are given by E^{++++} and E^{++--}. They are both negative and almost of the same size. From this we conclude that the spin independent and the spin dependent parts of V^{δ}_{pp} have the same importance in the production of pairing correlations in nuclei in a relativistic theory of the nuclear many-body problem. In the case of the lighter isotopes ^{108}Sn and ^{114}Sn E^{++--} is larger than E^{++++}, for ^{120}Sn we observe the opposite. Finally, the sizes of E^{----} and of E^{+-+-} are only about 1% of the the previous two terms, therefore they may be neglected in the discussion.

In Table 4.2 we repeat the same investigation for the relativistic pairing interaction s, v^0. In this case E^{++--} is zero, because $\mathbf{v}$ is not considered and, therefore E_{pair} results mainly from E^{++++} being E^{----} E^{+-+-} negligible. This situation is analogous to the case of the Gogny force.

In Table 4.3 we study the contributions of the different mesons to the total pairing energy for the relativistic (s, v) interaction of Eq. (4.11). s provides the largest attractive term, v^0 the repulsive one, and $\mathbf{v}$ another attractive term.

So far, all the results have been obtained starting from an antisymmetric pairing tensor. As already mentioned, this means that also the contribution of the antiparticles has been taken into account in the calculation of κ, it has been calculated using Eq. (4.10). In this respect it is still an open question whether the contribution of the antiparticles leads to a divergent term in κ, as they do in ρ. However, since in our subspace the antiparticles give a finite contribution to κ, we have investigated whether they influence the pairing properties of finite nuclei. In Fig. 4.9 we show the components κ_{++}, κ_{+-}, and κ_{--} of the relativistic pairing tensor κ in coordinate space and we study the contribution of the negative energy solutions of the Dirac equation. The solid and the dashed lines show the pairing tensor calculated with and without the contribution of the antiparticles.

A	E_{pair}	E^{++++}	E^{----}	E^{++--}	E^{+-+-}
108	-14.1	-6.81	-0.059	-7.25	0.036
114	-12.4	-6.11	-0.049	-6.25	0.040
120	-15.1	-7.75	-0.053	-7.38	0.088

Table 4.1: Total neutron pairing energy and contributions of the terms given in Eq.s (4.18)-(4.21) for the isotopes ^{108}Sn,^{114}Sn, and ^{120}Sn. The energies, given in MeV, are obtained with the relativistic pairing potential given in Eq. (4.11) for the cutoff $c_0 = 0.116$. In the pairing tensor the antiparticles are included.

A	E_{pair}	E^{++++}	E^{----}	E^{++--}	E^{+-+-}
108	-12.0	-12.0	-0.024	0.00	0.076
114	-12.1	-12.2	-0.022	0.00	0.112
120	-15.1	-15.2	-0.053	0.00	0.132

Table 4.2: Total neutron pairing energy and contributions of the terms given in Eq.s (4.18)-(4.21) for the isotopes ^{108}Sn,^{114}Sn, and ^{120}Sn. The energies, given in MeV, are obtained with the relativistic (s, v^0) pairing potential given in Eq. (4.11) for $c_0 = 0.207$. In the pairing tensor the antiparticles are included.

A	E_{pair}	E^{s}	E^{v^0}	$E^{\mathbf{v}}$
108	-14.1	-20.7	13.9	-7.27
114	-12.4	-18.6	12.5	-6.28
120	-13.3	-20.2	13.6	-6.68

Table 4.3: Total neutron pairing energy and contributions of the single meson as given in Eq. (4.11). The parameter $c_0 = 0.116$ is used in the calculations. The energies are in MeV.

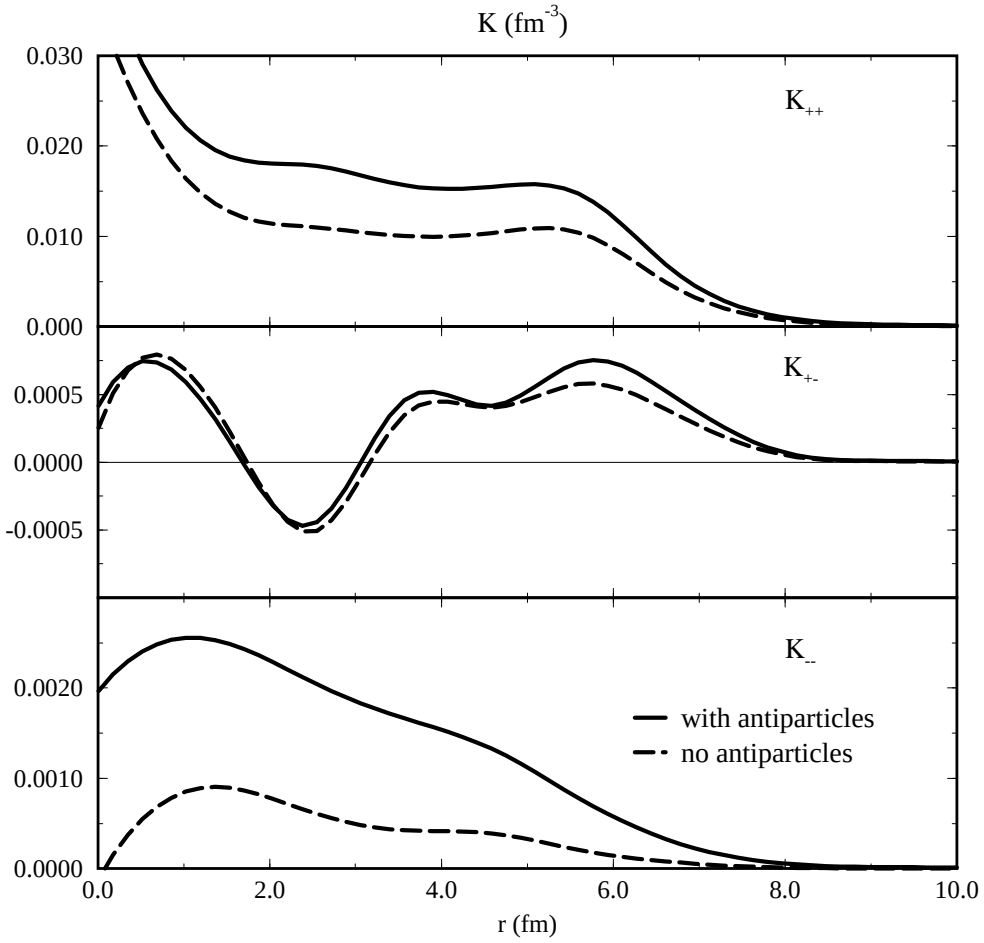

Figure 4.9: Self-consistent neutron pairing tensor components κ_{++},κ_{+-},and κ_{--} given in Eq. (4.10), as a function of the radial coordinate for ^{120}Sn. The calculations are performed by using the relativistic pairing potential given in Eq. (4.11) for $c_0 = 0.116$. The solid line shows the results obtained by considering also the negative energy solutions of the Dirac equation, while the dashed line shows the calculations in the no-sea approximation.

In the lower part of the figure we plot κ_{--}: we observe that the calculation without antiparticle is very much reduced compared to the full calculation. This result can be understood because the $\tilde{g}$ are the large components of the negative energy solutions of the Dirac equation. In particular, for small r they differ of a factor 3 and, as a consequence, the contribution of $\mathbf{v}$ to the pairing field is considerably reduced. In the middle part of the figure, we show κ_{+-} and in this case there is no considerable difference between the calculations with or without antiparticles. Finally, in the upper part of the figure we plot κ_{++}. In this case the calculation in the no-sea approximation is also reduced with respect to the full calculation, but the difference is less pronounced than in the case of κ_{--}. This agrees with the fact that the $\tilde{f}$ are the small components of the antiparticle solutions of the Dirac equation. Performing self-consistent RHB calculations with the pairing tensor calculated with and without antiparticles we have found considerably different results for the pairing energy. For example, a calculation of the nucleus ^{120}Sn with the cutoff $c_0 = 0.116$ gives a pairing energy E_{pair} of about -15 MeV when the pairing tensor includes the antiparticle solutions, while it gives a pairing energy of about -4 MeV if the pairing tensor is considered in the no-sea approximation. Therefore, the effect of the antiparticles is larger on the spin-dependent part of the relativistic pairing interaction.

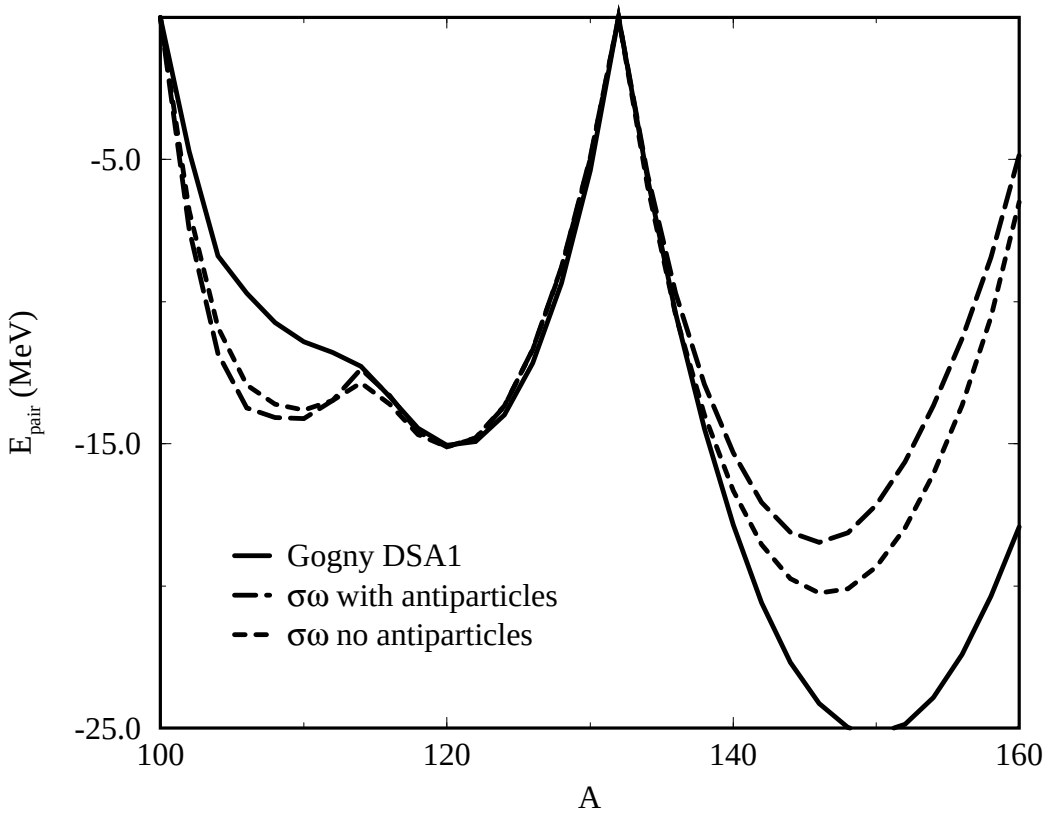

Figure 4.10: Neutron pairing energy of the even isotopes of Sn, as a function of the mass number A, calculated with the relativistic pairing interaction given in Eq. (4.11) for $c_0 = 0.116$ with and without antiparticles in the pairing tensor κ, and with non-relativistic Gogny force DSA1.

In the following we investigate whether the calculation of the relativistic pairing tensor κ given in Eq. (4.10) calculated in the no-sea approximation may resolve the discrepancy between $E^{\sigma,\omega}_{pair}$ and E^{G}_{pair} when also the antiparticles are considered. As already mentioned, the results which have just been presented, have been obtained by calculating κ as given in Eq. (4.10). In Fig. 4.10 we display the pairing energy as a function of the mass number for different RHB models. The solid line refers to the RHB model NL3+Gogny. In this case no antiparticles are considered in the calculation of the pairing tensor. The long dashed line corresponds to the RHB model NL3+(σ,ω) pairing potential with $c_0 = 0.116$, and the dashed line to the RHB model NL3+(σ,ω) pairing interaction for which the pairing tensor is calculated in the no-sea approximation, i.e. in Eq. (4.10) the terms containing $\tilde{f}$ and $\tilde{g}$ are omitted. Also in this case, neglecting the antiparticles contribution to κ leads to a much smaller pairing energy and therefore the cutoff parameter must be readjusted. It is observed that in the mass regions $100 \leq A \leq 114$ and $134 \leq A \leq 160$ the calculation of the pairing tensor in the no-sea approximation does not influence the results for E_{pair} very much, therefore it may be concluded that the discrepancy in the pairing energies obtained

A	E_{pair}	E^{++++}	E^{----}	E^{++--}	E^{+-+-}
108	-13.6	-9.32	-0.017	-4.32	0.049
114	-12.9	-8.94	-0.014	-3.96	0.057
120	-15.1	-10.8	-0.015	-4.43	0.116

Table 4.4: Total neutron pairing energy and contributions of the terms given in Eq.s (4.18)-(4.21) for the isotopes ^{108}Sn,^{114}Sn, and ^{120}Sn. The energies, given in MeV, are obtained with the relativistic (s, v) pairing potential given in Eq. (4.11) for $c_0 = 0.142$. The pairing tensor is calculated in the no-sea approximation.

with the fully relativistic RHB model and the RHB model NL3+Gogny is mainly due to the space-like component of the ω-meson.

In Table 4.4 we investigate the effects of the antiparticle on the different terms contributing to E_{pair}. Also in this case, the main contributions to E_{pair} originates from the negative terms E^{++++} and E^{++--}, which is now only about 40% of E^{++++}. This can be explained by the fact that in the no-sea approximation κ_{--} is more reduced that κ_{++} because the $\tilde{g}$ are the large components and the $\tilde{f}$ the small components of the antiparticles. As a consequence, the contribution of $\mathbf{v}$ is more quenched than the one of s and v^0.

Chapter 5

Relativistic HF Theory

The Lagrangian density (1.1) of the relativistic RMF theory is considered to be an effective Lagrangian in connection with the mean-field and the no-sea approximations. The equations of motion are derived from the classical variational principle, and, therefore, exchange terms are not included. The meson fields and their couplings are assumed to parametrize the G-matrix for the nucleon-nucleon scattering in the nuclear medium and possibly quantum field effects on the nucleons. The situation is fully analogous to the non-relativistic effective Hamiltonian in connection with Hartree-Fock calculations, as for example Skyrme forces, which are developed to parametrize the non-relativistic nucleon-nucleon G-matrix [Va73].

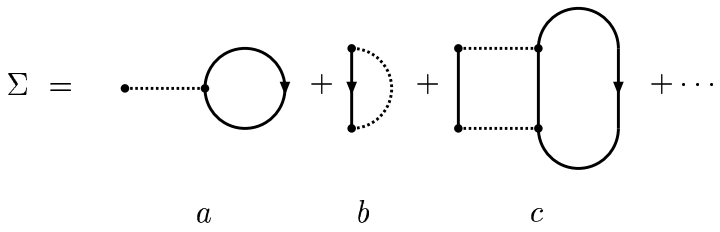

The figure illustrates the non-relativistic hierarchy of approximations for the many-body problem for the mass operator Σ which describes the difference between the free and the dressed Green's functions of a nucleon. Graph a represents the mean-field contributions, graph b the exchange term, and graph c the ladder series and higher corrections (e.g. core polarization diagrams). The according levels of approximations are: graph a corresponds to a Hartree theory, graphs $a + b$ correspond to the Hartree-Fock treatment, and graphs $a+b+c$ to the Brueckner theory. Although the situation is more involved in the relativistic case because also the quantum field effects have to be reduced in addition to the many-body effects, the relativistic hierarchy of approximations for the mass operator of the

nucleon Σ may again be illustrated by the same figure, and the stages of development can be taken analogously to the non-relativistic theory. One has to notice, anyway, that this representation ceases to distinguish the effects of the Dirac sea from the effects of the valence nucleons. However, in the contest of the mean-field and no-sea approximations the graph $a + b$ correspond to the relativistic Hartree-Fock.

As already discussed in Chapter 2, starting from a quantized version of the theory, Green's functions techniques allow the derivation of the relativistic HF (RHF) equations, which are technically much more difficult to solve than the relativistic Hartree (RH) equations. Another problem that has to be faced in going from a RH to a RHF approximation, is the treatment of the non-linear self energies of the σ-meson. As it is well known, these terms are essential for a quantitative description of finite nuclei properties, but their exchange term is not defined. So far, various relativistic models have been proposed and the corresponding RHF equations solved for infinite nuclear matter and finite nuclei. Although in the first models, self-energies of the σ-meson were neglected, they showed that the inclusion of the exchange term for isovector mesons changed considerably the properties of nuclear matter and finite nuclei. For example, in Ref.s [BMM85, BMG87] the RHF equations derived from the linear version of the (σ, ω)-, (σ, ω, π)-, and $(\sigma, \omega, \pi, \rho)$-models have been solved for nuclear matter and finite nuclei in coordinate space and it has been found that in going from the RH to the RHF approximation, meson masses and coupling constants have to be renormalized by $15 - 20\%$ in order to reproduce nuclear matter and finite nuclei properties. However, in the framework of these relativistic linear models, it was not possible to obtain a good description of the spin-orbit interaction and of the total binding energy. In order to include the self-interactions of the scalar field, two "philosophies" have been followed up to now. In one case (see Ref. [RWW90]), the σ self-energies were considered on the Hartree level, while the σ-meson exchange was treated in the Hartree-Fock approximation. In the second case (see Ref.s [BFG93, SMQ97]), a linearization recipe was introduced to treat them in the Hartree-Fock approximation.
Due to their more complex structure, the solution of the RHF equations is computationally much more involved than the solution of the Hartree equations. Together with the fact that the parameters set has to be readjusted, this means that to fit an effective force in the HF approximations is technically much more complicated than on the Hartree level.

In the next Sections we present a RHF model for the description of the nuclear many-body systems. Our starting point is a OBE interaction in the ph-channel containing the σ-, ω-, ρ-, and π-meson as degrees of freedom. Only the Fock term of the pion-exchange interaction is included explicitly, while the interactions originating form the exchanges of the σ-, ω-, and ρ-meson are considered at the Hartree level. This first approximation is justified by the fact that the masses of these mesons are large, and, as a consequence, the range of their interaction is very small. In the limit $m_m \to \infty$ we obtain zero-range forces. In this case the exchange term of the force has the same force of the direct term, up to a different factor (see Ref. [VB72]). We take the experimental values for the pion mass and coupling constant. Therefore the free parameters are the same as those in the RH approximation: i.e. the meson masses m_σ, m_ω, and m_ρ, and the coupling constants g_σ, g_ω, g_ρ, g_2, and g_ρ, and we would like to fit the same properties of finite nuclei used for the non-linear set NL3. Since m_π and f_π are fixed, to work in an expansion

of the Harmonic Oscillator wave functions (HOWF) is the most effective way to fit the parameters for the new effective force. In fact, in this way, the matrix elements for the pion exchange are calculated in the basis of the HOWFs only once, and then the HF equations are solved iteratively and at each iteration the pion exchange contribution is added to the Hamiltonian h. Pairing is treated in the BCS approximation. In addition, the RHF equations have to be solved for infinite nuclear matter in order to see if the nuclear saturation can be reproduced by the new force.

The rest of the Chapter is organized as follows: in Section 5.1 the RHF equations for nuclear matter are presented for the model that we use to fit the new force. As the fit to the finite nuclei properties requires a long time and it is now in progress, we present preliminary results for the parameters set obtained by fitting only the nuclear matter properties, and it will be shown that although they look reasonable, they do not work for finite nuclei. Therefore a fit to the finite nuclei properties is necessary. In Section 5.3 we present the general RHF equations for finite nuclei, and, finally, in Section 5.4 we apply them to the linear (σ, ω)- and (σ, ω, π)-model of Ref. [BMG87], in which the RHF equations were solved in coordinate space. First, we repeat some calculation for the bulk properties of the nuclei considered in Ref. [BMG87] for checking our numerics. In addition, we investigate also the exchange term contribution to the Hartree-Fock energies of the single meson exchanges for the (σ, ω)- and (σ, ω, π) models. As it is well known that the inclusion of the pion exchange modifies considerably the isospin dependence of the force from the Hartree approximation, we consider not only the stable double magic nuclei of Ref. [BMG87], but also the exotic short-lived ^{48}Ni, ^{100}Sn, and ^{132}Sn for which the isospin is stronger. We present now the RHF equations for infinite nuclear matter for the model previously discussed.

5.1 Relativistic HF Theory for Nuclear Matter

Since the RHF equations for nuclear matter have already been discussed extensively in the literature, see for example Ref. [BMM85] and the references therein, in this Section we only briefly remind the most important points. The Hartree-Fock equations are obtained by defining an approximate effective Hamiltonian H_0 in terms of an approximate field operator $\psi_0(x)$ satisfying the following Dirac equation

$$(-i\gamma^\mu \partial_\mu + M + \Sigma)\psi_0(x) = 0, \tag{5.1}$$

We now consider the baryon self-energy Σ produced by the meson exchanges. As already pointed out in Ref. [HS83, SW86], in nuclear matter, due to time-reversal and rotational invariance, Σ may be written quite generally as

$$\Sigma(\mathbf{p}) = \Sigma_S(p) + \gamma_0 \Sigma_0(p) + \boldsymbol{\gamma} \cdot \hat{\mathbf{p}} \Sigma_V(p), \tag{5.2}$$

where $\hat{\mathbf{p}}$ is the unit vector along $\mathbf{p}$. The different components of Σ, the scalar Σ_S, the time component Σ_0 and the space component Σ_V of the vector, are functions of $p = (E(p), \mathbf{p})$. This Ansatz for Σ leads to an equation for $\psi_0(x)$ in infinite medium formally identical to the equation for free particles. The solution is finally used to calculate the energy density per given volume Ω

$$\Omega\epsilon = \langle \phi_0 | H_0 | \phi_0 \rangle \equiv \langle T \rangle + \langle V \rangle \tag{5.3}$$

$M = 939.0$ (MeV)	
$m_\sigma = 522.521$ (MeV)	$g_\sigma = 10.150$
$m_\omega = 783.000$ (MeV)	$g_\omega = 12.774$
$m_\rho = 763.000$ (MeV)	$g_\rho = 3.548$
$m_\pi = 138.000$ (MeV)	$f_\pi/4\pi = 0.08$
$g_2 = -9.521$ (fm^{-1})	$g_3 = -26.790$

Table 5.1: Parameters of the preliminary effective interaction NLHF.

where $\langle T \rangle$ is the kinetic energy and $\langle V \rangle$ is the potential energy which consists of the direct and exchange terms, $\langle V_D \rangle$ and $\langle V_E \rangle$ respectively. The detailed expressions of the Dirac equation for ψ_0 and for ϵ are given in Appendix C.

5.1.1 Preliminary Fit

Although the Lagrangian parameters are usually obtained by a fitting procedure to some bulk properties of a set of spherical nuclei, due to the technical difficulties caused by the inclusion of the Fock term of π, we have done a preliminary fit of the Lagrangian parameters set using only nuclear matter properties, i.e. saturation density ρ_0, binding energy per particle $(E/A)_\infty$, nuclear matter incompressibility K, asymmetry energy J, and the effective mass M^*/M. In Table 5.1 we show the values for the new preliminary parameters set NLHF. The nucleon mass M is fixed to 939.0 MeV, the masses of the ω- and of the ρ-meson are also fixed to their empirical values of 783.0 and 763.0 MeV respectively, as well as the mass of the π-meson (138.0 MeV) and its coupling constant $f_\pi/4\pi$ (0.08). Then, we have calculated the charge radius and the total binding energy of two magic nuclei, the light ^{16}O and the heavy ^{208}Pb, in order to study whether a parameters set fitted only to nuclear medium properties, may lead to reasonable predictions for finite nuclei properties. From Table 5.2, in which the bulk properties of ^{16}O and ^{208}Pb are listed, we see that with the parameters set NLHF the total binding energies result in overbinding for the heavy nucleus and underbinding for the light one with respect to the experimental values also included in the Table. We can therefore draw the conclusion that a fitting procedure based on infinite nuclear matter only is not enough to make reasonable predictions for finite nuclei. It is therefore absolutely necessary to fit masses and couplings of the relativistic Lagrangian density to finite nuclei bulk properties. Such a fit is in progress now. The same set of spherical nuclei and the same bulk properties used for NL3 [LKR97] are considered.

5.2 Relativistic Hartree-Fock Theory for Finite Nuclei

Although the aim of our work is to adjust a new effective force containing only the exchange term of the pions in addition to the degrees of freedom of standard RH approximations, in this Section we develop the RHF equations for finite nuclei for the exchange

	^{16}O		^{208}Pb	
	E_{tot}	r_{ch}	E_{tot}	r_{ch}
NLHF	−135.82	2.699	−1611.94	5.517
Exp.	−127.62	2.730	−1636.47	5.503

Table 5.2: Total energies E and charge radius r_{ch} of ^{16}O and ^{208}Pb calculated with the preliminary set of parameters NLHF. The energies are in MeV and the charge radii in fm.

	g_σ	g_ω
(a) $(\sigma+\omega)_H$	8.862	13.802
(b) $(\sigma+\omega)_{HF}$	8.344	12.402
(c) $(\sigma+\omega+\pi)_{HF}$	8.200	12.493

Table 5.3: Isoscalar scalar σ and isoscalar vector ω meson coupling constants for the linear model in Ref. [BMG87]. All the parameters correspond to $m_\sigma = 440.0$ (MeV), $m_\omega = 783.0$ (MeV), and $m_\sigma = 763.0$ (MeV)

term of an arbitrary nucleon-meson vertex of the interaction Lagrangian density (1.1). We write the general expression for the RHF self-consistent field Γ^{HF}_{ac} and the energy E^{HF} energy. In Appendix H the explicit expressions of the self-consistent field for every nucleon-meson vertex considered in the model are given.

5.2.1 RHF Equations

As seen in Chapter 2, the relativistic Hartree-Fock equations may be derived from the canonical quantization of the meson fields. Therefore, we start here from the relativistic Hamiltonian h defined in Eq. (2.44) in which the mass operator as given in Eq. (2.44) by

$$\Sigma_{\alpha\gamma} = \delta_{\alpha\gamma} M + \Gamma^{HF}_{\alpha\gamma} \tag{5.4}$$

contains explicitly the direct and the exchange terms of the self-consistent field Γ^{HF}_{ac}

$$\begin{aligned} \Gamma^{HF}_{\alpha\gamma} &= \sum_{\beta\delta} (v_{\alpha\delta\gamma\beta} - v_{\alpha\delta\beta\gamma}) \rho_{\beta\delta} \\ &\equiv \Gamma^{H}_{\alpha\gamma} + \Gamma^{F}_{\alpha\gamma} \end{aligned} \tag{5.5}$$

where $v_{\alpha\delta\gamma\beta}$ are the relativistic two-body matrix elements of an OBE interaction and $\rho_{\beta\delta}$ is the relativistic generalized density matrix given in Eq. (4.11). The relativistic indices $\alpha \ldots$ have been defined in Eq.s (D.6) and (D.7). Since the Hartree approximation has been treated extensively in the literature, see for example Ref. [Ri96], in the following we concentrate on the exchange term of the RHF approximation. Explicitly the exchange term of the self-consistent field $\Gamma^{F}_{\alpha\gamma}$ of an arbitrary meson-exchange interaction m reads

$$\Gamma^{Fm}_{\alpha_1\alpha_3} = -\sum_{\alpha_2\alpha_4} \langle \alpha_1\alpha_2 | V_m | \alpha_4\alpha_3 \rangle \ \rho_{\alpha_4\alpha_2} \tag{5.6}$$

and the corresponding energy

$$E^{Fm}[\rho] = -\frac{1}{2} \sum_{\alpha_1\alpha_3} \rho_{\alpha_3\alpha_1} \ \Gamma^{Fm}_{\alpha_1\alpha_3}. \tag{5.7}$$

In this expression the sum runs also over neutron and proton states. The relativistic two-body matrix elements in Eq. (5.6) are given by

$$\langle \alpha_1\alpha_2 | V_m | \alpha_4\alpha_3 \rangle = \langle a_1 p_1 a_2 p_2 | \left(\gamma^0\Gamma^m\right)_{p_1p_4} \left(\gamma^0\Gamma^m\right)_{p_2p_3} D_m(r) | a_4 p_4 a_3 p_3 \rangle \tag{5.8}$$

where the meson propagators D_m are discussed in Appendix A. The expressions of the relativistic two-body matrix elements in terms of the HOWFs are given explicitly in Appendix D, E and F.

5.2.2 The Linear RHF/(σ, ω, π)-Model

As first application of the RHF equations for finite nuclei discussed in the previous Section, we consider the RHF/(σ, ω, π) model presented in Ref. [BMG87], in which the RHF equations have been solved in coordinate space. It contains the Hartree terms for the

mesons σ and ω, and the Fock terms for σ, ω and π, and no self-energies of the σ-meson are included. The investigations of ground state properties of the nuclei already studied in Ref. [BMG87] are a good test for our numerics which has been developed to solve the RHF equations as fast as possible in order to perform an effective fit of the new force parameters set. In fact, although fast, our method is based on an expansion of the nuclear wave functions in terms of Harmonic Oscillator wave functions, whose radial part is difficult to handle for large oscillator numbers.

In addition to the stable nuclei studied in Ref. [BMG87], we have considered also magic nuclei towards both the neutron and the proton driplines in order to investigate the role of the Fock terms on the properties of exotic nuclei, whose nuclear potential structure is expected to change significantly as the limit of the nuclear existence is approached. We have compared the results obtained with the RHF/(σ, ω, π)-model with the RH calculations performed with the parameters set NL3, whose predictions have been shown to be in good agreement with the experimental data of binding energies of the known stable nuclei and with the extrapolations for the exotic nuclei given in Ref. [AW93].

The rest of the Section is organized as follows: we first investigate the Fock term contributions of the different meson-exchange potential to the total Fock energy. Then, we turn our attention to the neutron and the proton spin-orbit splittings in isotopic chains of Ca and Sn nuclei. In this way we can see explicitly the role of the spin-isospin term of the nuclear force introduced the inclusion of the pion. Comparisons are always made between the RHF and the RH approaches and the available experimental data. Finally, we compare the neutron and the proton single-particle spectra.

Table 5.4 shows the binding energies per particle E/A, the rms charge radii r_c, and the proton spin-orbit splittings ΔE_{ls} of some double closed shell nuclei calculated in the framework of the RHF/(σ, ω, π)-model and of the RH theory. The used meson masses and couplings are given in Table 5.3 (parameters set c)) and in Table 1.1 respectively. First of all, the calculations for ^{16}O, ^{40}Ca, and ^{48}Ca are in excellent agreement with the results shown in Ref. [BMG87]. As already remarked, this constitutes a good test for our numerics in the case of light nuclei. However, one of the major problem that we have encountered concerned heavier nuclei, e.g. ^{208}Pb, whose ground state properties were not shown in Ref. [BMG87] in the framework of the (σ, ω, π)-model. In fact, in this case, more nuclear shells are occupied, and therefore, it is essential to treat the fast oscillating radial HOWFs with the greatest accuracy. To test our numerics for heavy nuclei, we have implemented a version of our code which used the NAG Library for the evaluation of the two-body matrix elements of the exchange term of the OBE interaction (5.8). The results of the two versions are the same up to the fifth-sixth digit. In addition to these nuclei, we have considered also ^{48}Ni, ^{100}Sn, ^{132}Sn, and ^{208}Pb in order to investigate the contribution of the pion-exchange in the case of large neutrons and protons excess. From the first column of the table we observe that in the framework of the RHF/(σ, ω, π)-model the nuclei are underbound. In the second part of the Table we show the E/A obtained with the parameters set NL3 of the RH theory. In this case, the results are in good agreement with the experimental data available for ^{16}O, ^{40}Ca, ^{48}Ca, and ^{208}Pb and with the extrapolations for the exotic ^{100}Sn, ^{132}Sn (see for example Ref. [AW93]). On the contrary RH and RHF calculations of the rms charge radii are in a better agreement, although r_c obtained with the (σ, ω, π)-model are somewhat larger than the r_c's given by

Nucleus	Dirac-Hartree-Fock			Dirac-Hartree		
	E/A	r_c	ΔE_{ls}	E/A	r_c	ΔE_{ls}
^{16}O	-3.10	2.91	5.04	-7.28	2.73	6.40
^{40}Ca	-4.90	3.59	7.07	-8.32	3.45	6.62
^{48}Ca	-5.36	3.57	3.54	-8.47	3.47	6.38
^{48}Ni	-4.01	3.86	4.62	-7.10	3.78	4.62
^{100}Sn	-5.38	4.55	1.73	-8.22	4.47	5.70
^{132}Sn	-6.03	4.73	1.20	-8.32	4.71	4.24
^{208}Pb	-5.81	5.52	1.08	-7.85	5.52	1.66

Table 5.4: Binding energy per particle E/A, rms charge radii r_c, and proton spin-orbit splittings ΔE_{ls} calculated in the framework of the RHF (σ, ω, π) model (parameters set (c) of Table 5.4) and of the RMF theory with the parameters set NL3 (Table 1.1). E/A and the proton ΔE_{ls} for the $1p$ shell (^{16}O), $1d$ shell (^{40}Ca, ^{48}Ca, ^{48}Ni), and $1f$ shell (^{100}Sn, ^{132}Sn, and ^{208}Pb) are given in MeV; the rms charge radii are in fm.

RH. Probably this is a consequence of the lower binding energies. More interesting is the situation of the proton spin-orbit splittings ΔE_{ls}, defined by

$$\Delta_{LS} = E_{n,l,j=l-1/2} - E_{n,l,j=l+1/2}. \tag{5.9}$$

Apart from ^{48}Ca, we observe an overall reduction of ΔE_{ls} in going from the Hartree to the Hartree-Fock approximation. We will come back to this point later with further investigations of neutron and proton spin-orbit splittings for isotopic chains of Ca and Sn nuclei.

In Table 5.5 we consider the total energy of the Fock term of the OBE interaction E^F

$$E^F = \sum_m E^{Fm} \tag{5.10}$$

where the E^{Fm} are the contributions of the different mesons given in Eq. (5.7), and the index m stands for σ, ω, and π. As in RH approximations, E^F results from a subtle cancellation of the various meson fields. We first consider the σ-meson, responsible for the attraction in RH calculations: as expected, $E^{F\sigma}$ becomes positive, and it amounts to $\approx 21\%$ of the corresponding Hartree term. Second, we consider the π-meson. It is well known, see for instance Ref.s [BMG87, BMM85] that the OBE potential produced by the exchange of π in the pseudo-vector coupling scheme contains a repulsive contact interaction δ_π (see Appendix E.3). This δ-term is neglected in these calculations as often in the literature, with the argument that the short-range repulsion is already described by the ω-meson. In the second and third columns of Table 5.5, we show the contributions to the exchange energy of the pion. $E^{F\delta_\pi}$ is the energy originating from the δ-term and $E^{F\pi}$

Nucleus	$E^{F\sigma}$	$E^{F\pi}$	$E^{F\pi_\delta}$	$E^{F\omega^0}$	$E^{F\boldsymbol{\omega}}$	E^F
^{16}O	328.84	123.71	−191.09	−283.89	25.40	2.97
^{40}Ca	956.52	376.63	−569.00	−835.87	106.04	34.32
^{48}Ca	1231.53	497.25	−729.92	−1091.92	142.98	50.77
^{48}Ni	1201.63	487.39	−716.79	-1060.79	134.62	46.06
^{100}Sn	2725.34	1147.66	−1654.43	-2423.88	355.06	149.75
^{132}Sn	3675.13	1463.35	−2116.91	-3273.22	505.49	253.84
^{208}Pb	5864.47	2347.40	−3420.20	-5216.41	842.65	417.91

Table 5.5: Fock energies of the different mesons exchanges calculated in the framework of the RHF (σ, ω, π) model with the parameters set (c) of Table 5.3. E^{Fm} are expressed in MeV.

is the full contribution of the pion (containing the δ-term). In fact, only the difference $E^{F\pi} - E^{F\delta_\pi}$ enters in our calculations. The presence of the δ-force makes $E^{F\pi}$ positive, and, at the same time, the removal of the δ-force leaves $E^{F\pi}$ negative. The sum of these two terms results in the usual attractive term for the pions. Third, we consider the ω-meson for which the situation becomes more involved than in Hartree approximation. On the contrary to RMF theory, in which only the time component ω^0 of the ω-exchange potential does not vanish, in the RHF approximation also the spatial component $\boldsymbol{\omega}$ contributes. In particular, we observe that the Fock energy of ω^0 is negative, while that one of $\boldsymbol{\omega}$ is positive because of the Lorentz scalar product of the Dirac matrices in the two-body interaction term of the nuclear Hamiltonian. As already seen in Chapter 4 for the RHB theory, relativity separates the spin independent and the the spin dependent part of the nuclear force. This is due to the structure of the Dirac matrices that mixes large and small components of the self-consistent field and of the generalized density matrix. In the fourth and fifth columns we list the Fock energies corresponding to ω^0 and $\boldsymbol{\omega}$: $E^{F\omega^0}$ is attractive and it amounts to $\approx 22\%$ of the RH term of the ω-meson for all the nuclei in the Table. On the other side, $E^{F\boldsymbol{\omega}}$ is much smaller. This is due to the fact that the Dirac matrices $\boldsymbol{\gamma}^i$ in the nucleon-meson vertex $\Gamma^{\boldsymbol{\omega}}$ mixes large and small components of the self-consistent field and of the generalized density matrix. Finally, in the last column of the Table, the total Fock energies E^F as in Eq. (5.10) are given. We observe that it increases from the lighter to the heavier nuclei. In particular, the strength of E^F goes from $\approx 4.5\%$ of the total energy in ^{16}O up to $\approx 35\%$ in ^{208}Pb. This seems to be connected not only to the neutron excess, but also with the nuclear mass.

In order to investigate further the importance of the spin-isospin term of the nuclear interaction introduced by the exchange term of the π-meson, we explicitly write E^F of Eq. (5.7) as sum of the neutron and proton exchange energies E^{Fn} and E^{Fp} respectively:

$$\begin{aligned} E^F &= \sum_{13} \rho^n_{31} \Gamma^{Fn}_{13} + \sum_{13} \rho^p_{31} \Gamma^{Fp}_{13} \\ &\equiv E^{Fn} + E^{Fp}. \end{aligned} \tag{5.11}$$

Nucleus	E^{Fn}	E^{Fp}	E^{F}
^{16}O	1.94	1.03	2.97
^{40}Ca	19.48	14.86	34.34
^{48}Ca	47.51	3.26	50.77
^{48}Ni	6.59	39.46	46.05
^{100}Sn	83.98	65.79	149.77
^{132}Sn	256.54	−2.70	253.84
^{208}Pb	407.14	10.77	417.91

Table 5.6: Neutron and proton Fock energies calculated in the framework of the RHF (σ, ω, π) model with the parameters set (c) of Table 5.3. E^{Fn} and E^{Fp} are expressed in MeV.

Nucleus	$E^{F\sigma}$	$E^{F\omega^0}$	$E^{F\boldsymbol{\omega}}$	E^{F}
^{48}Ca	1298.10	−1099.34	155.58	354.34
^{48}Ni	1269.74	−1071.45	147.01	345.30
^{100}Sn	2880.09	−2450.52	390.52	820.09
^{132}Sn	3873.39	−3297.95	552.20	1127.64

Table 5.7: Fock energies of the different mesons exchanges calculated in the framework of the RHF (σ, ω) model with the parameters set (b) of Table 5.3. E^{Fm} are expressed in MeV.

In Table 5.6 we show the Fock energies of neutrons and protons in the second and third column respectively and the total exchange energy in the last column of the Table for the spherical nuclei previously considered. For the $N \approx Z$ nuclei, i.e. ^{16}O, ^{40}Ca, and ^{100}Sn, E^{Fn} and E^{Fp} have a comparable magnitude. For the nuclei with neutron or proton excess the situation is completely different: in the $N > Z$ case, i.e. ^{48}Ca, ^{132}Sn, and ^{208}Pb, E^{Fn} gives the bigger contribution to E^{F}, while in the $Z > N$ case, i.e. ^{48}Ni, E^{Fp} gives the larger contribution to E^{F}. In order to understand whether these results depend upon the isovector nature of the π-meson exchange, we follow two ways. First, only for the nuclei with neutron or proton excess, we repeat the same calculations just shown, using the RHF (σ, ω)-model of Ref. [BMG87] (parameters set (b) of Table 5.3). As this seems to suggest that the π-meson exchange is really responsible for this behavior, second, we try to isolate the neutrons and protons contributions to E^{Fn} and E^{Fp} in the contest of the RHF/(σ, ω, π)-model.

In analogy with the RHF/(σ, ω, π)-model, in Table 5.7 we list the σ- and ω-meson contributions to E^{F}. As before, E^{F} results from a cancellation of the various meson

Nucleus	E^{Fn}	E^{Fp}	E^{F}
^{48}Ca	214.88	139.45	354.33
^{48}Ni	145.01	200.30	345.31
^{100}Sn	423.92	396.17	820.09
^{132}Sn	774.02	353.62	1127.64

Table 5.8: Neutron and proton Fock energies calculated in the framework of the RHF (σ, ω) model with the parameters set (b) of Table 5.3. E^{Fn} and E^{Fp} are expressed in MeV.

contributions. In this case, the Fock terms are stronger than in (σ, ω, π)-model.

E^{Fn} and E^{Fp} are given in Table 5.8: in the RHF (σ, ω)-model they are always of comparable sizes. Therefore, it seems that the the π-meson exchange plays an important role.

To investigate further this discrepancy, we explicitly write E^{Fn} and E^{Fp} in terms of neutron and proton self-consistent fields. Using the two-body matrix elements of the isospin part of the nuclear interaction given in Appendix I for E^{Fn} we obtain

$$\begin{aligned} E^{Fn} &= \sum_{13} \rho^n_{31}\Gamma^n_{13} = \sum_{13} \rho^n_{31}(v_{1243}\rho^n_{42} + 2v_{1243}\rho^p_{42}) \\ &= E^{Fnn} + E^{Fnp} \end{aligned} \tag{5.12}$$

and, analogously for E^{Fp}

$$\begin{aligned} E^{Fp} &= \sum_{13} \rho^p_{31}\Gamma^p_{13} = \sum_{13} \rho^p_{31}(v_{1243}\rho^p_{42} + 2v_{1243}\rho^n_{42}) \\ &= E^{Fpp} + E^{Fpn}. \end{aligned} \tag{5.13}$$

E^{Fn} and E^{Fp} contain a $T = 0$ and a $T = 1$ contributions. From Appendix I, we see that the $T = 1$ originates from the exchange of both isoscalar and isovector meson, while the $T = 0$ only from the exchange of isovector meson and it gives the factor 2 in front of the matrix elements. Finally, we can remark that in Eq.s (5.12)-(5.13) E^{Fnn} and E^{Fpp} are different in size due to the neutron and the proton densities ρ^n and ρ^p, while it holds

$$E^{Fnp} = E^{Fpn}.$$

In Table 5.9 we list E^{Fnn}, E^{Fpp}, and E^{Fnp} and the corresponding E^{Fn} and E^{Fp} for the nuclei with neutron and proton excess. We notice that E^{Fnn} and E^{Fpp} are always positive, while E^{Fnp} is always negative, i.e. the π-meson exchange, which is responsible for the the Fock energy in the $T = 0$ channel binds the system. In addition, it is possible to state in ^{48}Ca, ^{132}Sn, and ^{208}Pb, the large E^{Fn} originates from the neutron excess ($E^{Fnn} > E^{Fpp}$), as well as in ^{48}Ni the large E^{Fp} originates from the proton excess ($E^{Fpp} > E^{Fnn}$).

Nucleus	E^{Fnn}	E^{Fpp}	E^{Fnp}	E^{Fn}	E^{Fp}
^{48}Ca	125.51	81.26	−78.00	47.51	3.26
^{48}Ni	83.60	116.47	−77.01	6.59	39.46
^{132}Sn	467.90	208.66	−211.36	256.54	−2.70
^{208}Pb	756.21	35.84	−349.07	407.14	10.77

Table 5.9: Neutron and proton Fock energies calculated in the framework of the RHF (σ, ω, π) model with the parameters set (c) of Table 5.3. The energies are expressed in MeV.

On the left and on the right side of Fig. 5.1 we display the energy splittings of spin-orbit neutron and proton partners for Ca isotopes respectively, as function of the mass number A. The filled circles refer to the RHF/(σ, ω, π)-model calculations, the stars to the results obtained with RMF (parameters set NL3), and the triangles are the experimental data. For the Ca isotopes with open shells, pairing has been treated with the filling approximation. Apart from the $2p$ shell of proton spin-orbit partners, the calculations of ΔE_{ls} show a linear A-dependence. We now consider the proton spin-orbit partners in the $1d$ shell. While the value of RMF decrease only slightly (fairly constant), those of the RHF/(σ, ω, π)-model show a much larger decrease (about 3 MeV). This is agreement with the results of Ref. [LGM00], in which the same investigation is made in the framework of different self-consistent relativistic and non-relativistic approaches. In particular, we may compare our results for the proton spin-orbit partners of this shell with the calculations of Ref. [LGM00], performed with the RHF/$(\sigma, \omega, \pi, \rho)$-model of Ref. [BMG87]. Both show the same strong dependence of ΔE_{ls} on the neutron number. In the framework of the RHF/(σ, ω, π)-model the proton $\Delta E_{ls}(1d)$ are 7.1 MeV for ^{40}Ca and 4.06 MeV for ^{48}Ca, while in the framework of the RHF/$(\sigma, \omega, \pi, \rho)$ model they are 8.01 MeV and 4.06 MeV respectively. We can thus conclude that the major responsible for the strong decrease of ΔE_{ls} in dependence on A is the light π-meson. We observe the same situation for the neutron spin-orbit partners in the $1d$ shell. There is still a linear decrease of ΔE_{ls}, of about 2.0 MeV in the RHF/(σ, ω, π)-model and of 0.5 MeV in RMF/NL3, which agrees fairly well with the experimental data, available for ^{40}Ca only. In the $1f$ shell we still observe a linear dependence of ΔE_{ls} on A for both neutrons and protons. However, while the proton and the neutron spin-orbit partners decrease of about 2.0 MeV and 1.0 MeV respectively in the RHF/(σ, ω, π)-model, they increase of about 2.0 MeV and 1.0 MeV in RMF. The only experimental data available for ^{48}Ca (see for example Ref.s [Ma93, Ma94]) is not reproduced by any of the two approaches. Finally, in the $2p$ shell the linear dependence of the ΔE_{ls} is still shown by the neutron spin-orbit partners: in this case RHF/(σ, ω, π) and RH/NL3 give the same predictions for ΔE_{ls} which decreases of about 0.6 MeV in going from $A = 40$ to $A = 48$. Again, none of the two approaches reproduces the experimental data. The results of the RHF and RH for the proton spin-orbit partners in the $2p$ shell are quite different and no linear dependence is observed anymore. In the first case, ΔE_{ls} increases from 1.2 MeV at $A = 40$ to 1.4 MeV at $A = 42$, and then decreases till about 1.1

MeV at $A = 48$. RMF predicts a smooth increase of ΔE_{ls} only of about 0.1 MeV along all the Ca isotopic chain. In general, the predictions of the two relativistic approaches agrees better for ^{40}Ca and ^{42}Ca, i.e. for $N \approx Z$, than for heavier isotopes. This suggests that the effects of the Fock terms are stronger in nuclei with a large neutron excess. This is particularly interesting in relation with the still open question of the isospin dependence of the spin-orbit splittings.

In Fig. 5.2 we plot the energy splittings of spin-orbit neutron and proton partners for Sn isotopes. The notations used are the same as in the previous Figure. In this case pairing has been included with the BCS approximation. As input values, we have taken the results of the average neutron pairing gaps $\langle \Delta_N \rangle$ obtained with the RHB calculations of Ref. [LVR98]. We have considered the shells $1f$, $1g$, and $1h$. Apart from the proton $1h$ shell in which it is constant, we observe that RMF always predicts a decrease of ΔE_{ls} in going from $A = 100$ to $A = 132$. In every shell that we have considered it decreases of about 2.0 MeV although for neutron is somewhat larger. In the framework of the RHF/(σ, ω, π) model the behavior of ΔE_{ls} is very different: it always starts at a minimum value, then it increases till $A = 116$, and, finally, it decreases again till $A = 132$. For each shell we find $\Delta E_{ls}(100) > \Delta E_{ls}(132)$. Considering the proton spin-orbit splittings for the $1f$ shell and making a comparison with the results shown in Ref. [LGM00], we can conclude again that the main responsible for the different behavior of ΔE_{ls} in the RHF approach is due to the π-meson, while the ρ-meson tensor and vector-tensor terms seems to shift the spin-orbit splittings of about 1.0 MeV along all the isotopic chain. From the Figures 5.1 and 5.2 we have observed that the spin-orbit splitting is reduced in going from the RH to the RHF approaches to the nuclear many-body problem. Although the Fock terms of the isoscalar σ- and ω-meson are included, also this is mainly due to the isospin dependence of the exchange term of the π-meson. This question is important because the isospin dependence is supposed to be one of the factors contributing to significant structural changes in nuclei with large neutron excess.

In order to understand whether the magnitude of the splittings of spin-orbit partners depend on the neutron excess, in Table 5.10 - 5.14 we show neutron and proton single particle states in $N \approx Z$ nuclei, namely ^{16}O, ^{40}Ca, and ^{100}Sn, and in nuclei with a large neutron excess $N > Z$, namely ^{132}Sn and ^{208}Pb. The experimental data are taken from Ref. [IEM01] where an isospin dependence of a mean spin-orbit potential is suggested also by the use of the latest experimental data on ^{132}Sn and of the extrapolation of the properties of nuclei with less neutron deficiency for ^{100}Sn. From the experimental values of the neutron and the proton single particle states, it is seen that in the $N \approx Z$ (see Tables 5.10-5.12) the spin-orbit splittings differ only from $1 - 2\%$, while in the $N > Z$ nuclei (see Tables 5.13-5.14) the neutron spin-orbit splitting is about 10% larger than the corresponding proton spin-orbit splittings. Going to the calculations of the two relativistic approaches to the nuclear many-body problem, we observe that the RHF/(σ, ω, π) model predicts a neutron spin-orbit splitting always about 10% stronger than the corresponding proton spin-orbit splitting in both $N \approx Z$ and $N > Z$ nuclei. On the other side, in the framework of RMF the neutron and the proton spin-orbit splittings differ from a few percent $(1 - 2)$ in almost all the considered cases in both $N \approx Z$ and $N > Z$ nuclei. From this, it follows that the spin-orbit splitting remains still an open question. It will be interesting to see how it will be described in the framework of the non-linear Dirac Hartree-Fock model.

Neutrons				Protons			
nlj	Exp.	RHF	RH	nlj	Exp.	RHF	RH
$1d_{3/2}$	(0.94)	2.45	1.02	$1d_{3/2}$	(4.40)	5.02	3.97
$2s_{1/2}$	-3.27	-1.49	-2.43	$2s_{1/2}$	-0.11	1.23	0.49
$1d_{5/2}$	-4.14	-2.41	-4.83	$1d_{5/2}$	-0.60	0.81	-1.38
$1p_{1/2}$	-15.67	-11.00	-15.25	$1p_{1/2}$	-12.13	-7.43	-11.46
$1p_{3/2}$	(-21.84)	-16.69	-21.27	$1p_{3/2}$	(-18.45)	-12.94	-17.85
$1p$	6.17	5.69	6.02	$1p$	6.32	5.51	6.39
$1d$	4.18	4.86	5.85	$1d$	5.00	4.21	5.35

Table 5.10: Neutron and proton single particle states of ^{16}O, and spin-orbit of the $1p$ and $1d$ shells. RHF and RH refer to the σ, ω, π-model and to NL3 respectively. The energies are expressed in MeV.

Neutrons				Protons			
nlj	Exp.	RHF	RH	nlj	Exp.	RHF	RH
$1f_{5/2}$	-3.48	1.03	-1.43	$1f_{5/2}$	3.86	6.90	5.13
$2p_{1/2}$	-4.42	-1.24	-2.12	$2p_{1/2}$	2.64	4.21	3.83
$2p_{3/2}$	-6.42	-2.99	-3.86	$2p_{3/2}$	0.63	2.93	2.39
$1f_{7/2}$	-8.36	-6.66	-8.65	$1f_{7/2}$	-1.09	0.18	-1.64
$1d_{3/2}$	-15.64	-12.51	-16.18	$1d_{3/2}$	-8.33	-5.40	-8.83
$2s_{1/2}$	-18.11	-14.46	-17.00	$2s_{1/2}$	-10.85	-7.33	-9.68
$1d_{5/2}$	-21.64	-19.86	-22.89	$1d_{5/2}$	-14.33	-12.47	-15.45
$1f$	4.88	7.69	7.22	$1f$	4.95	6.72	6.77
$2p$	2.00	1.75	1.74	$2p$	2.01	1.28	1.44

Table 5.11: Neutron and proton single particle states of ^{40}Ca, and spin-orbit of the $1f$ and $2p$ shells. RHF and RH refer to the σ, ω, π-model and to NL3 respectively. The energies are expressed in MeV.

Neutrons				Protons			
nlj	Sys.	RHF	RH	nlj	Sys.	RHF	RH
$1h_{11/2}$	$-8.6(5)$	-2.43	-5.82	$1g_{7/2}$	$3.90(15)$	3.97	3.97
$2d_{3/2}$	$-9.2(5)$	-6.49	-7.30	$2d_{5/2}$	$3.00(80)$	5.28	4.37
$3s_{1/2}$	$-9.3(5)$	-6.19	-6.79	$1g_{9/2}$	$-2.92(20)$	0.38	-3.67
$1g_{7/2}$	$-10.93(20)$	-9.56	-10.00	$2p_{1/2}$	$-3.53(20)$	-4.37	-5.19
$2d_{5/2}$	$-11.13(20)$	-7.82	-9.09	$2p_{3/2}$	-6.38	-5.19	-6.55
$1g_{9/2}$	$-17.93(20)$	-13.54	-17.72	$1f_{5/2}$	-8.71	-9.39	-9.70
$2p_{1/2}$	$-18.38(20)$	-18.66	-19.66				
$1g$	7.00	3.98	7.72	$1g$	6.82	3.59	6.74

Table 5.12: Neutron and proton single particle states of ^{100}Sn, and spin-orbit of the $1g$ shell. RHF and RH refer to the σ, ω, π-model and to NL3 respectively. The energies are expressed in MeV.

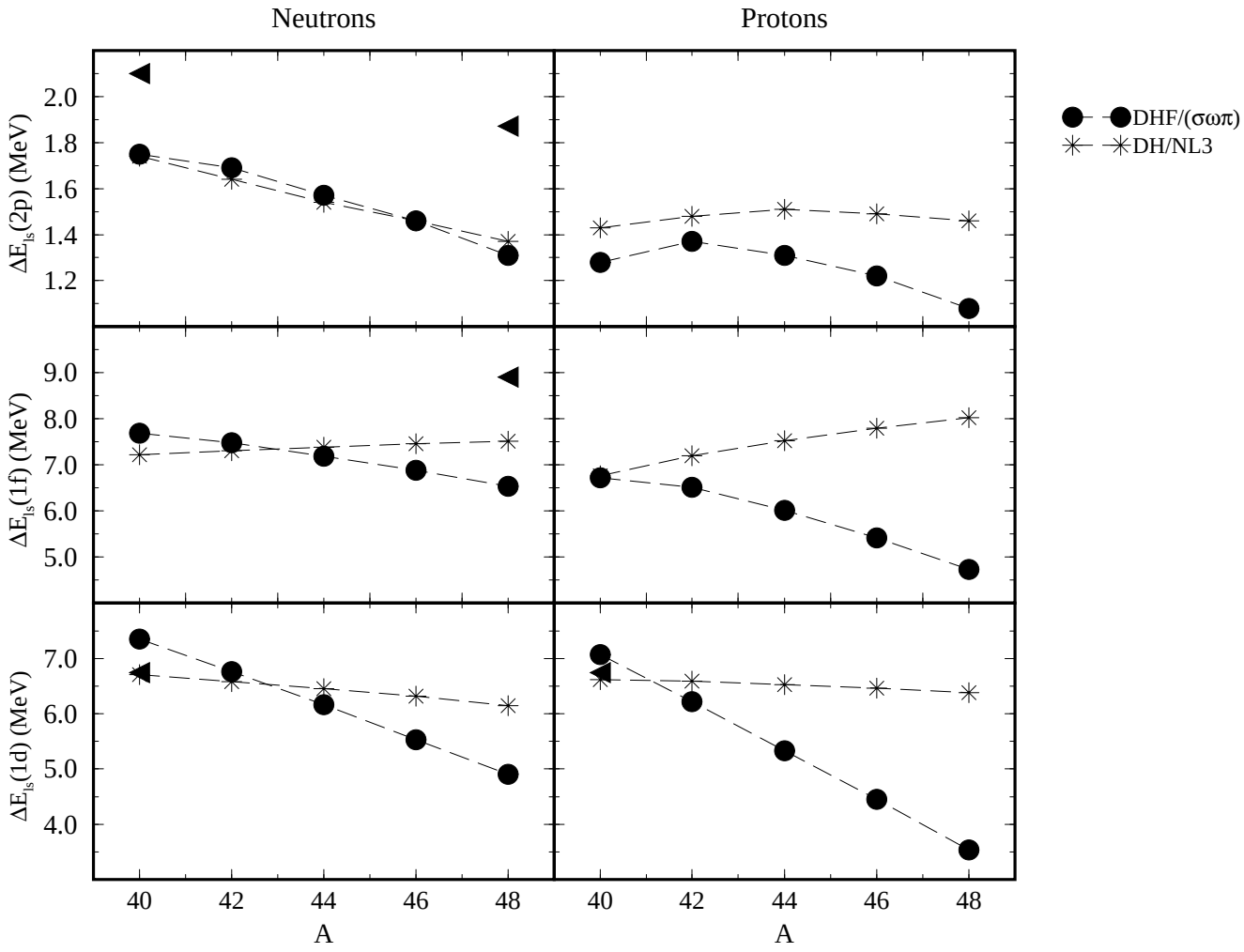

Figure 5.1: Energy splittings between spin-orbit partners for neutron and proton levels on the left and on the right side of the figure respectively in Ca isotopes, as functions of the mass number. The filled circles refer to the RHF/(σ, ω, π)-model calculations, the stars to the RH/NL3 calculations, and the triangles are the experimental data.

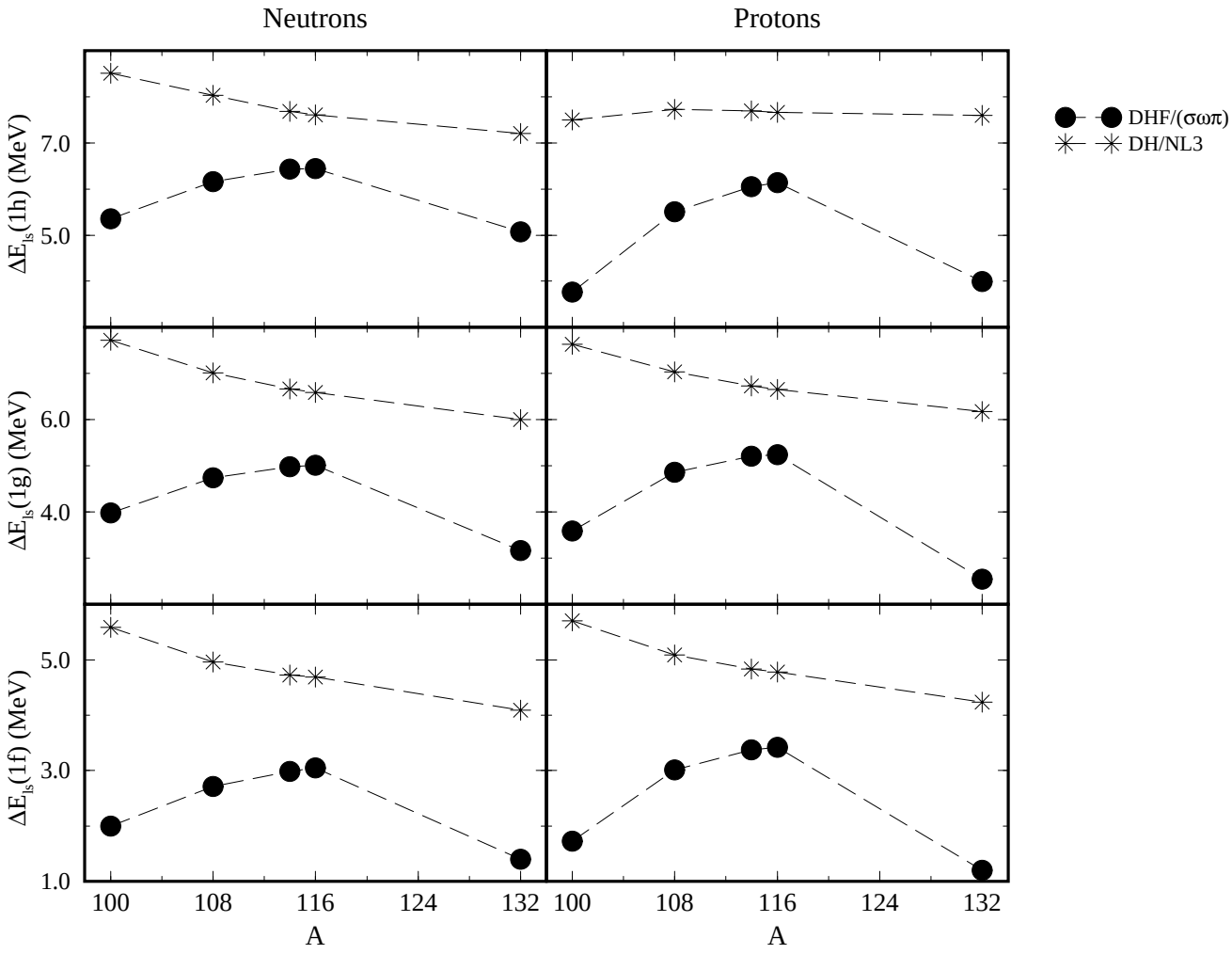

Figure 5.2: Energy splittings between spin-orbit partners for neutron and proton levels on the left and on the right side of the figure respectively in Sn isotopes, as functions of the mass number. The filled circles refer to the RHF/(σ, ω, π)-model calculations, the stars to the RMF/NL3 calculations.

Neutrons				Protons			
nlj	Exp.	RHF	RH	nlj	Exp.	RHF	RH
$2f_{5/2}$	-0.58	-0.46	0.09	$3s_{1/2}$	(-6.83)	-1.36	-4.27
$3p_{1/2}$	(-0.92)	-0.74	-0.21	$1h_{11/2}$	-6.84	1.22	-5.30
$1h_{9/2}$	-1.02	-1.80	-0.44	$2d_{3/2}$	-7.19	-2.29	-5.26
$3p_{3/2}$	-1.73	-1.11	-0.54	$2d_{5/2}$	-8.67	-3.36	-7.00
$2f_{7/2}$	-2.58	-1.82	-1.32	$1g_{7/2}$	-9.63	-6.86	-9.94
$2d_{3/2}$	-7.31	-9.54	-8.75	$1g_{9/2}$	-15.71	-9.41	-16.12
$1h_{11/2}$	-7.55	-6.87	-7.64	$2p_{1/2}$	-16.07	-13.87	-17.02
$3s_{1/2}$	-7.64	-9.08	-8.33				
$2d_{5/2}$	-8.96	-11.00	-10.45				
$1g_{7/2}$	-9.74	-14.04	-12.29				
$2d$	1.65	1.46	1.70	$2d$	1.48	1.07	1.74

Table 5.13: Neutron and proton single particle states of ^{132}Sn, and spin-orbit of the $2d$ shell. RHF and RH refer to the σ, ω, π-model and to NL3 respectively. The energies are expressed in MeV.

Neutrons				Protons			
nlj	Exp.	RHF	RH	nlj	Exp.	RHF	RH
$3d_{3/2}$	-1.40	-0.46	-0.01	$3p_{1/2}$	0.17	5.25	2.60
$2g_{7/2}$	-1.44	-0.81	-0.56	$2f_{5/2}$	-0.68	3.56	0.56
$4s_{1/2}$	-1.90	-0.79	-0.36	$3p_{3/2}$	-0.97	4.73	1.84
$1j_{15/2}$	-2.09	-0.14	-0.48	$1i_{13/2}$	-2.19	4.74	-1.02
$3d_{5/2}$	-2.37	-1.14	-0.63	$2f_{7/2}$	-2.90	2.09	-1.44
$1i_{11/2}$	-3.16	-3.80	-2.97	$1h_{9/2}$	-3.80	-1.73	-4.60
$2g_{9/2}$	-3.94	-2.74	-2.50	$3s_{1/2}$	-8.01	-4.90	-8.15
$3p_{1/2}$	-7.37	-8.11	-7.65	$2d_{3/2}$	-8.36	-6.30	-9.25
$2f_{5/2}$	-7.94	-9.50	-9.09	$1h_{11/2}$	-9.36	-4.53	-10.20
$3p_{3/2}$	-8.27	-8.79	-8.40	$2d_{5/2}$	-10.04	-7.38	-10.88
$1i_{13/2}$	-9.00	-8.95	-9.60	$1g_{7/2}$	-12.18	-12.42	-15.04
$2f_{7/2}$	-10.07	-11.42	-11.11				
$1h_{9/2}$	-10.78	-14.75	-13.39				
$2f$	2.13	1.92	2.02	$2f$	1.93	1.47	2.00

Table 5.14: Neutron and proton single particle states of ^{208}Pb, and spin-orbit of the $2f$ shell. RHF and RH refer to the σ, ω, π-model and to NL3 respectively. The energies are expressed in MeV.

Conclusions and Outlook

To conclude this work we summarize the most significant results that have been obtained and give some hints for possible future extensions and investigations.

Motivated by the facts that a relativistic theory of pairing is still an open question and the existing relativistic Hartree-Fock models have given results for properties of finite nuclei very much less satisfactory than relativistic Hartree approximations, in this thesis we have followed two lines of research: namely a relativistic Hartree-Bogoliubov approximation and a relativistic Hartree-Fock model for the description of the nuclear many-body problem. Applications to infinite nuclear matter and to finite nuclei have shown interesting relativistic dynamical effects.

The essential ingredients for a relativistic Hartree-Bogoliubov theory are: a fully relativistic treatment of the *pp*-channel and a realistic pairing interaction, i.e. the K-matrix.

First, we have investigated pairing correlations in infinite nuclear matter in the $^1S_0$ channel by using a relativistic BCS approximation: the successful non-linear parameters set NL1 of the RMF theory in the *ph*-channel and the relativistic bare interaction of the Bonn group in the *pp*-channel lead to a description of pairing properties in good agreement with non-relativistic calculations based on the Gogny force, a phenomenological potential fitted to experimental data of finite nuclei. As a consequence, one can hope that also pairing properties of finite nuclei may be successfully described in a relativistic self-consistent theory with a realistic pairing interaction.

In symmetric nuclear matter, we have calculated the contributions of the various meson exchange potentials to the pairing gap at the Fermi surface. As expected there is a large cancellation between the strongly repulsive ω-exchange and the large attractive σ-exchange that dominates the essential region of small momenta. The contribution of the other mesons is smaller, but not negligible because of this cancellation. For densities close to saturation, differencies between the relativistic and non-relativistic calculations have been observed, and we have shown that they originate from the strong repulsion in the bare NN interaction at high densities. An interesting question for the future is to investigate whether the polarization effects might reduce these discrepancies.

Finally, we have also shown that it is possible to construct simpler relativistic pairing interactions with finite range based only on the the σ- and ω-exchange, which reproduce pairing properties obtained by using the Bonn potential. For future investigations, it would be interesting to use these phenomenological interactions in RHB calculations for finite nuclei.

Second, we have presented the RHB equations for finite nuclei treating the *pp*-channel in a fully relativistic way. By constructing a simple phenomenological relativistic pairing potential with zero-range, attractive in the scalar and repulsive in the vector channel, we

have investigated for the first time how pairing properties of finite nuclei are produced in the framework of a relativistic field theory. An application of the model to a isotopic chain of Sn nuclei has shown interesting new effects due to relativity: in particular, in a fully relativistic treatment of the *pp*-channel it turns out that, although small, the matrix elements of the pairing tensor given by the product of two small components of the Dirac spinors give large contribution to the pairing field because they are connected to the very strong spin dependent part of the interaction. Thus, the spin independent and the spin dependent parts of the relativistic pairing interaction mix the small and the large pairing tensor components whose contributions to the total pairing field result to have the same size.

We have also investigated whether the antiparticles affect the properties of pairing in a fully relativistic treatment of the *pp*-channel. We have found that they contribute more to the spin dependent part of the interaction than to the spin independent term. However, a readjustment of the force parameters leads to similar results for the pairing properties in both the cases.

Comparisons of the pairing energy obtained with this model and with RHB calculations using the Gogny force in the *pp*-channel for the Sn isotopic chain considered suggest that within a fully relativistic treatment the pairing field depends rather weakly on the level density. This is mainly due to the strong contribution of the spin dependent term of the interaction.

Furthermore, comparisons between ground state properties calculated with the relativistic and non-relativistic pairing forces with those obtained from the experimental data show a better agreement in the case of the new fully relativistic treatment of the *pp*-channel.

Although a relativistic treatment of the *pp*-channel seems to be quite successful, this model is still a very simple approximation of the realistic pairing potential. The essential shortcoming is that the parameters of the pairing force have to be readjusted for each isotopic chain. They also depend on the number of shells used in the calculations. This suggests that future fully relativistic HB calculations for finite nuclei should use a more realistic pairing potential.

Finally, due to the fact that RMF approximations do not contain a spin-isospin term of the form $\sigma_1 \cdot \sigma_2 \tau_1 \cdot \tau_2$ and a tensor term of the nuclear force, we have proposed a new relativistic Hartree-Fock model for the description of the nuclear many-body system. Since, up to now, the numerical complexity of the RHF equations has not permitted to determine a good set of parameters for the new force, one of our main result has been the development of a fast numerical technique which allows an accurate fitting procedure. A preliminary fit only to properties of infinite nuclear matter and calculations of ground state properties of finite nuclei have shown that the new parameters cannot reproduce the properties of finite systems. Therefore, it is needed to consider finite nuclei properties in the fit and the determination of the new set is now in progress.

As a test of our new numerical method we have repeated previous calculations of ground state properties of spherical nuclei for a linear (σ, ω)- and a (σ, ω, π)-model and we have found good agreement for all the results. Moreover, by studying the Fock term of relativistic meson exchange potentials, we have seen that, as in the case of pairing correlation, relativity mixes large and small components of the generalized density matrix. As expected, the Fock energies of the σ and ω meson-exchange potential have opposite

sign of the corresponding direct term and the π-meson gives a negative contribution once that the spurious contact term is eliminated.

Furthermore, we have investigated the effect of the Fock terms, and that one of the pions in particular, on the spin-orbit splitting. It is well known that this term is naturally described in a relativistic approach to the nuclear many-body system. However, all the successful RMF approximations include only the ρ-meson for the isospin dependence. We have found that the π-meson with its $\sigma_1 \cdot \sigma_2 \tau_1 \cdot \tau_2$ and tensor terms produces essential contributions to the isospin dependence of the spin-orbit splitting. Calculations of the energy splittings of the spin-orbit partners in isotopic chains of Ca and Sn nuclei with the linear RHF model and comparisons with results obtained with the standard parameters set NL3 have shown that the effect of the pion is extremely large in particular for the nuclei with a larger neutron to proton ratio.

There are only few experimental data for the isospin dependence of the spin-orbit splitting. In particular, so far, there is no evidence for the strong influence of the tensor terms. Therefore we need further theoretical and experimental investigations in order to be able to make reliable predictions for nuclear structure phenomena far from the valley of stability.

Appendix A

One-Meson-Exchange Interactions

In this Appendix we write explicitly the relativistic one-boson-exchange (OBE) interactions which are used in the applications of the relativistic Hartree-Bogoliubov model and of the relativistic Hartree-Fock approximation presented in Chapters 3 and 4 and in Chapter 5 respectively. As already seen in Chapter 2, starting from the nucleon-meson vertex functions Γ^m given in Eq.s (2.12)-(2.16), the quantization of the meson fields allows the definition of a relativistic two-body potential as given in Eq.(2.40), in which the propagator $D_m(\mathbf{r}_1, \mathbf{r}_2)$ is simply of the Yukawa type. However, as pointed out in Chapter 2, for a microscopic understanding of pairing correlations in nuclear systems a bare interaction, or a phenomenological potential adjusted to a bare interaction, has to be used. As shown in detail in Ref. [MHE87, Er74], for the description of free NN scattering data, so-called form factors F_m, functions of the squared transferred momentum $\mathbf{q}^2$, have to be inserted at each vertex of the OBE diagram. Physically, they take into account the extended structure of the nucleons and assure the convergence of the dynamical equations. Of course, the introduction of $F_m(\mathbf{q}^2)$ in the nucleon-meson vertices leads to a more complicated expression of the propagator D_m in Eq.(2.40).

For the meson m ($m = \sigma, \omega, \rho \ldots$), the relativistic OBE interaction V_m reads

$$V_m(1,2) = g_m^2(\gamma^0\Gamma_\mu)_1 D_m^{\mu\nu}(1,2)(\gamma^0\Gamma_\nu)_2, \tag{A.1}$$

in which $D_m^{\mu\nu}$ are the meson propagators and they will be discussed in more details at the end of the section, and the indices 1 and 2 refer to the first and second particle. For a static problem, the OBE interaction (A.1) reads

$$v_\sigma(1,2) = -g_\sigma^2\gamma_1^0 D_\sigma(1,2)\gamma_2^0 \tag{A.2}$$

for the exchange of the isoscalar scalar $\sigma-$meson,

$$v_\omega(1,2) = +g_\omega^2(\gamma^0\gamma_\mu)_1 D_\omega^{\mu\nu}(1,2)(\gamma^0\gamma_\nu)_2 \tag{A.3}$$

for the exchange of the isoscalar vector ω-meson,

$$v_\pi(1,2) = -\left(\frac{f_\pi}{m_\pi}\right)^2 (\gamma^0\gamma^5\boldsymbol{\gamma})_1\vec{\tau}_1\cdot\vec{\tau}_2\boldsymbol{\nabla}_1\boldsymbol{\nabla}_2 D_\pi(1,2)(\gamma^0\gamma^5\boldsymbol{\gamma})_2 \tag{A.4}$$

for the exchange of the isovector π (only pv coupling is considered),

$$v_\rho^V(1,2) = +g_\rho^2(\gamma^0\gamma_\mu\vec{\tau})_1\vec{\tau}_1\cdot\vec{\tau}_2 D_\rho^{\mu\nu}(1,2)(\gamma^0\gamma_\nu\vec{\tau})_2 \tag{A.5}$$

for the isovector vector term of the ρ-meson,

$$v_\rho^T(1,2) = + \left(\frac{f_\rho}{2M}\right)^2 q^\lambda \sigma_{1\lambda\mu} q^{\lambda'} \sigma_{2\lambda'\nu} \vec{\tau}_1 \cdot \vec{\tau}_2 D_\rho^{\mu\nu}(1,2) \tag{A.6}$$

and, finally, for the isovector vector-tensor term of the ρ-meson,

$$v_\rho^{VT}(1,2) = i\frac{f_\rho g_\rho}{2M}\left[\gamma_2^\lambda \sigma_{1\lambda\mu} q_\nu - \sigma_{2\mu\lambda} q_\nu \gamma_1^\lambda\right] \vec{\tau}_1 \cdot \vec{\tau}_2 D_\rho^{\mu\nu}(1,2) \tag{A.7}$$

In Eq.s (A.2)-(A.7), the fully relativistic meson propagator in coordinate space $D_m^{\mu\nu}(1,2)$ is the Fourier transformation of the propagator in momentum space $D_m^{\mu\nu}(\mathbf{q},\omega)$

$$D_m^{\mu\nu}(\mathbf{r},\omega) = \int \frac{d^3q}{(2\pi)^3} \mathrm{e}^{i\mathbf{qr}} D_m^{\mu\nu}(\mathbf{q},\omega), \tag{A.8}$$

where $D_m^{\mu\nu}(\mathbf{q},\omega)$ is given by

$$D_m(\mathbf{q},\omega) = \frac{1}{-\omega^2 + \mathbf{q}^2 + m_m^2 - i\eta} F_m^2(\mathbf{q}^2) \quad \text{for scalar mesons,} \tag{A.9}$$

$$D_m^{\mu\nu}(\mathbf{q},\omega) = \frac{g^{\mu\nu} - q^\mu q^\nu / m_m}{-\omega^2 + \mathbf{q}^2 + m_m^2 - i\eta} F_m^2(\mathbf{q}^2) \quad \text{for vector mesons.} \tag{A.10}$$

$F_m(\mathbf{q}^2)$ are the form factors applied to each nucleon-meson vertex Γ^m. Since the term $q_\mu q_\nu / m_m$ in Eq.(A.10) may be omitted because vector mesons are coupled to the conserved nucleon sources j_μ and since retardation effects in the mesons propagation are neglected (i.e. $\omega^2 << q^2 + m_m^2$), the functions (A.9) and (A.10) reduce simply to

$$\begin{aligned} D_m(\mathbf{q}) &= \frac{1}{\mathbf{q}^2 + m_m^2} F_m^2(\mathbf{q}^2) \\ D_m^{\mu\nu}(\mathbf{q}) &= \frac{g^{\mu\nu}}{\mathbf{q}^2 + m_m^2} F_m^2(\mathbf{q}^2). \end{aligned} \tag{A.11}$$

From Eq.(A.11) it follows that in coordinate space, the propagators depend only on the relative coordinate

$$D_m(1,2) = D_m(r) \tag{A.12}$$

where $r = |\mathbf{r}_1 - \mathbf{r}_2|$. For the investigations presented in this thesis, three kind of form factors have been considered, namely

$$F_m(\mathbf{q}^2) = \begin{cases} 1 & \text{(a)} \\ \left(\frac{\Lambda_m^2 - m_m^2}{\Lambda_m^2 + \mathbf{q}^2}\right)^{n_m}, \ \frac{\Lambda^2}{\Lambda^2 + \mathbf{q}^2} & \text{(b)} \\ \mathrm{e}^{-\mathbf{q}/4\Lambda^2} & \text{(c)} \end{cases}, \tag{A.13}$$

in which m_m are the meson masses and Λ_m, and Λ are the cutoff masses in the form factors. In the RHF approach to the nuclear many-body problem discussed in Chapter 5, no form factors have been applied to the nucleon-pion vertex Γ^π. Therefore, for F_m given by Eq.(A.13a), the meson propagator in coordinate space reads simply

$$D_m(r) = \frac{1}{4\pi} \frac{\mathrm{e}^{-m_m r}}{r} \tag{A.14}$$

However, it has to be noticed that in this case the derivatives $\boldsymbol{\nabla}_1 \cdot \boldsymbol{\nabla}_2$ in the pseudo-vector, tensor, and vector-tensor OBE interactions in Eq.s(A.4), (A.6), and (A.7) produce a zero-range term in the nuclear interaction. Since this contact force would be in reality suppressed by short-range correlations due to the repulsion of the NN potential at short distances (i.e. ω-meson exchange), by analogy with what is done in non-relativistic calculations, the spurious δ component is removed from the potential part of the nuclear Hamiltonian by subtracting the zero-rank tensor term of the NN potential coming from π, ρ^T, and ρ^{VT}

$$D_{m_\delta}(1,2) = \frac{1}{3}\int \frac{d^3q}{(2\pi)^3} \mathrm{e}^{i\mathbf{qr}}. \tag{A.15}$$

The form factors given in Eq.s (A.13b) and (A.13c) have been used for the investigations of pairing correlations in nuclear matter discussed in Chapter 3. In particular, the first expression in Eq.(A.13b) is the form factor applied to a nucleon-meson vertex in the Bonn potential [Ma89], while the second one refers to a phenomenological interaction introduced in Ref. [TM99]. For the Bonn potential form factor, a direct integration [AS64, PBM86] in momentum space of Eq.(A.11) leads to the following expressions of the meson propagator in coordinate space. For $n_m = 1$

$$D_m(r) = \frac{1}{4\pi}\left(\frac{e^{-m_m r}}{r} - \frac{e^{-\Lambda_m r}}{r} + \frac{m_m^2 - \Lambda_m^2}{2\Lambda_m} e^{-\Lambda_m r}\right), \tag{A.16}$$

and for $n_m = 2$

$$\begin{aligned} D_m(r) \;=\; & \frac{1}{4\pi}\left[\frac{e^{-m_m r}}{r} - \frac{e^{-\Lambda_m r}}{r} + \frac{m_m^2 - \Lambda_m^2}{2\Lambda_m} e^{-\Lambda_m r}\right. \\ & - \frac{(\Lambda_m^2 - m_m^2)^2}{8}\left(\frac{e^{-\Lambda_m r}}{\Lambda_m^3} + \frac{r e^{-\Lambda_m r}}{\Lambda_m^2}\right) \\ & \left. - \frac{(\Lambda_m^2 - m_m^2)^3}{16}\left(\frac{e^{-\Lambda_m r}}{\Lambda_m^5} + \frac{r e^{-\Lambda_m r}}{\Lambda_m^4} + \frac{r^2 e^{-\Lambda_m r}}{3\Lambda_m^3}\right)\right]. \end{aligned} \tag{A.17}$$

The Fourier transformation of Eq.(A.11) for the phenomenological pairing interaction in Ref. [TM99] is analogous to Eq.(A.18) apart from the constants in front of the various terms. We can thus remark that the introduction of a form factor of monopole type leads to smooth the divergence at $r = 0$ by means of a second Yukawa type potential depending on the cutoff mass and with opposite sign of the first Yukawa, and an exponential potential. Finally, a direct integration [AS64, PBM86] of Eq.(A.11) with a gaussian cut off of Eq. (A.13c), gives

$$\begin{aligned} D_m(r) \;=\; & -\frac{\mathrm{e}^{m_m^2/\Lambda^2}}{8\pi}\left[\frac{2}{r}\sinh m_m r + \frac{\mathrm{e}^{-m_m r}}{r}\mathrm{erf}\left(\frac{m_m}{\Lambda} - \frac{\Lambda}{2}r\right)\right. \\ & \left. - \frac{\mathrm{e}^{-m_m r}}{r}\mathrm{erf}\left(\frac{m_m}{\Lambda} + \frac{\Lambda}{2}r\right)\right]. \end{aligned} \tag{A.18}$$

where the error function erf$z$ is defined by

$$\mathrm{erf}z = \frac{2}{\sqrt{\pi}}\int_0^z \mathrm{e}^{-t^2} dt. \tag{A.19}$$

We notice that in this case the error function erf prevent any divergence in the meson propagator.

A.1 Limit for Infinite Meson Mass: Point Couplings

A zero-range approximation of a relativistic OBE interaction is obtained by considering the limit of infinite meson mass $m_m \to \infty$. In this case the propagator

$$D_m^{\infty}(r) = \pm\, C_m^2 \int \frac{d^3q}{(2\pi)^3} \mathrm{e}^{i\mathbf{q}\cdot\mathbf{r}} = \pm\, C_m^2\ \delta(\mathbf{r}_1 - \mathbf{r}_2) \tag{A.20}$$

where the coupling constant is now defined by $C_m^2 = \left(\frac{g_m}{m_m}\right)^2$.

Appendix B

Relativistic BCS for Infinite Nuclear Matter: Two-body Matrix Elements

In Chapter 3, the calculation of the pairing gap at the Fermi surface in infinite nuclear matter is performed in the BCS approximation. Therefore the eigenvalues and the eigenfunctions of the Dirac equation for a spin-1/2 particle propagating in a uniform nuclear medium (3.8) are needed together with a pairing interaction in order to solve the gap equation (3.22). In this Appendix, we briefly remind the solution of the Dirac equation in this case, and we write the pairing two-body matrix elements of OBE interaction in momentum space. Moreover, we explicitly list the nucleon-meson amplitudes $v_{pp}(\mathbf{k},\mathbf{p})$ for a generic form factor F_m and calculate their average over the angle $v_{pp}(k,p)$ given in Eq.(3.23) for the three form factors considered in Eq.(A.13a,b,c).

The plane wave Dirac spinors corresponding to the eigenvalues $\epsilon(k)$ given in Eq.(3.9) are characterized by momentum $\mathbf{k}$ and spin s, $\alpha=(\mathbf{k},s)$ and read

$$\psi_\alpha^{(+)}(x) = \frac{1}{\sqrt{2\pi}^3}\mathrm{e}^{-ikx}u_{\mathbf{k}s}, \tag{B.1}$$

$$\psi_\alpha^{(-)}(x) = \frac{1}{\sqrt{2\pi}^3}\mathrm{e}^{+ikx}v_{\mathbf{k}s}, \tag{B.2}$$

for positive and negative energies respectively, with

$$u_{\mathbf{k}s} = \sqrt{\frac{E^*+M^*}{2E^*}}\begin{pmatrix}\chi_s\\ \frac{\boldsymbol{\sigma}\cdot\mathbf{k}}{E^*+M^*}\chi_s\end{pmatrix} \tag{B.3}$$

$$v_{\mathbf{k}s} = \sqrt{\frac{E^*+M^*}{2E^*}}\begin{pmatrix}\frac{\boldsymbol{\sigma}\cdot\mathbf{k}}{E^*+M^*}\chi_s\\ \chi_s\end{pmatrix}. \tag{B.4}$$

Working in the formalism of the second quantization and using Eq.s (B.3)-(B.4) as basis, the interaction between tow nucleons may be written as

$$V=\frac{1}{2}\sum_{\alpha_1\alpha_2\alpha_3\alpha_4}V_{\alpha_1\alpha_2\alpha_3\alpha_4}b^+_{\alpha_1}b^+_{\alpha_2}b_{\alpha_4}b_{\alpha_3}, \tag{B.5}$$

where $b^+_{\mathbf{k}s}$ are creation operators for particles states, and $V_{\alpha_1\alpha_2\alpha_3\alpha_4}$ the matrix elements (not yet antisymmetrized) of the two-body potential. For the OBE interaction given in

Eq.s (A.2)-(A.7) they read explicitly

$$V^{\sigma}_{\mathbf{k}_1 s_1 \mathbf{k}_2 s_2 \mathbf{k}_3 s_3 \mathbf{k}_4 s_4} = -g_\sigma^2 \delta_{\mathbf{k}_1+\mathbf{k}_2,\mathbf{k}_3+\mathbf{k}_4} \frac{\bar{u}_{\mathbf{k}_1 s_1} u_{\mathbf{k}_3 s_3} \bar{u}_{\mathbf{k}_2 s_2} u_{\mathbf{k}_4 s_4}}{\mathbf{q}^2 + m_\sigma^2} F_\sigma^2(\mathbf{q}^2), \tag{B.6}$$

$$V^{\omega}_{\mathbf{k}_1 s_1 \mathbf{k}_2 s_2 \mathbf{k}_3 s_3 \mathbf{k}_4 s_4} = +g_\omega^2 \delta_{\mathbf{k}_1+\mathbf{k}_2,\mathbf{k}_3+\mathbf{k}_4} \frac{\bar{u}_{\mathbf{k}_1 s_1} \gamma^\mu u_{\mathbf{k}_3 s_3} \bar{u}_{\mathbf{k}_2 s_2} \gamma_\mu u_{\mathbf{k}_4 s_4}}{\mathbf{q}^2 + m_\omega^2} F_\omega^2(\mathbf{q}^2), \tag{B.7}$$

$$V^{\pi}_{\mathbf{k}_1 s_1 \mathbf{k}_2 s_2 \mathbf{k}_3 s_3 \mathbf{k}_4 s_4} = -\frac{f_\pi^2}{m_\pi^2} \delta_{\mathbf{k}_1+\mathbf{k}_2,\mathbf{k}_3+\mathbf{k}_4} \frac{\bar{u}_{\mathbf{k}_1 s_1} \gamma^5 \vec{\tau}\mathbf{q} u_{\mathbf{k}_3 s_3} \bar{u}_{\mathbf{k}_2 s_2} \gamma_5 \vec{\tau}\mathbf{q} u_{\mathbf{k}_4 s_4}}{\mathbf{q}^2 + m_\pi^2} F_\pi^2(\mathbf{q}^2), \tag{B.8}$$

$$V^{\rho}_{\mathbf{k}_1 s_1 \mathbf{k}_2 s_2 \mathbf{k}_3 s_3 \mathbf{k}_4 s_4} = +g_\rho^2 \delta_{\mathbf{k}_1+\mathbf{k}_2,\mathbf{k}_3+\mathbf{k}_4} \frac{\bar{u}_{\mathbf{k}_1 s_1} \gamma^\mu \vec{\tau} u_{\mathbf{k}_3 s_3} \bar{u}_{\mathbf{k}_2 s_2} \gamma_\mu \vec{\tau} u_{\mathbf{k}_4 s_4}}{\mathbf{q}^2 + m_\omega^2} F_\rho^2(\mathbf{q}^2). \tag{B.9}$$

For the solution of the gap equation (3.22) the antisymmetrized matrix elements

$$\langle \mathbf{k}s, \tilde{\mathbf{k}s} | V | \mathbf{p}s', \tilde{\mathbf{p}s'} \rangle - \langle \mathbf{k}s, \tilde{\mathbf{k}s} | V | \tilde{\mathbf{p}s'}, \mathbf{p}s' \rangle \tag{B.10}$$

are needed. In Eq.(B.10) the tilde denotes the time-reversed states, i.e.

$$|\tilde{\mathbf{k}s}\rangle = \mathcal{T} |\mathbf{k}s\rangle. \tag{B.11}$$

Since the gap parameter $\Delta(k)$ in the state $S = 0$, $T = 1$ depends only on the absolute value of the momentum k and not on the spin index s, the evaluation of the matrix elements in Eq.(B.10) yields for the direct term

$$v^d_{pp}(\mathbf{k}, \mathbf{p}) = \mp \frac{1}{4} \frac{1}{(\mathbf{k}-\mathbf{p})^2 + m_m^2} \sum_{ss'} \bar{u}_{\mathbf{k}s} \Gamma^m u_{\mathbf{p}s'} \bar{\tilde{u}}_{\mathbf{k}s} \Gamma^m \tilde{u}_{\mathbf{p}s'} \tag{B.12}$$

and for the exchange term

$$v^a_{pp}(\mathbf{k}, \mathbf{p}) = \pm \frac{1}{4} \frac{1}{(\mathbf{k}+\mathbf{p})^2 + m_m^2} \sum_{ss'} \bar{u}_{\mathbf{k}s} \Gamma^m \tilde{u}_{\mathbf{p}s'} \bar{\tilde{u}}_{\mathbf{k}s} \Gamma^m u_{\mathbf{p}s'}. \tag{B.13}$$

The vertices Γ^m are given in Eq.s (2.12)-(2.16). Trace techniques [IZ80] and replacing the vector $\mathbf{p}$ by $-\mathbf{p}$ in the integral in the gap equation (3.22), it may be shown that the direct and the exchange terms give the same contribution, and therefore the total two-body matrix elements v_{pp} in the gap equation is simply

$$v_{pp}(\mathbf{k}, \mathbf{p}) = \mp \frac{M^{*2}}{2E^*(k)E^*(p)} \frac{\mathrm{Tr}[\Lambda_+(\mathbf{k}) \Gamma \Lambda_+(\mathbf{p}) \gamma^0 \mathcal{T}^\dagger \Gamma^\dagger \mathcal{T} \gamma^0]}{(\mathbf{k}-\mathbf{p})^2 + m_m^2} \tag{B.14}$$

where

$$\Lambda_+(\mathbf{p}) = \frac{\not{p} + M^*}{2M^*} \tag{B.15}$$

is the projector onto positive energy solution [IZ80] and

$$\mathcal{T} = i\gamma^1\gamma^3 K \tag{B.16}$$

is the representation of the time reversal operator in Dirac space.
The two-body matrix elements given in Eq.(B.14) have to be finally integrated over the angle between $\mathbf{k}$ and $\mathbf{p}$ as given in Eq.(3.23) in order to be used in the solution of the gap equation (3.22). Since the integration depends on the form factors F_m, in the following sections we present the final expressions of $v_{pp}(k, p)$ for the three different form factors given in Eq. (A.13) used for the solution of the gap equation.

B.1 Bonn Potential

The relativistic Bonn potential [MHE87],[Ma89] is a bare interaction defined as sum of one-boson-exchange (OBE) of six mesons, namely σ, ω, $\vec{\pi}$, $\vec{\rho}$, $\vec{\eta}$, and $\vec{\delta}$, and the tensor and the vector-tensor term of the ρ-meson are included. According to the Landau's theory of superfluid systems [Mi67, Mi68] it therefore corresponds to the first diagram of the K-matrix (see Section 2.2) which should be used to solve the gap equation. In momentum space, the Bonn potential two-body matrix elements $v_{pp}(\mathbf{k},\mathbf{p})$ are given in Eq.s (B.6)-(B.9) in which the form factors $F_m(\mathbf{q}^2)$ read

$$F_m(\mathbf{q}^2) = \left(\frac{\Lambda_m^2 - m_m^2}{\Lambda_m^2 + \mathbf{q}^2}\right)^{n_m} \tag{B.17}$$

where m_m and Λ_m are the meson and the cutoff masses respectively, and n_m can be 1 or 2. Carrying out analytically the integration over the angle (3.23), the final form of the Bonn potential which enters into the gap equation (3.22) may be written as

$$v_{pp}(k,p) = \frac{1}{8E(k)E(p)kp}\sum_i \chi_i \left(A_i(k,p)\Theta_i(k,p) + B_i(k,p)\Phi_i(k,p) + C_i(k,p)\Upsilon_i(k,p)\right) \tag{B.18}$$

where $i = \sigma, \omega, \vec{\pi}, \vec{\rho}, \vec{\eta}$, and $\vec{\delta}$, the functions $\Theta_i(k,p)$, $\Phi_i(k,p)$ and $\Upsilon_i(k,p)$ are defined by

$$\Theta_i(k,p) = \log\frac{(k+p)^2+m_i^2}{(k-p)^2+m_i^2}\,\frac{(k-p)^2+\Lambda_i^2}{(k+p)^2+\Lambda_i^2} \tag{B.19}$$

$$\Phi_i(k,p) = (\Lambda_i^2 - m_i^2)\left(\frac{1}{(k+p)^2+\Lambda_i^2} - \frac{1}{(k-p)^2+\Lambda_i^2}\right) \tag{B.20}$$

$$\Upsilon_i(k,p) = (\Lambda_i^2 - m_i^2)^2 \log\frac{(k+p)^2+\Lambda_i^2}{(k-p)^2+\Lambda_i^2} \tag{B.21}$$

and the coefficients $A_i(k,p)$, $B_i(k,p)$ and $C_i(k,p)$ are given in Table B.1. Finally, the functions $a(k,p)$, $b(k,p)$, and $c(k,p)$ in Table B.1 are defined by

$$a(k,p) = 4M^{*2} - (E_k - E_p)^2 \tag{B.22}$$

$$b(k,p) = 4(2E_kE_p - M^{*2}) \tag{B.23}$$

$$c(k,p) = 4E_kE_p + (E_k + E_p)^2. \tag{B.24}$$

The meson masses m_m, cutoff masses Λ_m, and coupling constants g_m are given in Table B.2.

B.2 Phenomenological Pairing Interactions

B.2.1 Monopole Form Factor

In the left side of Fig. 3.14 we display Δ_{k_F} obtained by using the phenomenological relativistic pairing interaction introduced in [TM99]. This is based on the exchange of a σ- and of a ω-meson and a monopole form factor

$$F(\mathbf{q}^2) = \frac{\Lambda^2}{\mathbf{q}^2 + \Lambda^2} \tag{B.25}$$

i	χ_i	$A_i(k,p)$	$B_i(k,p)$	$C_i(k,p)$
σ	$-\ g_\sigma^2$	$a(k,p) - m_\sigma^2$	$a(k,p) - \Lambda_\sigma^2$	
ω	$+\ g_\omega^2$	$b(k,p)$	$b(k,p)$	
π_{pv}	$+\left(\frac{f_\pi}{m_\pi}\right)^2$	$p^2 - k^2 - m_\pi^2\ a(k,p)$	$p^2 - k^2 - \Lambda_\pi^2\ a(k,p)$	
ρ^V	$+\ g_\rho^2$	$b(k,p)$	$b(k,p)$	
ρ^T	$-\left(\frac{f_\rho}{2M}\right)^2$	$\left(c(k,p) + m_\rho^2\right) m_\rho^2$	$\left(c(k,p) + \Lambda_\rho^2\right) \Lambda_\rho^2$	1
ρ^{VT}	$+2\frac{f_\rho g_\rho}{M} M^*$	m_ρ^2	Λ_ρ^2	
δ	$-\ g_\delta^2$	$a(k,p) - m_\delta^2$	$a(k,p) - \Lambda_\delta^2$	
η_{pv}	$+\left(\frac{f_\eta}{m_\eta}\right)^2$	$p^2 - k^2 - m_\eta^2\ a(k,p)$	$p^2 - k^2 - \Lambda_\eta^2\ a(k,p)$	

Table B.1: The functions $A_i(k,p)$, $B_i(k,p)$, and $C_i(k,p)$ for the relativistic pairing interaction based on the Bonn potential.

		Potential A		Potential B		Potential C	
	m_α (MeV)	$g_\alpha^2/4\pi$	Λ_α (GeV)	$g_\alpha^2/4\pi$	Λ_α (GeV)	$g_\alpha^2/4\pi$	Λ_α (GeV)
π	138.03	14.9	1.05	14.6	1.2	14.6	1.3
η	548.8	7	1.5	5	1.5	3	1.5
ρ	769	0.99	1.3	0.95	1.3	0.95	1.3
ω	782.6	20	1.5	20	1.5	20	1.5
δ	983	0.7709	2.0	3.1155	1.5	5.0742	1.5
σ	550	8.3141	2.0	8.0769	2.0	8.0279	1.8

Table B.2: Parameters sets of the relativistic Bonn OBE Potential [Ma89]. The pseudovector coupling is used for the mesons π and η.

i	χ_i	$A_i(k,p)$	$B_i(k,p)$
σ	$-\ g_\sigma^2\Lambda_\sigma^4$	$\frac{a(k,p)-m_\sigma^2}{(\Lambda_\sigma^2-m_\sigma^2)^2}$	$\frac{a(k,p)-\Lambda_\sigma^2}{\Lambda_\sigma^2-m_\sigma^2}$
ω	$+\ g_\omega^2\Lambda_\omega^4$	$\frac{b(k,p)}{(\Lambda_\omega^2-m_\omega^2)^2}$	$\frac{b(k,p)}{\Lambda_\omega^2-m_\omega^2}$

Table B.3: The functions $A_i(k,p)$ and $B_i(k,p)$ for the relativistic pairing interaction with a monopole form factor applied to each nucleon-meson vertex.

is applied to each meson-nucleon vertex. In this case the total potential can be written as

$$v_{pp}(k,p) = \frac{1}{8E(k)E(p)kp} \sum_{i=\sigma,\omega} \chi_i \left(A_i(k,p)\Theta_i(k,p) + B_i(k,p)\Phi_i(k,p)\right) \tag{B.26}$$

in which the coefficients χ_i, the functions $A_i(k,p)$ and $B_i(k,p)$ are given in Table B.2. There, the functions $a(k,p)$, and $b(k,p)$ are defined in Eq.s(B.22)-(B.23).

B.2.2 Gaussian Form Factor

We have constructed a phenomenological relativistic pairing interaction also based on the exchange of a σ- and of a ω-meson, but with a form factor of gaussian type:

$$F(\mathbf{q}^2) = \mathrm{e}^{-(\mu q/2)^2} \tag{B.27}$$

Starting from the parameters set NL2, we have fixed the cutoff parameter μ to 140.0 MeV or 0.7 fm, therefore we have chosen the same value used in the Gogny force, in order to assure the convergence of the RHB equations. We have then scaled the coupling constants g_σ and g_ω in order to reproduce the pairing gap at the Fermi surface obtained by the Bonn potential or the Gogny force. The meson masses have not been changed. The total potential can be written as

$$v_{pp}(k,p) = \frac{1}{8E(k)E(p)kp} \sum_{i=\sigma,\omega} \chi_i \left(A_i(k,p)\Theta_i(k,p) + B_i(k,p)\Phi_i(k,p)\right) \tag{B.28}$$

where the functions $\Theta_i(k,p)$ and $\Phi_i(k,p)$ are given by

$$\begin{aligned} \Theta_i(k,p) &= \mathrm{e}^{-\mu^2/2m_i^2}\mathrm{e}^{-\mu^2(k^2+p^2)} \left(\ln\frac{(k+p)^2+m_i^2}{(k-p)^2+m_i^2}\right. \\ &+ \left.\sum_{n=1}^{\infty}\frac{1}{nn!}\left(\frac{\mu^2}{2}\right)^n\left[(m_i^2+(k+p)^2)^n-(m_i^2+(k-p)^2)^n\right]\right) \end{aligned} \tag{B.29}$$

$$\Phi_i(k,p) = \frac{4}{\mu^2}\mathrm{e}^{-\mu^2(k^2+p^2)/2}\sinh(\mu^2 kp), \tag{B.30}$$

the coefficients χ_i, and the functions $A_i(k,p)$ and $B_i(k,p)$ are given in Table B.3. There the functions $a(k,p)$ and $b(k,p)$ are given in Eq.s Eq.s(B.22)-(B.23).

i	χ_i	$A_i(k,p)$	$B_i(k,p)$
σ	$-\ g_\sigma^2$	1	$a(k,p) - m_\sigma^2$
ω	$+\ g_\omega^2$	0	$b(k,p)$

Table B.4: The functions $A_i(k,p)$ and $B_i(k,p)$ for the relativistic pairing interaction with a gaussian form factor applied to each nucleon-meson vertex.

In the limit $\mu \to 0$ $v_{pp}(k,p)$ tends to the expression obtained by using a simple one-meson-exchange potential [KR91].

Appendix C

Relativistic HF Theory for Infinite Nuclear Matter

With the ansatz for the mass operator Σ given in Eq.(5.2), the Dirac equation (5.1) for the spinor ψ_0 becomes

$$(\boldsymbol{\gamma} \cdot \mathbf{p}^* + M^*)u(\mathbf{p}, s) = \gamma_0 E^* u(\mathbf{p}, s) \tag{C.1}$$

where the starred quantities are defined by

$$\begin{aligned} \mathbf{p}^*(p) &= \mathbf{p} + \hat{\mathbf{p}}\Sigma_V(p), \\ M^*(p) &= M + \Sigma_S(p), \\ E^*(p) &= E(p) - \Sigma_0(p). \end{aligned} \tag{C.2}$$

Here M^* is the usual scalar effective mass of the baryon, and E^* the single particle energy

$$E^{*2} = \mathbf{p}^{*2} + M^{*2}. \tag{C.3}$$

Eq.(C.1) is formally identical to the Dirac equation for a free particle, and therefore its positive energy solution may be written as

$$u(\mathbf{p}, s) = \left(\frac{E^* + M^*}{2E^*}\right)^{1/2} \begin{pmatrix} 1 \\ \frac{\boldsymbol{\sigma}\cdot\mathbf{p}^*}{E^*+M^*} \end{pmatrix} \chi_s \tag{C.4}$$

(see also eq. (B.3)). As said in Section 5.1, the energy density can be calculated as in Eq.(5.3). In the following we write explicitly the kinetic term $\langle T \rangle$, the direct and the exchange terms of the potential, $\langle V_D \rangle$ and $\langle V_E \rangle$ respectively, for the non-linear (σ, ω, π)-model that we consider to fit the parameters of the new force.
Using standard trace techniques and the projection operator onto positive energy states (see Eq.s (B.14) and (B.15)), $\langle T \rangle$ becomes simply

$$\langle T \rangle = \frac{2}{\pi^2} \int_0^{p_F} p^2 dp \; (pp^* + MM^*). \tag{C.5}$$

With the inclusion of non-linear σ terms, the direct part of the potential energy $\langle V_D \rangle$ reads

$$\langle V_D \rangle = \frac{1}{2}(m_\sigma \sigma)^2 + g_\sigma \sigma \rho_S - \frac{1}{2}(m_\omega \omega)^2 + g_\omega \omega \rho_V + \frac{g_2}{3}\sigma^3 + \frac{g_3}{4}\sigma^4 \tag{C.6}$$

A_π	B_π	C_π
$-3\frac{f_\pi^2}{m_\pi^2}m_\pi^2\theta$	$-3\frac{f_\pi^2}{m_\pi^2}m_\pi^2\theta$	$6\frac{f_\pi^2}{m_\pi^2}[(p^2+p'^2)\phi - pp'\theta]$

Table C.1: The functions $A_\pi(k,p)$ and $B_\pi(k,p)$ and $C_\pi(k,p)$ for the exchange potential energy $\langle V_E\rangle$ of the π-meson.

where the scalar density ρ_S and the vector density ρ_V read

$$\rho_S = \frac{2}{\pi^2}\int_0^{p_F} p^2 dp\, \frac{M^*(p)}{E^*}. \tag{C.7}$$

$$\rho_V = \frac{2}{3\pi^2}p_F^3. \tag{C.8}$$

The exchange potential energy $\langle V_E\rangle$ originates from the pions only. It can be expressed as

$$\langle V_E\rangle = \frac{1}{(2\pi)^4}\int_0^{p_F} pdp\, p'dp' \left[A_\pi(p,p') + \frac{M^*(p)}{E^*(p)}\frac{M^*(p')}{E^*(p')}B_\pi(p,p') + \frac{p^*(p)}{E^*(p)}\frac{p^*(p)}{E^*(p)}C_\pi(p,p')\right] \tag{C.9}$$

where the functions A_π, B_π and C_π are listed in Table C.1 in terms of the functions

$$\theta(p,p') = \log\left[\frac{m_\pi^2+(p+p')^2}{m_\pi^2+(p-p')^2}\right], \tag{C.10}$$

$$\phi(p,p') = \frac{p^2+p'^2+m_\pi^2}{4pp'}\theta(p,p') - 1.$$

This expression includes the removal of the zero-range interaction in the pseudovector-pion contribution.
The self-energies (5.2) are obtained by differentiating $\langle V\rangle$ by respect to $u(\mathbf{p},s)$. They read

$$\Sigma_S(p) = -\left(\frac{g_\sigma}{m_\sigma}\right)^2\rho_S + \frac{1}{(4\pi)^2}\frac{1}{p}\int_0^{p_F} p'dp'\hat{M}(p')B(p,p') \tag{C.11}$$

$$\Sigma_0(p) = \left(\frac{g_\omega}{m_\omega}\right)^2\rho_V + \frac{1}{(4\pi)^2}\frac{1}{p}\int_0^{p_F} p'dp'A(p,p'), \tag{C.12}$$

$$\Sigma_V(p) = \frac{1}{(4\pi)^2}\frac{1}{p}\int_0^{p_F}\hat{P}(p')C(p,p'). \tag{C.13}$$

Appendix D

Relativistic Two-Body Matrix Elements For Finite Nuclei

A general expression for two-body matrix elements of the relativistic one-boson-exchange (OBE) interaction given in Eq. (A.1) reads

$$\langle \alpha_1 \alpha_2 | V_m | \alpha_3 \alpha_4 \rangle = \int d^3r_1 d^3r_2 \; \bar{\psi}_1(\mathbf{r}_1) \; \bar{\psi}_2(\mathbf{r}_2) \; V_m(|\mathbf{r}_1 - \mathbf{r}_2|) \; \psi_3(\mathbf{r}_1) \; \psi_4(\mathbf{r}_2). \tag{D.1}$$

$\psi_k(\mathbf{r}_i)$ are Dirac spinors. For spherical nuclei they have the form

$$\psi_k(\mathbf{r}) = \begin{pmatrix} f_k(\mathbf{r}) \\ i g_k(\mathbf{r}) \end{pmatrix} \chi_{t_k}(t) = \begin{pmatrix} f_{n_k}(r) | s_k l_k j_k m_k \rangle \\ i g_{n_k}(r) | s_k \tilde{l}_k j_k m_k \rangle \end{pmatrix} \chi_{t_k}(t) \tag{D.2}$$

where χ_{t_k} is the isospin wave function and $\phi_{s_k l_k j_k m_k}$

$$|sljm\rangle = \sum_{m_l m_s} C(s m_s l m_l | jm) Y_{l m_l}(\Omega) \chi_{m_s} \tag{D.3}$$

is the spin spherical harmonics of the nucleon k with spin $s_k = \frac{1}{2}$. In Eq. (D.2) the orbital angular momenta l and $\tilde{l}$ are determined by the spin j and the parity π as

$$\kappa = (j + \frac{1}{2}), \quad l = j + \frac{1}{2}, \quad \tilde{l} = j - \frac{1}{2}, \quad \text{for} \quad \pi = (-)^{j+\frac{1}{2}} \tag{D.4}$$

and

$$\kappa = -(j + \frac{1}{2}), \quad l = j - \frac{1}{2}, \quad \tilde{l} = j + \frac{1}{2}, \quad \text{for} \quad \pi = (-)^{j-\frac{1}{2}}. \tag{D.5}$$

In Eq. (D.1) the index $\alpha \equiv (a, p)$ denotes the complete set of quantum numbers that define the single particle state, and, in particular the index a refers to the radial quantum number, the spin, the orbital and total angular momenta, and the isospin, i.e.

$$a = (n, s, l, j, m, t). \tag{D.6}$$

Relativity introduces the additional index p that labels the large and small components of $\psi_k(\mathbf{r}_i)$. Therefore it can assume only two values

$$p = (+, -) \qquad\qquad \bar{p} = (-, +). \tag{D.7}$$

Writing explicitly the OBE interaction V_m and using the momentum representation of the propagator given in Eq.(A.8) and after neglecting retardation the relativistic two-body matrix elements given in Eq. (D.1) may be rewritten as

$$\begin{aligned}\langle\alpha_1\alpha_2|V_m|\alpha_3\alpha_4\rangle &= g_m^2\int\frac{d^3q}{(2\pi)^3}\int d^3r_1d^3r_2\,\bar{\psi}_1(\mathbf{r}_1)\Gamma_\mu^m\psi_3(\mathbf{r}_1)\;\mathrm{e}^{i\mathbf{q}(\mathbf{r}_1-\mathbf{r}_2)}D_m^{\mu\nu}(q)\bar{\psi}_2(\mathbf{r}_2)\Gamma_\nu^m\psi_4(\mathbf{r}_2)\\ &= g_m^2\int\frac{d^3q}{(2\pi)^3}\langle 1\;|\Gamma_\mu\mathrm{e}^{i\mathbf{qr}}|3\;\rangle\,D_m^{\mu\nu}(q)\;\langle\;2|\Gamma_\nu\mathrm{e}^{-i\mathbf{qr}}|4\rangle. \qquad \text{(D.8)}\end{aligned}$$

This is the final expression that has be to be calculated explicitly. Moreover, since we study only spherical nuclei it is convenient to calculated the two-body matrix elements coupled to zero total angular momentum J. In the following Sections, the expression of the coupled two-body matrix elements given in Eq. (D.8) are given explicitly for the OBE interactions in Eq.s (A.2), (A.3), and (A.5). The case of a pseudo-vector coupling is treated separately because it is more complicated.

D.1 Multipole Expansion

Using the multipole expansion for plane waves

$$\mathrm{e}^{i\mathbf{kr}} = 4\pi\sum_{LM} i^L j_L(kr)Y^*_{LM}(\hat{\mathbf{k}})Y_{LM}(\hat{\mathbf{r}}) \qquad \text{(D.9)}$$

we obtain

$$\langle 1\;2|V_m|3\;4\rangle = (4\pi g_m)^2\sum_{LM}\int\frac{q^2dq}{(2\pi)^3}\langle 1\;|\Gamma_\mu\,j_L(qr)Y_{LM}|3\;\rangle D_m^{\mu\nu}(q)\langle 2|\Gamma_\nu\,j_L(qr)Y^*_{LM}|4\;\rangle \qquad \text{(D.10)}$$

D.2 jj-Coupled Matrix Elements

D.2.1 Direct Term

We now calculate the two-body matrix elements coupled to good angular momentum. Introducing the index $|k\rangle = (a_kp_k)$ to shorten the notation, for the direct term we obtain

$$\begin{aligned}\langle 1\;2|V_m|3\;4\rangle_d^J &= \sum_{m_1m_3}(-)^{j_3-m_3}C(j_1m_1j_3-m_3|JM)\times\\ &\quad\times\sum_{m_4m_2}(-)^{j_2-m_2}C(j_4m_4j_2-m_2|JM)\times\\ &\quad\times\langle j_1m_1\;j_2m_2|V_m|j_3m_3\;j_4m_4\rangle \qquad \text{(D.11)}\end{aligned}$$

Using the reduced matrix elements

$$\langle j_1 m_1 \ |Q_{JM}|j_3 m_3 \ \rangle = \frac{(-)^{j_3-m_3}}{\sqrt{2J+1}} C(j_1 m_1 j_3 - m_3 | JM) \langle j_1 \ ||Q_J||j_3 \rangle \tag{D.12}$$

we find for the vertices Γ, which do not depend on the spin (1, γ_0,γ_5)

$$\begin{aligned} \langle 1 \ 2|V_m|3 \ 4\rangle_d^J &= \frac{(4\pi g_m)^2}{2J+1}(-)^{j_2-j_4} \int \frac{q^2 dq}{(2\pi)^3} \\ &\times \langle 1 \ ||\Gamma_m \, j_J(qr) Y_J||3 \ \rangle D_m(q) \langle 2||\Gamma_m \, j_J(qr) Y_J||4 \ \rangle \end{aligned} \tag{D.13}$$

and for vertices which carry spin (for instance spatial part of the vector mesons: $\Gamma_i = \gamma_i$)

$$\begin{aligned} \langle 1 \ 2|V_m|3 \ 4\rangle_d^J &= \sum_L \frac{(4\pi g_m)^2}{2J+1}(-)^{j_2+j_4+L+J} \int \frac{q^2 dq}{(2\pi)^3} \\ &\times \langle 1 \ ||j_L(qr) \, [\vec{\gamma} \, Y_L]_J \, ||3 \ \rangle D_m(q) \langle 2||j_L(qr) \, [\vec{\gamma} \, Y_L]_J \, ||4 \ \rangle \end{aligned} \tag{D.14}$$

$\sigma-$meson: $\Gamma = 1$

$$\langle 1 \ ||\Gamma_\sigma \, j_J(qr) Y_J||3 \ \rangle = \langle j_1||Y_J||j_3\rangle \, \langle 1|\gamma_0 j_J(qr)|3\rangle, \tag{D.15}$$

with:

$$\langle 1|\gamma_0 j_J(qr)|3\rangle = \int r^2 dr \, j_J(qr) \, (f_1^*(r) f_3(r) - g_1^*(r) g_3(r)) \, . \tag{D.16}$$

and

$$\begin{aligned} \langle 1 \ 2|V_\sigma|3 \ 4\rangle_d^J &= \frac{(4\pi g_\sigma)^2}{2J+1}(-)^{j_2-j_4} \langle j_1||Y_J||j_3\rangle \, \langle j_2||Y_J||j_4\rangle \\ &\times \int \frac{q^2 dq}{(2\pi)^3} \langle 1 \ | \, \gamma_0 j_J(qr)|3 \ \rangle D_\sigma(q) \langle 2| \, \gamma_0 j_J(qr)|4 \ \rangle \end{aligned} \tag{D.17}$$

For $J = 0$, $j_1 = j_3$, and $j_2 = j_4$ this means

$$\begin{aligned} \langle 1 \ 2|V_\sigma|3 \ 4\rangle_d^0 &= \delta_{\kappa_1 \kappa_3} \delta_{\kappa_2 \kappa_2} \hat{j}_1 \hat{j}_2 4\pi g_\sigma^2 \\ &\times \int \frac{q^2 dq}{(2\pi)^3} \langle 1 \ | \, \gamma_0 j_0(qr)|3 \ \rangle D_\sigma(q) \langle 2| \, \gamma_0 j_0(qr)|4 \ \rangle \end{aligned} \tag{D.18}$$

$\omega-$ and $\rho-$meson

- for the time-like part of the ω- and ρ-meson: $\Gamma = \gamma^0$

$$\langle 1 \ ||\Gamma_{\omega_0} \, j_J(qr) Y_J||3 \ \rangle = \langle j_1||Y_J||j_3\rangle \, \langle 1 \ | \, j_J(qr)|3\rangle \, , \tag{D.19}$$

with:

$$\langle 1|j_J(qr)|3\rangle = \int r^2 dr \, j_J(qr) \, (f_1^*(r) f_3(r) + g_1^*(r) g_3(r)) \tag{D.20}$$

and

$$\begin{aligned} \langle 1 \ 2|V_{\omega_o}|3 \ 4\rangle_d^J &= \frac{(4\pi g_\omega)^2}{2J+1}(-)^{j_2-j_4} \langle j_1||Y_J||j_3\rangle \, \langle j_2||Y_J||j_4\rangle \\ &\times \int \frac{q^2 dq}{(2\pi)^3} \langle 1 \ | \, j_J(qr)|3 \ \rangle D_\omega(q) \langle 2| \, j_J(qr)|4 \ \rangle \end{aligned} \tag{D.21}$$

For $J=0$, $j_1=j_3$, and $j_2=j_4$ this means

$$\begin{aligned}\langle 1\ 2|V_{\omega_0}|3\ 4\rangle_d^0 &= \delta_{\kappa_1\kappa_3}\delta_{\kappa_2\kappa_2}\hat{j}_1\hat{j}_2 4\pi g_\omega^2 \\ &\times \int \frac{q^2dq}{(2\pi)^3}\langle 1\mid j_0(qr)|3\rangle D_\omega(q)\langle 2|\, j_0(qr)|4\rangle \end{aligned} \tag{D.22}$$

- for the spatial part of the ω- and ρ-mesons: $\Gamma=\boldsymbol{\alpha}$

$$\begin{aligned}\langle 1\ ||j_L(qr)\,[\boldsymbol{\alpha}\,Y_L]_J\,||3\rangle &= -\Big\{\langle l_1 j_1||\,[\vec{\sigma}Y_L]_J\,||\tilde{l}_3 j_3\rangle\, i\int r^2dr j_L(qr) f_1^*(r) g_3(r) \\ &- \langle \tilde{l}_1 j_1||\,[\vec{\sigma}Y_L]_J\,||l_3 j_3\rangle\, i\int r^2dr j_L(qr) g_1^*(r) f_3(r)\Big\}\end{aligned} \tag{D.23}$$

The minus sign comes from the fact that $\boldsymbol{\omega}$ originates an attractive interaction. For $J=0$, $j_1=j_3$, and $j_2=j_4$ this means (with Eq. (J.19)

$$\begin{aligned}\langle 1\ 2|V_{\boldsymbol{\omega}}|3\ 4\rangle_d^0 &= -(4\pi g_\omega)^2\int\frac{q^2dq}{(2\pi)^3} \\ &\times\langle 1\ ||\,j_1(qr)\,[\boldsymbol{\alpha}Y_1]_0\,||\ 3\rangle\, D_\omega(q)\,\langle 2\ ||\,j_1(qr)\,[\boldsymbol{\gamma}Y_1]_0\,||\ 4\rangle \\ &= --\hat{j}_1\hat{j}_2\,4\pi g_\omega^2\int\frac{q^2dq}{(2\pi)^3}\int r_1^2dr_1\, j_1(qr_1)\,[f_1^*(r_1)g_3(r_1)-g_1^*(r_1)f_3(r_1)] \\ &\times D_\omega(q)\int r_2^2dr_2\, j_1(qr_2)\,[f_2^*(r_2)g_4(r_2)-g_2^*(r_2)f_4(r_2)]\end{aligned} \tag{D.24}$$

D.2.2 The Exchange Term

The exchange term is defined as

$$\begin{aligned}&\langle 12|V|34\rangle_{ex}^J \\ &= \sum_{m_1m_3}(-)^{j_3-m_3}C(j_1m_1j_3-m_3|JM)\sum_{m_4m_2}(-)^{j_2-m_2}C(j_4m_4j_2-m_2|JM) \\ &\times\langle j_1m_1j_2m_2|V|j_4m_4j_3m_3\rangle \\ &= \sum_\lambda(2\lambda+1)(-)^{j_3+j_4+J+\lambda}\left\{\begin{array}{ccc} j_1 & j_3 & J\\ j_2 & j_4 & \lambda\end{array}\right\}\langle 12|V|43\rangle_d^\lambda\end{aligned} \tag{D.25}$$

We therefore obtain for vertices Γ, which do not depend on the spin (1, γ_0,γ_5)

$$\begin{aligned}\langle 1\ 2|V_m|3\ 4\rangle_{ex}^J &= (4\pi g_m)^2\sum_\lambda(-)^{j_2+j_4+J+\lambda}\left\{\begin{array}{ccc} j_1 & j_3 & J\\ j_2 & j_4 & \lambda\end{array}\right\} \\ &\times\int\frac{q^2dq}{(2\pi)^3}\langle 1\ ||\Gamma_m\, j_\lambda(qr)Y_\lambda||4\ \rangle\, D_m(q)\,\langle 2||\Gamma_m\, j_\lambda(qr)Y_\lambda||3\ \rangle\end{aligned} \tag{D.26}$$

and for those, which depend on the spin (γ_i)

$$\begin{aligned}\langle 1\ 2|V_m|3\ 4\rangle_{ex}^J &= (4\pi g_m)^2\sum_\lambda(-)^{j_2-j_4+J+L}\left\{\begin{array}{ccc} j_1 & j_3 & J\\ j_2 & j_4 & \lambda\end{array}\right\} \\ &\times\int\frac{q^2dq}{(2\pi)^3}\langle 1\ ||j_L(qr)\left[\vec{\Gamma}_m Y_L\right]_\lambda||4\rangle\, D_m(q)\,\langle 2||j_L(qr)\left[\vec{\Gamma}_m Y_L\right]_\lambda||3\rangle\end{aligned} \tag{D.27}$$

$\sigma-$meson

$$\langle 1\ 2|V_\sigma|3\ 4\rangle^J_{ex} = (4\pi g_\sigma)^2 \sum_\lambda (-)^{j_2+j_4+J+\lambda} \left\{ \begin{array}{ccc} j_1 & j_3 & J \\ j_2 & j_4 & \lambda \end{array} \right\} \langle j_1||Y_\lambda||j_4\rangle\langle j_2||Y_\lambda||j_3\rangle$$
$$\times \int \frac{q^2dq}{(2\pi)^3} \langle 1|\gamma_0 j_\lambda(qr)|4\rangle\, D_\sigma(q)\, \langle 2|\gamma_0 j_\lambda(qr)|3\rangle \qquad \text{(D.28)}$$

For $J=0$, $j_1=j_3$ and $j_2=j_4$ this means:

$$\langle 1\ 2|V_\sigma|3\ 4\rangle^0_{ex} = \delta_{j_1 j_3}\delta_{j_2 j_4}\hat{j}_1\hat{j}_2 \sum_\lambda \frac{1+(-)^{l_1+l_2+\lambda}}{2}(2\lambda+1) \left(\begin{array}{ccc} j_1 & \lambda & j_2 \\ -\frac{1}{2} & 0 & \frac{1}{2} \end{array} \right)^2$$
$$\times 4\pi g_\sigma^2 \int \frac{q^2dq}{(2\pi)^3} \langle 1|\gamma_0 j_\lambda(qr)|4\rangle\, D_\sigma(q)\, \langle 2|\gamma_0 j_\lambda(qr)|3\rangle \qquad \text{(D.29)}$$

$\omega-$ and $\rho-$mesons

- for the time-like part of the ω- or ρ-meson:

$$\langle 1\ 2|V_{\omega_0}|3\ 4\rangle^J_{ex} = \sum_\lambda (-)^{j_2+j_4+J+\lambda} \left\{ \begin{array}{ccc} j_1 & j_3 & J \\ j_2 & j_4 & \lambda \end{array} \right\} \langle j_1||Y_\lambda||j_4\rangle\langle j_2||Y_\lambda||j_3\rangle$$
$$\times (4\pi g_\omega)^2 \int \frac{q^2dq}{(2\pi)^3} \langle 1|j_\lambda(qr)|4\rangle\, D_\omega(q)\, \langle 2|j_\lambda(qr)|3\rangle \qquad \text{(D.30)}$$

  For $J=0$, $j_1=j_3$, $l_1=l_3$ and $j_2=j_4$, $l_2=l_4$ this means:

$$\langle 1\ 2|V_{\omega_0}|3\ 4\rangle^0_{ex} = \delta_{j_1 j_3}\delta_{j_2 j_4}\hat{j}_1\hat{j}_2 \sum_\lambda \frac{1+(-)^{l_1+l_2+\lambda}}{2}(2\lambda+1) \left(\begin{array}{ccc} j_1 & \lambda & j_2 \\ -\frac{1}{2} & 0 & \frac{1}{2} \end{array} \right)^2$$
$$\times 4\pi g_\omega^2 \int \frac{q^2dq}{(2\pi)^3} \langle 1|j_\lambda(qr)|4\rangle\, D_\omega(q)\, \langle 2|j_\lambda(qr)|3\rangle \qquad \text{(D.31)}$$

- For the spatial part of the $\omega-$ and $\rho-$mesons
  For $J=0$, $j_1=j_3$ and $j_2=j_4$, the matrix elements given in Eq.(D.28) become

$$\langle 1\ 2|V_{\boldsymbol{\omega}}|3\ 4\rangle^0_{ex} = -\delta_{j_1 j_3}\delta_{j_2 j_4} \frac{1}{\hat{j}_1\hat{j}_2} \sum_{\lambda L} (-)^{j_1+j_2+\lambda+L}\ (4\pi g_\omega)^2 \qquad \text{(D.32)}$$
$$\times \int \frac{q^2dq}{(2\pi)^3}\ \langle 1||j_L(qr)\left[\vec{\Gamma}_\omega Y_L\right]_\lambda||4\rangle\, D_\omega(q)\, \langle 2||j_L(qr)\left[\vec{\Gamma}_\omega Y_L\right]_\lambda||3\rangle$$

  where the reduced matrix elements are given by Eq.(D.24).

D.2.3 The Pairing Term

The pairing term is defined as

$$\langle 12|V|34\rangle^J_{pp} \qquad \text{(D.33)}$$
$$= \sum_{m_1 m_2} C(j_1 m_1 j_2 m_2|JM) \sum_{m_3 m_4} C(j_3 m_3 j_4 m_4|JM) \langle j_1 m_1 j_2 m_2|V|j_3 m_3 j_4 m_4\rangle$$
$$= \sum_\lambda (2\lambda+1)(-)^{j_3+j_4+J} \left\{ \begin{array}{ccc} j_1 & j_2 & J \\ j_4 & j_3 & \lambda \end{array} \right\} \langle 12|V|34\rangle^\lambda_d \qquad \text{(D.34)}$$

We therefore obtain for vertices Γ, which do not depend on the spin (1, γ_0,γ_5)

$$\begin{aligned}\langle 1\ 2|V_m|3\ 4\rangle^J_{pp} &= \sum_\lambda (-)^{j_2+j_3+J} \left\{ \begin{array}{ccc} j_1 & j_2 & J \\ j_4 & j_3 & \lambda \end{array} \right\} \\ &\times (4\pi g_m)^2 \int \frac{q^2 dq}{(2\pi)^3} \langle 1\ ||\Gamma_m\, j_\lambda(qr) Y_\lambda||3\rangle D_m(q) \langle 2||\Gamma_m\, j_\lambda(qr) Y_\lambda||4\ \rangle \end{aligned} \tag{D.35}$$

and for those, which depend on the spin (γ_i)

$$\begin{aligned}\langle 1\ 2|V_m|3\ 4\rangle^J_{pp} &= \sum_{\lambda L} (-)^{j_2-j_3+L+J+\lambda} \left\{ \begin{array}{ccc} j_1 & j_2 & J \\ j_4 & j_3 & \lambda \end{array} \right\} \\ &\times (4\pi g_m)^2 \int \frac{q^2 dq}{(2\pi)^3} \langle 1\ ||j_L(qr) \left[\vec{\Gamma}_m Y_L\right]_\lambda ||3\rangle D_m(q) \langle 2\ ||j_L(qr) \left[\vec{\Gamma}_m Y_L\right]_\lambda ||4\rangle. \end{aligned} \tag{D.36}$$

$\sigma-$meson

$$\begin{aligned}\langle 1\ 2|V_\sigma|3\ 4\rangle^J_{pp} &= \sum_\lambda (-)^{j_2+j_3+J} \left\{ \begin{array}{ccc} j_1 & j_2 & J \\ j_4 & j_3 & \lambda \end{array} \right\} \langle j_1||Y_\lambda||j_3\rangle \langle j_2||Y_\lambda||j_4\rangle \\ &\times (4\pi g_\sigma)^2 \int \frac{q^2 dq}{(2\pi)^3} \langle 1|\gamma_0 j_\lambda(qr)|3\rangle\, D_\sigma(q)\, \langle 2|\gamma_0 j_\lambda(qr)|4\rangle \end{aligned} \tag{D.37}$$

For $J=0$, $j_1=j_2$, and $j_3=j_4$, this means

$$\begin{aligned}\langle 1\ 2|V_\sigma|3\ 4\rangle^0_{pp} &= \delta_{j_1 j_2}\delta_{j_3 j_4}\hat{j}_1\hat{j}_3 \sum_\lambda \frac{1+(-)^{l_1+l_3+\lambda}}{2} (-)^\lambda (2\lambda+1) \begin{pmatrix} j_1 & \lambda & j_3 \\ -\frac{1}{2} & 0 & \frac{1}{2} \end{pmatrix}^2 \\ &\times 4\pi g_\sigma^2 \int \frac{q^2 dq}{(2\pi)^3} \langle 1|\gamma_0 j_\lambda(qr)|3\rangle\, D_\sigma(q)\, \langle 2|\gamma_0 j_\lambda(qr)|4\rangle \end{aligned} \tag{D.38}$$

$\omega-$ and $\rho-$mesons

- for the time-like part of the ω- or ρ-meson:

$$\begin{aligned}\langle 1\ 2|V_{\omega_0}|3\ 4\rangle^J_{pp} &= \sum_\lambda (-)^{j_2+j_3+J} \left\{ \begin{array}{ccc} j_1 & j_2 & J \\ j_4 & j_3 & \lambda \end{array} \right\} \langle j_1||Y_\lambda||j_3\rangle \langle j_2||Y_\lambda||j_4\rangle \\ &\times (4\pi g_\omega)^2 \int \frac{q^2 dq}{(2\pi)^3} \langle 1|j_\lambda(qr)|3\rangle\, D_\omega(q)\, \langle 2|j_\lambda(qr)|4\rangle \end{aligned} \tag{D.39}$$

For $J=0$, $j_1=j_2$ and $j_3=j_4$ this means

$$\begin{aligned}\langle 1\ 2|V_{\omega_0}|3\ 4\rangle^0_{pp} &= \delta_{j_1 j_2}\delta_{j_3 j_4}\hat{j}_1\hat{j}_3 \sum_\lambda \frac{1+(-)^{l_1+l_3+\lambda}}{2} (-)^\lambda (2\lambda+1) \begin{pmatrix} j_1 & \lambda & j_3 \\ -\frac{1}{2} & 0 & \frac{1}{2} \end{pmatrix}^2 \\ &\times 4\pi g_\omega^2 \int \frac{q^2 dq}{(2\pi)^3} \langle 1|j_\lambda(qr)|3\rangle\, D_\omega(q)\, \langle 2|j_\lambda(qr)|4\rangle \end{aligned} \tag{D.40}$$

- for the spatial part of the $\omega-$ and $\rho-$mesons
  For $J = 0$, $j_1 = j_2$ and $j_3 = j_4$, the matrix elements given in Eq.(D.37) become

$$\begin{aligned} \langle 1\ 2|V_{\boldsymbol{\omega}}|3\ 4\rangle^0_{pp} &= -\delta_{j_1 j_2}\delta_{j_3 j_4}\frac{1}{\hat{j}_1\hat{j}_3}\sum_{\lambda L}(-)^{L+1}\ (4\pi g_\omega)^2 \\ &\times \int \frac{q^2 dq}{(2\pi)^3}\ \langle 1||j_L(qr)\left[\vec{\Gamma}_\omega Y_L\right]_\lambda||3\rangle\ D_\omega(q)\ \langle 2||j_L(qr)\left[\vec{\Gamma}_\omega Y_L\right]_\lambda||4\rangle \end{aligned} \tag{D.41}$$

  where the reduced matrix elements are given by Eq.(D.24).

Appendix E

Pseudo-Vector Coupling: Two-body Matrix Elements

As the Dirac spinors defined in Eq.(D.2) are time-independent, the vertex and the propagator of the $\vec{\pi}$-meson (pv-coupling) reduce to

$$\vec{\Gamma}_\pi^{(pv)} = \gamma_5 \vec{\tau} \boldsymbol{\gamma} \tag{E.1}$$

$$D_\pi^{(pv)}(1,2) = -\frac{1}{4\pi} \boldsymbol{\nabla}_{\mathbf{r}_1} \frac{\mathrm{e}^{-m_\pi |\mathbf{r}_1 - \mathbf{r}_2|}}{|\mathbf{r}_1 - \mathbf{r}_2|} \boldsymbol{\nabla}_{\mathbf{r}_2} \tag{E.2}$$

$$D_\pi^{(pv)}(q) = -\frac{1}{q^2 + m_\pi^2} \tag{E.3}$$

respectively. Therefore, the two-body matrix elements in the momentum space representation become

$$\langle 1\ 2|V_\pi^{(pv))}|3\ 4\rangle = \left(\frac{f_\pi}{m_\pi}\right)^2 \int \frac{d^3q}{(2\pi)^3} \int d^3r_1 d^3r_2\, \bar{\psi}_1(\mathbf{r}_1)\, \bar{\psi}_2(\mathbf{r}_2) \tag{E.4}$$

$$\times\, \vec{\boldsymbol{\Gamma}}_1 \cdot \vec{\nabla}_{\mathbf{r}_1}\, \mathrm{e}^{i\mathbf{q}(\mathbf{r}_1 - \mathbf{r}_2)}\, D_\pi(q)\, \overleftarrow{\nabla}_{\mathbf{r}_2} \cdot \vec{\boldsymbol{\Gamma}}_2\, \psi_3(\mathbf{r}_1)\, \psi_4(\mathbf{r}_2) \tag{E.5}$$

$$= \left(\frac{f_\pi}{m_\pi}\right)^2 \int \frac{d^3q}{(2\pi)^3} \langle 1\ |\, \vec{\boldsymbol{\Gamma}}_1 \cdot \nabla_{\mathbf{r}} \mathrm{e}^{i\mathbf{qr}} |3\ \rangle\, D_\pi(q)\ \langle\ 2|\nabla_{\mathbf{r}} \cdot\ \vec{\boldsymbol{\Gamma}}_2 \mathrm{e}^{-i\mathbf{qr}}|4\rangle$$

For the moment we neglect the isospin dependence, and we concentrate on the angular part of the matrix elements. A multipole expansion given in Eq. (D.9) of the plane waves of Eq.(E.4), and an integration over the transferred momentum angles Ω_q, gives

$$\langle 1\ 2|V_\pi^{(pv)}|3\ 4\rangle = (4\pi \frac{f_\pi}{m_\pi})^2 \sum_{LM_L} \int \frac{q^2\, dq}{(2\pi)^3} \quad \langle 1\,|\gamma_0\gamma_5\, \boldsymbol{\gamma} \cdot \nabla_{\mathbf{r}}\, j_L(qr)\, Y_{LM_L}(\Omega)|3\rangle \tag{E.6}$$

$$\times\, D_\pi(q)\, \langle 2\,|\gamma_0\gamma_5 \boldsymbol{\gamma} \cdot \nabla_{\mathbf{r}}\, j_L(qr) Y^*_{LM_L}(\Omega)|4\rangle,$$

where the integrals over the coordinates still contain the gradient of Bessel functions and spherical harmonics. Writing explicitly

$$\gamma_0\gamma_5\, \boldsymbol{\gamma} \cdot \nabla_{\mathbf{r}}\, j_L(qr) Y_{LM_L}(\Omega) = \begin{pmatrix} -\boldsymbol{\sigma} \cdot \nabla_{\mathbf{r}} & 0 \\ 0 & -\boldsymbol{\sigma} \cdot \nabla_{\mathbf{r}} \end{pmatrix} j_L(qr) Y_{LM_L}(\Omega), \tag{E.7}$$

and using the gradient formula for the Bessel functions

$$\begin{aligned}\nabla_{\mathbf{r}} j_L(qr) Y_{LM_L}(\Omega) &= \sqrt{\frac{L+1}{2L+1}}\, q\, j_{L+1}(qr) \boldsymbol{Y}_{LL+1M_L}(\Omega) \\ &+ \sqrt{\frac{L}{2L+1}}\, q\, j_{L-1}(qr) \boldsymbol{Y}_{LL-1M_L}(\Omega) \end{aligned} \tag{E.8}$$

in which the vector spherical harmonics $\boldsymbol{Y}_{JlM}$ are given by

$$\boldsymbol{Y}_{JlM}(\Omega) = \sum_{m_l m_s} C(lm_l 1m_s|JM)\, \boldsymbol{e}_{m_s}\, Y_{mm_l}(\Omega) \tag{E.9}$$

and $\boldsymbol{e}_{m_s}$ are the spin spherical unit vectors, allows us to remove the gradient from the integrands and to rewrite them as a linear combination of Bessel functions and vector spherical harmonics. After recoupling spin and angular momentum, we obtain

$$\begin{aligned}\boldsymbol{\sigma} \cdot \nabla_{\mathbf{r}}\, j_L(qr) Y_{LM_L}(\Omega) &= \sqrt{\frac{L+1}{2L+1}}\, q\, j_{L+1}(qr)\, \left[\sigma Y_{L+1}\right]_{LM_L} \\ &+ \sqrt{\frac{L}{2L+1}}\, q\, j_{L-1}(qr)\, \left[\sigma Y_{L-1}\right]_{LM_L}. \end{aligned} \tag{E.10}$$

Therefore, the relativistic uncoupled two-body matrix elements of the π-meson (pv-coupling) read

$$\begin{aligned}\langle 1\,2|V_\pi^{(pv)}|3\,4\rangle &= (4\pi \frac{f_\pi}{m_\pi})^2 \sum_{LM_L} \int \frac{q^4 dq}{(2\pi)^3} \left\{ \sqrt{\frac{L+1}{2L+1}}\, \langle 1|j_{L+1}(qr)\, [\Sigma\, Y_{L+1}]_{LM_L}\, |3\,\rangle \right. \\ &+ \left. \sqrt{\frac{L}{2L+1}}\, \langle 1|j_{L-1}(qr)\, [\Sigma\, Y_{L-1}]_{LM_L}\, |3\,\rangle \right\} D_\pi(q) \\ &\times \left\{ \sqrt{\frac{L+1}{2L+1}}\, \langle 2|j_{L+1}(qr)\, [\Sigma\, Y_{L+1}]_{L-M_L}\, |4\,\rangle \right. \\ &+ \left. \sqrt{\frac{L}{2L+1}}\, \langle 2|j_{L-1}(qr)\, [\Sigma\, Y_{L-1}]_{L-M_L}\, |4\,\rangle \right\}, \end{aligned} \tag{E.11}$$

where

$$\boldsymbol{\Sigma} = \gamma_5 \gamma^0 \boldsymbol{\gamma} = \begin{pmatrix} \boldsymbol{\sigma} & 0 \\ 0 & \boldsymbol{\sigma} \end{pmatrix}. \tag{E.12}$$

E.1 jj-Coupled Matrix Elements

In the following we calculate the relativistic two-body matrix elements of the π-meson coupled to good angular momentum.

E.1.1 Direct Term

For the direct term we have

$$\begin{aligned}\langle 1\ 2|V_\pi^{(pv)}|3\ 4\rangle_d^J &= \sum_{m_1 m_3}(-)^{j_3-m_3}C(j_1 m_1 j_3 - m_3|JM)\times \\ &\times\sum_{m_4 m_2}(-)^{j_2-m_2}C(j_4 m_4 j_2 - m_2|JM)\times \\ &\times\langle j_1 m_1\ j_2 m_2|V_\pi^{(pv)}|j_3 m_3\ j_4 m_4\rangle \end{aligned} \tag{E.13}$$

Using the reduced matrix elements given in Eq.(D.12), we obtain for the direct term of the π-meson matrix elements

$$\langle 1\ 2|V_\pi^{(pv)}|3\ 4\rangle_d^J = (4\pi\frac{f_\pi}{m_\pi})^2\frac{(-)^{j_2-j_4}}{(2J+1)^2}\int\frac{q^4dq}{(2\pi)^3} \tag{E.14}$$

$$\begin{aligned}\times\ & \{(J+1)\ \langle n_1 j_1||j_{J+1}(qr)\,[\Sigma\, Y_{J+1}]_J\,||n_3 j_3\rangle\, D_\pi(q)\,\langle n_2 j_2||j_{J+1}(qr)\,[\Sigma\, Y_{J+1}]_J\,||n_4 j_4\rangle \\ +\ & \sqrt{J(J+1)}\,\langle n_1 j_1||j_{J+1}(qr)\,[\Sigma\, Y_{J+1}]_J\,||n_3 j_3\rangle\, D_\pi(q)\,\langle n_2 j_2||j_{J-1}(qr)\,[\Sigma\, Y_{J-1}]_J\,||n_4 j_4\rangle \\ +\ & \sqrt{J(J+1)}\,\langle n_1 j_1||j_{J-1}(qr)\,[\Sigma\, Y_{J-1}]_J\,||n_3 j_3\rangle\, D_\pi(q)\,\langle n_2 j_2||j_{J+1}(qr)\,[\Sigma\, Y_{J+1}]_J\,||n_4 j_4\rangle \\ +\ & J\langle n_1 j_1||j_{J-1}(qr)\,[\Sigma\, Y_{J-1}]_J\,||n_3 j_3\rangle\, D_\pi(q)\,\langle n_2 j_2||j_{J-1}(qr)\,[\Sigma\, Y_{J-1}]_J\,||n_4 j_4\rangle\end{aligned}$$

where the reduced matrix elements read

$$\begin{aligned}\langle n_1 j_1||j_{J+1}(qr)\ [\Sigma Y_{J+1}]_J\,||n_3 j_3\rangle &= \langle l_1 j_1||\,[\sigma Y_{J+1}]_J\,||l_3 j_3\rangle\int r^2dr\, j_{J+1}(qr)f^*_{n_1}(r)f_{n_3}(r) \\ &+ \langle \tilde{l}_1 j_1||\,[\sigma Y_{J+1}]_J\,||\tilde{l}_3 j_3\rangle\int r^2dr\, j_{J+1}(qr)g^*_{n_1}(r)g_{n_3}(r)\end{aligned} \tag{E.15}$$

and so on.

E.1.2 Exchange Term

As already seen, the exchange term is defined as

$$\langle 12|V_\pi^{(pv)}|34\rangle_{ex}^J = \sum_\lambda(2\lambda+1)(-)^{j_3+j_4+J+\lambda}\left\{\begin{array}{ccc} j_1 & j_3 & J \\ j_2 & j_4 & \lambda\end{array}\right\}\langle 12|V_\pi^{(pv)}|43\rangle_d^\lambda \tag{E.16}$$

Therefore we obtain

$$\langle 12|V_\pi^{(pv)}|34\rangle_{ex}^J = \sum_\lambda\frac{(-)^{j_2+j_4+J+\lambda}}{2\lambda+1}\left\{\begin{array}{ccc} j_1 & j_3 & J \\ j_2 & j_4 & \lambda\end{array}\right\}(4\pi\frac{f_\pi}{m_\pi})^2\int\frac{q^4dq}{(2\pi)^3} \tag{E.17}$$

$$\times\ \{(\lambda+1)\ \langle n_1 j_1||j_{\lambda+1}(qr)\,[\Sigma\, Y_{\lambda+1}]_\lambda\,||n_4 j_4\rangle\ \ D_\pi(q)\,\langle n_2 j_2||j_{\lambda+1}(qr)\,[\Sigma\, Y_{\lambda+1}]_\lambda\,||n_3 j_3\rangle$$

$$+ \quad \sqrt{\lambda(\lambda+1)}\,\langle n_1 j_1||j_{\lambda+1}(qr)\,[\Sigma\,Y_{\lambda+1}]_\lambda\,||n_4 j_4\rangle\,D_\pi(q)\,\langle n_2 j_2||j_{\lambda-1}(qr)\,[\Sigma\,Y_{\lambda-1}]_\lambda\,||n_3 j_3\rangle$$

$$+ \quad \sqrt{\lambda(\lambda+1)}\,\langle n_1 j_1||j_{\lambda-1}(qr)\,[\Sigma\,Y_{\lambda-1}]_\lambda\,||n_4 j_4\rangle\,D_\pi(q)\,\langle n_2 j_2||j_{\lambda+1}(qr)\,[\Sigma\,Y_{\lambda+1}]_\lambda\,||n_3 j_3\rangle$$

$$+ \quad \lambda\,\langle n_1 j_1||j_{\lambda-1}(qr)\,[\Sigma\,Y_{\lambda-1}]_\lambda\,||n_4 j_4\rangle\,D_\pi(q)\,\langle n_2 j_2||j_{\lambda-1}(qr)\,[\Sigma\,Y_{\lambda-1}]_\lambda\,||n_3 j_3\rangle\}$$

E.1.3 Pairing Term

The pairing term is defined as

$$\langle 12|V_\pi^{(pv)}|34\rangle_{ex}^J = \sum_\lambda (2\lambda+1)(-)^{j_3+j_4+J} \left\{ \begin{array}{ccc} j_1 & j_2 & J \\ j_4 & j_3 & \lambda \end{array} \right\} \langle 12|V_\pi^{(pv)}|34\rangle_d^\lambda \quad \text{(E.18)}$$

Therefore we obtain

$$\langle 12|V_\pi^{(pv)}|34\rangle_{pp}^J = \sum_\lambda \frac{(-)^{j_2+j_3+J}}{2\lambda+1} \left\{ \begin{array}{ccc} j_1 & j_2 & J \\ j_4 & j_3 & \lambda \end{array} \right\} (4\pi\frac{f_\pi}{m_\pi})^2 \int \frac{q^4 dq}{(2\pi)^3}$$

$$\times \quad \{(\lambda+1)\ \ \langle n_1 j_1||j_{\lambda+1}(qr)\,[\Sigma\,Y_{\lambda+1}]_\lambda\,||n_3 j_3\rangle \quad D_\pi(q)\,\langle n_2 j_2||j_{\lambda+1}(qr)\,[\Sigma\,Y_{\lambda+1}]_\lambda\,||n_4 j_4\rangle$$

$$+ \quad \sqrt{\lambda(\lambda+1)}\,\langle n_1 j_1||j_{\lambda+1}(qr)\,[\Sigma\,Y_{\lambda+1}]_\lambda\,||n_3 j_3\rangle\,D_\pi(q)\,\langle n_2 j_2||j_{\lambda-1}(qr)\,[\Sigma\,Y_{\lambda-1}]_\lambda\,||n_4 j_4\rangle$$

$$+ \quad \sqrt{\lambda(\lambda+1)}\,\langle n_1 j_1||j_{\lambda-1}(qr)\,[\Sigma\,Y_{\lambda-1}]_\lambda\,||n_3 j_3\rangle\,D_\pi(q)\,\langle n_2 j_2||j_{\lambda+1}(qr)\,[\Sigma\,Y_{\lambda+1}]_\lambda\,||n_4 j_4\rangle$$

$$+ \quad \lambda\,\langle n_1 j_1||j_{\lambda-1}(qr)\,[\Sigma\,Y_{\lambda-1}]_\lambda\,||n_3 j_3\rangle\,D_\pi(q)\,\langle n_2 j_2||j_{\lambda-1}(qr)\,[\Sigma\,Y_{\lambda-1}]_\lambda\,||n_4 j_4\rangle\}$$

E.2 Matrix Elements Coupled to $J = 0^+$

Introducing the Slater integral as

$$S^{k_1 k_2}_{n_1 l_1 n_2 l_2 n_3 l_3 n_4 l_4} = \frac{2}{\pi} \int q^4 dq \, \langle n_1 l_1 | j_{k_1}(qr) | n_3 l_3 \rangle \, D_\pi(q) \, \langle n_2 l_2 | j_{k_1}(qr) | n_4 l_4 \rangle \tag{E.19}$$

we write the coupled matrix elements as follows.

E.2.1 Direct Term

$$\langle 1\,2 | V_\pi^{(pv)} | 3\,4 \rangle^0_d = (\frac{f_\pi}{m_\pi})^2 \langle l_1 j_1 || \left[\Sigma Y_1\right]_0 || l_3 j_3 \rangle \, \langle l_2 j_2 || \left[\Sigma Y_1\right]_0 || l_4 j_4 \rangle \, S^{1\,1}_{n_1 l_1 n_2 l_2 n_3 l_3 n_4 l_4} \tag{E.20}$$

E.2.2 Exchange Term

$$\begin{aligned}
\langle 1\,2 | V_\pi^{(pv)} | 3\,4 \rangle^0_{ex} &= (\frac{f_\pi}{m_\pi})^2 \frac{(-)^{j_1 - j_2}}{\hat{j}_1 \hat{j}_2} \sum_\lambda \frac{1}{2\lambda + 1} \\
&\times \Big[(\lambda + 1) \, \langle l_1 j_1 || \left[\Sigma Y_{\lambda+1}\right]_\lambda || l_4 j_4 \rangle \, \langle l_2 j_2 || \left[\Sigma Y_{\lambda+1}\right]_\lambda || l_3 j_3 \rangle \, S^{\lambda+1\,\lambda+1}_{n_1 l_1 n_2 l_2 n_4 l_4 n_3 l_3} \\
&+ \sqrt{\lambda(\lambda+1)} \, \langle l_1 j_1 || \left[\Sigma Y_{\lambda+1}\right]_\lambda || l_4 j_4 \rangle \, \langle l_2 j_2 || \left[\Sigma Y_{\lambda-1}\right]_\lambda || l_3 j_3 \rangle \, S^{\lambda+1\,\lambda-1}_{n_1 l_1 n_2 l_2 n_4 l_4 n_3 l_3} \\
&+ \sqrt{\lambda(\lambda+1)} \, \langle l_1 j_1 || \left[\Sigma Y_{\lambda-1}\right]_\lambda || l_4 j_4 \rangle \, \langle l_2 j_2 || \left[\Sigma Y_{\lambda+1}\right]_\lambda || l_3 j_3 \rangle \, S^{\lambda-1\,\lambda+1}_{n_1 l_1 n_2 l_2 n_4 l_4 n_3 l_3} \\
&+ \lambda \, \langle l_1 j_1 || \left[\Sigma Y_{\lambda-1}\right]_\lambda || l_4 j_4 \rangle \, \langle l_2 j_2 || \left[\Sigma Y_{\lambda-1}\right]_\lambda || l_3 j_3 \rangle \, S^{\lambda-1\,\lambda-1}_{n_1 l_1 n_2 l_2 n_4 l_4 n_3 l_3} \Big]
\end{aligned} \tag{E.21}$$

E.2.3 Pairing Term

$$\begin{aligned}
\langle 1\,2 | V_\pi^{(pv)} | 3\,4 \rangle^0_{pp} &= (\frac{f_\pi}{m_\pi})^2 \frac{1}{\hat{j}_1 \hat{j}_3} \sum_\lambda (-)^\lambda \frac{1}{2\lambda + 1} \\
&\times \Big[(\lambda + 1) \, \langle l_1 j_1 || \left[\Sigma Y_{\lambda+1}\right]_\lambda || l_3 j_3 \rangle \, \langle l_2 j_2 || \left[\Sigma Y_{\lambda+1}\right]_\lambda || l_4 j_4 \rangle \, S^{\lambda+1\,\lambda+1}_{n_1 l_1 n_2 l_2 n_3 l_3 n_4 l_4} \\
&+ \sqrt{\lambda(\lambda+1)} \, \langle l_1 j_1 || \left[\Sigma Y_{\lambda+1}\right]_\lambda || l_3 j_3 \rangle \, \langle l_2 j_2 || \left[\Sigma Y_{\lambda-1}\right]_\lambda || l_4 j_4 \rangle \, S^{\lambda+1\,\lambda-1}_{n_1 l_1 n_2 l_2 n_3 l_3 n_4 l_4} \\
&+ \sqrt{\lambda(\lambda+1)} \, \langle l_1 j_1 || \left[\Sigma Y_{\lambda-1}\right]_\lambda || l_3 j_3 \rangle \, \langle l_2 j_2 || \left[\Sigma Y_{\lambda+1}\right]_\lambda || l_4 j_4 \rangle \, S^{\lambda-1\,\lambda+1}_{n_1 l_1 n_2 l_2 n_3 l_3 n_4 l_4} \\
&+ \lambda \, \langle l_1 j_1 || \left[\Sigma Y_{\lambda-1}\right]_\lambda || l_3 j_3 \rangle \, \langle l_2 j_2 || \left[\Sigma Y_{\lambda-1}\right]_\lambda || l_4 j_4 \rangle \, S^{\lambda-1\,\lambda-1}_{n_1 l_1 n_2 l_2 n_3 l_3 n_4 l_4} \Big]
\end{aligned} \tag{E.22}$$

E.3 δ-Force in Pseudo-Vector Coupling

The matrix elements of a OBE interaction with pseudo-vector coupling given in Eq. (E.4) contain a contact term in the central spin dependent channel of the force. Similarly to the non-relativistic case, it is argued that the short-range correlations mask the action of this divergent term, and, therefore, it has to be removed from the expression of the matrix elements. In this Section we show how it arises and how to remove it. The two-body matrix elements of one-pion exchange interaction given in Eq.(E.4) may be rewritten as

$$\begin{aligned}\langle 1\ 2|V_\pi^{(pv))}|3\ 4\rangle &= \left(\frac{f_\pi}{m_\pi}\right)^2 \int \frac{d^3q}{(2\pi)^3} \int d^3r_1 d^3r_2\, \psi_1^\dagger(\mathbf{r}_1)\, \boldsymbol{\Sigma}_1 \cdot \mathbf{q}\, \psi_3(\mathbf{r}_1) \\ &\times \ \mathrm{e}^{i\mathbf{q}(\mathbf{r}_1-\mathbf{r}_2)}\, D_\pi(q)\, \psi_2^\dagger(\mathbf{r}_2)\, \boldsymbol{\Sigma}_2 \cdot \mathbf{q}\, \psi_4(\mathbf{r}_2) \end{aligned} \tag{E.23}$$

where the pion propagator is given in Eq. (E.3) with $F_\pi = 1$ and $\boldsymbol{\Sigma}$ is the Dirac matrix given in Eq. (E.12). In order to see how the δ-force arises, it is more convenient to restrict the discussion to the non-relativistic case, therefore, instead of the Dirac matrix $\boldsymbol{\Sigma}$ we simply consider the non-relativistic spin, i.e.

$$\boldsymbol{\Sigma} \cdot \mathbf{q} \longrightarrow \boldsymbol{\sigma} \cdot \mathbf{q}$$

Let us consider the scalar products between the spin of the nucleon 1 and 2 and the transferred momentum $\mathbf{q}$ given in Eq. (E.23): writing $\mathbf{q}$ in terms of spherical harmonics of rank 1 $Y_{1m},\ m = -1, 0, 1$ as

$$\mathbf{q} = q\sqrt{\frac{4\pi}{3}} \sum_m (-)^m Y_{1-m} \mathbf{e}_m$$

where $\mathbf{e}_m$ is the unitary vector along the axis, and the scalar product $\boldsymbol{\sigma} \cdot \mathbf{Y}$ as a zero-rank tensor by using the relation $[\sigma Y_1]_0 = -1/\sqrt{3}\ \boldsymbol{\sigma} \cdot \mathbf{Y}$, we obtain the following identity

$$\boldsymbol{\sigma}_1 \cdot \mathbf{q}\ \boldsymbol{\sigma}_2 \cdot \mathbf{q} = \frac{4\pi}{3} q^2 \boldsymbol{\sigma}_1 \cdot \mathbf{Y}_1\ \boldsymbol{\sigma}_2 \cdot \mathbf{Y}_1 = 3\frac{4\pi}{3}\ q^2\ [\sigma_1 Y_1]_0\ [\sigma_2 Y_1]_0. \tag{E.24}$$

Recoupling the angular and the spin part of the zero-rank tensors, leads to have

$$\boldsymbol{\sigma}_1 \cdot \mathbf{q} \boldsymbol{\sigma}_2 \cdot \mathbf{q} = \frac{1}{3}\ q^2\ \boldsymbol{\sigma}_1 \cdot \boldsymbol{\sigma}_2 + \frac{4\pi}{3}\ q^2\ (\sigma_1\sigma_2)_2\ (Y^1 Y^2)_2. \tag{E.25}$$

Thus, in the two-body matrix elements of a pseudo-vector coupling a tensor of rank 0 and a tensor of rank 2 are contained. Considering the product of the propagator $D_\pi(q)$ with the term of rank 0 given in Eq.s (E.3) and (E.25) respectively, it may be written as

$$\frac{1}{3}\frac{q^2}{q^2+m_\pi^2}\boldsymbol{\sigma}_1 \cdot \boldsymbol{\sigma}_2 = \frac{1}{3}\left(1 + \frac{m_\pi^2}{q^2+m_\pi^2}\right)\boldsymbol{\sigma}_1 \cdot \boldsymbol{\sigma}_2 \tag{E.26}$$

in which the constant term $\frac{1}{3}$ is the δ-force in momentum space. Therefore, going back to the relativistic structure of the problem, in order to eliminate the effect of the contact

term in the matrix elements of the one-pion exchange interaction, we have to subtract a two-body matrix element of the form

$$\begin{aligned}\langle 1\ 2|V_{\delta_\pi}^{(pv))}|3\ 4\rangle &= -\frac{1}{3}\left(\frac{f_\pi}{m_\pi}\right)^2\int\frac{d^3q}{(2\pi)^3}\int d^3r_1 d^3r_2\,\bar{\psi}_1(\mathbf{r}_1)\,\bar{\psi}_2(\mathbf{r}_2)\\ &\times\ \boldsymbol{\Sigma}_1\cdot\boldsymbol{\Sigma}_2\ \mathrm{e}^{i\mathbf{q}(\mathbf{r}_1-\mathbf{r}_2)}\ \psi_3(\mathbf{r}_1)\,\psi_4(\mathbf{r}_2)\end{aligned}\tag{E.27}$$

Using the multipole expansion for the plane wave given in Eq. (D.9), the previous expression reads

$$\begin{aligned}\langle 1\ 2|V_{\delta_\pi}^{(pv))}|3\ 4\rangle &= -\frac{1}{3}\left(\frac{f_\pi}{m_\pi}\right)^2\sum_{L\lambda\mu}(-)^{L+1+\lambda+\mu}\langle l_1j_1|[\Sigma_1Y_L]_{\lambda\mu}|l_3j_3\rangle\langle l_2j_2|[\Sigma_2Y_L]_{\lambda\mu}|l_4j_4\rangle\\ &\times\ S^\lambda_{n_1l_1n_2l_2n_3l_3n_4l_4}\end{aligned}\tag{E.28}$$

where the Slater integral $S^\lambda_{n_1l_1n_2l_2n_3l_3n_4l_4}$ is defined in Eq. (F.1). However, using the orthogonality relation of the Bessel functions it can be noticed that it does not depend on λ in the case of a δ-force and it reads

$$S^\lambda_{n_1l_1n_2l_2n_3l_3n_4l_4}=S_{n_1l_1n_2l_2n_3l_3n_4l_4}=\int r^2drR_{n_1l_1}(r)R_{n_2l_2}(r)R_{n_3l_3}(r)R_{n_4l_4}(r).\tag{E.29}$$

The direct two-body matrix elements coupled to a total momentum J become

$$\begin{aligned}\langle 1\ 2|V_{\delta_\pi}^{(pv))}|3\ 4\rangle^J_d &= -\frac{1}{3}\left(\frac{f_\pi}{m_\pi}\right)^2\frac{1}{2J+1}(-)^{j_2+j_4+J}S_{n_1l_1n_2l_2n_3l_3n_4l_4}\\ &\times\ \sum_L(-)^L\langle l_1j_1||[\Sigma Y_L]_J||l_3j_3\rangle\langle l_2j_2||[\Sigma Y_L]_J||l_4j_4\rangle\end{aligned}\tag{E.30}$$

By using Eq. (D.25) the two-body matrix elements for the exchange term coupled to a total momentum J read

$$\begin{aligned}\langle 1\ 2|V_{\delta_\pi}^{(pv))}|3\ 4\rangle^J_{ex} &= -\frac{1}{3}\left(\frac{f_\pi}{m_\pi}\right)^2 S_{n_1l_1n_2l_2n_3l_3n_4l_4}\\ &\times\ \sum_{\lambda L}(-)^{j_2-j_4+J+L}\left\{\begin{array}{ccc} j_1 & j_3 & J\\ j_2 & j_4 & \lambda\end{array}\right\}\langle l_1j_1||[\Sigma Y_L]_\lambda||l_4j_4\rangle\langle l_2j_2||[\Sigma Y_L]_\lambda||l_3j_3\rangle\end{aligned}\tag{E.31}$$

and the matrix elements coupled to a total momentum $J=0$ with $j_1=j_3$ and $j_2=j_4$ become

$$\begin{aligned}\langle 1\ 2|V_{\delta_\pi}^{(pv))}|3\ 4\rangle^0_{ex} &= -\frac{1}{3}\left(\frac{f_\pi}{m_\pi}\right)^2 S_{n_1l_1n_2l_2n_3l_3n_4l_4}\\ &\times\ \frac{1}{\hat{j}_1\hat{j}_2}\sum_{\lambda L}(-)^{j_1+j_2+\lambda+L}\langle l_1j_1||[\Sigma Y_L]_\lambda||l_4j_4\rangle\langle l_2j_2||[\Sigma Y_L]_\lambda||l_3j_3\rangle.\end{aligned}\tag{E.32}$$

Appendix F

Slater Integrals

From the previous two Appendices, we have seen that the Slater integrals in the two-body matrix elements of a OBE interaction read

$$S^{\lambda}_{n_1 l_1 n_2 l_2 n_3 l_3 n_4 l_4} = \frac{2}{\pi}\int_0^\infty q^2\, dq\ \langle 1|\Gamma_\mu j_\lambda(qr)|3\rangle\ D^{\mu\nu}_m(q)\langle 2|\Gamma_\nu j_\lambda(qr)|4\rangle \tag{F.1}$$

for the mesons $\sigma,\ \omega,\ \rho$, and $\vec{\pi}$ (pseudo-scalar coupling), and

$$S^{\lambda_1\lambda_2}_{n_1 l_1 n_2 l_2 n_3 l_3 n_4 l_4} = \frac{2}{\pi}\int_0^\infty q^4\, dq\ \langle 1|\vec{\Gamma}_{pv} j_{\lambda_1}(qr)|3\rangle\ D_{pv}(q)\langle 2|\vec{\Gamma}_{pv} j_{\lambda_2}(qr)|4\rangle \tag{F.2}$$

for the $\vec{\pi}$-meson (pseudo-vector coupling). In this notation $|k\rangle$ represent the relativistic radial wave functions. In the following, we calculate the Slater integrals for the nonrelativistic wave functions of a harmonic oscillator. In particular, an analytical expression for the radial matrix elements of spherical Bessel functions are determined.

F.1 Harmonic Oscillator Wave Functions

The normalized wave functions of a three-dimensional oscillator with an oscillator length $b = \sqrt{\hbar/m\omega}$ 3DHOWF can be written as

$$\psi_{nlm_l}(\mathbf{r}) = R_{nl}(r)Y_{lm_l}(\Omega). \tag{F.3}$$

where

$$R_{nl}(r) = b^{-\frac{3}{2}}\Phi_{nl}(\frac{r}{b})\mathrm{e}^{-\frac{r^2}{2b^2}}. \tag{F.4}$$

with the quantum numbers $n = 0, 1, \ldots,$ $l = 0, 1, \ldots,$. Working in units of the oscillator length $x = r/b$ the radial functions $\Phi_{nl}(x)$ are expressed in terms of Laguerre polynomials $L_n^{(l+\frac{1}{2})}(x^2)$

$$\Phi_{nl}(x) = N_{nl}\, x^l L_n^{(l+1/2)}(x^2) \tag{F.5}$$

with

$$L_n^{(l+\frac{1}{2})}(x^2) \;=\; (l+n+\frac{1}{2})!\sum_{q=0}^{n}\frac{(-)^q}{(n-q)!q!(l+q+\frac{1}{2})!}x^{2q} \tag{F.6}$$

$$= 2N_{nl}^{-2} \sum_{q=0}^{n} \left(\begin{array}{c} n \\ q \end{array} \right) \frac{(-)^q}{(l+q+\frac{1}{2})!} x^{2q}, \tag{F.7}$$

$$= \sum_{q=0}^{n} \frac{(-)^q}{q!} \left(\begin{array}{c} l+n+\frac{1}{2} \\ n-q \end{array} \right) x^{2q}, \tag{F.8}$$

and the normalization constants N_{nl} are given by

$$N_{nl} = \sqrt{\frac{2n!}{(n+l+\frac{1}{2})!}}. \tag{F.9}$$

The orthonormality relation is

$$\int r^2 dr\, R_{nl}(r) R_{n'l}(r) = \int x^2 dx\, \Phi_{nl}(x) \Phi_{n'l}(x) \mathrm{e}^{-x^2} = \delta_{nn'}. \tag{F.10}$$

As the oscillator wave functions form a complete set, the product of two oscillator functions can be expressed as a linear combination of oscillator functions. This is the addition theorem of oscillator functions

$$\psi^*_{n_1 l_1 m_{l_1}}(\mathbf{r}) \psi_{n_2 l_2 m_{l_2}}(\mathbf{r}) = b^{-\frac{3}{2}} \sum_{n_3 l_3} T^{n_3 l_3}_{n_1 l_1 n_2 l_2} \langle l_1 m_{l_1} | Y^*_{l_3 m_{l_3}} | l_2 m_{l_2} \rangle \psi_{n_3 l_3 m_{l_3}}(\mathbf{r}) \mathrm{e}^{-r^2/2b^2} \tag{F.11}$$

where $T^{n_3 l_3}_{n_1 l_1 n_2 l_2}$ are referred as Talman coefficients [Ta70]. Multiplying by $Y^*_{l_3 m_{l_3}}$ and integrating over $d\Omega$, a similar theorem for the radial functions

$$\Phi_{n_1 l_1}(x) \Phi_{n_2 l_3}(x) = \sum_{n_3} T^{n_3 l_3}_{n_1 l_1 n_2 l_2} \Phi_{n_3 l_3}(x) \tag{F.12}$$

$$R_{n_1 l_1}(r) R_{n_2 l_3}(r) = b^{-\frac{3}{2}} \sum_{n_3} T^{n_3 l_3}_{n_1 l_1 n_2 l_2} R_{n_3 l_3}(r) \mathrm{e}^{-\frac{r^2}{2b^2}} \tag{F.13}$$

is obtained. It holds for arbitrary values of l_3 satisfying $|l_1 - l_2| \leq l_3 \leq l_1 + l_2$ and $l = (l_1 + l_2 + l_3)/2$ integer. Using the orthogonality of the radial functions, we obtain

$$T^{n_3 l_3}_{n_1 l_1 n_2 l_2} = \int x^2 dx\, \Phi_{n_1 l_1}(x) \Phi_{n_2 l_2}(x) \Phi_{n_3 l_3}(x) \mathrm{e}^{-x^2} \tag{F.14}$$

$$= N_{n_1 l_1} N_{n_2 l_2} N_{n_3 l_3} \int dx x^{2l+2} L_{n_1}^{(l_1+\frac{1}{2})}(x^2) L_{n_2}^{(l_2+\frac{1}{2})}(x^2) L_{n_3}^{(l_3+\frac{1}{2})}(x^2) \mathrm{e}^{-x^2} \tag{F.15}$$

where $l = \frac{1}{2}(l_1 + l_2 + l_3)$ is an integer number. We expand $L_{n_1}^{(l_1+1/2)}(x^2)$ and $L_{n_2}^{(l_2+1/2)}(x^2)$ as in Eq. (F.6) and using

$$\int_0^\infty dy\, y^{\sigma+\frac{1}{2}} L_n^{(l+\frac{1}{2})}(y) e^{-y} = (\sigma + \frac{1}{2})! (-)^n \left(\begin{array}{c} \sigma - l \\ n \end{array} \right) \tag{F.16}$$

we find

$$T^{n_3 l_3}_{n_1 l_1 n_2 l_2} = \frac{2N_{n_3 l_3}}{N_{n_1 l_1} N_{n_2 l_2}} \sum_{q_1 q_2} \prod_{i=1,2} \frac{(-)^{q_i}}{(l_i + q_i + \frac{1}{2})!} \left(\begin{array}{c} n_i \\ q_i \end{array} \right) \int dy y^{q_1+q_2+l+\frac{1}{2}} L^{l_3+\frac{1}{2}}_{n_3}(y) \mathrm{e}^{-y}$$

$$= 2 \frac{N_{n_3 l_3}}{N_{n_1 l_1} N_{n_2 l_2}} \frac{n_1! n_2!}{n_3!} b^{n_3 l_3}_{n_1 l_1 n_2 l_2} \qquad \text{(F.17)}$$

where the coefficients $b^{n_3 l_3}_{n_1 l_1 n_2 l_2}$ are defined as

$$b^{n_3 l_3}_{n_1 l_1 n_2 l_2} = (-)^{n_3} \sum_{q_1=0}^{n_1} \sum_{q_2=0}^{n_2} \frac{(-)^{q_1+q_2} (q_1 + q_2 + (l_1 + l_2 + l_3)/2 + \frac{1}{2})!}{q_1! q_2! (n_1 - q_1)! (n_2 - q_2)! (q_1 + l_1 + \frac{1}{2})! (q_2 + l_2 + \frac{1}{2})!}$$

$$\times \frac{(q_1 + q_2 + (l_1 + l_2 - l_3)/2)!}{(q_1 + q_2 + (l_1 + l_2 - l_3)/2 - n_3)!} \qquad \text{(F.18)}$$

F.2 Nonrelativistic Slater Integrals

As nonrelativistic form of the Slater integrals, we take

$$S^{\lambda}_{n_1 l_1 n_2 l_2 n_3 l_3 n_4 l_4} = \frac{2}{\pi} \int_0^{\infty} q^2 \, dq \, \langle n_1 l_1 | j_\lambda(qr) | n_3 l_3 \rangle \, D_m(q) \langle n_2 l_2 | j_\lambda(qr) | n_4 l_4 \rangle. \qquad \text{(F.19)}$$

This expression is identical to Eq.(F.1) apart from the fact that we have now omitted the nucleon-meson vertices. In Eq.(F.19) the radial matrix element of a spherical Bessel function j_λ

$$\langle n_1 l_1 | j_\lambda(qr) | n_2 l_2 \rangle = \int_0^{\infty} r^2 \, dr \; R_{n_1 l_1}(r) j_\lambda(qr) R_{n_2 l_2}(r) \qquad \text{(F.20)}$$

can be explicitly calculated. The addition theorem given in Eq.(F.13) and the expansion of the resulting harmonic oscillator wave function $R_{n_3 l_3}$ in terms of polynomials (Eq.s (F.4)-(F.6)) lead to the following expression

$$\langle n_1 l_1 | j_\lambda(qr) | n_2 l_2 \rangle = \sum_{n_3} N_{n_3 l_3} T^{n_3 l_3}_{n_1 l_1 n_2 l_2} (n_3 + l_3 + \frac{1}{2})! \sum_{m=0}^{n_3} \frac{(-)^m}{(n_3 - m)! m! (m + l_3 + \frac{1}{2})!}$$

$$\times \sqrt{\frac{\pi}{2bq}} \int_0^{\infty} dx \; x^{2m+l_3-1/2+2} e^{-x^2} J_{\lambda+1/2}(bqx), \qquad \text{(F.21)}$$

in which $x = \frac{r}{b}$ and J_μ is a Bessel function of half integer order. For l_3 we choose $l_3 = l_1 + l_2$. Using

$$\int_0^{\infty} dx \; x^\mu e^{-x^2} \, J_\nu(\beta x) = \frac{\beta^\nu \Gamma(\frac{\nu}{2} + \frac{\mu}{2} + \frac{1}{2})}{2^{\nu+1} \Gamma(\nu + 1)} \, e^{-\beta^2/4} \, {}_1F_1(\frac{1 + \nu - \mu}{2}, \nu + 1, \frac{\beta^2}{4}) \qquad \text{(F.22)}$$

and the relation between the confluent hypergeometric function ${}_1F_1$ and the generalized Laguerre polynomials $L^{(\alpha)}_n$

$${}_1F_1(-n, \alpha + 1, x) = \frac{n! \alpha!}{(n + \alpha)!} \, L^{(\alpha)}_n(x) \qquad \text{(F.23)}$$

we arrive

$$\begin{aligned}\langle n_1 l_1|j_\lambda(qr)|n_2 l_2\rangle &= b^{3/2}\frac{\sqrt{\pi}}{2}\sqrt{n_1!}\sqrt{n_2!}\sqrt{(n_1+l_1+\frac{1}{2})!}\sqrt{(n_2+l_2+\frac{1}{2})!}\\ &\times \sum_{n_3} b^{n_3 l_3}_{n_1 l_1 n_2 l_2}\sum_{m=0}^{n_3}\frac{(-)^m}{(n_3-m)!m!(m+l_3+\frac{1}{2})!}(m+\frac{l_3-\lambda}{2})!e^{-b^2q^2/8}\\ &\times \frac{1}{N_{m+\frac{l_3-\lambda}{2}\lambda}}R_{m+\frac{l_3-\lambda}{2}\lambda}(\frac{bq}{2}).\end{aligned} \tag{F.24}$$

in which $\frac{l_3-\lambda}{2}$ is integer. Exchanging the order of the sums over n_3 and m

$$\sum_{n_3=0}^{n_1+n_2}\sum_{m=0}^{n_3} = \sum_{m=0}^{n_1+n_2}\sum_{n_3=m}^{n_1+n_2} \tag{F.25}$$

and using the explicit expression for the $b^{n_3 l_3}_{n_1 l_1 n_2 l_2}$ given in Eq.(F.18) with $l_3 = l_1 + l_2$, we find

$$\begin{aligned}\langle n_1 l_1|j_\lambda(qr)|n_2 l_2\rangle &= \frac{\sqrt{\pi}}{2}\sqrt{n_1!}\sqrt{n_2!}\sqrt{(n_1+l_1+\frac{1}{2})!}\sqrt{(n_2+l_2+\frac{1}{2})!}\\ &\times \sum_{m=0}^{n_1+n_2}\frac{(-)^m}{(n_3-m)!m!(m+l_3+\frac{1}{2})!}(m+\frac{l_3-\lambda}{2})!\frac{e^{-b^2q^2/8}}{N_{m+\frac{l_3-\lambda}{2}\lambda}}\\ &\times R_{m+\frac{l_3-\lambda}{2}\lambda}(\frac{bq}{2})\sum_{q_1 q_2,0}^{n_1,n_2}\frac{(-)^{q_1+q_1}(q_1+q_2+l_1+l_2+\frac{1}{2})!(q_1+q_2)!}{q_1!q_2!(n_1-q_1)!(n_2-q_2)!(q_1+l_1+\frac{1}{2})!(q_2+l_2+\frac{1}{2})!}\\ &\times \sum_{n_3=m}^{q_1+q_2}\frac{(-)^{n_3}}{(n_3-m)!(q_1+q_2-n_3)!}.\end{aligned} \tag{F.26}$$

In Eq.(F.26) we have replaced the upper limit of the sum over n_3, n_1+n_2 with q_1+q_2. This comes from the condition $q_1+q_2 \geq n_3$. Introducing the index

$$\mu = m + \frac{l_3-\lambda}{2} \tag{F.27}$$

the matrix elements of a Bessel functions can be simply rewritten as

$$\begin{aligned}\langle n_1 l_1|j_\lambda(qr)|n_2 l_2\rangle &= \frac{\sqrt{\pi}}{2}\sqrt{n_1!}\sqrt{n_2!}\sqrt{(n_1+l_1+\frac{1}{2})!}\sqrt{(n_2+l_2+\frac{1}{2})!}\\ &\times \sum_{\mu=\mu_m}^{\mu_M}\frac{(-)^{\mu-\mu_m}}{(\mu-\mu_m)!(\mu-\mu_m+l_3+\frac{1}{2})!}\mu!\frac{e^{-b^2q^2/8}}{N_{\mu\lambda}}R_{\mu\lambda}(\frac{bq}{2})\\ &\times \sum_{q_1 q_2,0}^{n_1,n_2}\frac{(-)^{q_1+q_1}(q_1+q_2+l_1+l_2+\frac{1}{2})!(q_1+q_2)!}{q_1!q_2!(n_1-q_1)!(n_2-q_2)!(q_1+l_1+\frac{1}{2})!(q_2+l_2+\frac{1}{2})!}\\ &\times \sum_{n_3=\mu-\mu_m}^{q_1+q_2}\frac{(-)^{n_3}}{(n_3-\mu+\mu_m)!(q_1+q_2-n_3)!}\end{aligned} \tag{F.28}$$

where $\mu_m = \frac{l_3-\lambda}{2}$ and $\mu_M = n_1 + n_2 + \mu_m$. With the new variable

$$\nu = n_3 - \mu + \mu_m \tag{F.29}$$

that changes the inner sum as

$$\sum_{n_3=\mu-\mu_m}^{q_1+q_2} = \sum_{\nu=0}^{q_1+q_2-\mu+\mu_m} \tag{F.30}$$

we obtain

$$\begin{aligned}
\langle n_1 l_1 | j_\lambda(qr) | n_2 l_2 \rangle &= \frac{\sqrt{\pi}}{2}\sqrt{n_1!}\sqrt{n_2!}\sqrt{(n_1+l_1+\frac{1}{2})!}\sqrt{(n_2+l_2+\frac{1}{2})!} \\
&\times \sum_{\mu=\mu_m}^{\mu_M} \frac{(-)^{\mu-\mu_m}}{(\mu-\mu_m)!(\mu-\mu_m+l_3+\frac{1}{2})!}\mu! \frac{e^{-b^2q^2/8}}{N_{\mu\lambda}} R_{\mu\lambda}(\frac{bq}{2}) \qquad \text{(F.31)} \\
&\times \sum_{q_1 q_2,0}^{n_1,n_2} \frac{(-)^{q_1+q_1}(q_1+q_2+l_1+l_2+\frac{1}{2})!(q_1+q_2)!}{q_1!q_2!(n_1-q_1)!(n_2-q_2)!(q_1+l_1+\frac{1}{2})!(q_2+l_2+\frac{1}{2})!} \\
&\times \frac{(-)^{\mu-\mu_m}}{(q_1+q_2-\mu+\mu_m)!} \sum_{\nu=0}^{q_1+q_2-\mu+\mu_m} (-)^\nu \left(\begin{array}{c} q_1+q_2-\mu+\mu_m \\ \nu \end{array} \right)
\end{aligned}$$

where the sum over ν may be carried out using the relation

$$\sum_{k=0}^{n} (-)^k \left(\begin{array}{c} n \\ k \end{array} \right) = \delta_{0n}. \tag{F.32}$$

Therefore, the matrix elements of a spherical Bessel function read

$$\langle n_1 l_1 | j_\lambda(qr) | n_2 l_2 \rangle = \sqrt{\frac{\pi}{8}} e^{-b^2q^2/8} \sum_{\mu=\mu_m}^{\mu_M} A^{\mu\lambda}_{n_1 l_1 n_2 l_2} R_{\mu\lambda}(\frac{bq}{2}) \tag{F.33}$$

where the coefficients $A^{\mu\lambda}_{n_1 l_1 n_2 l_2}$ are defined by

$$\begin{aligned}
A^{\mu\lambda}_{n_1 l_1 n_2 l_2} &= \sqrt{n_1!}\sqrt{n_2!}\sqrt{(n_1+l_1+\frac{1}{2})!}\sqrt{(n_2+l_2+\frac{1}{2})!}\sqrt{\mu!}\sqrt{(\mu+\lambda+\frac{1}{2})!} \\
&\times \sum_{q_1 q_2,0}^{n_1,n_2} \frac{\delta_{0 q_1+q_2-\mu+\mu_m}}{q_1!q_2!(n_1-q_1)!(n_2-q_2)!(q_1+l_1+\frac{1}{2})!(q_2+l_2+\frac{1}{2})!}. \qquad \text{(F.34)}
\end{aligned}$$

These coefficients are always positive. Thus, the nonrelativistic Slater integrals given in Eq. (F.19) may be rewritten as

$$\begin{aligned}
S^\lambda_{n_1 l_1 n_2 l_2 n_3 l_3 n_4 l_4} &= \frac{1}{4} \sum_{\mu_1=\mu_{m_1}}^{\mu_{M_1}} \sum_{\mu_2=\mu_{m_2}}^{\mu_{M_2}} \qquad \text{(F.35)} \\
&\times \int_0^\infty q^2 dq e^{-b^2q^2/4} R_{\mu_1\lambda}(\frac{bq}{2}) D_m(q) R_{\mu_2\lambda}(\frac{bq}{2}).
\end{aligned}$$

Analogous considerations apply to the Slater integrals for the pseudo-vector coupling.

Appendix G

Relativistic HB Theory for Finite Nuclei

In this Appendix we write the expressions of the pairing fields and energies of the σ- and ω-exchange interactions which habe been used in the relativistic HB calculations for finite nuclei presented in Chpater 4. Explicitly

- for the σ-meson

$$\Delta^{\sigma}_{a_1 p_1 a_2 p_2} = \sum_{a_3 a_4} \langle a_1 p_1 a_2 p_2 | \gamma^0_{13} \gamma^0_{24} D_\sigma | a_3 p_1 a_4 p_2 \rangle \kappa_{a3 p_1 a4 p_2} \tag{G.1}$$

$$E^{\sigma}_{pair} = \frac{1}{4} \sum_{\alpha_1 \alpha_2 a_3 a_4} \kappa_{a_2 p_2 a_1 p_1} \langle a_1 p_1 a_2 p_2 | \gamma^0_{13} \gamma^0_{24} D_\sigma | a_3 p_1 a_4 p_2 \rangle \kappa_{a_3 p_1 a_4 p_2} \tag{G.2}$$

- for the ω^0-meson

$$\Delta^{\omega^0}_{a_1 p_1 a_2 p_2} = \sum_{a_3 a_4} \langle a_1 p_1 a_2 p_2 | \mathbf{I}_{13} \mathbf{I}_{24} D_\omega | a_3 p_1 a_4 p_2 \rangle \kappa_{a3 p_1 a4 p_2} \tag{G.3}$$

$$E^{\omega^0}_{pair} = \frac{1}{4} \sum_{\alpha_1 \alpha_2 a_3 a_4} \kappa_{a_2 p_2 a_1 p_1} \langle a_1 p_1 a_2 p_2 | \mathbf{I}_{13} \mathbf{I}_{24} D_\omega | a_3 p_1 a_4 p_2 \rangle \kappa_{a_3 p_1 a_4 p_2} \tag{G.4}$$

- for the $\boldsymbol{\omega}$-meson

$$\Delta^{\boldsymbol{\omega}}_{a_1 p_1 a_2 p_2} = \sum_{a_3 a_4} \langle a_1 p_1 a_2 p_2 | \boldsymbol{\alpha}_{13} \cdot \boldsymbol{\alpha}_{24} D_\omega | a_3 \bar{p}_1 a_4 \bar{p}_2 \rangle \kappa_{a_2 \bar{p}_1 a_4 \bar{p}_3} \tag{G.5}$$

$$E^{\boldsymbol{\omega}}_{pair} = \frac{1}{4} \sum_{\alpha_1 \alpha_2 a_3 a_4} \kappa_{a_2 p_2 a_1 p_1} \langle a_1 p_1 a_2 p_2 | \boldsymbol{\alpha}_{13} \cdot \boldsymbol{\alpha}_{24} D_\omega | a_3 \bar{p}_1 a_4 \bar{p}_2 \rangle \kappa_{a_2 \bar{p}_1 a_4 \bar{p}_3} \tag{G.6}$$

The meson propagators D_m are given in Eq.s (A.11) in which the form factors F_m depend on the interaction used in the pp-channel.

Appendix H

Relativistic HF Theory for Finite Nuclei

In this Appendix we write the expressions of the selfconsistent fields and energies of the Fock term of the OBE interactions that have been used for the relativistic Hartree-Fock calculations presented in Section 5.2. Explicitly

- for the σ-meson

$$\Gamma^{F\sigma}_{a_1p_1a_3p_3} = \sum_{a_2a_4}\langle a_1p_1a_2p_3|\gamma^0_{14}\gamma^0_{23}D_\sigma|a_4p_1a_3p_3\rangle\rho_{a_2p_1a_4p_3} \quad \text{(H.1)}$$

$$E^{F\sigma}_{exc} = -\frac{1}{2}\sum_{\alpha_1a_2\alpha_3a_4}\rho_{a_3p_3a_1p_1}\langle a_1p_1a_2p_3|\gamma^0_{14}\gamma^0_{23}D_\sigma|a_4p_1a_3p_3\rangle\rho_{a_2p_1a_4p_3} \quad \text{(H.2)}$$

- for the ω^0-meson

$$\Gamma^{F\omega^0}_{a_1p_1a_3p_3} = \sum_{a_2a_4}\langle a_1p_1a_2p_3|\mathbf{I}_{14}\mathbf{I}_{23}D_\omega(r)|a_4p_1a_3p_3\rangle\rho_{a_2p_1a_4p_3} \quad \text{(H.3)}$$

$$E^{F\omega^0}_{exc} = -\frac{1}{2}\sum_{\alpha_1a_2\alpha_3a_4}\rho_{a_3p_3a_1p_1}\langle a_1p_1a_2p_3|\mathbf{I}_{14}\mathbf{I}_{23}D_\omega|a_4p_1a_3p_3\rangle\rho_{a_2p_1a_4p_3} \quad \text{(H.4)}$$

- for the $\boldsymbol{\omega}$-meson

$$\Gamma^{F\boldsymbol{\omega}}_{a_1p_1a_3p_3} = \sum_{a_2a_4}\langle a_1p_1a_2\bar{p}_3|\boldsymbol{\alpha}_{14}\cdot\boldsymbol{\alpha}_{23}D_\omega|a_4\bar{p}_1a_3p_3\rangle\rho_{a_2\bar{p}_1a_4\bar{p}_3} \quad \text{(H.5)}$$

$$E^{F\boldsymbol{\omega}}_{exc} = -\frac{1}{2}\sum_{\alpha_1a_2\alpha_3a_4}\rho_{a_3p_3a_1p_1}\langle a_1p_1a_2\bar{p}_3|\boldsymbol{\alpha}_{14}\cdot\boldsymbol{\alpha}_{23}D_\omega|a_4\bar{p}_1a_3p_3\rangle\rho_{a_2\bar{p}_1a_4\bar{p}_3} \quad \text{(H.6)}$$

- for the $\vec{\pi}$ (pseudo-vector coupling)

$$\Gamma^{F\vec{\pi}}_{a_1p_1a_3p_3} = \sum_{a_2a_4}\langle a_1p_1a_2p_3|\boldsymbol{\Sigma}_{14}\cdot\boldsymbol{\Sigma}_{23}D_\pi|a_4p_1a_3p_3\rangle\rho_{a_2p_1a_4p_3} \quad \text{(H.7)}$$

$$E^{F\vec{\pi}}_{exc} = -\frac{1}{2}\sum_{\alpha_1a_2\alpha_3a_4}\rho_{a_3p_3a_1p_1}\langle a_1p_1a_2p_3|\boldsymbol{\Sigma}_{14}\cdot\boldsymbol{\Sigma}_{23}D_\pi|a_4p_1a_3p_3\rangle\rho_{a_2p_1a_4p_3} \quad \text{(H.8)}$$

- for the δ-term in the $\vec{\pi}$ (pseudo-vector coupling)

$$\Gamma^{F\delta_\pi}_{a_1p_1a_3p_3} = \sum_{a_2a_4}\langle a_1p_1a_2p_3|\mathbf{\Sigma}_{14}\cdot\mathbf{\Sigma}_{23}D_{\delta_\pi}|a_4p_1a_3p_3\rangle\rho_{a_2p_1a_4p_3} \tag{H.9}$$

$$E^{F\delta\pi}_{exc} = -\frac{1}{2}\sum_{\alpha_1a_2\alpha_3a_4}\rho_{a_3p_3a_1p_1}\langle a_1p_1a_2p_3|\mathbf{\Sigma}_{14}\cdot\mathbf{\Sigma}_{23}D_{\delta_\pi}|a_4p_1a_3p_3\rangle\rho_{a_2p_1a_4p_3} \tag{H.10}$$

The meson propagators D_m for the mesons σ, ω, ρ, and π (pseudo-scalar coupling) are given in Eq.s (A.11) and the form factor is simply 1, and the meson propagator of the π-meson (pseudo-vector coupling) is given in Eq. (E.2) and the propagator the δ-term in the pseudo-vector term of π is

$$D_{\delta_\pi}(r) = \frac{1}{3}\left(\frac{f_\pi}{m_\pi}\right)^2\delta(\mathbf{r}_1-\mathbf{r}_2) = \frac{1}{3}\left(\frac{f_\pi}{m_\pi}\right)^2\int\frac{d^3q}{(2\pi)^3}\,\mathrm{e}^{i\mathbf{q}\cdot(\mathbf{r}_1-\mathbf{r}_2)} \tag{H.11}$$

Appendix I

Two-body Matrix Elements for the Isospin

In this Appendix we consider explicitly the two-body matrix elements of the isospin part of a OBE interaction as they enter into the pairing fields Δ of the DHB approximation and into the self-consistent field Γ of the DHF approximation.
Denoting with V_τ the isospin part of the OBE interaction, one has

$$V_\tau^S = \mathbb{I}_1 \mathbb{I}_2 \tag{I.1}$$

for isoscalar mesons, and

$$V_\tau^V = \vec{\tau}_1 \cdot \vec{\tau}_2 = 4t_{1z}t_{2z} + 2t_{1+}t_{2-} - 2t_{1-}t_{2+} \tag{I.2}$$

I.1 Two-body Matrix Elements for the Isospin in the *pp*-Channel

As we consider $T = 1$ pairing only, the neutron and proton pairing fields simply read

$$\Delta_{12}^n = \sum_{34} \langle 1n\ 2n|V_\tau|3n\ 4n\rangle\ \kappa_{34}^n \tag{I.3}$$

$$\Delta_{12}^p = \sum_{34} \langle 1p\ 2p|V_\tau|3p\ 4p\rangle\ \kappa_{34}^p \tag{I.4}$$

In this notation $|1\rangle$ contains all the quantum numbers which label the state, except the isospin one. The two-body matrix elements for the pairing channel are

$$\langle n\,n| \begin{pmatrix} \mathbb{I}_1\mathbb{I}_2 \\ \vec{\tau}_1 \cdot \vec{\tau}_2 \end{pmatrix} |n\,n\rangle = \begin{pmatrix} 1 \\ 1 \end{pmatrix}. \tag{I.5}$$

It holds

$$\langle n\,n|V_\tau|n\,n\rangle = \langle p\,p|V_\tau|p\,p\rangle. \tag{I.6}$$

I.2 Two-body Matrix Elements for the Isospin in the ph-Channel

We consider as an example the self-consistent field for neutrons. Using the previuos notation for the quantum numbers, it reads

$$\Gamma^n_{13} = \sum_{24} \langle 1n\,2n|V_\tau|3n\,4n\rangle\ \rho^n_{42} + \langle 1n\,2p|V_\tau|3n\,4p\rangle\ \rho^p_{42} \tag{I.7}$$

$$- \langle 1n\,2n|V_\tau|4n\,3n\rangle\ \rho^n_{42} - \langle 1n\,2p|V_\tau|4p\,3n\rangle\ \rho^p_{42}. \tag{I.8}$$

Analogously for the self-consistent field of the protons. The two-body matrix elements for pure neutron or proton states are the same as Eq.(I.5) for the direct and the exchange terms, while for mixed states they read

$$\langle n\,p| \begin{pmatrix} \mathbb{I}_1\mathbb{I}_2 \\ \vec{\tau}_1\cdot\vec{\tau}_2 \end{pmatrix} |n\,p\rangle = \begin{pmatrix} 1 \\ -1 \end{pmatrix}. \tag{I.9}$$

for the direct term, and

$$\langle n\,p| \begin{pmatrix} \mathbb{I}_1\mathbb{I}_2 \\ \vec{\tau}_1\cdot\vec{\tau}_2 \end{pmatrix} |p\,n\rangle = \begin{pmatrix} 0 \\ 2 \end{pmatrix}. \tag{I.10}$$

for the exchange term. We remark that the isospin independent part of the interaction gives no contribution to the exchange term in the isospin space. As for the pairing case, the isospin symmetry of the nuclear force leads to

$$\langle n\,p|V_\tau|n\,p\rangle = \langle p\,n|V_\tau|p\,n\rangle \tag{I.11}$$

Appendix J

Appendix: Auxiliary Formulas

$$\begin{pmatrix} j_1 & j_2 & j_3 \\ m_1 & m_2 & m_3 \end{pmatrix} \begin{Bmatrix} j_1 & j_2 & j_3 \\ l_1 & l_2 & l_3 \end{Bmatrix} \tag{J.1}$$
$$= \sum_{\mu_1\mu_2\mu_3} (-)^{l_1+l_2+l_3+\mu_1+\mu_2+\mu_3} \begin{pmatrix} j_1 & l_2 & l_3 \\ m_1 & \mu_2 & -\mu_3 \end{pmatrix} \begin{pmatrix} l_1 & j_2 & l_3 \\ -\mu_1 & m_2 & \mu_3 \end{pmatrix} \begin{pmatrix} l_1 & l_2 & j_3 \\ \mu_1 & -\mu_2 & m_3 \end{pmatrix}$$

$$\begin{pmatrix} J_{12} & J_{34} & J \\ M_{12} & M_{34} & M \end{pmatrix} \begin{Bmatrix} J_{12} & J_{34} & J \\ j_1 & j_3 & J_{13} \\ j_2 & j_4 & J_{24} \end{Bmatrix} \tag{J.2}$$
$$= \sum_{\substack{m_1m_2 \\ m_3m_4}} \begin{pmatrix} j_1 & j_2 & J_{12} \\ m_1 & m_2 & M_{12} \end{pmatrix} \begin{pmatrix} j_3 & j_4 & J_{34} \\ m_3 & m_4 & M_{34} \end{pmatrix} \begin{pmatrix} j_1 & j_3 & J_{13} \\ m_1 & m_3 & -m_1-m_3 \end{pmatrix}$$
$$\times \begin{pmatrix} j_2 & j_4 & J_{24} \\ m_2 & m_4 & -m_2-m_4 \end{pmatrix} \begin{pmatrix} J_{13} & J_{24} & J \\ -m_1-m_3 & -m_2-m_4 & M \end{pmatrix}$$

Recoupling for the ph-channel:

$$\sum_{m_1m_2} \sum_{m_3m_4} \sum_{\lambda\mu} (-)^{j_3-m_3} C(j_1m_1j_3-m_3|JM)(-)^{j_2-m_2} C(j_4m_4j_2-m_2|JM) \times$$
$$(-)^{j_4-m_4} C(j_1m_1j_4-m_4|\lambda\mu)(-)^{j_3-m_3+\mu} C(j_2m_2j_3-m_3|\lambda-\mu)$$
$$= (-)^{j_2+j_4+J+\lambda}(2\lambda+1) \begin{Bmatrix} j_1 & j_3 & J \\ j_2 & j_4 & \lambda \end{Bmatrix} \tag{J.3}$$

and

$$\sum_{m_1m_2} \sum_{m_3m_4} \sum_{\lambda\mu} (-)^{j_3-m_3} C(j_1m_1j_3-m_3|JM)(-)^{j_2-m_2} C(j_4m_4j_2-m_2|JM) \times$$
$$(-)^{j_4-m_4} C(j_1m_1j_4-m_4|\lambda\mu)(-)^{j_2-m_2} C(j_3m_3j_2-m_2|\lambda\mu)$$
$$= (-)^{j_3+j_4+J+\lambda}(2\lambda+1) \begin{Bmatrix} j_1 & j_3 & J \\ j_2 & j_4 & \lambda \end{Bmatrix} \tag{J.4}$$

Recoupling for the pp-channel:

$$\begin{aligned}
&\sum_{m_1 m_2}\sum_{m_3 m_4}\sum_{\lambda\mu} C(j_1 m_l j_2 m_2|JM)C(j_3 m_3 j_4 m_4|JM)\times \\
&\times(-)^{j_3-m_3}C(j_1 m_1 j_3 - m_3|\lambda\mu)(-)^{j_4-m_4+\mu}C(j_2 m_2 j_4 - m_4|\lambda-\mu) \\
= \;& (-)^{j_2+j_3+J}(2\lambda+1)\left\{\begin{array}{ccc} j_1 & j_2 & J \\ j_4 & j_3 & \lambda \end{array}\right\} \qquad \text{(J.5)}
\end{aligned}$$

and

$$\begin{aligned}
&\sum_{m_1 m_2}\sum_{m_3 m_4}\sum_{\lambda\mu} C(j_1 m_1 j_2 m_2|JM)C(j_3 m_3 j_4 m_4|JM)\times \\
&(-)^{j_3-m_3}C(j_1 m_1 j_3 - m_3|\lambda\mu)(-)^{j_2-m_2}C(j_4 m_4 j_2 - m_2|\lambda\mu) \\
= \;& (-)^{j_3+j_4+J}(2\lambda+1)\left\{\begin{array}{ccc} j_1 & j_2 & J \\ j_4 & j_3 & \lambda \end{array}\right\} \qquad \text{(J.6)}
\end{aligned}$$

$$\left(\begin{array}{ccc} \frac{1}{2} & l & j \\ -\frac{1}{2} & 0 & \frac{1}{2} \end{array}\right) = (-)^{j-\frac{1}{2}}\frac{1}{\sqrt{2}}\frac{1}{\sqrt{2l+1}} \qquad \text{(J.7)}$$

$$\left\{\begin{array}{ccc} j_1 & L & j_2 \\ l_2 & \frac{1}{2} & l_1 \end{array}\right\}\left(\begin{array}{ccc} l_1 & L & l_2 \\ 0 & 0 & 0 \end{array}\right) = -\frac{1+(-)^{l_1+l_2+L}}{2}\frac{1}{\hat{l}_1\hat{l}_2}\left(\begin{array}{ccc} j_1 & L & j_2 \\ -\frac{1}{2} & 0 & \frac{1}{2} \end{array}\right) \qquad \text{(J.8)}$$

$$\left\{\begin{array}{ccc} \frac{1}{2} & l_1 & j_1 \\ \frac{1}{2} & l_2 & j_2 \\ S & L & J \end{array}\right\}\left(\begin{array}{ccc} l_1 & L & l_2 \\ 0 & 0 & 0 \end{array}\right) = \qquad \text{(J.9)}$$

$$\frac{1+(-)^{l_1+l_2+L}}{2}\frac{(-)^L}{\hat{l}_1\hat{l}_2}\left\{\delta_{S0}\,\delta_{LJ}\frac{(-)^{l_2+j_2+\frac{1}{2}+L}}{\sqrt{2}\,\hat{L}}\left(\begin{array}{ccc} j_1 & J & j_2 \\ \frac{1}{2} & 0 & -\frac{1}{2} \end{array}\right) + \right.$$

$$\left.\delta_{S1}\left[\frac{(-)^{l_2+j_2+\frac{1}{2}}}{\sqrt{6}}\left(\begin{array}{ccc} S & L & J \\ 0 & 0 & 0 \end{array}\right)\left(\begin{array}{ccc} j_1 & J & j_2 \\ \frac{1}{2} & 0 & -\frac{1}{2} \end{array}\right) - \frac{1}{\sqrt{3}}\left(\begin{array}{ccc} S & L & J \\ -1 & 0 & 1 \end{array}\right)\left(\begin{array}{ccc} j_1 & J & j_2 \\ \frac{1}{2} & -1 & \frac{1}{2} \end{array}\right)\right]\right\}$$

Reduced matrix elements:

$$(j_1 m_1|Q_{\lambda\mu}|j_2 m_2) = \frac{(-)^{j_2-m_2}}{\sqrt{2\lambda+1}}C(j_1 m_1 j_2 - m_2|\lambda\mu)(j_1||Q_\lambda||j_2) \qquad \text{(J.10)}$$

This yields:

$$\begin{aligned}
(\frac{1}{2}||1||\frac{1}{2}) &= \sqrt{2} && \text{(J.11)} \\
(\frac{1}{2}||\sigma||\frac{1}{2}) &= \sqrt{6} && \text{(J.12)} \\
\langle l||Y_\lambda||l'\rangle &= \frac{(-)^l}{\sqrt{4\pi}}\hat{\lambda}\,\hat{l}\hat{l}'\left(\begin{array}{ccc} l & \lambda & l' \\ 0 & 0 & 0 \end{array}\right) && \text{(J.13)}
\end{aligned}$$

$$\langle l||Y_0||l'\rangle = \delta_{ll'}\sqrt{\frac{2l+1}{4\pi}} \tag{J.14}$$

$$\langle lj||Y_J||l'j'\rangle = \frac{1+(-)^{l+l'+J}}{2}\frac{\hat{j}\hat{j}'\hat{J}}{\sqrt{4\pi}}(-)^{j-\frac{1}{2}}\begin{pmatrix} j & J & j' \\ -\frac{1}{2} & 0 & \frac{1}{2}\end{pmatrix} \tag{J.15}$$

$$\langle l'j'||Y_J||lj\rangle = (-)^{j-j'}\langle lj||Y_J||l'j'\rangle \tag{J.16}$$

$$\langle lj||Y_0||l'j'\rangle = \delta_{ll'}\delta_{jj'}\sqrt{\frac{2j+1}{4\pi}} \tag{J.17}$$

and

$$\langle lj||\left[\sigma Y_L\right]_J||l'j'\rangle = \hat{j}\hat{j}'\hat{J}\langle||\sigma||\rangle\langle l||Y_L||l'\rangle\begin{Bmatrix} \frac{1}{2} & \frac{1}{2} & 1 \\ l & l' & L \\ j & j' & J\end{Bmatrix}, \tag{J.18}$$

Using Eq. (J.3) this yields

$$\begin{aligned}\langle lj||\left[\sigma Y_L\right]_J||l'j'\rangle = {} & \frac{1+(-)^{l+l'+L}}{2}\frac{\hat{j}\hat{j}'\hat{L}\hat{J}}{\sqrt{4\pi}}(-)^{l+L}\left[(-)^{l'+j'+\frac{1}{2}}\begin{pmatrix} 1 & L & J \\ 0 & 0 & 0\end{pmatrix}\begin{pmatrix} j & J & j' \\ \frac{1}{2} & 0 & -\frac{1}{2}\end{pmatrix}\right. \\ & \left.-\sqrt{2}\begin{pmatrix} 1 & L & J \\ -1 & 0 & 1\end{pmatrix}\begin{pmatrix} j & J & j' \\ \frac{1}{2} & -1 & \frac{1}{2}\end{pmatrix}\right].\end{aligned}$$

and

$$\langle lj||\left[\sigma Y_1\right]_0||l'j'\rangle = \frac{1-(-)^{l+l'}}{2}\,\delta_{jj'}\sqrt{\frac{2j+1}{4\pi}} \tag{J.19}$$

The conjugation relation between the spin-dependent matrix elements yields

$$\langle l'j'||\left[\sigma Y_L\right]_J||lj\rangle = (-)^{j'+j+L+J}\langle lj||\left[\sigma Y_L\right]_J||l'j'\rangle \tag{J.20}$$

Bibliography

[AS64] M. Abramowitz and I.A. Stegun, *Handbook of Mathematical Functions*, Dover Publications, INC, New York (1964)

[AW93] G. Audi and A.H. Wapstra, *Nucl. Phys.* A 565 (1993) 1

[BB77] J. Boguta and A.R. Bodmer, *Nucl. Phys.* A 292 (1977) 43

[BCL90] M. Baldo, J. Cugnon, A. Lejeune and U. Lombardo, *Nucl. Phys.* A 515 (1990) 409

[BFG93] P. Bernardos, V.N. Fomenko, N. Van Giai, M. López-Quelle, S. Marcos, R. Niembro and L. Savushkin, *Phys. Rev.* C 48 (1993) 2665

[BGG84] J.F. Berger, M. Girod and D. Gogny, *Nucl. Phys.* A 428 (1984) 32c

[BI87] P.J. Blundel and M.J. Iqbal, *Phys. Lett.* B 196 (1983) 295

[BL84] D. Bailin and A. Love, *Phys. Rep.* 107C (1984) 325

[BM90] R. Brockmann and R. Machleidt, *Phys. Rev.* C 42 (1990) 1965

[BMG87] A. Bouyssy, J.F. Mathiot, N. Van Giai and S. Marcos, *Phys. Rev.* C 36 (1987) 380

[BMM85] A. Bouyssy, S. Marcos, J.F. Mathiot and Nguyen Van Giai, *Phys. Rev. Lett.* 55 (1985) 1731

[BMP58] A. Bohr, B.R. Mottelson and D. Pines, *Phys. Rev.* 110 (1958) 936

[Br78] R. Brockmann, *Phys. Rev.* C 18 (1978) 1510

[BT92] R. Brockmann and H. Toki, *Phys. Rev. Lett.* 68 (1992) 3408

[BW63] W. Brenig and H. Wagner, *Z. Phys.* 173 (1963) 484

[CCD70] F. Coester, S. Cohen, B.D. Day and C.M. Vincent *Phys. Rev.* C 1 (1970) 769

[CCD93] J.M.C. Chen, J.W. Clark, R.D. Davè and V.V. Khodel, *Nucl. Phys.* A 455 (1993) 59

[CH00] B.V. Carlson and D. Hirata, *Phys. Rev.* C 62 (2000) 054310

[Ch77] S.A. Chin, *Ann. Phys. (N.Y.)* 108 (1977) 301

[CW74] S.A. Chin and J.D. Walecka, *Phys. Lett.* B 52 (1974) 24

[DFT84] J. Dobaczewski, H. Flocard, J. Trenier, *Nucl. Phys.* A 422 (1984) 103

[DG80] J. Decharge and D. Gogny, *Phys. Rev.* C 21 (1980) 1568

[DG90] R.M. Dreizler and E.K.U. Gross; *Density Functional Theory*, Springer Verlag, Heidelberg (1990)

[DNW96] J. Dobaczewski, W. Nazarewicz, T.R. Werner, J.F. Berger, C.R. Chinn and J. Dechargé, *Phys. Rev.* C 38 (1996) 2089

[DT56] H.P. Dürr and E. Teller, *Phys. Rev.* 101 (1956) 494

[Ed60] A.R. Edmonds, *Angular Momentum in Quantum Mechanics*, Princeton University Press (Princeton), (1960)

[EEH96] O. Elgaroy, L. Engvik, M. Hjorth-Jensen and E. Osnes, *Nucl. Phys.* A 604 (1996) 466

[EH98] O. Elgaroy and M. Hjorth-Jensen *Condensed Matter Theories* 13 (1998) 191

[Er74] E. Erkelenz, *Phys. Rep.* 13 (1974) 191

[FPS89] R.J. Furnstahl, R.J. Perry and B.D. Serot, *Phys. Rev.* C 40 (1989) 321

[GCF96] F.B. Guimarães, B.V. Carlson and T. Frederico, *Phys. Rev.* C 54 (1996) 2385

[Gi97] J.N. Ginocchio, *Phys. Rev. Lett.* 77 (1997) 4149

[GLE96] T. Gonzales-Llarena, J.L. Egido, G.A. Lalazissis and P. Ring, *Phys. Lett.* B 379 (1996) 13

[Go58] L.P. Gorkov, *Sov. Phys.* JETP 7 (1958) 505

[GR93] Y.K. Gambhir and P. Ring *Mod. Phys. Lett.* A 8 (1993) 787

[GR94] I.S. Gradshtein and I.M. Ryzhik, *Table of Integrals, Series and Products*, Academic Press (1994)

[GRT90] Y.K. Gambhir, P. Ring and A. Thimet, *Ann. Phys. (N.Y.)* 511 (1990) 129

[GRW89] J. Götz, J. Ramschütz, F. Weber and M.K. Weigel, *Phys. Lett.* B 226 (1989) 213

[HK64] P. Hohenberg and W. Kohn, *Phys. Rev.* B 136 (1964) 864

[HS83] C.J. Horowitz and B.D. Serot, *Nucl. Phys.* A 399 (1983) 529

[HS84] C.J. Horowitz and B.D. Serot, *Phys. Lett.* B 140 (1984) 181

[IEM01] V.I. Isakov, K.I. Erokhina, H. Mach, M. Sanchez-Vega and B. Fogelberg, *nucl-th/0101029*

[IZ80] C. Itzykson and J.B. Zuber, *Quantum Field Theory*, McGraw Hill, New York (1980)

[JG89] R.O. Jones and O. Gunnarson, *Rev. Mod. Phys.* 61 (1989) 689

[JT55] M.H. Johnson and E. Teller, *Phys. Rev.* 98 (1955) 783

[KR91] H. Kucharek and P. Ring, *Z. Phys.* A 339 (1991) 23

[KRS89a] H. Kucharek, P. Ring and P. Schuck, *Z. Phys.* A 334 (1989) 119

[KRS89b] H. Kucharek, P. Ring, P. Schuck, R. Bengtsson and M. Girod, *Phys. Lett.* B 216 (1989) 249

[KS65] W. Kohn and L. Sham, *Phys. Rev.* 137 (1965) 1697

[La59] L.D. Landau, *Sov. Phys.* JETP 8 (1959) 70

[LGM00] M. Lopez-Quelle, N. Van Giai, S. Marcos and L.N. Savushkin, *Phys. Rev.* C 61 (2000) 064321

[LKR97] G.A. Lalazissis, J. König and P. Ring, *Phys. Rev.* C 55 (1997) 540

[LLR80] M. Lacombe, B. Loiseaux, J.-M. Richard, R. Vinh Mau, J. Côté, D. Pirès and R. de Tourreil, *Phys. Rev.* C 21 (1980) 861

[LVP98a] G.A. Lalazissis, D. Vretenar, W. Pöschl and P. Ring, *Nucl. Phys.* A 632 (1998) 363

[LVP98b] G.A. Lalazissis, D. Vretenar, W. Pöschl and P. Ring, *Phys. Lett.* B 418 (1998) 7

[LVR01] G.A. Lalazissis, D. Vretenar and P. Ring, *Nucl. Phys.* A 679 (2001) 481

[LVR98] G.A. Lalazissis, D. Vretenar and P. Ring, *Phys. Rev.* C 57 (1998) 2294

[LVR99] G.A. Lalazissis, D. Vretenar and P. Ring, *Nucl. Phys.* A 650 (1999) 133

[Mi67] A.B. Migdal, *Theory of Finite Fermi Systems, Applications to Atomic Nuclei*, Wiley Interscience, New York (1967)

[Mi68] A.B. Migdal, *Nuclear Theory: the Quasiparticle Method*, W.A. Benjamin, Inc., New York (1968)

[Ma89] R. Machleidt,*Adv. Nucl. Phys.* 19 (1989) 189

[Ma93] G. Mairle, *Nucl. Phys.* B 304 (1993) 39

[Ma94] G. Mairle, *Z. Phys.* A 350 (1994) 285

[Ma98] M. Matsuzaki, *Phys. Rev.* C 58 (1998) 3407

[Me98] J. Meng, *Phys. Rev.* C 57 (1998) 1229

[MHE87] R. Machleidt, K. Holinde and Ch. Elster, *Phys. Rep.* 149 (1987) 1

[MR96] J. Meng and P. Ring, *Phys. Rev. Lett.* 77 (1996) 3963

[MRS89] P. Massen, Th. Rijken and J. de Swart, *Phys. Rev.* C 40 (1989) 40

[MSS96] R. Machleidt, F. Sammarrucca and Y. Song, *Phys. Rev.* C 53 (1996) R1483

[MT01] M. Matsuzaki and T. Tanigawa, *Nucl. Phys.* A 683 (2001) 406

[NuP00] *Radioactive Nuclear Beam Facilities*, NuPECC, April 2000

[PBM86] A.P. Prudnikov, Yu.A. Brychkov and O.I. Marichev, *Integrals and Series*, Gordon and Breach Science Publishers (1986), Vol. 1,2

[PRB87] W. Pannert, P. Ring and J. Boguta, *Phys. Rev. Lett.* 59 (1987) 2420

[PVL97] W. Pöschl, D. Vretenar, G.A. Lalazissis and P. Ring, *Phys. Rev. Lett.* 79 (1997) 3841

[Ri96] P. Ring, *Prog. Part. Nucl. Phys.* 37 (1996) 193

[RIA00] *Scientific Opportunities with Fast Fragmentation Beams from RIA*, MSU, March 2000

[RRM86] P.G. Reinhard, M. Rufa, J. Maruhn, W. Greiner and J. Friedrich, *Z. Phys.* A 323 (1986) 13

[RS80] P. Ring and P. Schuck, *The Nuclear Many-body Problem*, Springer Verlag, Heidelberg (1980)

[Ru94] A. Rummel, *Diplomarbeit, TUM, 1994*

[RWW90] J. Ramschütz, F. Weber and M.K. Weigel, *J. Phys.* G 16 (1990) 987

[Sc51] L.I. Schiff, *Phys. Rev.* 84 (1951) 1

[Sk59] T.H.R. Skyrme, *Nucl. Phys.* 9 (1959) 615

[SMM91] K.W. Schmid, H. Müther and R. Machleidt, *Nucl. Phys.* A 530 (1991) 14

[SMQ97] L. Savushkin, S. Marcos, M. López-Quelle, P. Bernardos, V.N. Fomenko and R. Niembro, *Phys. Rev.* C 55 (1997) 167

[SNR93] M.M. Sharma, M.A. Nagarajan and P. Ring, *Phys. Lett.* B 312 (1993) 377

[SW86] B.D. Serot and J.D. Walecka, *Adv. Nucl. Phys.* 16 (1986) 1

[Ta70] J.D. Talman, *Nucl. Phys.* A 141 (1970) 273

[Ta72] T. Takatsuka, *Prog. Theor. Phys.* 48 (1972) 1517

[TM99] T. Tanigawa and M. Matsuzaki, *Prog. Theor. Phys.* 102 (1999) 897

[Va73] D. Vautherin, *Phys. Rev.* C 7 (1973) 296

[VB72] D. Vautherin and D.M. Brink, *Phys. Rev.* C 5 (1972) 626

[VLR98] D. Vretenar, G.A. Lalazissis, and P. Ring, *Phys. Rev.* C 57 (1998) 3071

[Wa74] J.D. Walecka, *Ann. Phys. (N.Y.)* 83 (1974) 491

[Wa88] D.A. Wasson, *Phys. Lett.* B 210 (1988) 41

[We70] F. Wegner, *Nucl. Phys.* A 141 (1970) 609

[WPC00] R.B. Wiringa, S.C. Pieper, J. Carlson and V.R. Pandharipande, *Phys. Rev.* C 62 (2000) 014001

[WSA84] R.B. Wiringa, R.A. Smith and T.L. Ainsworth, *Phys. Rev.* C 29 (1984) 1207

[ZMR91] Z.Y. Zhu, H.J. Mang and P. Ring, *Phys. Lett.* B 254 (1991) 325